UNIVERSITY OF TRIESTE

DOCTORAL THESIS

Climate change impact on flood hazard over Italy

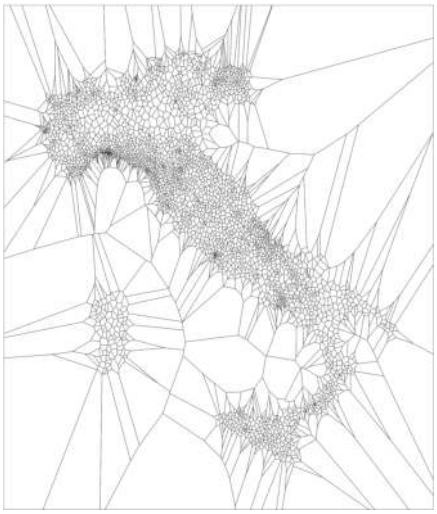

Author:
Adriano FANTINI

Supervisor:
Erika Coppola

PhD Course in Earth Science, Fluid-Dynamics, and Mathematics, XXXI cycle
Department of Mathematics and Geosciences

'There is a pleasure in the pathless woods
There is a rapture on the lonely shore
There is society where none intrudes
By the deep Sea, and music in its roar:
I love not Man the less, but Nature more'

George Byron

Abstract

Floods are one of the most devastating natural disasters, with strong impacts on both society and economy. Flood hazard estimation is an essential tool for protecting the population from floods both financially, via insurance policies, and physically, via water management and engineering. In Europe, different kinds of flood maps are usually produced with different methods by governments, regional agencies, or insurance and re-insurance companies. In the last decades, however, new approaches based on hydrological and hydraulical modelling emerged as viable, which allows for a more robust and reproducible physically-based estimation of flood extent and water level. In this work a multimodel approach has been adopted, with a hydrological model driven by multiple sources of precipitation input data, generating discharge data for a given region or basin for a long time period. The discharge is then fed to a hydrodynamic model which produces of flood extents and, if necessary, other variables such as flood depth or flow speed. Extreme value analysis is also used to derive any Return Period value (ranging from 10 to 500 years) starting from a shorter observational record, by assuming a given distribution for extreme events.

Over Italy, flood hazard has not yet been evaluated using a unified method. We propose a methodology to simulate flood hazard for any return period, based on a model chain comprised of three models: the Regional Climate Model RegCM, the hydrological model CHyM and the hydraulical model CA2D. For the time being only domains covering the complete Italian territory were simulated, but no limitation is in place that would prevent this technique from being applied to any domain worldwide, provided that the necessary input data is available.

In order to provide observed precipitation data as input to the hydrological model, we created a new product called GRIPHO (GRidded Italian Precipitation Hourly Observations), which consists of quality checked hourly precipitation observations over the complete Italian territory. We validate GRIPHO against other state-of-the-art precipitation datasets over Italy, showing good performance in reproducing both mean and extreme precipitation: GRIPHO is comparable with the high resolution ARCIS and EURO4M-APGD datasets in Northern Italy, and shows finer spatial details and more consistent extremes than E-OBS in the rest of the domain.

Two regional climate simulations, one run in perfect boundary mode (with ERA-Interim) and one a scenario simulation (driven with HadGEM, RCP8.5), are described and validated over the Italian territory. Both simulations show good agreement with observation in several precipitation and temperature metrics, for both extreme and mean climate. The projected climate change signal is also evaluated, finding, on average, increased extreme precipitation even in areas where mean precipitation decreases.

Three hydrological simulations, driven by both observations and regional climate model outputs, are described. Validation is carried out against a set of discharge stations, finding generally good performance of the CHyM model for the regions where observations are available. Using different metrics, we assess the future changes in mean and extreme discharge for the Italian territory, finding strong increases in possible flood proxies. In particular, mean discharge is projected to increase (decrease) in Northern Italy in winter (summer), which is directly linked to changes in mean precipitation over the Po river basin. In winter and autumn, maximum yearly discharges increase by 50% in several Italian regions, with summer and spring showing more mixed results. 100-year Return Period discharges are projected to increase over most of Italy by more than 100% by the end of the century. Similarly, the frequency of exceedance of extreme discharge thresholds drastically increases in the future scenario compared to the reference period, with changes for the 100-year threshold exceeding 500% for several rivers in Italy, including the Po river.

Finally, we present preliminary results over the whole Italian territory for flood maps for different Return Periods, as produced by a hydraulic model fed by simulated discharge data. The resulting maps are compatible with the currently available products obtained from regional environment agencies, but have the advantage of being produced with a coherent, scientific methodology.

Acknowledgements

This PhD project is the outcome of the work of many people: the core team was composed by Erika Coppola, Francesca Raffaele, Rita Nogherotto and myself. Graziano Giuliani and Fabio di Sante also were instrumental to several parts of the project thanks to their technical insight.

Whenever fitting, specific acknowledgements are given inside the text or in footnotes, but here I would especially like to thank all of my colleagues at the ICTP Earth System Physics group, which funded the project and hosted me during my PhD.
In particular, I thank Rita, Francesca and Erika, for sharing this adventure with me: thanks for being patient when I was stubborn, for being understanding when I made mistakes. I can only imagine it's not always easy to work with a pedantic and introvert person like myself.
Thanks to Graziano and Ivan, without whom the mysteries of computing would often have remained just that: mysteries. I thank the colleagues and friends of a time now gone, Bianca, Csaba, Stefano, Ramon, Irene: our paths have crossed, and I hope they will again.

But most of all I want to thank those who, during these three years, more than colleagues have been friends. Giorgio, for putting up with me all this time; Fabio, for teaching by example (to play table football, of course); Costanza, for that one ice cream, and for more to come; James, for being the most down to cheese guy; Rita once again, for the moral support and the reality checks in harsh times; Marco, for the smile always ready.
Thank you, friends, for the most important thing: because you made going to work not a chore, but a pleasure.

I have a short memory. I am certain I am forgetting someone, and if that's you, reader, I beg your pardon. If you think you deserve my gratitude, well, you probably do: thank you.

Author's note

This thesis has been compressed for uploading and is missing hyperlinks. The original version, containing full-resolution images and hyperlinks, can be obtained from http://users.ictp.it/~afantini/PhD_thesis/PhD_thesis_final_15feb2019.pdf or by requesting it to adr.fantini@gmail.com.

Contents

List of Figures

List of Tables

Dedicated to Anna and to Sofia

Chapter 1

Introduction

1.1 Project objectives and overview

The aim of this thesis is to assess flood hazard over the complete Italian domain for both the present day climate and for future projections. Due to the requirements of a strictly physically-based reproducible scientific approach, a framework consisting in a model chain of three tried-and-tested models, spanning climate, hydrology, and hydraulics, was developed. This thesis thus describes a truly inter-disciplinary approach to flood hazard modelling. The work described here was partially funded by the Allianz Insurance Company.

In order to obtain a reliable representation of flood hazard, model calibration and evaluation were performed using several observational datasets of precipitation, discharge and flood extent. In particular, a new gridded hourly precipitation dataset for the complete Italian territory was developed in conjunction with the University of L'Aquila, Italy. The development of such dataset represents an important step in the scientific process described in this thesis since, to our knowledge, no database suitable for driving a high-resolution hourly hydrological model is currently available over Italy. Both flood proxies consisting in several extreme discharge metrics and simulated floods extents are analysed in this work.

1.1.1 Scientific significance and research questions

The impact of climate change on atmospheric Essential Climate Variables (ECVs), such as temperature and precipitation, has been subject of several studies in the last decades, and is relatively well-known. As detailed in section 1.3, under a business-as-usual scenario, precipitation extremes are generally projected to increase both in frequency and in intensity. However, how changes in atmospheric ECVs affect derived variables is less clear, especially for extreme events at small spatial and temporal scales. Flooding, in particular, is one archetype of extreme event which might be significantly affected by changes in climate patterns, due to the simple fact that increased extreme precipitation leads to increased flooding; the link between precipitation and floods is not necessarily linear: due to the complexities derived

from snow accumulation and melting, underground water flow and local channel characteristics, the change in flood hazard might differ in pattern and intensity compared to that of extreme precipitation. Assessing the spatial and temporal change patterns of these two variables is a research topic of great interest, and one which requires high resolution data to be able to decode the signal at small spatial scales. In this work, we look not only at how these factors change in a climate scenario, but also at how they are related to each other.

Flooding strongly affects society and economy, both on the large and small scales, and flood hazard is increasingly taken into consideration by policymakers and companies, which require up-to-date historical data and future projections. For this reason, the interest in flood hazard studies has been soaring in the last decades, and recently a new model chain approach has emerged as viable, at least on the continental scale. Here, climate, hydrological and hydraulic models work in concert to provide physically-based flood hazard projections for possible future scenarios. In this regard, several studies improved the knowledge of the projected changes over large basins, especially over Europe. These works, however, rarely offer enough insight over future small scale flood hazards over specific areas, and studies focusing on changes for any individual European country are quite rare. In fact, the model chain approach is rarely employed for high resolution analysis due to the sheer size of the domains and the resulting computing challenges. By focusing on a single country, however, computational requirements become manageable, which allows the testing of this methodology at unprecedented spatial and temporal scales.
Therefore, this thesis focuses on one specific region (Italy) with the aim of providing high resolution, usable information to companies and policymakers alike. In this sense, this work represents an advancement in large scale flood hazard projection compared to previous studies, being the first application of the model chain approach over a single European country.

In short, the main research questions addressed by this work are:

- Can a model chain of climate, hydrological and hydraulic models reliably reproduce flood hazard at high resolution over the selected domain?
- How does climate change impact flood hazard over Italy, in terms of intensity, frequency and seasonality?
- Is the change in flood hazard linearly connected with changes in precipitation extremes, or are the spatial or temporal patterns different between the two?

1.1.2 The structure of this thesis

This thesis is structured in 6 chapters. In the upcoming sections of the current chapter a general overview on flood risk, flood hazard and flood modelling is given, including a discussion on the current knowledge of flood hazard in the study domain. Chapter 2 details the different types of observational dataset used through this project,

with particular attention to precipitation. A new hourly precipitation dataset over Italy, named GRIPHO, is presented in chapter 3, where it is described and validated. Chapter 4 describes the methodologies and models used to produce precipitation, discharges and flood extents. The results of the simulations with the three models are presented and discussed in chapter 5. Finally, chapter 6 gives a summary of the work done and of the future prospects.

1.2 Flood hazard: an overview

Floods are some of the most devastating natural disasters, with severe negative impacts on both the societal and economic scale. According to the Centre for Research on the Epidemiology of Disasters, several thousand people are killed every year by floods worldwide, with a yearly average of about 5700 deaths and 82.6 million people affected in the period 2006–2015 (Guha-sapir et al., 2011). Flood-related damages, up to $34 billion yearly, account for one third (Munich RE, 2000) to one quarter (Guha-sapir et al., 2011) of the total disaster damage claimed worldwide, with damages amounting to billion $15.45 in the USA alone in 2016. For Europe in particular, floods have caused about billion €100 in damages in the period 1986–2006 (CEA, 2007).

For these reasons, flood forecasting and risk estimation are an essential tool for protecting the population from flood-related damages both financially, via insurance policies, and physically, via water management and engineering.

1.2.1 Flood types, risk and hazard

According to the European Union Floods Directive, a flood is defined by the 'temporary covering by water of land not normally covered by water' (European Union Floods Directive, 2007). Three main types of floods are usually recognised (see Kron, 2005), each having its own characteristics:

Storm surge Storm surges can occur when low pressure systems, strong winds and/or high tides combine to cause high waters in coastal areas. This type of floods is especially frequent in regions where strong cyclonic development can take place.

Flash floods Flash floods are extremely fast floods that are characterised by a short timescale, usually below 6 hours. They can be caused by very strong, sudden precipitation (especially in urban areas where waterways are severely constrained) or by catastrophic events, such as dam failures and landslides.

River floods River floods, associated with unusually strong and persistent precipitation and snow melt, are instead characterised by a longer life cycle, up to several days. They are usually caused by the gradual increase in river discharge, to the point where water level overtops levees or overflows river banks. The time scale of riverine floods is usually dependant on the size of the catchment.

River floods are the only type of floods considered in this work.

The impact of floods on society can be evaluated statistically via the concepts of risk and hazard. Despite being often used as interchangeable terms, risk and hazard have very different meanings in scientific language. Risk is usually defined as the product of the probability of an event happening (the hazard) with its possible consequences (see e.g. De Moel et al., 2009; Kron, 2002; Merz et al., 2007). These can be further split into two different aspects, exposure and coping factor, so that (IPCC, 2012):

$$\text{RISK} = \underbrace{\overbrace{\text{HOW OFTEN}}^{\text{RETURN PERIOD}}}_{\text{HAZARD}} \times \underbrace{\overbrace{\text{WHAT}}^{\text{EXPOSURE}} \times \overbrace{\text{HOW}}^{\text{COPING}}}_{\text{CONSEQUENCES}}$$

Exposure refers to the amount and value of physical and societal goods at risk; the coping factor instead relates to the capability of dealing with the effects of the event. A very rich and populated area, for example, might have very high exposure to flood damages (large population displaced and physical damage) but also very high capacity to manage floods (thanks, for example, to well-devised evacuation plans and physical protection infrastructure). Conversely, a poor region, in which damages are going to be lower, might also have poorly implemented contingency plans and infrastructure, resulting in more severe consequences.
While policymakers tend to focus the efforts of risk mitigation mainly towards the reduction of exposure and improvements in the coping factor, in this thesis we are primarily concerned with flood hazard, usually measured by its Return Period RP:

$$\text{RP} = \frac{\Delta t + 1}{N_{events}}$$

Statistically, the Return Period of any event can be considered as the inverse of the probability that the event will occur in any year. As an example, a 100-year flood is a flood that has a probability of occurring of 1% in any given year.

1.2.2 Methods of flood hazard estimation

Flood hazard can be assessed via proxies, such as the recurrence of extreme discharge events, as well as by creating simulated flood maps. Different kinds of flood maps are usually produced with different methods by governments, regional agencies, or insurance and re-insurance companies. The resulting fragmentation often makes it hard to distinguish between solid, scientifically-based approaches and less reliable methods, especially since the level of uncertainty is rarely provided. Especially in the case of private companies, the methods and input data used for obtaining flood maps are often undisclosed, resulting in products that cannot be considered scientifically-based and reproducible (De Moel et al., 2009).

Historically, flood hazard was estimated via the analysis of historical discharge and flooding records and by surveying local people. The statistical analysis of

these observations can however be misleading, as extreme floods are exceptionally rare events and long observational periods, in excess of a few tens of years, have little chance of being available. This major limitation can be partially addressed by researching into documentary evidence of past floods (Kjeldsen et al., 2014; Reed, 2002), but these are often equally hard to come by and can be hard to properly interpret.

In the last decades, however, new approaches based on hydrological and hydraulic modelling emerged as viable (Alfieri et al., 2014; Barredo et al., 2007; Bell et al., 2007; Dankers and Feyen, 2009; De Moel et al., 2009; Demir and Kisi, 2016; Feyen et al., 2011; Merz et al., 2014; Paprotny et al., 2017; Rojas et al., 2012; Serinaldi and Kilsby, 2017; Van Alphen et al., 2009; Veijalainen et al., 2010). In this model chain approach, a hydrological simulation, driven by precipitation data, generates discharge data for a given region or basin for a long period of time; this discharge is then fed to a second hydrodynamic model which reproduces hypothetical flood extents and, if necessary, other variables such as flood depth or flow speed. In order to extend the analysis to long Return Periods, extreme value analysis can be applied to the simulated discharge, assuming a given distribution for extreme events and performing a fit over the available data. This model chain approach has the advantage of being very flexible, potentially requiring precipitation data instead of discharge data, which are generally less readily available. Additionally, this technique can work on virtually any domain including ungauged ones, if precipitation data from large scale datasets is used as input. This opens the door for multi-regional and cross-catchment analysis.

Of course, there are downsides to this approach too: a large amount of observational data, for calibration and evaluation, is still advisable (the larger, the better); moreover, having a model working off another model's output, in what constitutes an offline model chain, can make the estimation of the uncertainty of the final output more difficult.
As stated, uncertainties arise from the driving data, from the model configurations and choice, and from insufficiently precise description of the physical phenomena object of investigation. In the case of flood hazard estimation, one more important source of uncertainty is the generally followed assumption that flood defences and river levees and banks will not fail; additionally, for heavily managed rivers, water management can reduce flood hazard by diverting additional water to reservoirs (Alfieri et al., 2016; Huntjens et al., 2010, see e.g.), other rivers, or agricultural areas. As is the case for most similar studies (Alfieri et al., 2014, see e.g.), water management was not taken into consideration in this work.

1.2.3 Different kinds of flood maps

As highlighted in the previous section, the generic term 'flood maps' can refer to several different products, from historical "flooded point" references, to extreme

discharge estimations, to economic risk maps. De Moel et al. (2009) gives an overview of 6 different types (see figure 1.1):

A) Flooded points in historical records

B) Flooded area probability, each year, for different Return Periods (10, 100 and 500 years)

C) Flooded area water depth for a given Return Period

D) Qualitative flood danger, usually calculated as a combination of Return Period, depth, flow speed or other factors

E) Qualitative flood risk, including information on population density and other societal variables

F) Quantitative flood risk, showing information on direct economic damage

In this thesis work the focus is on producing Return Period and flood depth maps, which are the variables usually necessary for modelling flood impact and thus required by policymakers, modellers and insurance companies. Extreme discharge and precipitation are also analysed as proxies for floods.

1.3 Past, present and future of extreme climatological and hydrological events

In the last century little to no change in average river runoff occurred for unmanaged rivers (Dai, 2016; Dai et al., 2009), and despite few studies indicating an increase in observed extreme streamflows and river flooding (Mallakpour and Villarini, 2015; Stevens et al., 2016), these results can vary wildly from region to region (see e.g. Do et al., 2017). Due to uncertainties in both the driving and the hydrological models (Donnelly et al., 2017; Gosling et al., 2017), there is no general agreement on the observed changes (Hall et al., 2014; Kundzewicz, 2012; Kundzewicz et al., 2010; Robson, 2002). In Europe, recent changes in flood timings in winter and spring have been highlighted by Blöschl et al. (2017), although the spatial variability of the signal is high, with 'earlier spring snowmelt floods in northeastern Europe, later winter floods around the North Sea and parts of the Mediterranean coast owing to delayed winter storms, and earlier winter floods in western Europe caused by earlier soil moisture maxima'.
Summing up the observed trends in flood hazard, the IPCC Fifth Assessment Report (Jiménez Cisneros et al., 2014, section 3.2.7) states: 'There is *low confidence*, due to *limited evidence*, that anthropogenic climate change has affected the frequency and magnitude of floods at global scale (Kundzewicz et al., 2013). The strength of the evidence is limited mainly by lack of long-term records from unmanaged catchments.'.

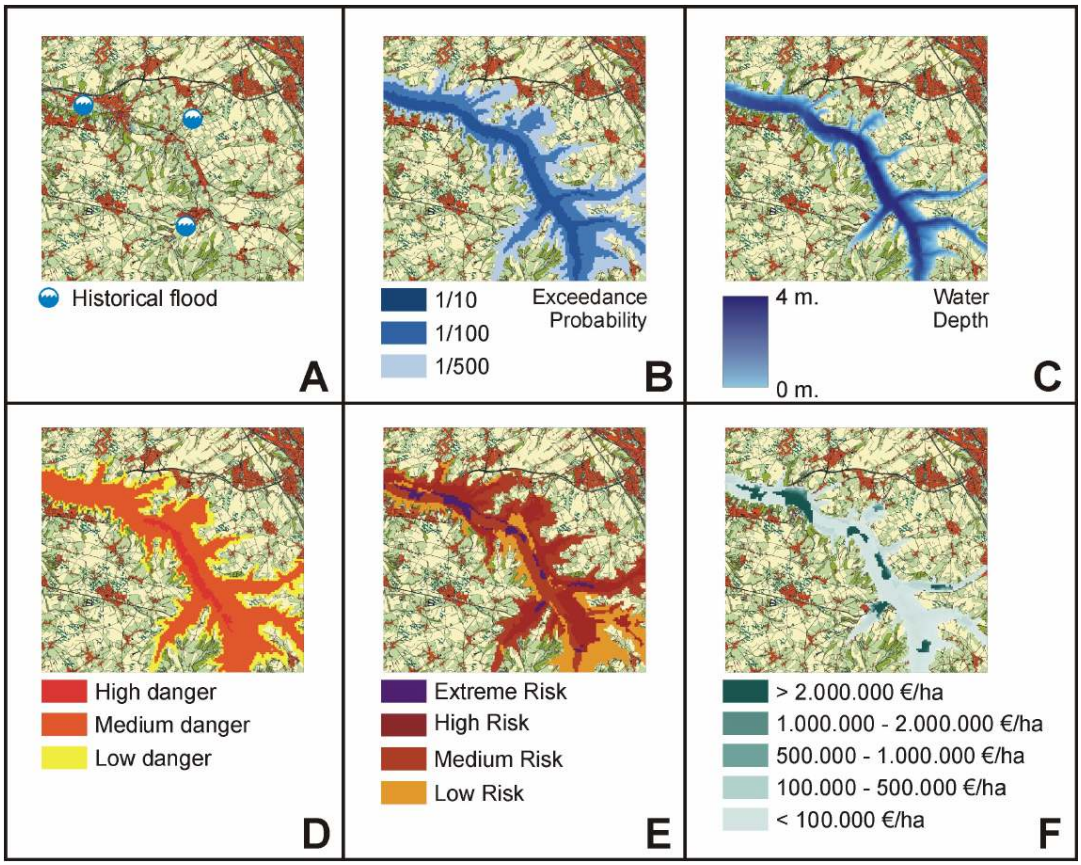

FIGURE 1.1: A depiction of 6 different flood map types, from De Moel et al. (2009), Figure 2. Refer to section 1.2.3 for description of the panels.

The Earth is currently undergoing a relatively rapid warming period which is, according to climate scientists, primarily linked to anthropogenic activity (Anderegg et al., 2010; IPCC WG1, 2013). Climate change affects all aspects of the atmospheric system, including the events which are usually associated with floods, such as extremely strong or prolonged periods of rain. Increases in heavy precipitations are more correlated with the total amount of moisture in the air (growing by approximately 7% $^{\circ}C^{-1}$ according to the Clausius-Clapeyron equation) than with changes in mean precipitation (Allen and Ingram, 2002), so that increases in extreme rainfall might happen even in regions with decreasing total precipitation.
In the Fifth Assessment Report (IPCC WG1, 2013, section 12.4.5.5), the IPCC Working Group 1 stated regarding extreme precipitation events:

> Return Periods are projected to be reduced by about 10 to 20% $^{\circ}C^{-1}$ over the most of the mid-latitude land masses with larger reductions over wet tropical regions (Kharin et al., 2013). Hence, extreme precipitation events will very likely be more intense and more frequent in these regions in a warmer climate. Reductions in return values (or equivalently, increases in Return Period) are confined to convergent oceanic regions where circulation changes have reduced the available water vapour.

This projected increase in extreme precipitation events all over the globe (see figure 1.2 for a map of changes) and in Europe in particular is supported by numerous studies (e.g. Christensen and Christensen, 2004; Durman et al., 2001; Fowler and Kilsby, 2003; Frei et al., 2006; Gobiet et al., 2014; Goubanova and Li, 2007; Klein Tank and Können, 2003; Pal et al., 2004; Púčik et al., 2017; Rajczak et al., 2013; Roudier et al., 2016; Tramblay and Somot, 2018) showing high likelihood of increasing frequency and/or intensity of such events before the end of the century, even in regions where the total precipitation is supposed to decrease. As a consequence of the projected increment in extreme precipitation events, however, floods and flood-related damages are destined to rise in most areas of the world, despite improving flood protection infrastructures. The increase in risk is primarily due to higher exposure in flood-prone areas, which are on average very attractive for socioeconomic human activities (Alfieri et al., 2016; Barredo, 2009; Hirabayashi and Kanae, 2009; Kron, 2005; Mitchell, 2003; Munich RE, 2015 and IPCC, 2014, section 3.4.8).
Jongman et al. (2012) calculated that the total exposure to flood disasters, which is reported at $27 to 46 T globally in 2010, is going to more than triple (to $80 to 158 T) in 2050. In Europe, according to some studies (Alfieri et al., 2015b; Forzieri et al., 2017; Rojas et al., 2013 and Valentini et al., 2014, section 23.3.1.2), the current annual population affected is expected to significantly increase by the 2080s, with annual damages growing up to 20-fold, if no change occurs in the current climate mitigation politics. Forzieri et al. (2017) specifically estimates casualties related to river flood events to increase by 54% (106 more lives claimed per year) under the A1B emission scenario (IPCC, 2000). Multiple sectors are going to be affected, with worsening

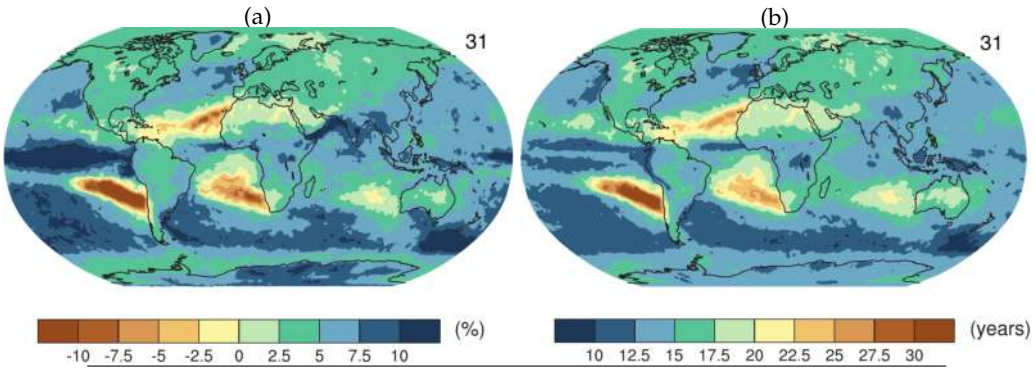

FIGURE 1.2: Annual maximum daily precipitation changes in an ensemble median of all CMIP5 models, according to IPCC WG1 (2013, section 12.4.5.5, figure 12.27).
In panel a, percent change in 20-year return values per 1 °C of local warming, 2081–2100 relative to the 1986–2005 reference period.
In panel b, the average 2081–2100 Return Period (in years) corresponding to the typical 1986–2005 20-year return values; regions of no change would have Return Periods of 20 years.

conditions in particular for electricity transport, road infrastructure and water and waste management (Forzieri et al., 2018).

As stated, the strongest driver for increasing flood risk is high exposure primarily due to growing population density. The other main factor, flood hazard, is also generally projected to increase according to the majority of studies, with the recently published IPCC Special Report "Global Warming of 1.5 °C" stating (IPCC, 2018, section 3.3.5): 'A global warming of 1.5°C would also lead to an expansion of the global land area with significant increases in runoff *(medium confidence*) as well as to an increase in flood hazard in some regions (*medium confidence*) compared to present day conditions.'

The projections are, however, very dependant on the region (or even basin) of interest, as local flood-related climatic characteristic can differ greatly from one location to another. Global studies (Alfieri et al., 2017; Arnell and Gosling, 2016; Dankers et al., 2014; Hirabayashi et al., 2008, 2013; Milly et al., 2002), for example, generally agree in finding increasing likelihood of flood events in the future for Southern Asia, Western Russia, Canada and the Northern Andes, but some highlight decreasing likelihood for most of Europe and the Amazon Basin (see e.g. Arnell and Gosling (2016), Dankers et al. (2014) and Hirabayashi et al. (2013) and figure 1.3). The resolution of such large scale studies, however, is usually not fine enough to resolve the details of some river catchments (Gosling et al., 2011; Whitfield, 2012) especially for European basins, which are typically small in size.
Smaller scale studies over the European continent (e.g. Alfieri et al., 2015a; Alfieri et al., 2018; Dankers and Feyen, 2009; Feyen et al., 2011; Prudhomme et al., 2003) generally find increasing flood hazard in most basins, especially in terms of higher frequency more than of higher magnitude (Alfieri et al., 2015a; Lehner et al., 2006), but large regional variations can be found due to different climatic characteristics.

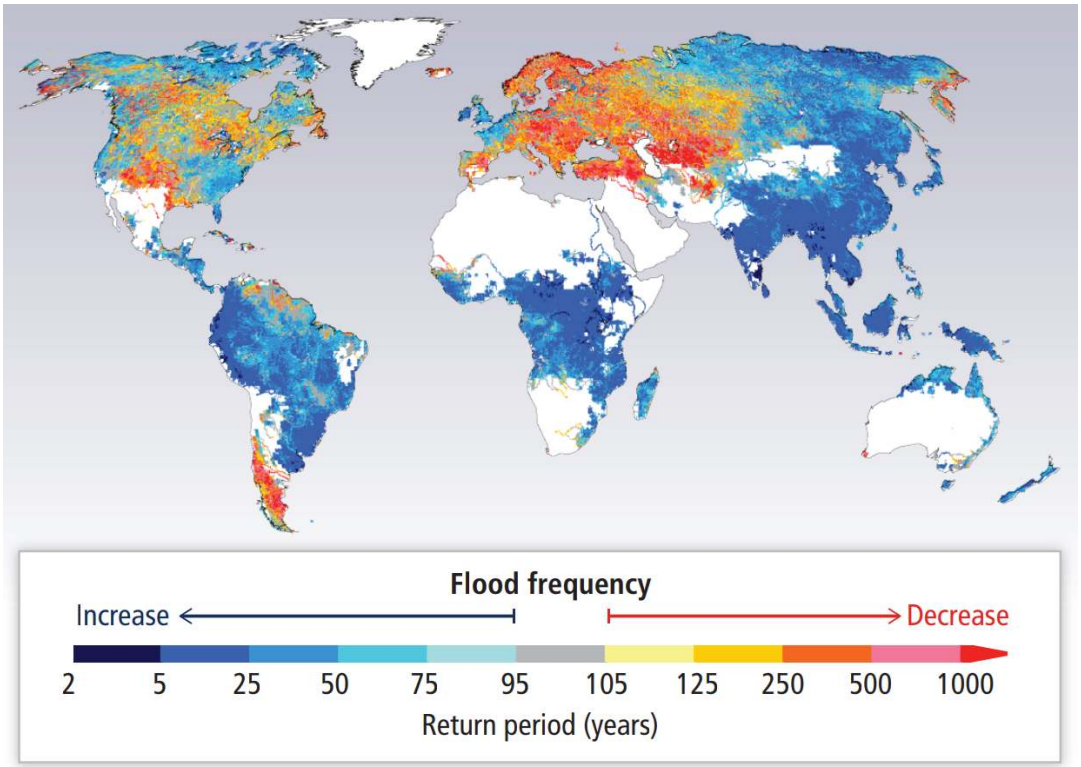

FIGURE 1.3: Future world flood hazard map: 1971–2000 to 2071–2100 change as estimated by Hirabayashi et al. (2013), using 11 Coupled Model Intercomparison Project Phase 5 (CMIP5) models under the RCP8.5 ("business-as-usual") scenario. Figure taken from IPCC (2014, section 3.4.8).

As can be expected, the changes generally show strong seasonality, with increased discharges and frequency of flood events mostly concentrating in autumn and winter, and shifts in the flood regimes usually towards earlier and stronger winter floods (e.g. Arheimer and Lindström, 2015; Coppola et al., 2014; Middelkoop et al., 2001).

1.4 Flood hazard in the study domain

This thesis focuses its attention specifically on flood hazard in Italy. The region is frequently affected by severe inundation events, with 584 reported casualties, 50 missing, 462 injured and 168254 evacuees in the last 50 years due to flooding only (excluding flood-induced landslides, see Istituto di Ricerca per la Protezione Idrologica and Consiglio Nazionale delle Ricerche, 2018). Observed heavy precipitation trends in the last century indicate a general decrease of total precipitation, but an increase in extreme events (Brunetti, 2004; Brunetti et al., 2001, 2004). Recent flood events with several casualties, caused primarily by the inundation include floods in Polesine (1951, 84 casualties), Salerno (1954, 318), Tuscany (1966, 34), Piedmont (1994, 70), Campania (1998, 159), Piedmont (2000, 34), Liguria (2011, 13), Sardinia (2014, 18) and Tuscany (2017, 9).

Figure 1.4, obtained from the Polaris 2017 Periodic Report on Landslide and Flood Risk for the Italian Population (Istituto di Ricerca per la Protezione Idrologica and Consiglio Nazionale delle Ricerche, 2018), shows the human costs (in terms of casualties and evacuees) in the period 1967–2016. The most affected regions is the North-West, but catastrophic flood events occur all over Italy, having severely affected 920 out of 7982 municipalities in the last 50 years.

Despite the significant impact on the area, scientific studies concerning flood hazard estimation over the complete Italian domain are few: most works focus specifically on examining limited areas or basins (Di Salvo et al., 2017; Marchesini et al., 2016; Morelli et al., 2014; Sole et al., 2008), specific past events (Amadio et al., 2013; Marchi et al., 2010; Masoero et al., 2013; Norbiato et al., 2007; Santo et al., 2012), or target flood risk rather than hazard (Albano et al., 2017; Dottori et al., 2016; Salvati et al., 2010).

Some Italian regional protection agencies and basin authorities provide open-access flood hazard maps for their specific basin of interest. The Po River Basin Authority (AdbPo), for example, provides flood hazard maps for the whole Po basin (figure 1.5). These maps, however, have a few limitations for scientific work: they are rarely provided with accompanying vector data, the methodology is generally undisclosed, and maps from neighbouring agencies often do not agree with each other. Additionally, maps are often provided in numerous, separated image files with small extents, such as the maps provided by the Tevere River Basin Authority (ABTevere), which are comprised of 100 extremely small areas (figure 1.6). This fragmentation, while useful for small-scale studies, makes large-scale analysis much more difficult.

A national, complete, and scientifically-based homogenised flood hazard map over Italy does not exist. The only nation-wide flood hazard product available is the report *Dissesto idrogeologico in Italia: pericolosità e indicatori di rischio* (Trigila et al., 2018) from ISPRA, the Italian Superior Institute for the Ambient Protection and Research, in which the data from the single local agencies (often computed using undisclosed techniques) is merged and provided as vector data. Fluvial floods and storm surges are both considered, but no distinction is made in the output product.
Figures 1.7a to 1.7c show the ISPRA maps for high, medium and low hazard. The most affected areas are the Romagna, Valle D'Aosta, Piedmont, Lombardy and Tuscany regions, while the hazard is significantly lower towards the South and North-East of Italy. It is hard to discern whether regional differences (such as the increased risk in Valle D'Aosta compared to the neighbouring Piedmont or the relatively low hazard in the North-Eastern regions) come from real physical and meteorological diversities or from discrepancies in methodology and underlying data. Figure 1.7d shows the population count under a medium hazard category, grouped by municipality. Neighbourhoods of major cities, such as Turin, Milan, Venice and Rome, concentrate a large number of people in areas at risk of flooding, highlighting the importance, in these areas, of suitable emergency procedures and plans based on reliable data.

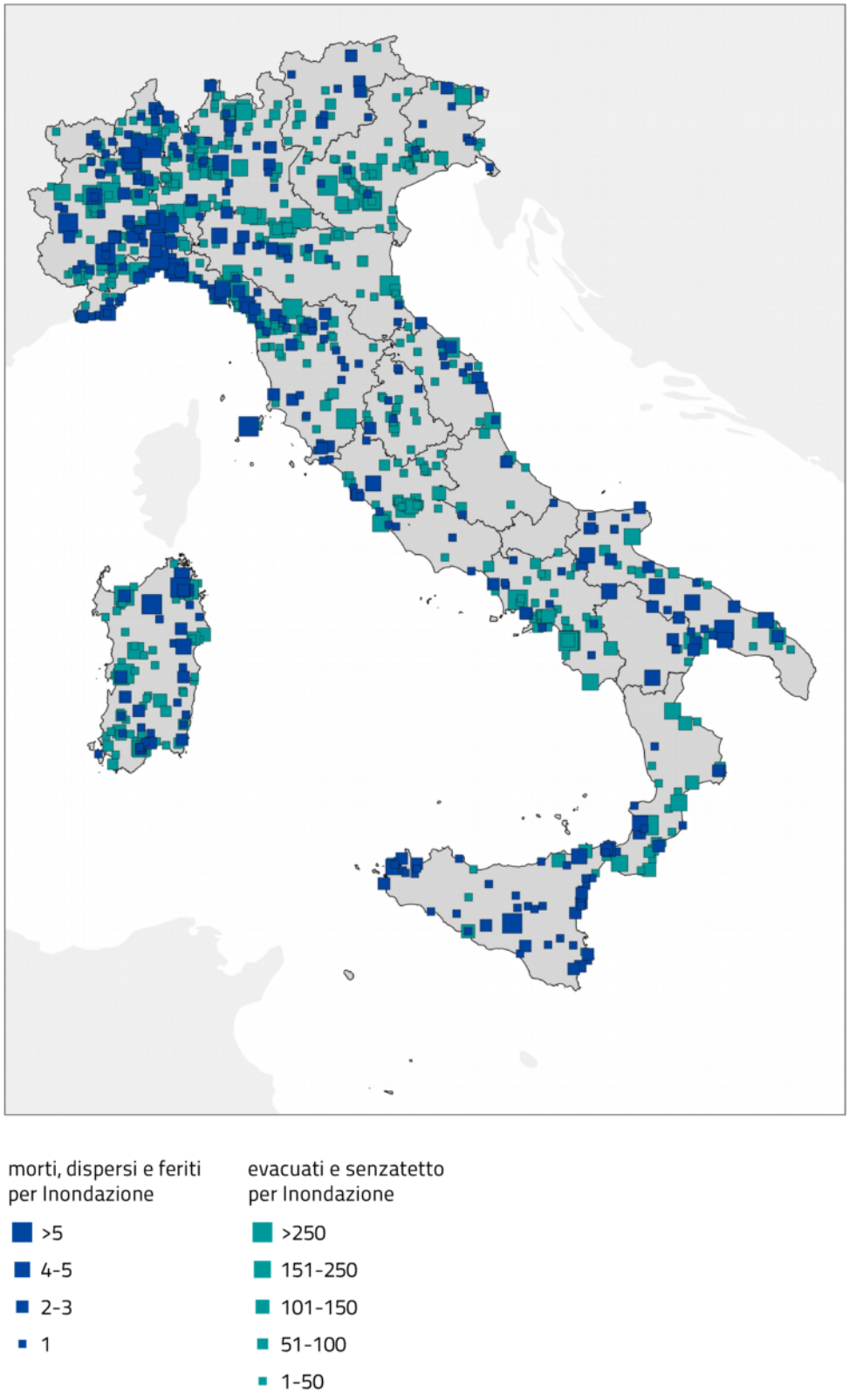

FIGURE 1.4: Map of human costs for all flood events in Italy between 1967 and 2016. In dark blue are deaths, missing and injured; in light blue evacuees and homeless due to flooding events. Figure taken from Istituto di Ricerca per la Protezione Idrologica and Consiglio Nazionale delle Ricerche (2018, page 14).

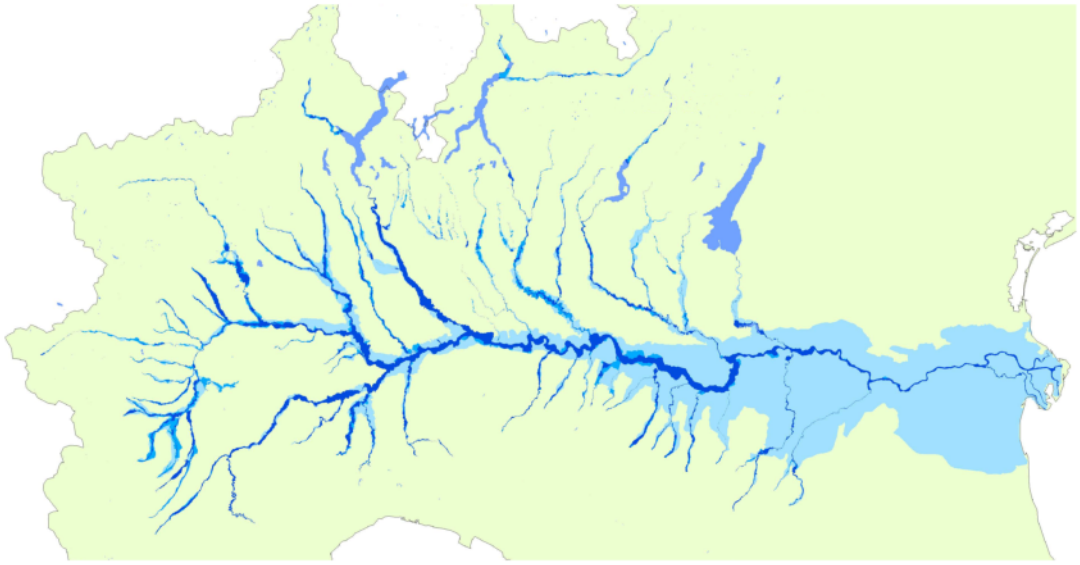

FIGURE 1.5: Flood hazard for the Po River Basin, as estimated by the Po River Basin Authority (AdbPo) (http://www.adbpo.gov.it/). Dark blue represents high flood hazard, with Return Period 10–20 years; medium blue 100–200 years; light blue 500 years. Open waters are in muted blue.

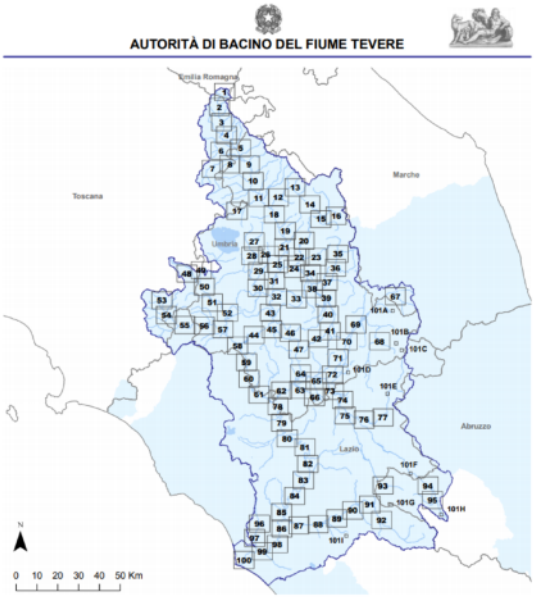

FIGURE 1.6: Union view of all 100 flood map extents provided by the Tevere River Basin Authority. From http://www.abtevere.it.

[%]	Hazard	N-W	N-E	Centre	South	Islands	Whole Italy
Population	High	2.9	7.1	3.6	2.2	1.2	3.5
	Medium	5.9	29.1	10.9	3.9	1.8	10.4
	Low	15.1	28.2	23.5	5.1	4.3	15.7
Families	High	3.0	7.1	3.5	2.2	1.2	3.6
	Medium	6.1	29.6	10.9	3.8	1.9	10.8
	Low	15.3	28.7	23.7	5.0	4.4	16.3
Buildings	High	2.9	6.6	3.8	2.4	1.3	3.4
	Medium	5.9	25.8	10.7	3.4	2.0	9.3
	Low	16.0	25.7	22.1	4.6	4.2	14.1
Companies	High	3.8	7.3	4.0	2.2	1.6	4.1
	Medium	7.1	29.9	13.2	4.4	2.4	12.4
	Low	16.3	27.7	28.5	5.8	5.2	18.4
Cultural heritage	High	9.8	11.9	3.2	2.5	2.4	6.8
	Medium	14.2	33.7	8.4	3.3	3.0	15.3
	Low	23.7	34.4	14.0	4.0	4.8	19.4

TABLE 1.1: Estimated percentage of population, families, buildings, companies and cultural heritage at three flood hazard levels, divided by Italian macroregion. High hazard corresponds to an estimated Return Period of 20–50 years; medium to 100–200 years; low to "extremely rare events". Macroregions are defined as follows:
N-W: Piedmont, Valle D'Aosta, Lombardy and Liguria; N-E: Trentino–Alto Adige, Veneto, Friuli–Venezia Giulia, Emilia–Romagna; Centre: Tuscany, Umbria, Marche, Lazio; South: Abruzzo, Molise, Campania, Puglia, Basilicata, Campania; Islands: Sicily, Sardinia.
Data from Trigila et al. (2018).

ISPRA estimates (table 1.1) 10.4% of the population, 12.4% of the companies, 15.3% of the cultural heritage and 8.4% of the surface area of Italy to be currently at medium risk of inundation (Return Period of 100 to 200 years), with higher values in the North and significantly lower hazard in the South and Isles.

Although no official national study on the topic is available, in the future flood hazard is generally projected to increase in the region by several European-wide studies, in contrast with the results of some global studies (see figure 1.3), albeit strong differences exist among the available studies. Most works focus on estimating the change in flood hazard by focusing on the intensity or recurrence time of extreme discharges, most often Q_{100}, the typical 100 year Return Period discharge.
Rojas et al. (2012) uses an ensemble of 12 bias-corrected simulations from the ENSEMBLES project to drive a single calibrated hydrological model (LISFLOOD) over all of Europe. Due to the large spatial extent, the study resolution is relatively low (5 km), thus reproducing only major rivers, which are not necessarily those contributing

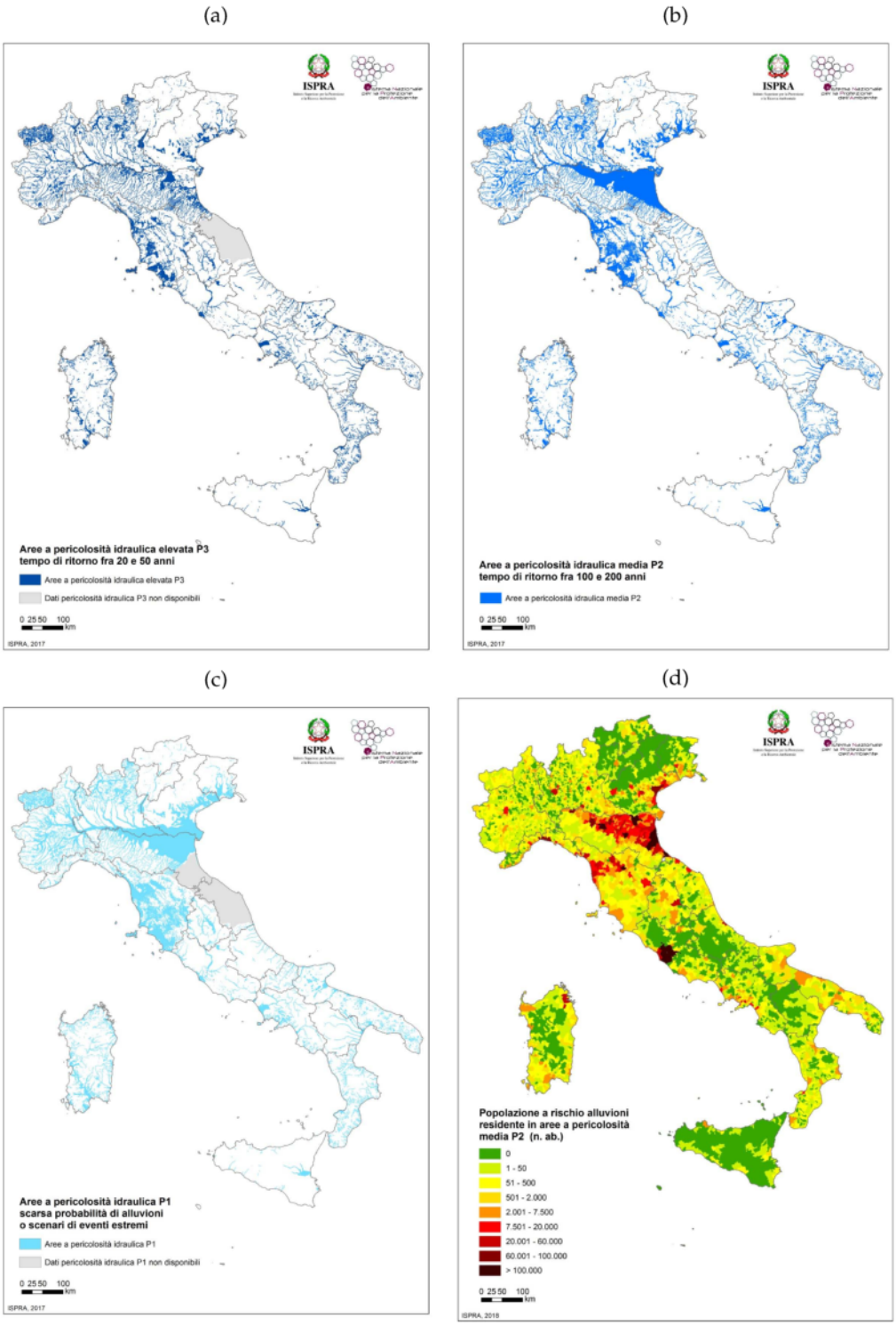

FIGURE 1.7: Flood hazard in Italy, according to Trigila et al. (2018, figures 2.1 to 2.3 and 4.25). In panel a, areas with low flood Return Period (high hazard, 20–50 years); in panel b, medium Return Period (100–200 years); in panel c, high Return Period ("extremely rare events"). In panel d, the number of people exposed to a medium hazard, by municipality. Areas where data is missing are colored in grey.

the most to flood hazard. The results (figure 1.8) generally indicate an increase in 100 year Return Period peak discharges (and thus flood intensity) under a climate change scenario (SRES A1B), when comparing the future (2071–2100) to the control period (1961–1990). The change is, however, strongly dependent on the model and the region of interest. In Italy, the rivers showing the greatest increase (and agreement between the 12 simulations) are those located in the North and fed by the Alpine range; changes in the Centre and South (both positive and negative) show lower agreement between models.
In a similar study, Thober et al. (2018) employs a multi-model ensemble of three hydrological models forced by five Global Climate Models under three different warming levels (1.5, 2 and 3 °C). The climate change results are generally in agreement with (Rojas et al., 2012) (despite some differences, especially in Scandinavia and the Baltic Republics), finding reduced flood hazard for Eastern Europe and Mediterranean regions, but increased hazard for North Italy (figure 1.9).
Dankers and Feyen (2009) and Feyen et al. (2011) show more conflicting results for Italy, with only the Po river seemingly subject to increased extreme peak discharges. In some studies (Alfieri et al., 2015a; Alfieri et al., 2015b; Donnelly et al., 2017; Roudier et al., 2016), on the other hand, a more uniform increase in high runoff events all over Western and Southern Europe and the Mediterranean is found (see e.g. figures 1.11 and 1.10). In these studies, the whole Italian territory shows a marked increase in flood-related variables, although the change in the Northern basins remains more evident.

The spatial (usually 5 km) and temporal (daily) resolution of the cited works is generally too low to capture the details of smaller river basins: the maps reported in these studies in fact only show major rivers in Italy. In this thesis work, which focuses only on the Italian domain, higher resolutions are possible while keeping the computational costs reasonable.

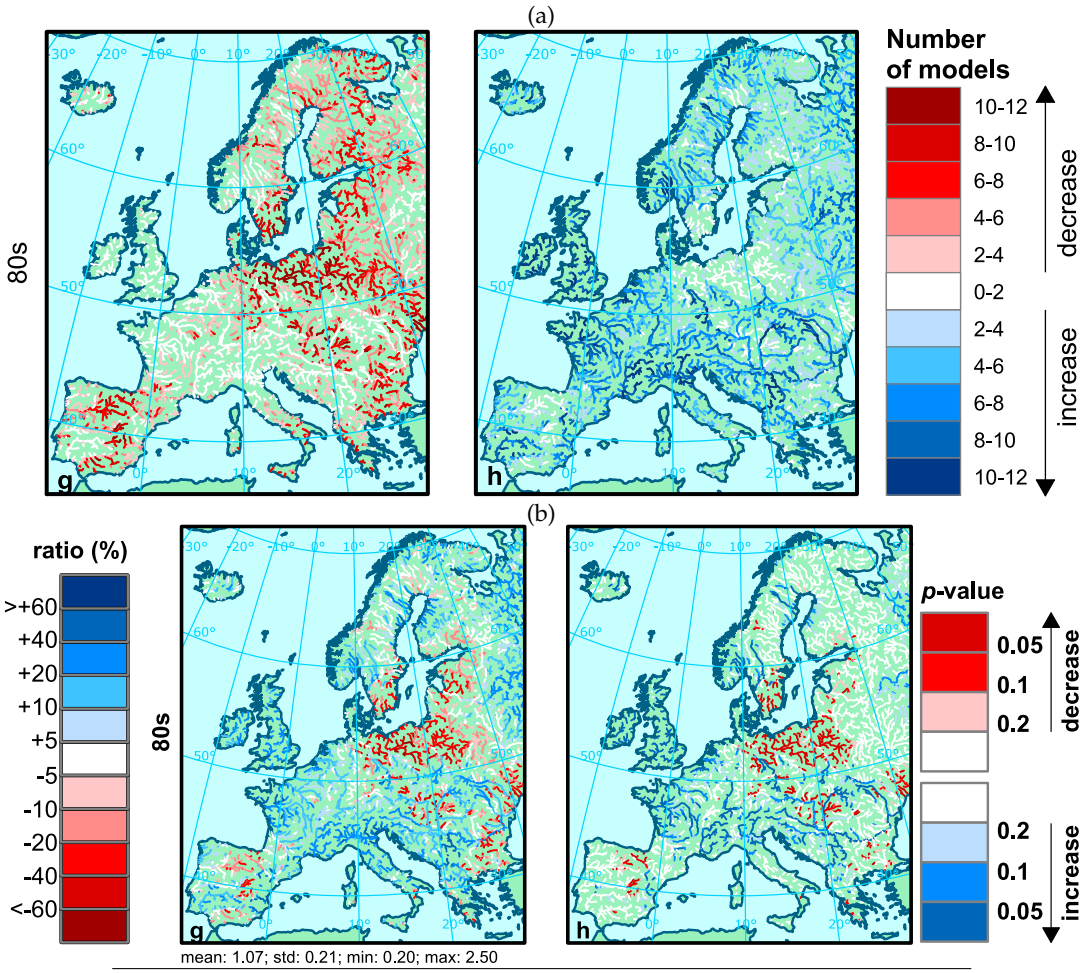

FIGURE 1.8: Change in extreme discharge (Q_{100}: peak annual discharge with 100 year Return Period), extracted from Rojas et al. (2012, figures 5 and 6). In the upper panels, the number of models agreeing in a decrease (left) or increase (right) in Q_{100} discharges by the end of the century, compared to the control period. In the lower panels, ensemble average of the change (left) and p-value of the signal (right).

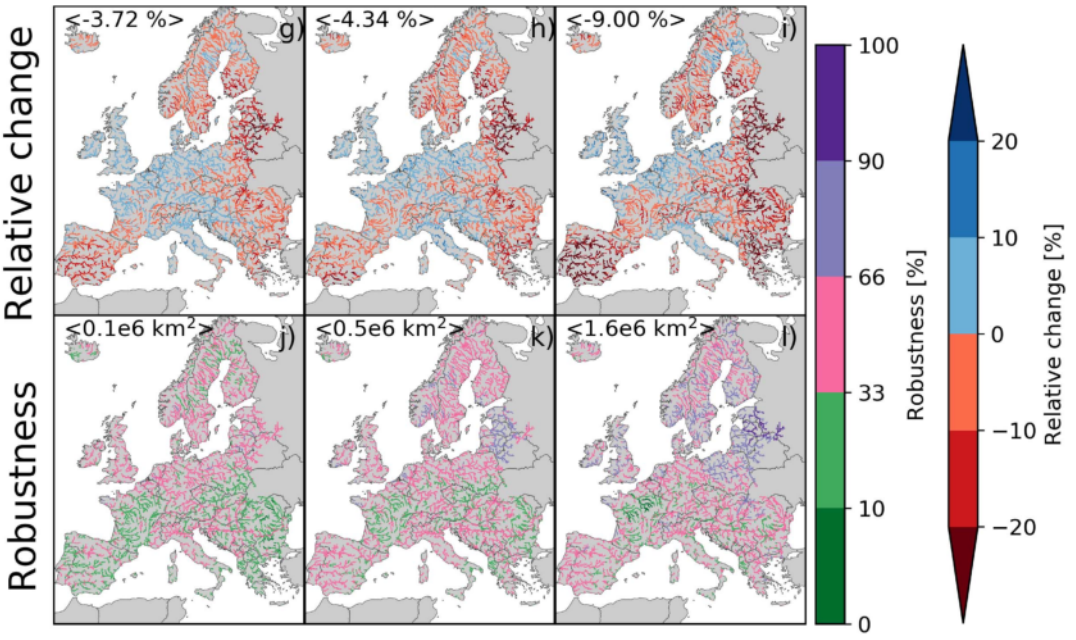

FIGURE 1.9: Change in high runoff (mean annual maximum runoff), extracted from Thober et al. (2018, figure 1). The three columns represent the three warming targets considered: +1.5 °C, +2 °C and +3 °C. In the top panel, the relative change compared to the reference period (1971–2000) and, in brackets, the spatial average. In the bottom panel, the percentage of ensemble members indicating robust changes and, in brackets, the area exhibiting changes with likelyhood greater than 66%.

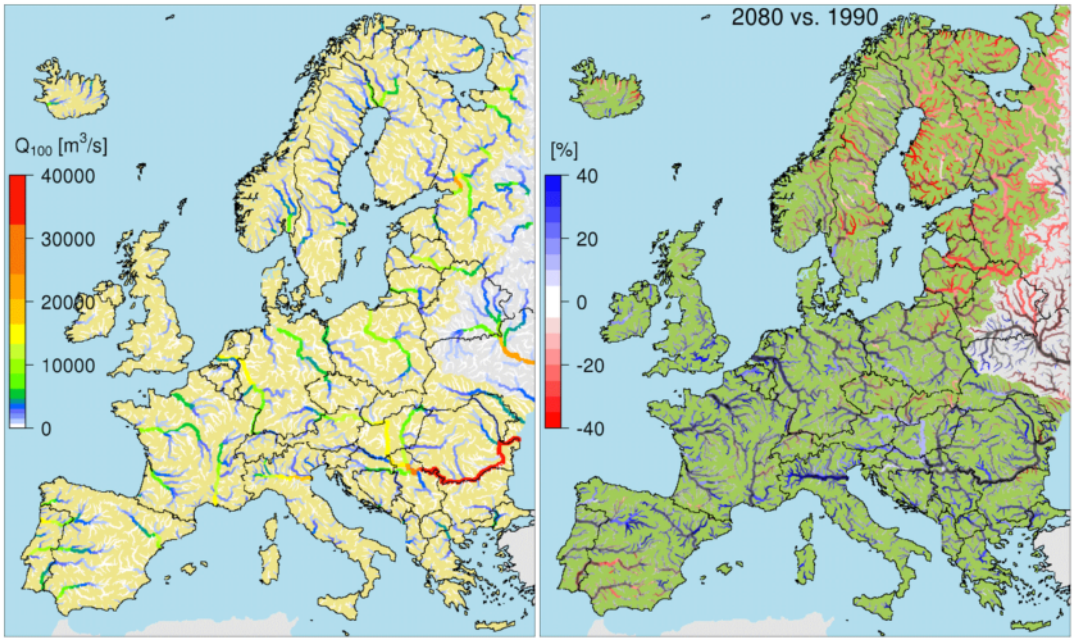

FIGURE 1.10: Extreme discharge (Q_{100}: peak annual discharge with 100 year Return Period), extracted from Alfieri et al. (2015a, figure 6). In the left panel, ensemble mean of the reference period (1976–2005); in the right panel, percentage change for the time slice 2066–2095.

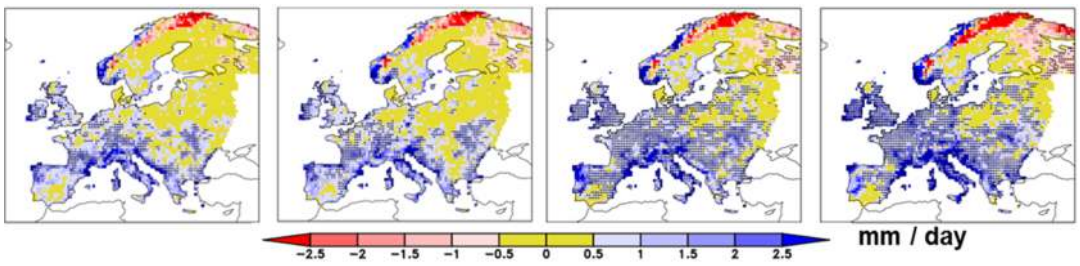

FIGURE 1.11: Change in high runoff (mean annual maximum runoff), extracted from Donnelly et al. (2017, figure 4). The four columns represent the four warming scenarios considered: +1.5 °C with RCP 2.6 and 4.5, +2 °C with RCP 2.6 and 4.5, +2 °C with RCP 4.5 and 8.5, +3 °C with RCP 4.5 and 8.5.

Chapter 2

Observational data

The main observational data used within this thesis are of four different kinds: precipitation, discharge, flood extent and terrain elevation. Due to the different peculiarities of each variable, they are treated separately in the following sections. Section 2.1 will give an overview of precipitation datasets available over the study domain, including a brief analysis of precipitation uncertainty employing eight different datasets (section 2.1.4). Sections 2.2 and 2.3 will describe the available discharge and flood observations, while in section 2.4 the choice of Digital Elevation Model for the subsequent hydrological and hydraulic simulations will be discussed.

2.1 Precipitation observations

Precipitation is probably the most difficult of all atmospheric climate variables to measure reliably, due to the huge spatio-temporal variability (especially in summer) and to the physical difficulty of setting up and maintaining a dense network of high-maintenance sensors. In our multi-model approach (see section 4.3), however, it is vital that the precipitation input data is of sufficient quality and resolution to provide information even about very local, fast thunderstorms, which can trigger flooding in smaller catchments. Moreover, it is important to analyse the longest time series possible, so that rare events, which by definition have a long Return Period, can be properly represented.

In this project, precipitation observations are utilised for calibration, for validation and for driving the hydrological model CHyM (see section 4.2).

2.1.1 Types of precipitation measurements

Precipitation measurements come from essentially three distinct sources:

In-situ Station observations are widely regarded to be the most reliable source of information for precipitation observations (Hughes, 2006). Several types of rain gauges exist, with the most common type of instrument being the *tipping bucket rain gauge* (figure 2.1). It consists of a small bucket of fixed size which fills up with precipitation and mechanically tips and empties, triggering a counting

switch, every (usually) 0.1 mm of rain. The buckets are usually heated, so that solid precipitation (snow, ice) is melted and correctly registered. Having moving parts means that most in-situ precipitation stations require constant and attentive maintenance, as ill-maintained sensors can easily get stuck (see figure 3.5a for an example). In general, in-situ precipitation measurements suffer greatly from the problem of gauge undercatch (see section 2.1.2), in which, due to strong winds, a smaller amount of precipitation than expected enters the measuring funnel. In-situ data usually offer the longest time-series of all precipitation measurements techniques, with some datasets reconstructing rainfall back to the 19th century: the HISTALP project (Auer et al., 2007), for example, provides rainfall on the Alpine range using data as old as the 1800; (Brunetti et al., 2006) goes as far as 1750 with monthly precipitation data over Italy. Uncertainties in in-situ data are mostly related with low station density and choice of gridding technique, so that different datasets can have significantly different climatology, especially in areas of low data availability (Prein and Gobiet, 2017). Additional details on station-based precipitation datasets, such as E-OBS and EURO4M-APGD, can be found in section 2.1.3.

Ground radar Available since the mid '80s, ground radar observations are obtained from data on the reflectivity of the atmosphere. Rain and water vapour reflect radar waves, and the analysis of this effect allows for estimation of precipitation and wind speed; however, the displayed data can differ from the rainfall actually measured at the surface by in-situ gauges, especially in areas of complex topography, where the radio waves can easily be shielded or reflected by mountain ranges (Germann et al., 2006; Wüest et al., 2010). On the other hand, the time and space resolution of radar-based datasets cannot be matched by in-situ data. Overall, radar observations are primarily used for weather prediction and analysis and for studying specific events (e.g. Bertato et al., 2003), but are sometimes also used as a tool for filling or extending other kinds of measurements.

Satellite Space-borne precipitation measurements (see Kidd and Levizzani, 2011, for an overview) have been available since the mid '70s and have been on the rise in both availability and reliability ever since. Much like radars, they scan the atmosphere with several frequencies (microwave and radio), and interpret the reflected waves according to specific algorithms. Their main advantage is the relatively high resolution and very large coverage, being available even in regions where no station or radar is in place. However, the physical limitations, different measurement techniques and algorithms used to retrieve precipitation from interferometry data introduce large uncertainties (Bartsotas et al., 2018; Bytheway and Kummerow, 2013; Maggioni et al., 2016; Sarachi et al., 2015; Tian and Peters-Lidard, 2010). Large advancements have occurred in satellite-based precipitation measurements since the early days of remote sensing from space,

FIGURE 2.1: A tipping bucket rain gauge, the most common type of precipitation measuring instrument, with the buckets exposed.

and there is no doubt that this data source is essential for global datasets; it is however generally found and agreed upon (Bowman, 2005; Gao and Liu, 2013; Prein and Gobiet, 2017; Rossi et al., 2017) that in regions where in-situ data is available (such as most of Europe) station-based datasets still provide more reliable data. Examples of global satellite-based precipitation datasets are PERSIANN, CMORPH, TRMM, GPCP and GPM (see table 2.1 for citations).

2.1.2 Gauge undercatch

The main source of uncertainty for in-situ precipitation observations is the phenomenon of *gauge undercatch*. This term indicates the underestimation of precipitation due to local turbulent effects around the gauge caused by the wind interacting with the sides of the instrument, as seen in figure 2.2. Gauge undercatch is hard to quantify, but it can severely impact the measurements of precipitation, especially for solid precipitation in windy days. According to some studies, underestimation of total precipitation can be as high as 30 to 40 % for some winter stations (Adam and Lettenmaier, 2003; Isotta et al., 2014; Kochendorfer et al., 2017a), with peaks of 80% in some cases (Kochendorfer et al., 2017b; Wolff et al., 2015). Shielded gauges, in which the collector is partially shielded from the wind (see figure 2.3), reduce, but do not eliminate this problem (Duchon and Essenberg, 2001).
Correcting precipitation datasets for gauge undercatch is possible, but detailed information about local station exposure and sensor type are necessary to perform reasonable estimates (see e.g. Adler et al., 2018; Johansson, 2002; Mohr, 2009). In the Norwegian observational dataset created by Mohr (2009), for example, the correction

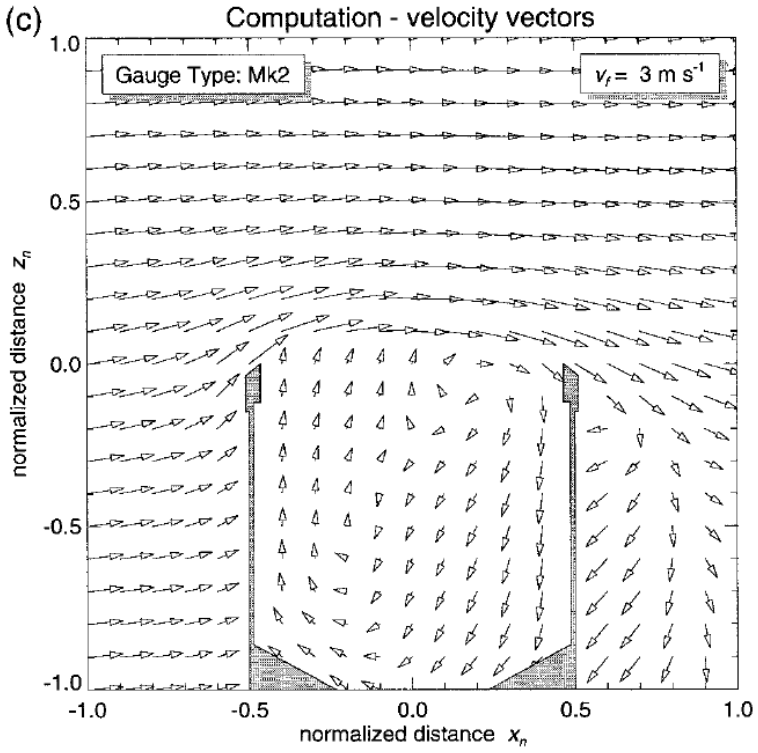

FIGURE 2.2: Wind velocity vectors around an unshielded gauge. Wind blowing precipitation away from the collector is the main cause of gauge undercatch. From Nešpor and Sevruk (1999).

method from Førland et al. (1996), is applied: each station is associated with an exposure index, and a correction factor ranging from 1.02 to 1.8 (depending on precipitation type and exposure) is applied. Observational datasets which are produced through data assimilation via a meteorological model (see e.g. Landelius et al., 2016; Vidal et al., 2010) often implicitly include correction factors.
Due to the complexity and variability of the datasets used through this thesis, and especially for the dataset described in chapter 3, no attempt at correcting for gauge undercatch was performed.

2.1.3 Precipitation datasets available over Italy

Table 2.1 lists some of the currently available gridded precipitation datasets covering the Italian territory. Two high-resolution, high-quality precipitation datasets for the Alps and Northern Italy (EURO4M-APGD and ARCIS) are available for a long observational period (38 and 55 years respectively); Central and Southern Italy, however, are only covered by European-wide and World-wide datasets, such as E-OBS, CHIRPS and the HMR reanalysis. In section 2.1.4, a few of these datasets will be compared.
Of those listed in table 2.1, only three high-resolution datasets provide sub-daily accumulations (PERSIANN-CDR, GPM and the UERRA reanalysis); of these, the PERSIANN-CDR reanalysis has been shown to perform poorly over Europe (Prein

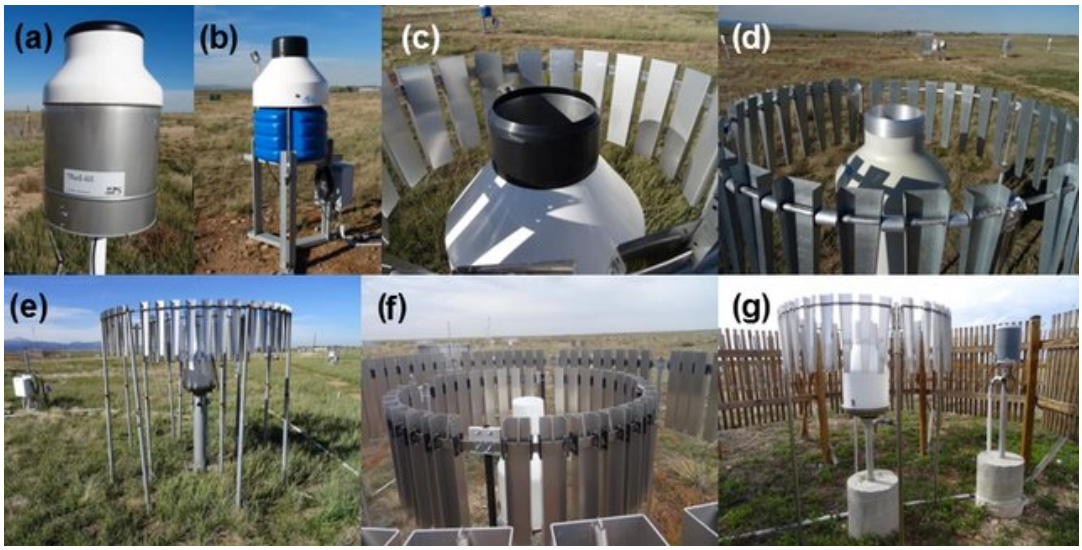

FIGURE 2.3: 7 different rain gauges. a) and b) are unshielded, the rest show an array of different shielding methods. From Kochendorfer et al. (2018).

and Gobiet, 2017), GPM is available only since 2014, and UERRA-HARMONIE is a relatively new reanalysis which has so far seen little use and validation. The precipitation dataset described in chapter 3 thus represents, to the author's knowledge, the first attempt at creating a sub-daily precipitation dataset deriving from in-situ observations specifically for the Italian territory.

2.1.4 Uncertainty in precipitation datasets

Due to low station density, gauge undercatch and homogenisation problems, precipitation datasets can show large differences between each other. In a study utilising seven regional high-resolution datasets, two gauge-based European-wide datasets, and seven global low-resolution datasets, Prein and Gobiet (2017) show large variability between different products, both in terms of mean and extreme precipitation; with correlations between different datasets sometimes lower than 0.5. Higher uncertainties are found, as can be expected, for extreme events and on the short-term temporal variability, while higher agreement is found on the shape of the annual cycle and on inter-annual and spatial variability.

As a brief assessment of precipitation uncertainty over Italy, in this section eight different daily precipitation datasets are compared under four different aspects: mean and extreme precipitation, precipitation distribution (probability density function) and annual cycle. The standard $R95_{ptot}$ and $R99_{ptot}$ indexes are used to assess extreme precipitation. They represent, for each grid point, the percentage of the total precipitation due to events higher than the 95th and 99th percentile of wet days

Name	Region	Period	Spatial res.	Time res.	Data source	Reference
E-OBS	Europe	1950–2017	0.25°	Daily	Station data	Haylock et al. (2008)
EURO4M-APGD	Alps	1971–2008	5 km	Daily	Station data	Isotta et al. (2014)
HMR	Europe	1979–2013	5.5 km	Daily	Reanalysis	Landelius et al. (2016)
ARCIS	North Italy	1961–2015	~ 5 km	Daily	Station data	Pavan et al. (2018)
ISAC/CNR	Italy	1961–1990	~ 1 km	Monthly	Station data	Crespi et al. (2017)
UERRA-HARMONIE	Europe	1960–now	11 km	Sub-daily	Reanalysis	Ridal et al. (2017)
CHIRPS	World	1981–now	0.05°	Daily	Station data + satellite	Funk et al. (2015)
CPC	World	1979–now	0.5°	Daily	Station data	Chen and Xie (2008)
CMORPH	World	1998–now	0.25°	Daily	Satellite	Joyce et al. (2004)
GPCC	World	1901–now	0.5°	Monthly	Station data	Schneider et al. (2014)
PERSIANN-CDR	World	1983–now	0.25°	Sub-daily	Satellite	Ashouri et al. (2015)
TRMM-TMPA	World	2000–now	0.5°	Daily	Satellite	Huffman et al. (2007)
UDEL	World	2001–2010	0.5°	Monthly	Station data	Willmott and Matsuura (2001)
GPM	World	2014–now	0.1°	Sub-daily	Satellite	Hou et al. (2014)
CRU	World	1901–2016	0.5°	Monthly	Station data	Harris et al. (2014)
GPCP	World	1996–2015	1°	Daily	Satellite	Adler et al. (2018)

TABLE 2.1: Non comprehensive list of some gridded precipitation datasets available over Italy. At Italian latitudes, 0.25° corresponds to about 20 km.

Dataset name	Period	Spatial res.	Data source
E-OBS	2000–2016	0.25°	Station data
EURO4M-APGD	2000–2008	5 km	Station data
HMR	2000–2013	5.5 km	Reanalysis
ARCIS	2000–2015	~ 5 km	Station data
CHIRPS	2000–2016	0.05°	Station data + satellite
CPC	2000–2016	0.5°	Station data
CMORPH	2000–2016	0.25°	Satellite
PERSIANN-CDR	2000–2016	0.25°	Satellite

TABLE 2.2: List of datasets used in the analysis of daily precipitation uncertainty carried over in section 2.1.4. At Italian latitudes, 0.25° corresponds to about 20 km. See table 2.1 for additional details and references.

respectively:

$$\mathrm{R95}_{ptot} = \frac{\sum_{PR>q95} PR}{\sum_{PR>1\,\mathrm{mm\,d^{-1}}} PR}\,, \tag{2.1}$$

where $q95$ is the 95th percentile of the daily precipitation PR for wet days.

Table 2.2 lists the eight datasets used for this analysis, with their respective time period, data source and resolution; further datasets and indices to be included in this study, such as drought metrics, are being considered for the final version of this analysis (Fantini and Coppola, 2019, in preparation). Of the available datasets, only ARCIS and EURO4M-APGD have a station density that can be considered dense compared to other high-resolution regional datasets over Europe (see Fantini et al., 2016; Prein and Gobiet, 2017). None of the station-based datasets considered in the analysis is gauge-corrected. The Italian territory is split into four distinct regions: North, Centre, South and Islands, which have distinct climatic characteristics. The analysis periods, for all datasets, start from 2000 and go up to the latest available data at the moment of this analysis. Since different remapping procedures can impact negatively on data quality (Diaconescu et al., 2015), in order to minimise uncertainties due to data manipulation all the datasets were analysed and plotted on their own original grid.

Figure 2.4 shows the seasonal average precipitation for the eight datasets; the extent of the four regions is highlighted in different colours in the maps. In Northern Italy, the two datasets with the highest station density, ARCIS and EURO4M-APGD, show similar patterns and precipitation intensities. Compared to these, the HMR reanalysis overestimates SON precipitation in the North-Eastern Alpine region, while consistently underestimating the precipitation in the Liguria region, which is an area of strong cyclogenesis and one of the most rainy in Italy. E-OBS, while spatially coherent with the high-resolution Northern datasets, cannot resolve the same fine scale details and generally underestimates average precipitation in the Northern region.

In Central and Southern Italy and in the Islands, no high-density station-based dataset

is available (but the one which will be presented and validated in chapter 3), so the E-OBS and HMR datasets represent the benchmark against which the other datasets must perform. Here, the CPC and CHIRPS datasets show similar patterns, with precipitation averages generally slightly above those of E-OBS, but in line with HMR. A precipitation high point is found in Calabria in winter in HMR, CPC and CHIRPS, but less in E-OBS. The CMORPH dataset shows particularly low precipitation in the colder months over the whole peninsula, underestimating precipitation in all seasons but JJA. PERSIANN-CDR, on the contrary, show extremely high precipitation averages across the whole period, similarly to the findings of Prein and Gobiet (2017). The annual cycle (figure 2.5) confirms the previous findings, with similar cycles across the four regions for E-OBS, HMR, CHIRPS, CPC, ARCIS and EURO4M-APGD, but extremely high precipitation for PERSIANN-CDR, with the opposite happening for CMORPH.

The spatial distribution of extreme precipitation can be assessed by figures 2.6 and 2.7. The three high resolution ARCIS, EURO4M-APGD and HMR datasets capture similar spatial details and amount of extremes in the North, with HMR slightly underestimating. In the other regions, large variability is present: CHIRPS almost completely lacks extremes, while CPC and PERSIANN-CDR show limited spatial variability across the regions. CMORPH, on the other hand, presents spatial patterns that are completely different from those obtained by the other products.
The Probability Density Functions of rainy days (figures 2.8 and 2.9) confirms the ability of ARCIS and HMR, in the North, to reproduce precipitation extremes not available in the other datasets. In the other regions, no clear picture seems to be discernible from the PDF data, with CHIRPS, CMORPH and HMR generally showing more intense extremes. In the South and in the Islands, E-OBS shows the least amount of extremes, while CMORPH continues to show much stronger seasonal variations compared to the other datasets.

These results show that the uncertainty associated with precipitation observations is often large, especially when it comes to precipitation extremes. In this analysis, two of the eight datasets considered (CMORPH and PERSIANN-CDR), both of which solely based on satellite data, showed very large biases (one underestimating, one overestimating) even in average precipitation, indicating that the performance of satellite-based products is insufficient in this specific region. Additionally, gauge undercatch is not taken into consideration in any of the station-based datasets employed in this brief analysis, thus uncertainty, especially for winter extreme events in mountainous regions, might be very large. On the positive side, the two Northern high-resolution datasets (EURO4M-APGD and ARCIS) show good agreement, with the HMR European reanalysis also showing good performance for mean precipitation (but a general underestimation of extremes compared to other datasets).

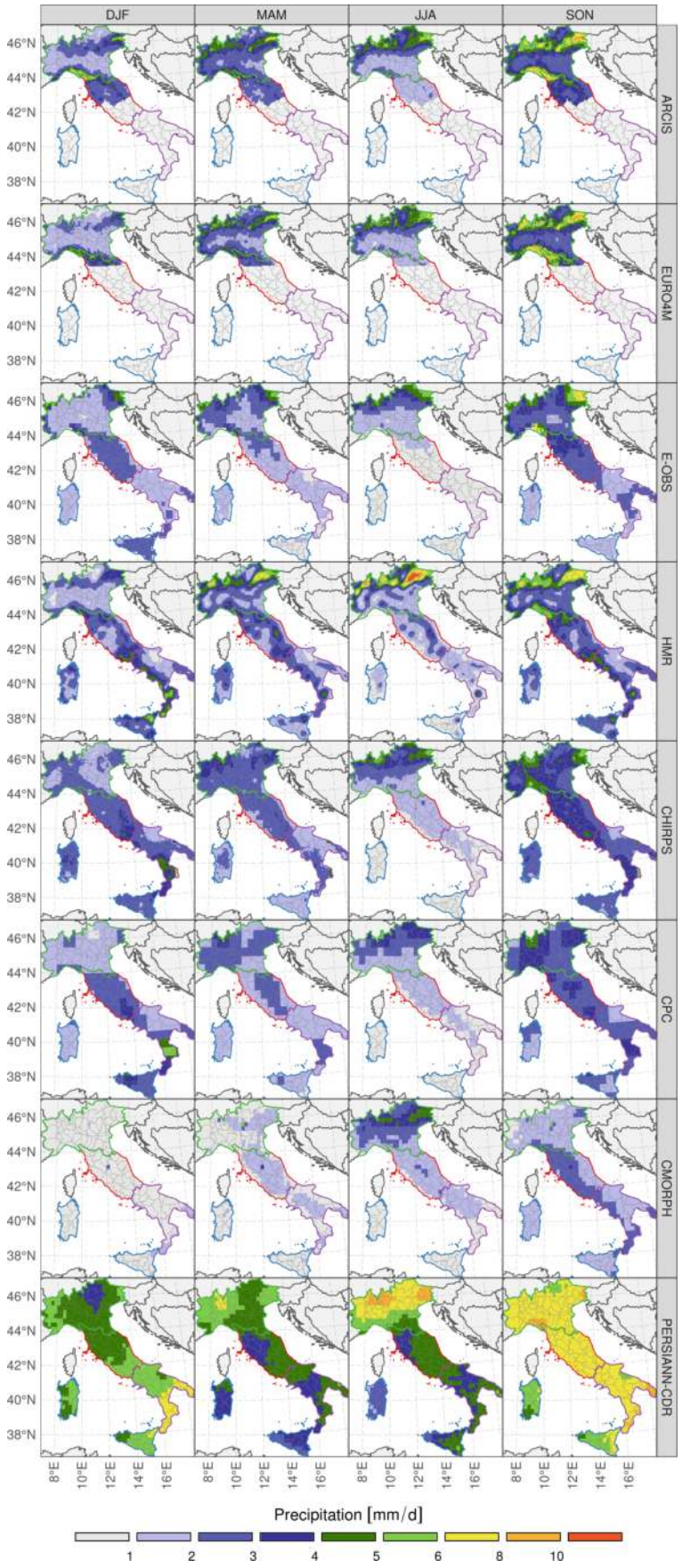

FIGURE 2.4: Average precipitation for the datasets in table 2.2. The four summarising regions for the annual cycle (figure 2.5) and the PDFs (figures 2.8 and 2.9) are highlighted in green (North), red (Centre), purple (South) and blue (Islands).

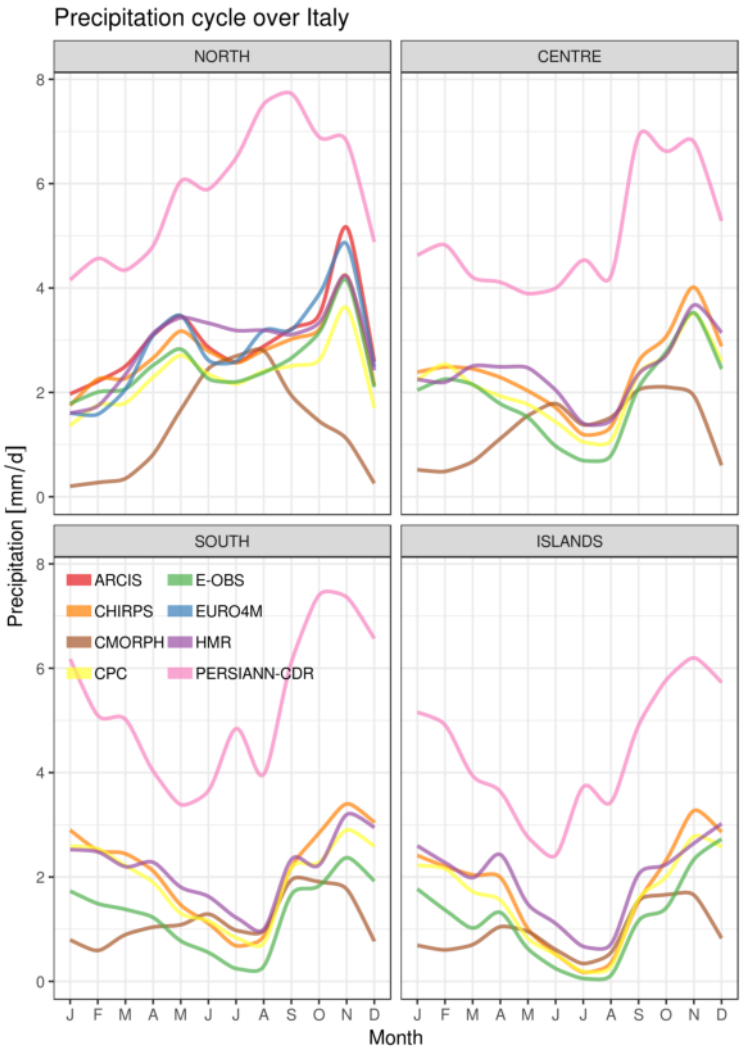

FIGURE 2.5: Annual cycle for average precipitation for the datasets in table 2.2. The four summarising regions are highlighted in figures 2.4, 2.6 and 2.7.

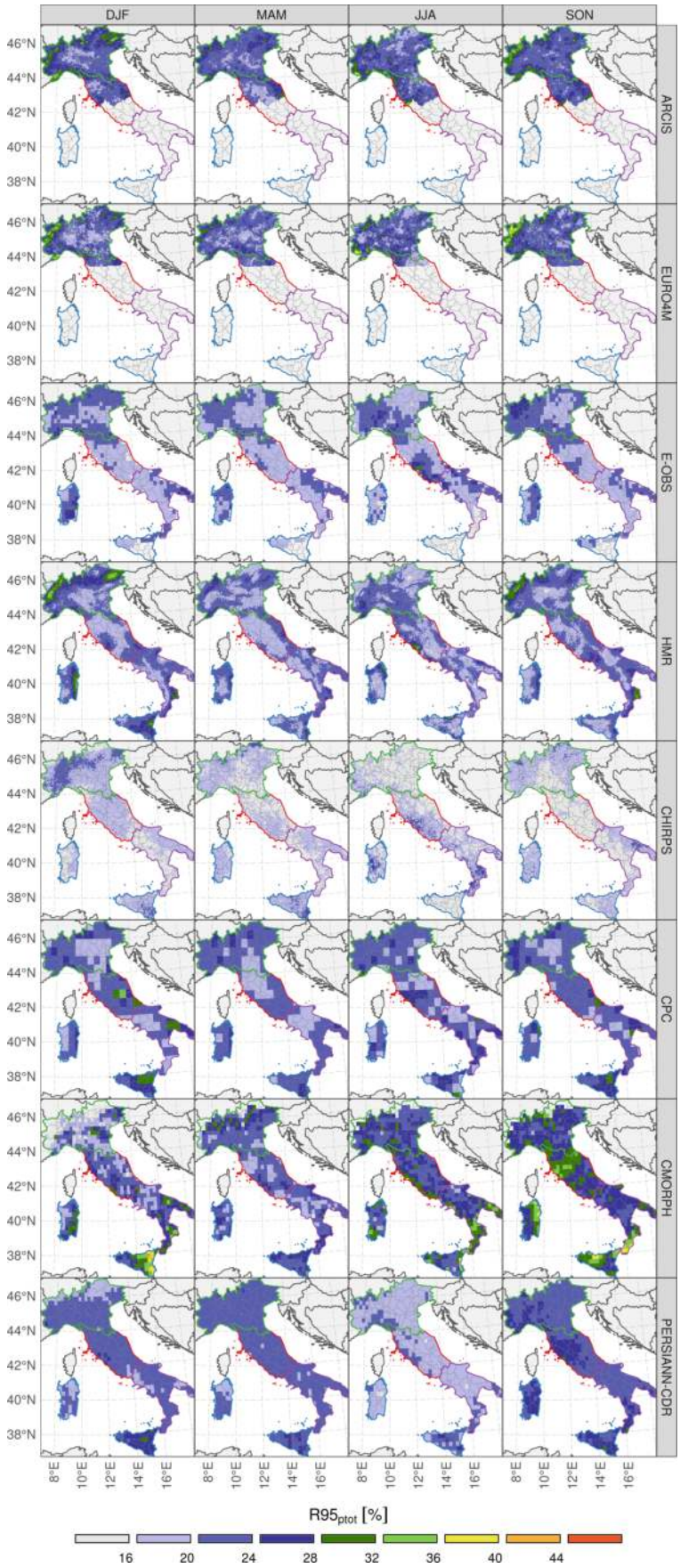

FIGURE 2.6: Extreme $R95_{ptot}$ precipitation for the datasets in table 2.2. $R95_{ptot}$ represents the percentage of precipitation due to precipitation events above the 95th percentile.

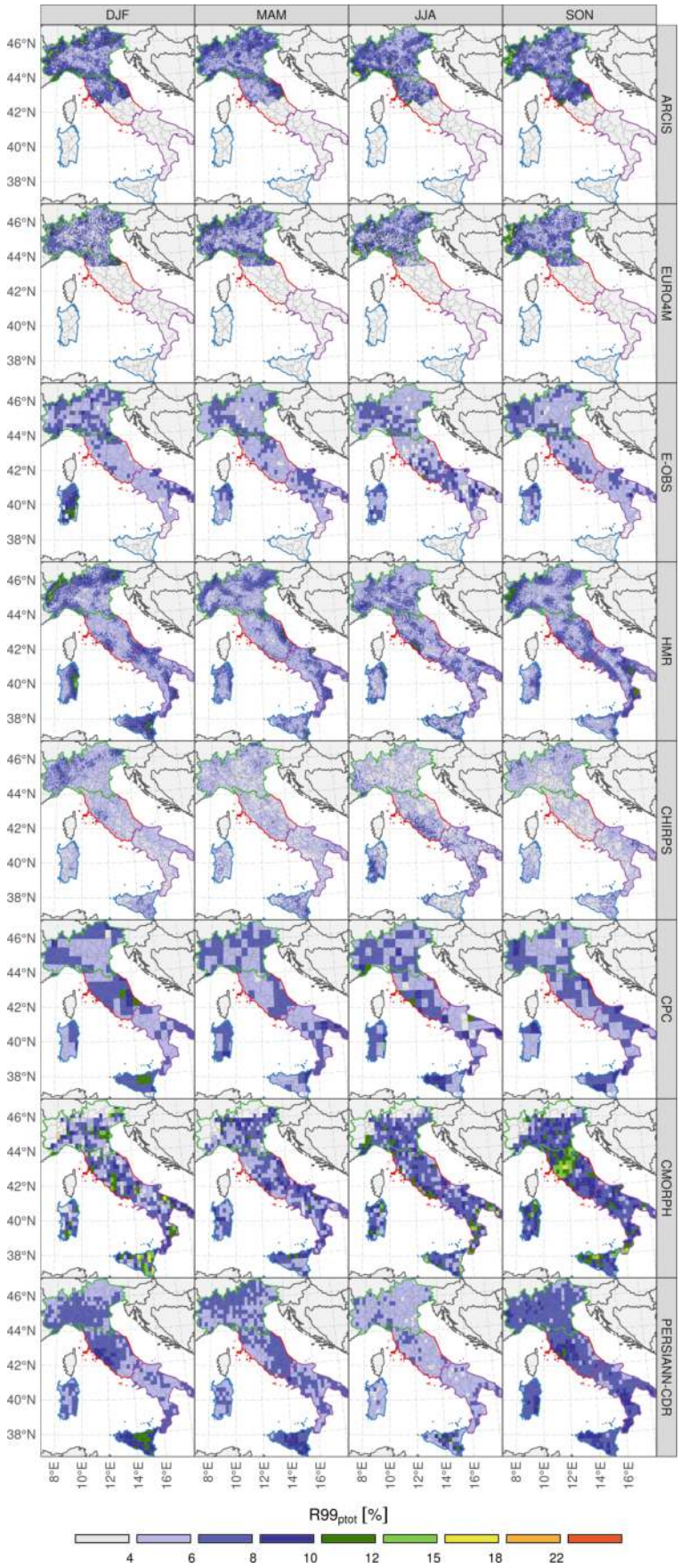

FIGURE 2.7: As figure 2.6, but for $R99_{ptot}$.

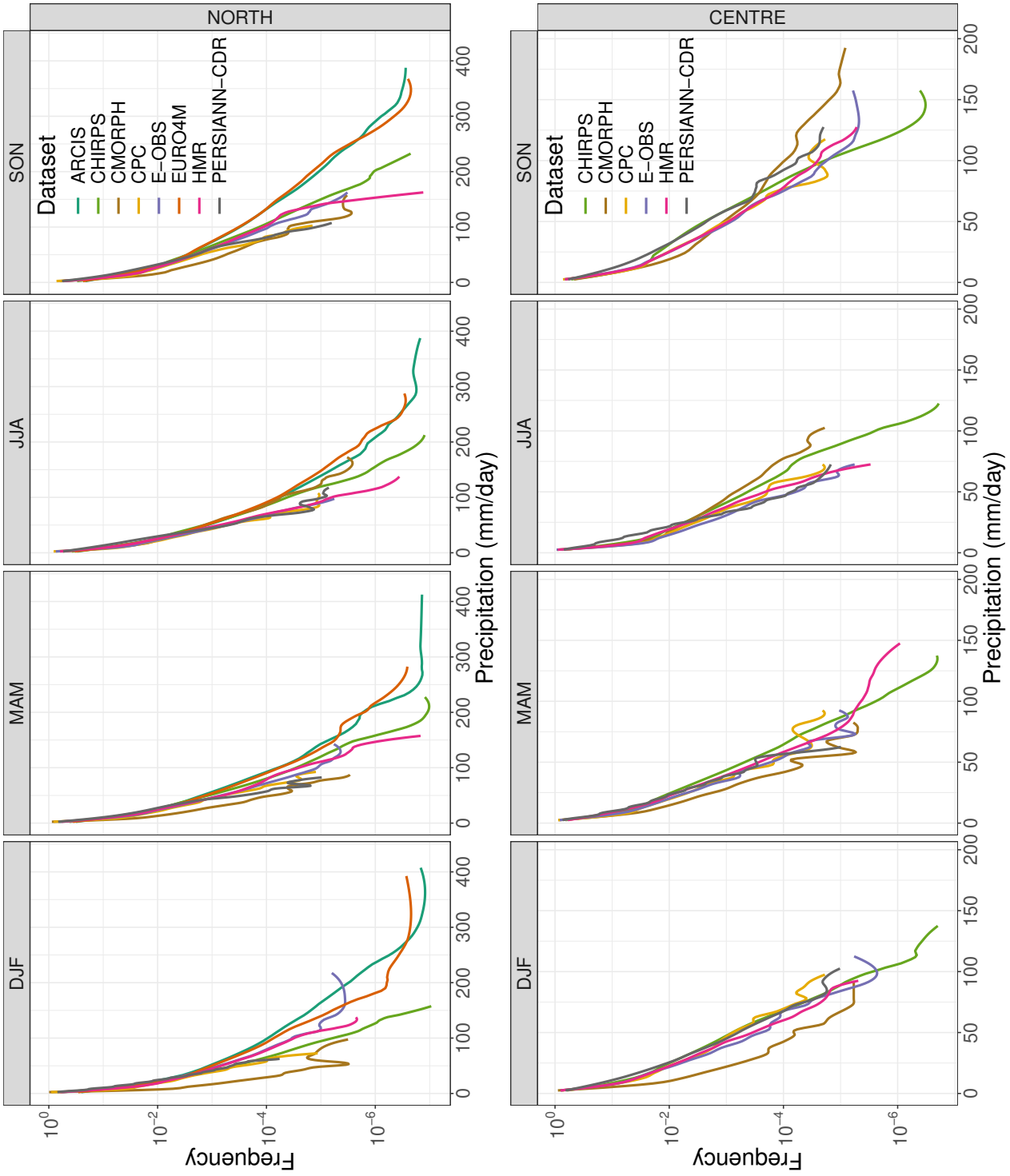

FIGURE 2.8: Daily precipitation Probability Density Functions for the datasets in table 2.2 for the North and Centre regions. The four summarising regions are highlighted in figures 2.4 and 2.6.

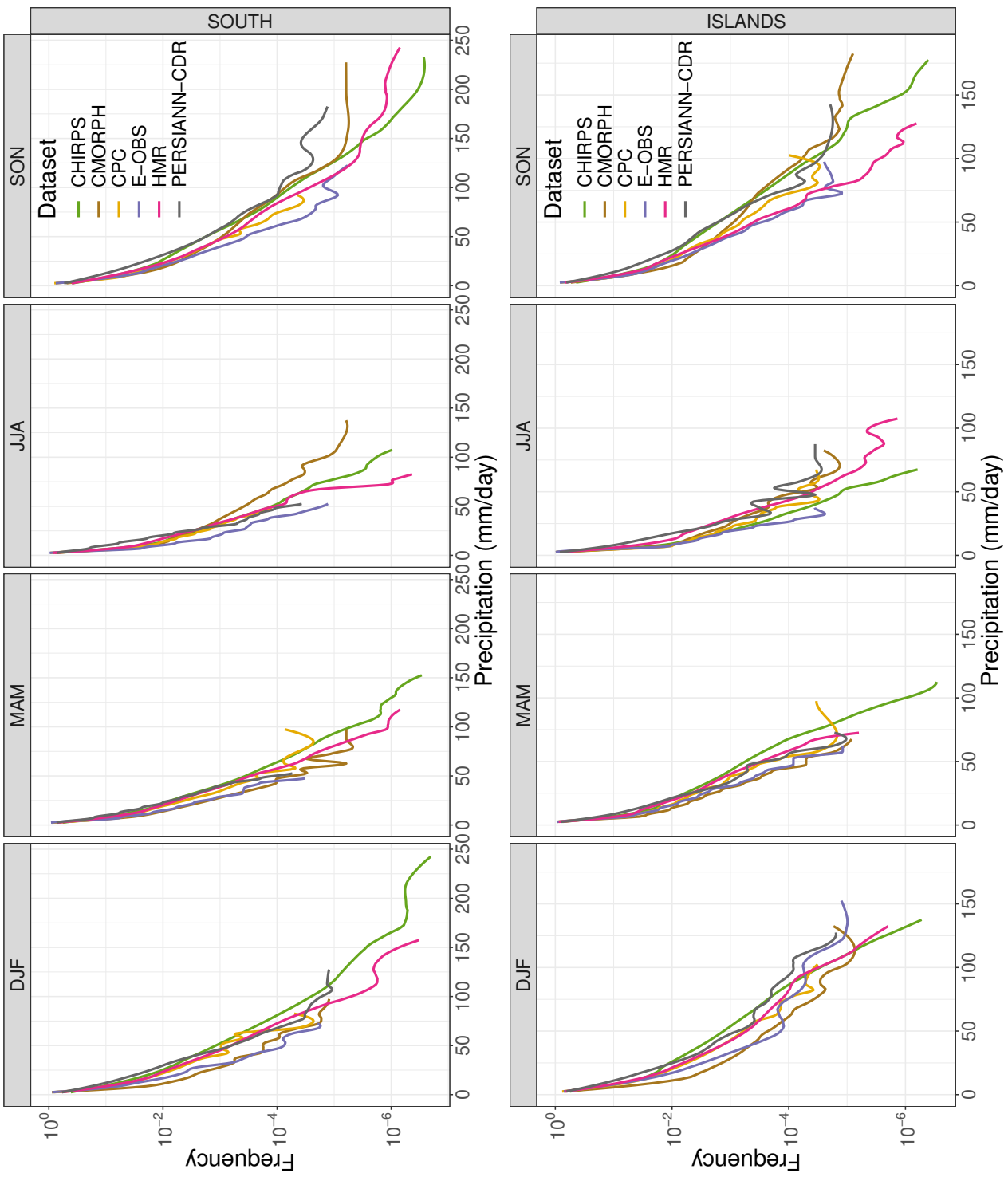

FIGURE 2.9: As figure 2.8, but for the South and Islands regions.

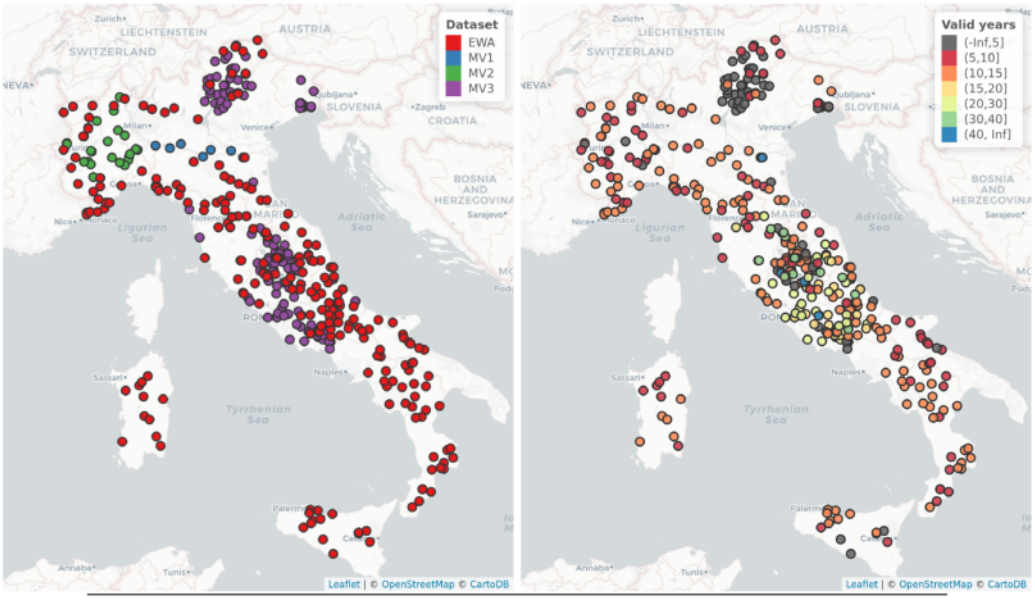

FIGURE 2.10: Source dataset (left) and time availability (right, in years) of the 414 discharge stations over the Italian territory, from the four datasets of table 2.3.

2.2 Discharge observations

River discharge observations are necessary to evaluate the performance of hydrological models. For a given river location, discharge is calculated from water level observations assuming a given *stage-discharge* (or *rating*) curve (Braca, 2008), which takes into account riverbed shape and water speed. Stage-discharge curves are extensively used in hydrology, but they necessitate constant updates due to the fact that stream channels constantly change due to erosion, deposition of debris, vegetation growth and presence of ice. As a consequence, despite being an irreplaceable tool, discharge measurements can sometimes be somewhat unreliable, especially for high flows (Di Baldassarre and Montanari, 2009).
In this thesis work, datasets of discharge from several sources are considered. Similarly to the precipitation dataset exposed in chapter 3, three hourly discharge datasets were provided by Prof. Marco Verdecchia[1], from the University of L'Aquila; to these, the standard European Water Archive (EWA, 2014), containing daily data from a collection of sources over Europe, was added. Due to the low number of daily discharge stations over Italy (only three according to the official reference[2]), the Global Runoff Data Centre (GRDC) database was not selected for use in this study.

Table 2.3 shows information about the four available datasets, while figure 2.10 shows the number of valid data years over Italy for each station, prior to any data checking. The coverage of the Italian territory is not complete, with two regions (Veneto and Puglia) being completely devoid of stations, and other areas (e.g. Trentino–Alto Adige) where temporal station coverage is low, often less than five years. Some stations even have no valid data at all. Station density and time availability are highest in Central Italy.
It has to be stressed that, in many cases, station locations were found to be erroneous (especially for the EWA dataset in Southern Italy); additionally, the time range with available observations varies wildly not only from dataset to dataset, but also within the same dataset. Data quality problems, ranging from stuck sensors (see e.g. figure 2.11) to extreme outliers, are present in all datasets.
For these reasons, when performing data analysis and validation, care has to be taken to select only stations that have a sufficiently long time range, without any noticeable systematic error. To this end, manual controls using several metrics (among which interquartile range, standard deviation to mean ratio, frequency of most common values, number of outliers) and comparison of nearby timeseries are carried out. However, only the most conspicuous errors are guaranteed to be removed by this procedure, and many inhomogeneities and suspicious timeseries remain in the datasets.
Similarly to all the other data sources used in this thesis, the four discharge datasets

[1] http://www.dsfc.univaq.it/it/ricercatori/44-verdecchia-marco.html
[2] ftp://ftp.bafg.de/pub/REFERATE/GRDC/website/grdc_referencestations_summary_countries.pdf

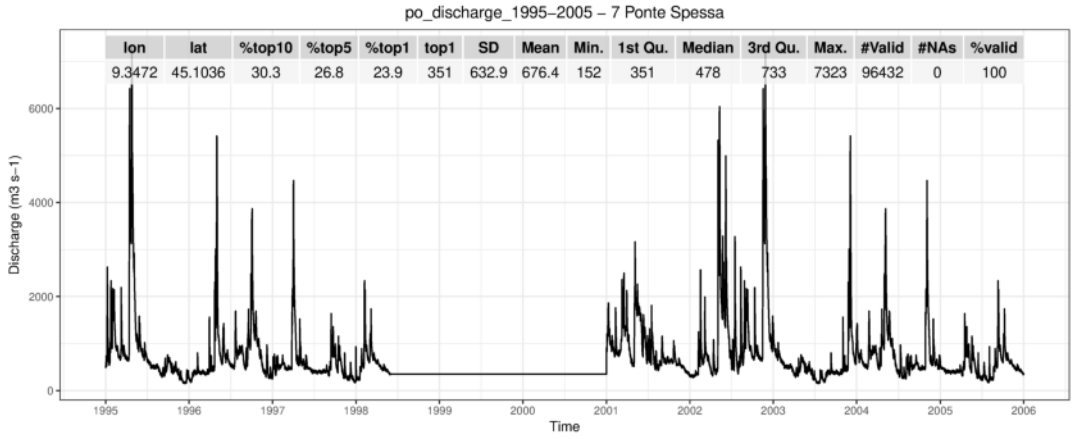

FIGURE 2.11: Example of a discharge station with a sensor stuck at 351 $m^3 s^{-1}$ for almost 3 years. Some station statistics used to assess station quality are listed at the top of the figure.

Dataset name	Region	Number of stations	Max period	Frequency	File type
MV1	Po river	7	1995–2005	Hourly	Fortran binary
MV2	Upper Po basin	43	2000–2010	Hourly	Fortran binary
MV3	Italy	152	2000–2016	Hourly	Fortran binary
EWA	Europe	4058 (231 in Italy)	1863–2013	Daily and monthly	Plain text

TABLE 2.3: Discharge datasets used in this thesis. See figure 2.10 for station locations in Italy. Datasets provided by Marco Verdecchia are named MV1 to MV3.

are converted to netCDF files compliant with the CF-1.7 conventions; for additional information on the rationale and the practical advantages of using of this file format, refer to section 3.1.1.

2.3 Flood extent observations

Flood extent observations are useful to validate and evaluate model performance against real world flood events. Unfortunately, availability of precise maps of flooded areas over Italy is lacking due to the aforementioned fragmentation of regional environment agencies and lack of national coordination. In the last decades, thanks to advancements in flood mapping techniques from satellite, by analysing Landsat, MODIS, Sentinel-1, SRTM and other remotely-retrieved data, several projects have started offering flood monitoring and maps with global or regional extent (see e.g. Brakenridge et al., 2003; Clement et al., 2017; Martinis and Rieke, 2015; Martinis et al.,

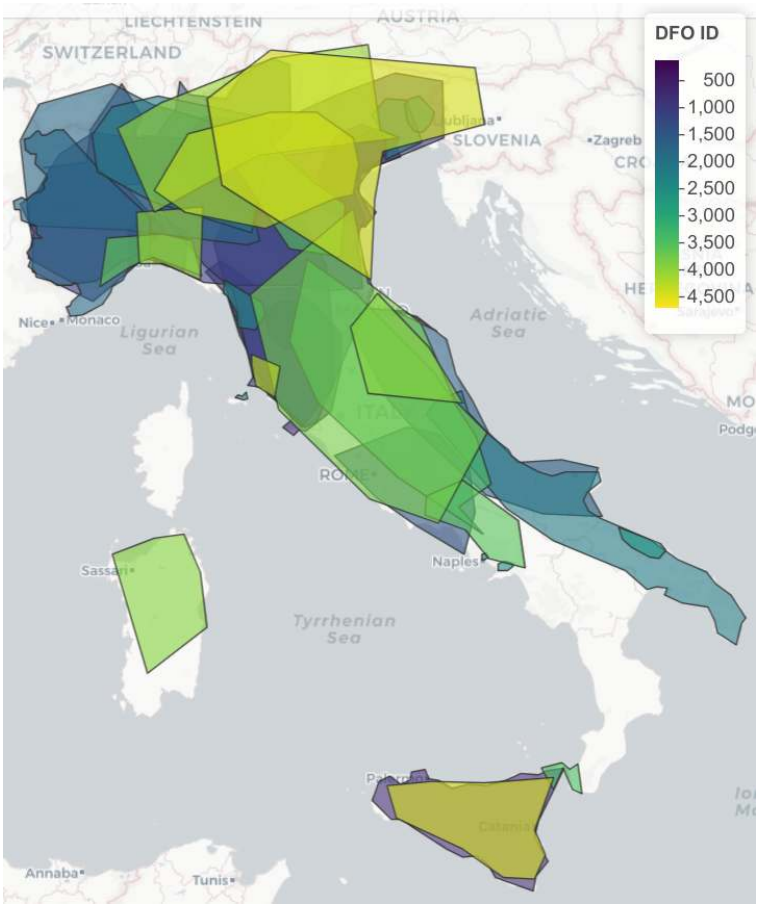

FIGURE 2.12: All areas in Italy affected by a flood event, as provided by the Dartmouth Flood Observatory (DFO). Areas are coloured by their DFO ID.

2013; Schlaffer et al., 2015; Smith, 1997; Westerhoff et al., 2013).
The Dartmouth Flood Observatory (DFO, G.R.Brakenridge, 2015), for example, provides metadata for all major events worldwide from 1985 to present, including shapefiles indicating affected areas. These are, however, extremely approximate and do not help in the precise identification of flooded areas (see figure 2.12); additionally, only 37 events are reported in Italy in the period 1985–present, in comparison with several hundred events listed by IRPI for the period 1967–present (figure 1.4).

The DFO also provides in-depth analysis for specific large events via the NASA-supported Global Flood Monitoring System (GFMS). Figure 2.13, for example, shows the November 2018 flooding in Northern Italy as detected by the DFO algorithms from satellite data: comparing with reported flooding by news sources, only a small part of the flooded areas in Northern Veneto and Liguria is included, and the Sicily flash flooding that caused 9 casualties is not reported at all. For comparison, the NASA NRT Global Flood Mission (Nigro et al., 2014) shows even less flooding for the same period and area (figure 2.14).

Several challenges in flood mapping still need to be overcome in order to provide

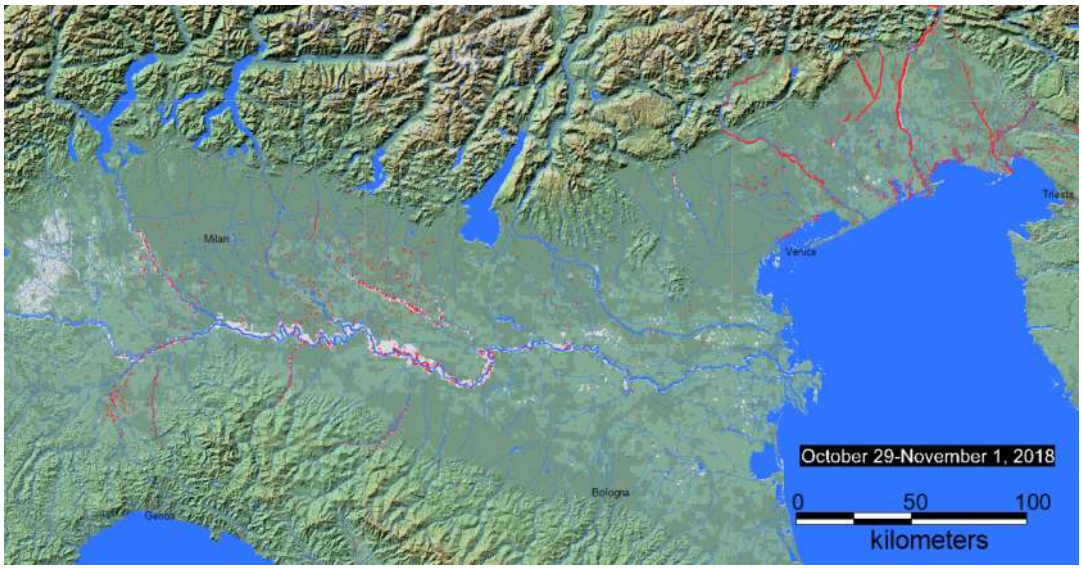

FIGURE 2.13: Flooded areas in Northern Italy for the November 2018 event, from the DFO archive (DFO event number 4699). Blue is reference water extent, grey is maximum water extent in the archive, and red is peak flooding for this event. Image from http://floodobservatory.colorado.edu/Events/4699/2018Italy4699.html.

reliable flood extent dataset for all major events. For example, small rivers often cannot be mapped or are severely underestimated by satellites due to the shielding effect of vegetation (Smith, 1997); algorithm details and calibration also add an additional level of uncertainty which is often difficult to quantify (Stephens et al., 2012).

Due to these challenges, the current focus of companies and research scientists seems to be mainly on near-real-time flood monitoring, short-term forecasting and long-term flood hazard mapping, rather than on validation of specific events. As such, few detailed observations of flood events are available over the Italian territory; tools such as the Aqueduct Global Flood Analyzer (Luo, 2015) from the World Resources Institute, the Web Portal from DFO[3] and the Global Surface Water Explorer (Pekel et al., 2016) from the European Joint Research Centre focus mainly on long-term flood hazard mapping and/or large scale events only. The Copernicus Global Flood Awareness System (GLOFAS Alfieri et al., 2013), instead, provides daily flood extents and short-term flood forecasts. The COSMO-SkyMed stellite constellation (Covello et al., 2010) has been used for evaluation of specific flood events (see e.g. Pierdicca et al., 2013; Pulvirenti et al., 2011; Refice et al., 2014), but the data availability seems to be limited. In short, very little information is currently available to validate inundation models against specific events over Italy: in this work, information from all of the above sources was taken into account and used when possible, given the above

[3] https://diluvium.colorado.edu/arcgis/apps/Viewer/index.html?appid=759d697577dd438ab7f2d48f605593d5

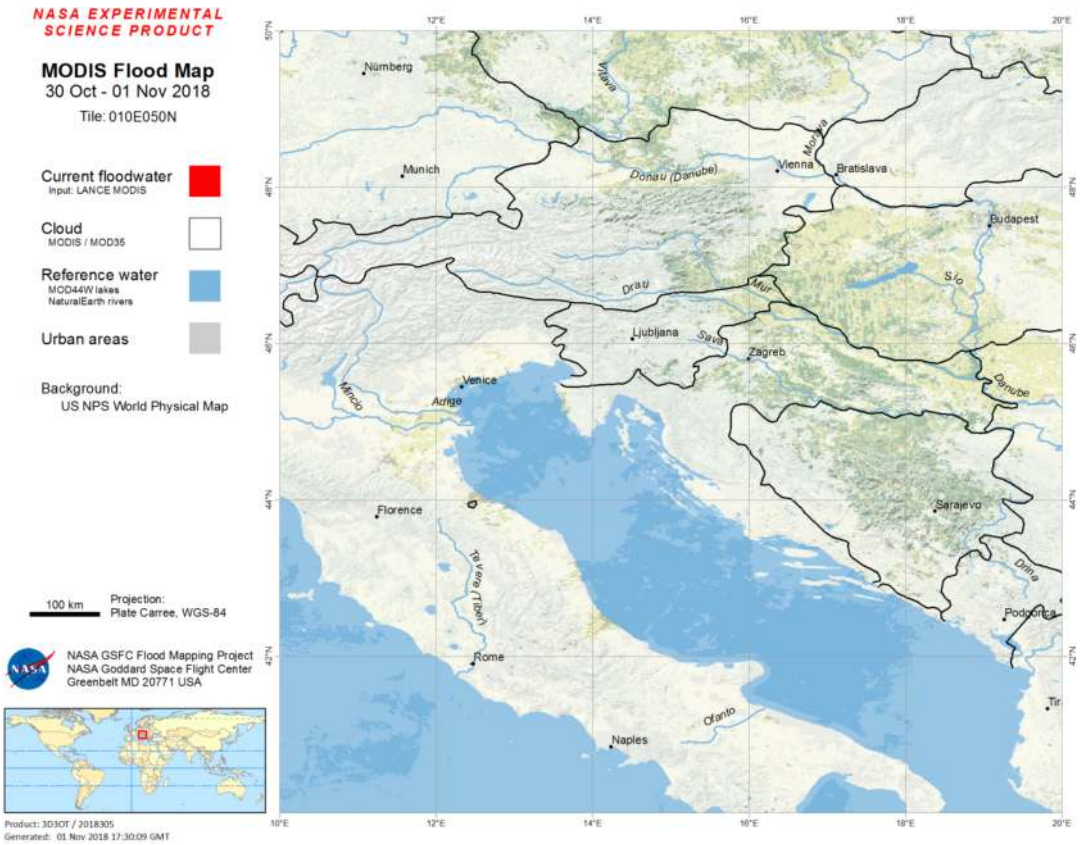

FIGURE 2.14: Flooded areas (or absence thereof) in North-Eastern Italy for the November 2018 event from the MODIS NASA NRT Global Flood Mission . Image from https://floodmap.modaps.eosdis.nasa.gov/getTile.php?location=010E050N&day=305&year=2018&product=3.

mentioned caveats.

2.4 Elevation observations

Elevation information for each location in the study area is necessary for the hydrological (CHyM, section 4.2) and hydraulic (CA-2D, section 4.4) models: the former uses elevation to reconstruct a realistic river network; the latter, instead, uses it to know where and how water can propagate in case of flooding. For both of these applications, high vertical accuracy, proper river routing and high horizontal resolution are necessary.

Satellite-based remote sensing techniques are the most common source of elevation data over the whole globe. Several publicly available datasets, such as SRTM, ASTER, TanDEM-X, GTOPO30 and AW3D30 use satellite sensing to infer terrain elevation and provide world coverage at resolutions ranging from 30 m to 1 km. Due to the nature of remote sensing via satellite, all of these datasets are affected by relatively large errors in the elevation, with vertical accuracies often of the order of several tens of meters. This makes them unsuitable for flood mapping especially of smaller basins and in flatlands.
A possible alternative is represented by datasets obtained by scanning the Earth's surface via LiDAR-equipped planes: these datasets, albeit very accurate, are usually very expensive for the end user (upwards of $\$10\,\mathrm{km}^{-2}$), especially if a large area is required.
A third option for hydrologists and flood modellers is to use specifically conditioned Digital Surface Models (the term is sometimes used interchangeably with Digital Elevation Models, or DEMs) which include information on the position and depth of rivers. This is the course taken within this thesis work.

2.4.1 The HydroSHEDS Digital Elevation Model

In this thesis, the HydroSHEDS[4] dataset (Lehner et al., 2013; Lehner et al., 2008) was selected to provide information not only about elevation data, but also river network and river depth. HydroSHEDS is based on different versions of NASA's 3 arc-second (about 90 m at the equator) SRTM satellite-based elevation data, with several other datasets used for control and void filling. Being a DSM, and not a DTM (Digital Terrain Model), HydroSHEDS, like most satellite-only products, is affected by surface features such as buildings, major roadways and vegetation. The DEM is hydrologically conditioned to reproduce river networks all over the globe using a mixture of automatic and manual techniques. In particular, the following algorithms are applied in order:

Deepening of open water surfaces Open waters such as lakes and oceans are deepened to insure proper flow towards them.

[4] Hydrological data and maps based on SHuttle Elevation Derivatives at multiple Scales

Weeding of coastal zone Coastal areas are lowered to account for higher vegetation height near the sea.

Stream burning Major river courses are carved into the surface to ensure proper river flow. A 500 m buffer is also carved around rivers to avoid sudden elevation changes and shape a smoother transition between the rivers and the surrounding areas.

Filtering Local filtering with a 3×3 kernel size to remove high points blocking the flow path.

Molding of valley courses Additional local algorithm to identify valley direction, using a 5×5 kernel.

Sink filling Filling of non-natural sinks which can impede river flow.

Carving through barriers Final step to ensure continuous flow through natural (e.g. lakes) and man-made (e.g. dams) objects.

Second conditioning After the barrier carving procedure, second application of the first six conditioning steps.

HydroSHEDS is particularly suited to the creation of a reliable river network for the CHyM model (see section 4.2.1), resulting in higher accuracy compared to the default 300 m Italian DEM that comes with the model. Additionally, an advantage of using a global DEM is that it is easy to extend the flood mapping procedure to any area of the world, without the need to have any additional data requirement.
At the time of writing, the CHyM model is also being tested for running directly on the HydroSHEDS river network, without any further conditioning procedure as carried out by the model by default.

HydroSHEDS comes as ESRI binary `.bil` files, and was converted to appropriate formats to use with our models (NetCDF for CHyM and ASCIIgrid for CA2D) using GDAL's `gdal_translate` tool (GDAL/OGR contributors, 2018).

2.4.2 Alternative elevation models

Several DEMs are publicly available under no fee for research use, both for specific regions and with worldwide extent. Table 2.4 shows a non-comprehensive list of commonly-used DEMs, with their availability, references and maximum resolution.

In figure 2.15 and 2.16, six of them are compared for a small ($0.3° \times 0.3°$) mountainous region in North-Eastern Italy, with reference to the Italian official PCN20 20 m DEM (whose elevation is displayed in figure 2.15). The region of choice, centred around the town of Belluno, includes deep valleys, a major lake towards the East and a large river (for the standards of the region) flowing through from North towards South-West. Table 2.5 shows mean, standard deviation, median and 5–95% quantile ranges for the bias with the reference dataset. Large variations of up to several tens of meters

DEM name	Region	Provider	Resolution	Data source	Coordinate system	Reference
PCN20	Italy	Italian ministry for the environment	20 m	Contour lines from Italian Military Geographic Institute (IGM) cartography	UTM 32N EPSG:32632	Provider site [a]
TINITALY/01	Italy	INGV	10 m	Mixed: satellite, cartography, LiDAR, ground data	UTM 32N EPSG:32632	Tarquini et al. (2007, 2012) [b]
ASTER GDEM-2	World	NASA	1 arc–second (about 30 m)	Satellite	Lat-Lon EPSG:4326	Provider site [c]
SRTM	World	NASA	1 arc–second (about 30 m)	Satellite	Lat-Lon EPSG:4326	Provider site [d]
EU-DEM	Europe	EEA	25 m	SRTM and ASTER	EPSG:3035 ETRS89-LAEA	Bashfield et al. (2011) and Józsa et al. (2014) [e]
TanDEM-X	World	DLR	90 m (free version)	Satellite	Lat-Lon EPSG:4326	Rizzoli et al. (2017) [f]
ALOS World 3D (AW3D30)	World	JAXA	1 arc–second (about 30 m)	Satellite	Lat-Lon EPSG:4326	Tadono et al. (2016) and Tadono et al. (2017) [g]
GTOPO30	World	USGS	30 arc–second (about 1 km)	Satellite	Lat-Lon EPSG:4326	USGS (1996) [h]
HYDRO1K	World	USGS	30 arc–second (about 1 km)	GTOPO30, hydrologically conditioned. Flow directions and river information available	Lat-Lon EPSG:4326	USGS (1996) [i]
HydroSHEDS	World	WWF	3 arc–second (about 90 m)	SRTM, hydrologically conditioned. Flow directions and river information available	Lat-Lon EPSG:4326	Lehner et al. (2013) and Lehner et al. (2008) [j]

TABLE 2.4: Non comprehensive overview of some free-to-use DEMs and DTMs available over Italy.

[a] http://www.pcn.minambiente.it
[b] http://tinitaly.pi.ingv.it/
[c] https://asterweb.jpl.nasa.gov/gdem.asp
[d] https://www2.jpl.nasa.gov/srtm/
[e] https://www.eea.europa.eu/data-and-maps/data/copernicus-land-monitoring-service-eu-dem
[f] https://geoservice.dlr.de/web/dataguide/tdm90/
[g] https://www.eorc.jaxa.jp/ALOS/en/aw3d30/index.htm
[h] https://lta.cr.usgs.gov/GTOPO30
[i] https://lta.cr.usgs.gov/HYDRO1K
[j] https://www.hydrosheds.org

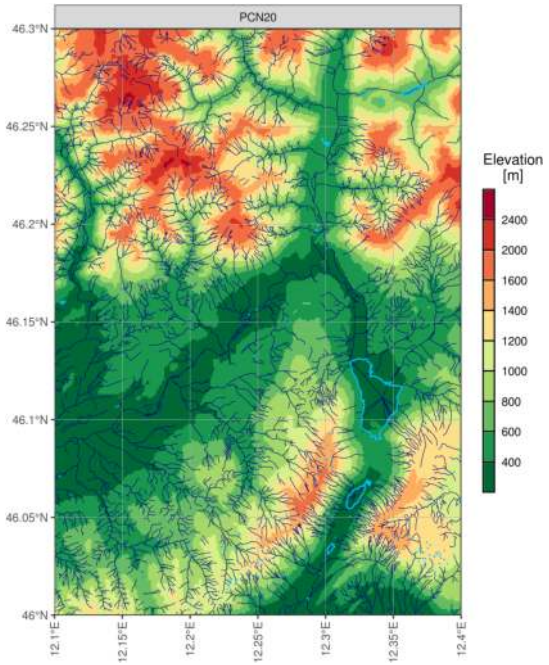

FIGURE 2.15: Elevation of the Italian PCN DEM at 20 m resolution; detail of a selected North-Eastern Italian region centred around the town of Belluno. Rivers (dark blue) and lakes (bright blue) are from the Interregional Centre for Information, Geographical and Statistical Systems (CISIS) DBPrior10K project[5].

can be found between the datasets (figure 2.16); additionally, one dataset (Nasa's SRTM) shows large no-data regions which would need to be filled in before usage with a hydrological model was possible. The conditioned version of HydroSHEDS is, on average, several meters deeper than the other datasets (18.4 m deeper than the non-conditioned version), with a 5–95% bias quantile range of −86 to 29 m, the widest among those considered. Carved flow paths are evident along the main course of the river and in the largest lake.

In general, the choice of Digital Elevation Model must be driven by the project's requirements, and not by average bias. In this case, a reliable river network representation was paramount, leading us to settle with HydroSHEDS as terrain model

DEM	Mean	StdDev	Q05	Median	Q95
ASTER	3.9	30.1	-21	1	36
HydroSHEDS Void Filled	0.4	57.8	-52	0	51
HydroSHEDS VF + Cond.	-16.4	59.7	-86	-11	29
JAXA AW3D30	5.0	19.6	-14	3	26
SRTM	4.7	14.1	-14	3	25
TINITALY/01	-0.6	14.1	-19.3	-0.6	17.7

TABLE 2.5: Statistics for the DEM comaparison of figure 2.16. All values are in meters.

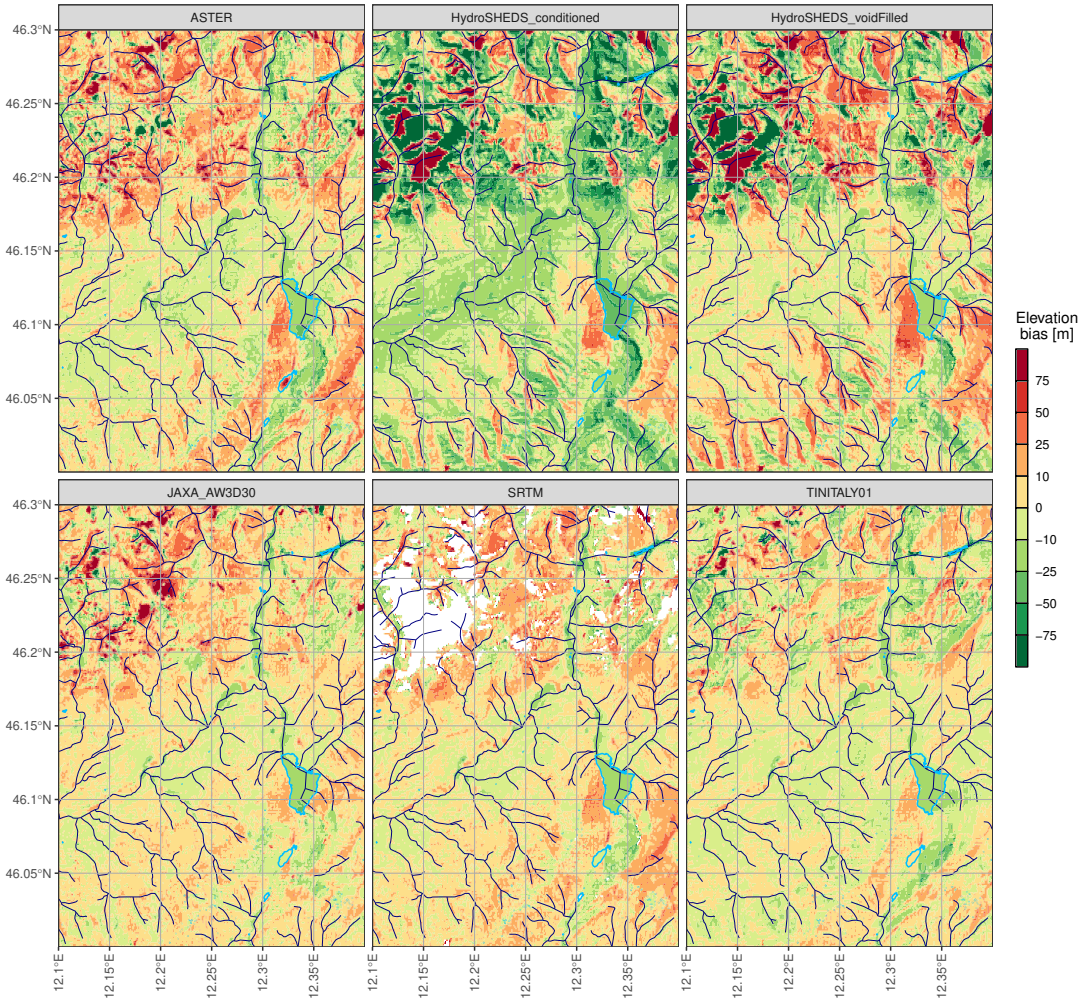

FIGURE 2.16: Example comparison of 6 DEMs (see table 2.4) over a small region in North-Eastern Italy centred around the town of Belluno. Elevation biases are calculated with reference to the national PCN20 DEM displayed in figure 2.15. Red means the DEM is higher than PCN20, green indicates the opposite. For the purpose of this example, all grids were warped to a common 300×300 0.001° resolution grid using bilinear resampling. Overlaid simplified rivers (dark blue) are obtained from the Italian Superior Institute for the Ambient Protection and Research (ISPRA) online catalogue SINAnet[6]; lakes (bright blue) are the same as figure 2.15.

of choice. Other global and regional elevation datasets were tested by attempting to reconstruct a reasonable river network via the hydrological model CHyM (section 4.2.1), but none allowed to reconstruct the rivers as well as the hydrologically conditioned HydroSHEDS.

Chapter 3

GRIPHO: developing an Italian high-resolution hourly precipitation dataset

In order to simulate flood hazard on the scale of a small catchment, high resolution precipitation data is needed. This is because the time scale for floods in small areas can be very short, due to the limited ability of small rivers to displace the large amounts of water that can fall in a relatively brief timespan. While model output can be easily obtained for this scope, observations provide a very important tool for validation and evaluation of the methodology. Therefore, in this thesis project, observations are used to drive some of the simulations described in the next chapter.

Most observational datasets over Italy and Europe are daily (see section 2.1.3 and table 2.1), which implies that very rapid precipitation extremes, which often occur in a few hours, are necessarily smoothed out when upscaled to a daily time scale. Analysing these extremes on an hourly time scale has the potential to provide better results for flood hazard analysis, especially for small catchments with a short water residence time. For this reason, one of the objectives of this thesis work was the creation of an hourly precipitation dataset that could serve as input to CETEMPS Hydrological Model (CHyM, Coppola et al., 2006; Tomassetti et al., 2005, see section 4.2 for details), the hydrological model of our choice, which is designed to easily digest hourly data as input and has been doing so operationally for quite some time at the CETEMPS Center of Excellence[1].
We thus developed what can be considered, as far as we know, the first hourly precipitation database over Italy using exclusively in-situ precipitation data as input. The dataset is named GRIPHO (GRidded Italian Precipitation Hourly Observations). This chapter will outline the work undergone in analysing, cleaning, gridding and validating GRIPHO. The resulting dataset is deemed of sufficient quality to be used in this project.

[1] http://cetemps.aquila.infn.it/

Later in the project, GRIPHO was used for driving the CHyM model simulations (section 4.2) and to validate the RegCM simulations (section 4.1.4).

3.1 Original input data

The first challenge when developing such a dataset is collecting the data: not always a single national agency can provide all the necessary information. Fragmentation of data sources, different input formats and different levels of quality checks are the main problems that need to be addressed. As previously mentioned, Italy lacks a national repository for meteorological data: regional agencies each have their own station network, data collection and cleaning procedures. Retrieving and homogenising all the necessary information from all regional agencies can prove to be a difficult task. In this case, the input data are provided by the CETEMPS Center of Excellence of the University of L'Aquila, as part of an agreement with the International Centre for Theoretical Physics. The dataset is the result of integration between different data sources; observations from 3712 precipitation stations located in all of Italy over the period from 2001 to 2016 are collected, validated and filtrated by different algorithms and then provided as a collection of yearly time series. Using this input data, a gridded hourly dataset was created and validated.

The input data is provided as yearly Fortran-style binary files. The time step is quarter-hourly, and the unit of measure reportedly mm h^{-1}. A single, separate metadata text file contains the following fields for each station:

- Station number [int]
- Station name [char]
- Province [char]
- Municipality [char]
- Latitude [dbl]
- Longitude [dbl]

No information on station type, height, exposure or any other metadata is provided. Due to the severe lack of metadata, correcting for gauge undercatch (see section 2.1.2) is deemed too complex for the scope of this project.
Any value less than 0 is considered to be a filling value (most often, this is the case with -10, -999 and -9999). The total size of the input database is about 3.9 GB for the period 2001 to 2016. In absence of any additional information, the first timestep of each yearly file is assumed to be at time January 1, 00:00:00 UTC, with the following timesteps separated by 15 minutes each.

3.1.1 Conversion to NetCDF

The first step for making use of this data is the conversion to a more user-friendly format. NetCDF[2] is chosen primarily due to its widespread use across all fields of climate science and to its ease of use and metadata integration. All modern programming languages offer one or more interfaces capable of reading self-describing NetCDF data. Additionally, NetCDF offers advanced options such as transparent compression and chunking, which can speed up reading and writing significantly. The latter, chunking, is a netCDF-4 feature which allows to tune a dataset for faster access along a specific dimension: this allows for two versions of the dataset to be created as separate files, one that assures very fast reads for the complete time-series of one single station, and one that optimised the reading of all station values for a single time-step. The industry-standard CF conventions (Eaton et al., 2009) version 1.7 are followed for the storing of metadata inside the files, the total size of which resulted to be around 650 MB.

3.1.2 Station spatial and temporal availability

Figure 3.1 shows the station distribution over the study area. The coverage of the Italian territory is very complete, with an average density of one station per 9×9 km^2, which is on par with most European high resolution observational datasets (see section 2.1.3 and Prein and Gobiet, 2017, for details). The overall spatial distribution is quite uniform over the complete Italian teritory, with generally lower density over less climatologically complex areas, such as the Po Plain.
Figure 3.2 shows the height distribution of the dataset, with station height values extracted from the HydroSHEDS void-filled Digital Elevation Model (Lehner et al., 2013; Lehner et al., 2008, also see section 2.4) at 0.000 83° (about 90 m) resolution, as opposed to the spatial distribution of all of the Italian territory. All elevations are well represented in the dataset, except very high elevations (above 3000 m), which is to be expected due to the difficulty in setting up and maintaining such stations. Such small underrepresentation of very high elevations should not impact the precipitation field in a noticeable way.

In figure 3.3, the number of available stations (stations whose value is not one of the possible NaN values) is plotted over each timestep for the whole Italian territory. Station availability grows significantly within the 16-year period, which implies that the total station density is not constant. While a variable number of stations is common for all station-based datasets (see for example Haylock et al., 2008, figure 2), in this case it is particularly evident, with the actual number of active stations growing from about 500 in 2001 to about 2600 in 2012. Moreover, in some timesteps (e.g. at the beginning of 2012) the number of stations falls momentarily close to zero and little to no data is reported. In order to keep the dataset as close as possible to

[2] https://www.unidata.ucar.edu/software/netcdf/

FIGURE 3.1: Station spatial distribution for the Italian in-situ hourly precipitation dataset. All 3712 stations in the dataset are shown, regardless of their temporal availability.

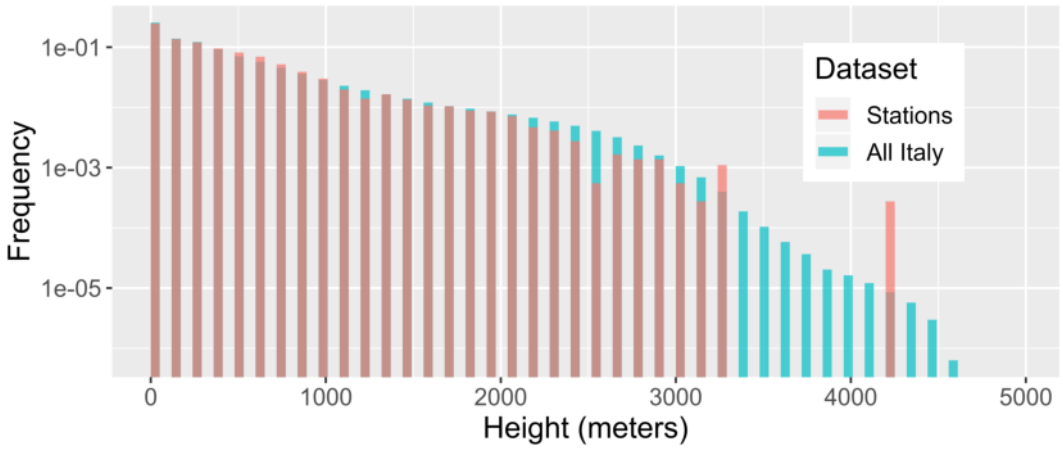

FIGURE 3.2: Station height distribution for the Italian in-situ hourly precipitation dataset (red), compared to all of the Italian territory (blue). Bin size is 120 m. Data from the HydroSHEDS void-filled Digital Elevation Model (Lehner et al., 2013; Lehner et al., 2008).

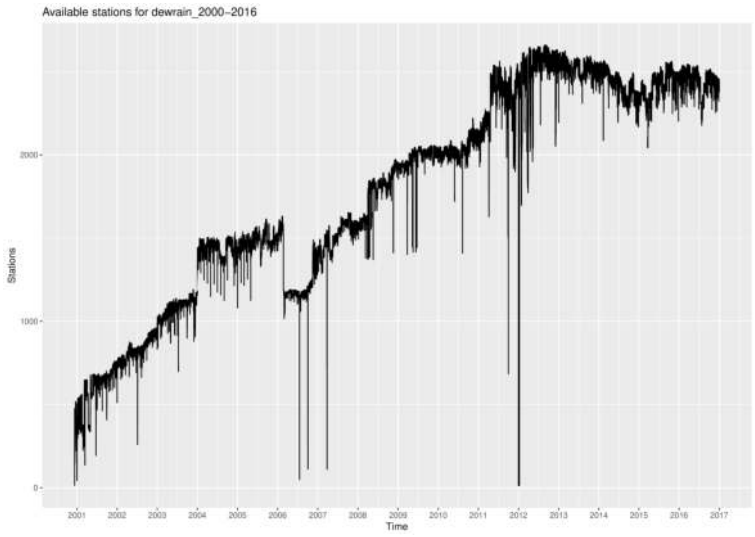

FIGURE 3.3: Timeseries of the number of available stations for each timestep in the input data for the Italian in-situ dataset GRIPHO.

raw station data, in the final product these voids are not filled in with alternative datasets or via interpolation, but are rather left as missing values.

Maps of the number of stations and valid timesteps per Italian region (figure 3.4) show very low data availability for some regions, likely as a result of some regional agencies providing only a few years of data to the original data collector. While some regions provided 12 or even 13 years (Piemonte, Calabria) of data, one region (Sicily) only has 3 valid years in total (figure 3.4b). When taking into account the total number of timesteps and the station density (figure 3.4f), Liguria and Friuli–Venezia Giulia come on top, with about 2000 valid values/km^2, in contrast with Trentino–Alto Adige and Sicily, both with less than 300 values/km^2.

As result of this initial analysis a large variability in the data availability is evident. Subsequent analysis (section 3.2) confirms the lack of station coverage for some regions, especially in the early 2000s. Once again, due to the lack of suitable hourly backup data for the whole period and region, these gaps are purposefully left in GRIPHO without any attempt at filling them.

3.2 Data checking, flagging and cleaning

Due to the fragmented nature of the data, which comes from a plethora of different regional agencies, the original data provider could not guarantee that any quality control procedure or checks were performed on the station data. As a result, understanding which eventual problems affect the input data represents the first priority in order to reduce the bias in the final product.
Several procedures are carried out in order to identify and remove errors and inconsistencies, such as:

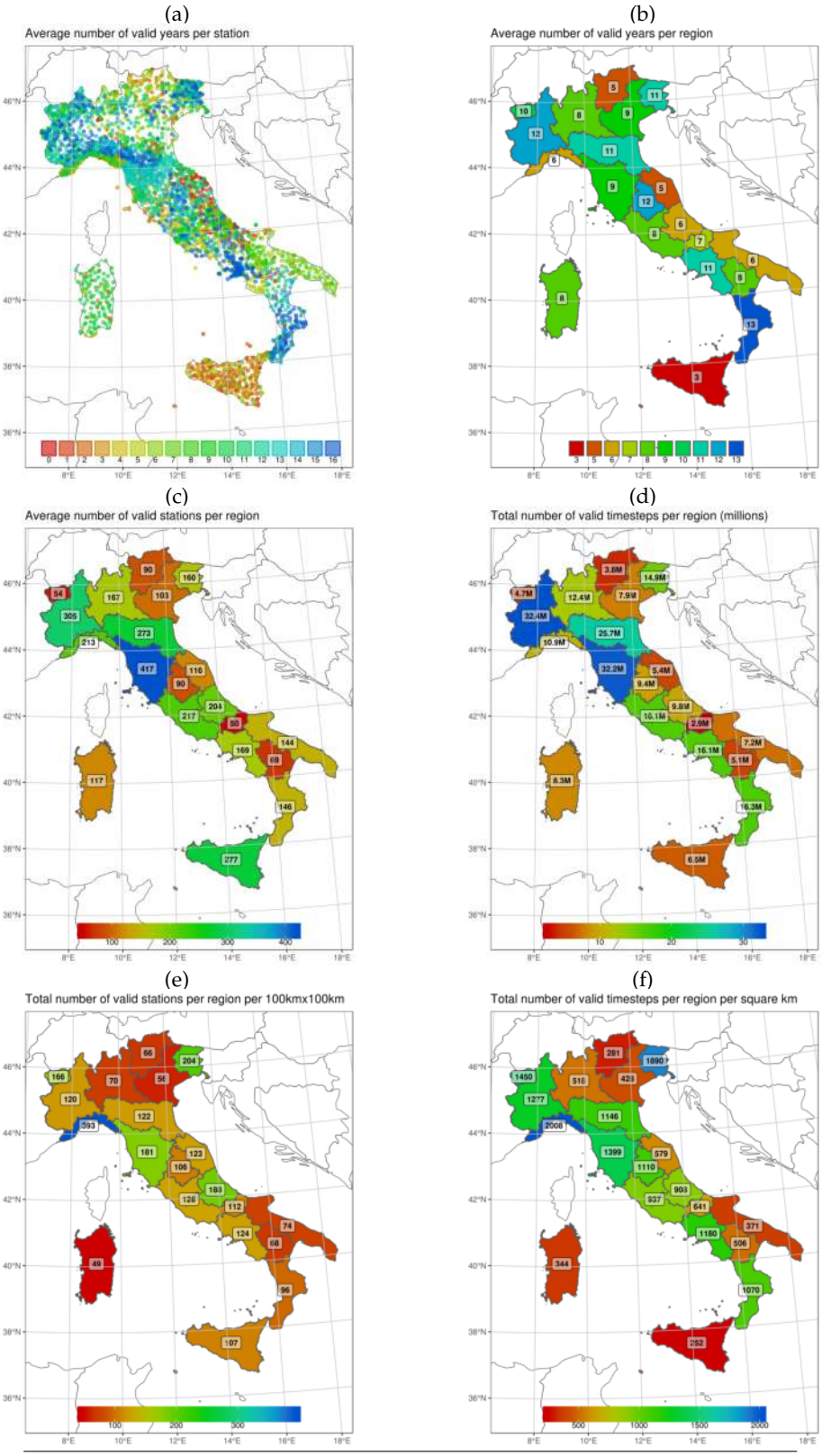

FIGURE 3.4: Analysis of station availability for the Italian in-situ hourly precipitation dataset GRIPHO; refer to the titles for the contents of each panel

- analysing spatial and temporal distribution of the stations (figures 3.2 and 3.3), also separated by region (figure 3.4);
- producing precipitation maps for each timestep and assembling into videos;
- manually analysing single station timeseries;
- automatic flagging of suspicious events in single station timeseries;
- automatic removal of extremely suspicious events;
- manual checking of monthly precipitation maps and statistics over the whole time period;

Due to the complexity of such procedure, no correction is attempted for those values that resulted to be erroneous or suspicious; additionally, no undercatch correction (see section 2.1.2) is applied due to the lack of the sufficient station metadata.

3.2.1 Station-by-station timeseries analysis and flagging

A manual temporal analysis was carried out independently for all 3712 stations in the original dataset. During this process several inconsistencies were discovered, in particular:

- the vast majority of data points are stored in round hours timesteps (timestamps ending in ':00' minutes), with only a handful values (less than 0.1%) stored in between. This indicates that most of the data is actually hourly, and not sub-hourly.
- Some stations (see e.g. figure 3.5a) seem to suffer from issues with stuck sensors, causing constant values to be reported for very long periods of time. This occurs most often with the $0\,\mathrm{mm\,h^{-1}}$ value, but some instances of constant values differing from zero (most often values close to zero) are present.
- A sizeable amount of extremely high outliers (see e.g. figure 3.5b) was detected. Sometimes this affects only a single station in a given area, indicating a fluke or error in the instrumentation; other times several neighbouring stations appear to show the same behaviour, indicating an issue in the data collection and processing.

To mitigate these problems, a multi-step approach of manual checking, driven by different metrics, is devised, comprising of 4 different steps:

1. Flagging of suspicious events using several metrics obtained from the literature (World Meteorological Organization, 2008). The description of the metrics can be found in table 3.1.
2. Identification of values above the historical maxima for the region of interest, which are considered erroneous and removed. Three different thresholds are used, one for hourly values ($200\,\mathrm{mm\,h^{-1}}$), one for monthly sums ($1800\,\mathrm{mm\,month^{-1}}$),

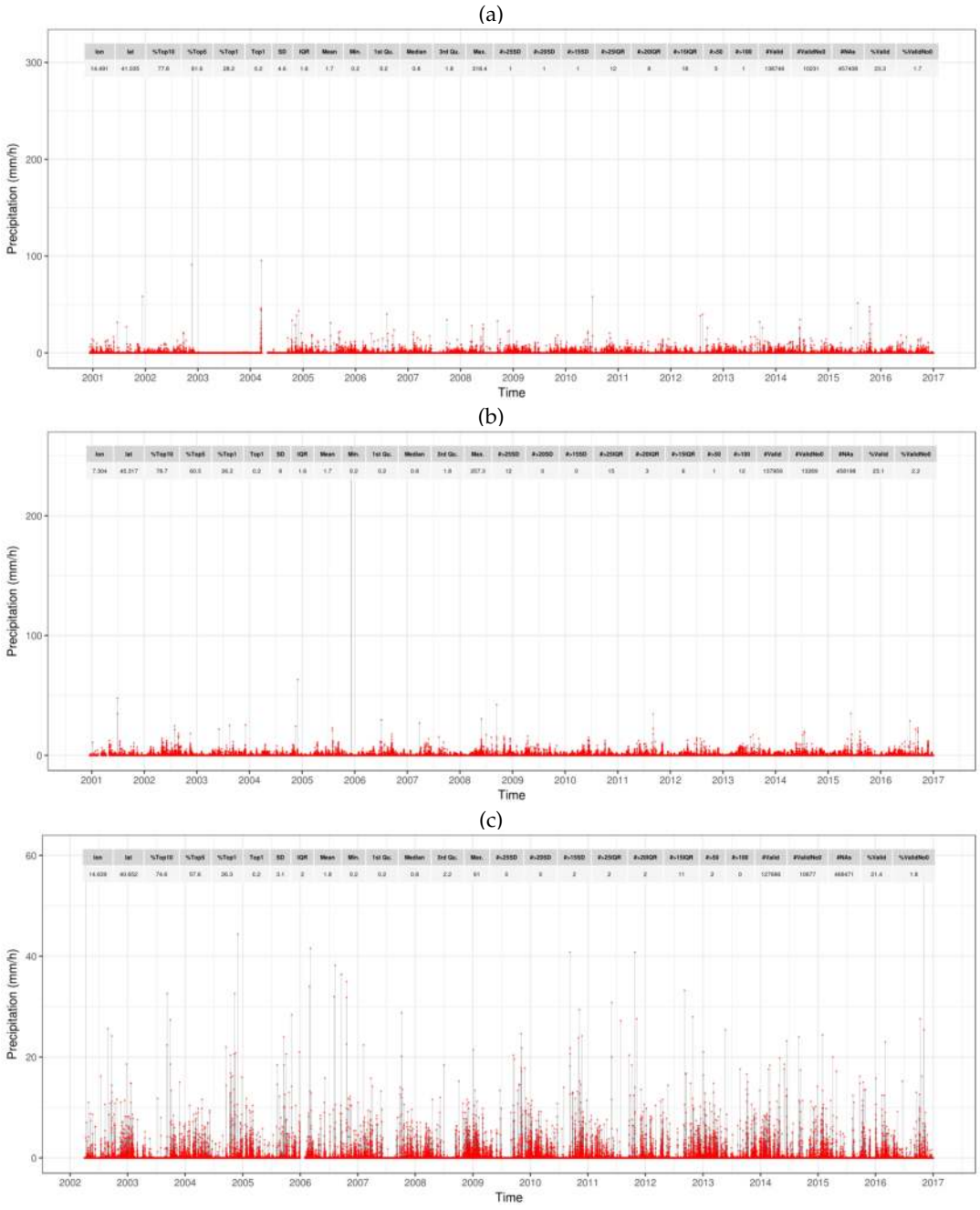

FIGURE 3.5: Three example precipitation timeseries from stations located in (top to bottom) Arienzo (Naples), Ala di Stura (Turin) and Maiori (Salerno). In panel a, the continuous zero values in 2003 indicate a stuck sensor. In panel b, a clear outlier at the end of 2005 can be considered an instrumental fluke with high certainty, due to the extremely high value above historical records. Panel c instead shows a station remarkable for its consistency and quality. Tables with some of the statistics computed for each station are also shown at the top of each panel.

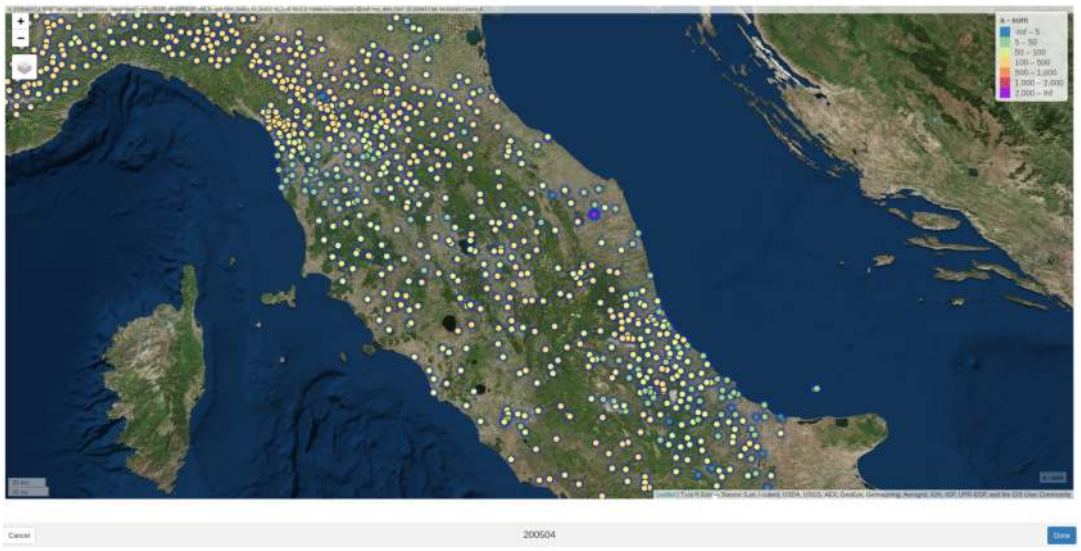

FIGURE 3.6: Example screenshot of one of the steps in the manual cleaning procedure for the hourly precipitation dataset GRIPHO. Here, for each month, stations are plotted on an interactive map coloured by their total precipitation amount. Clicking on a station pops up a timeseries plot for that station (figure 3.7), so that several neighbouring stations can be easily compared; clicking the blue circle surrounding a station selects it for exclusion from the dataset.

and one for extreme step changes with the previous/next timestep (100 mm h^{-1}). If these thresholds are exceeded more than 100 times in any given year, the entire year is removed. This filtering are carried out by the data provider, Marco Verdecchia, on the original binary data.

3. Second flagging of the values identical to step 1, to verify changes after the filtering occurred in 2. The results, shown in table 3.2, show that the vast majority of suspicious values are removed after the initial cleaning procedure. In particular, 99.7% of precipitation events above 100 mm h^{-1} are found to be unrealistic; the reduction drops to 76.3% for events between 50 and 100 mm h^{-1}. In total, 82.1% of the total flags are removed by applying this simple technique.

4. Visualisation and selection of problematic months for each station using some of the metrics of point item 1, aggregated on monthly scale and displayed via 192 (16 years $\times$ 12 months) interactive web maps (figures 3.6 and 3.7), in which suspicious stations for each month are manually compared with their neighbours and, if considered unreliable, removed.

As a result of this cleaning process, the reduction in the total number of valid data points results to be modest and especially concentrated in the last few years (figure 3.8). A brief overview of the improvement on the data quality obtained thanks to these simple procedures will be presented in section 3.4.

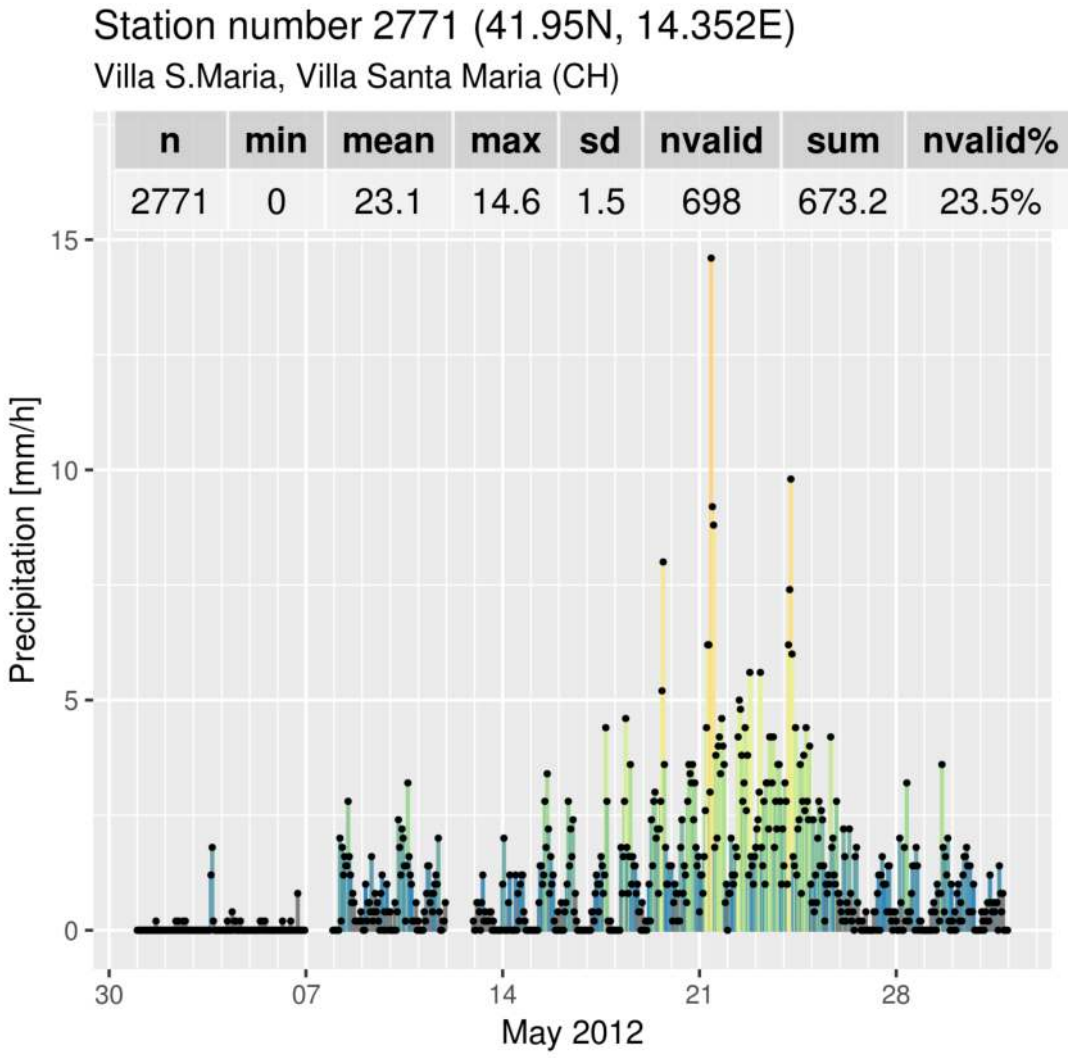

FIGURE 3.7: Example precipitation timeseries for May 2012 for a station in Southern Italy. Graphs like this are used to compare neighbouring stations in the procedure of figure 3.6. About 360000 of these graphs were generated.

Metric	Meaning
Total valid values	Number of values in the whole time series which are not one of the strings considered NA or negative
pr > Mean + nSD	Number of values greater than n standard deviations from the mean; $n = 10, 15, 20$
pr > Median + nIQR	Number of values greater than n interquartile ranges from the median; $n = 10, 15, 20$
100 > pr > 50 mm/h	Number of values greater than 50 mm h^{-1}, but smaller than 100 mm h^{-1}
pr > 100 mm/h	Number of values greater than 100 mm h^{-1}
%Top n	Percentage of values among the top n most common values, excluding 0; $n = 1, 5, 10$
% valid values	Total percentage of valid values
% valid values $\neq 0$	Total percentage of valid values which are not equal to 0

TABLE 3.1: Description of all the metrics used for flagging suspicious values before and after the first automated cleaning procedure, and for selecting complete months to remove in the last manual process.

Metric	Original	Filtered	% change
Total valid values	250M	244M	-2,6%
Total flags	324468	58008	-82.1%
pr > Mean + 20SD	3240	2538	-21.7%
pr > Median + 20IQR	49753	22519	-54.7%
100 > pr > 50 mm/h	21758	5171	-76.3%
pr > 100 mm/h	221822	711	-99.7%

TABLE 3.2: Selected metrics for suspicious values before and after automatic first stage filtering. See table 3.1 for a description of all metrics.

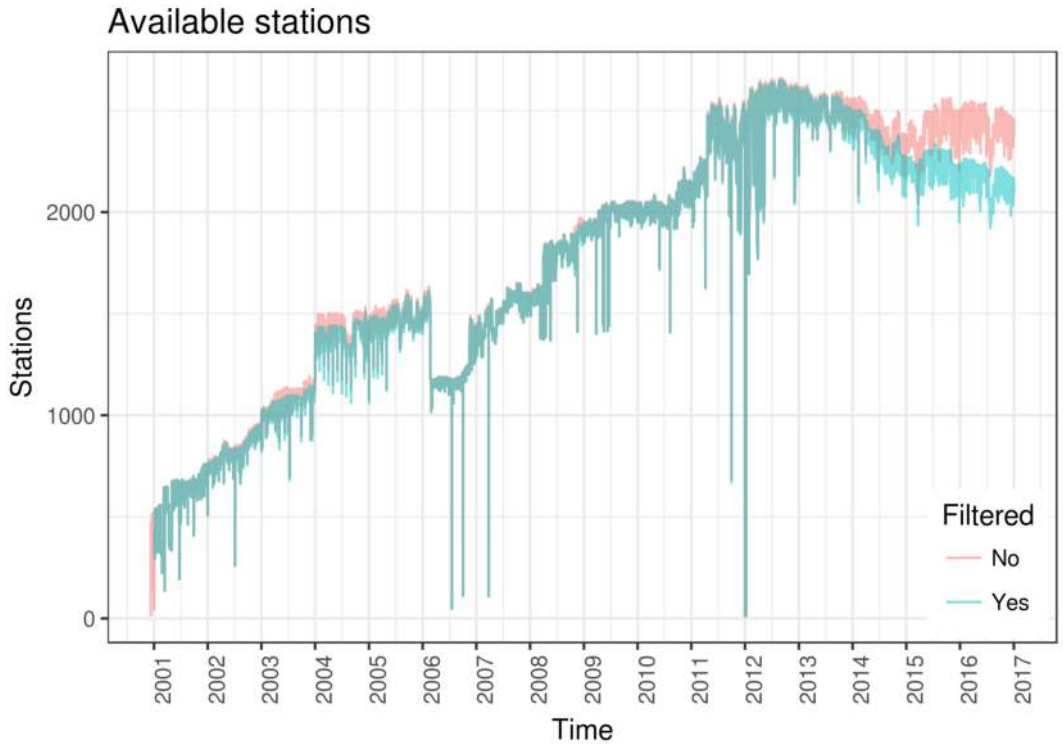

FIGURE 3.8: Timeseries of the number of available stations for each timestep in the input data for the Italian in-situ dataset, before and after the first-stage filtering.

3.3 Gridding and output format

To be able to compare the precipitation data with other similar products and with models, interpolating the station point data onto a grid is a necessary step. Our first approach to this issue uses a simple interpolation method; different techniques are currently being tested. The upcoming sections consist of a general view of the challenges that had to be faced, and the technical choices that were consequently made, while gridding the precipitation dataset described in this chapter.

3.3.1 Overview of gridding techniques

The interpolation of sparse data is a vast topic, with tens of different methods available, each with its own advantages and disadvantages. There is no general consensus on which is the best method for precipitation, which is particularly difficult to treat due to the extremely local aspect of the phenomena, both in time and in space (this is especially true in summer, when most precipitation is of convective nature). The precipitation datasets available over Europe (including those in table 2.1) use a plethora of different gridding techniques, some of which are listed in the following.

The de-facto standard E-OBS dataset (Haylock et al., 2008) uses a three step process:

daily anomalies are applied with kriging over a monthly field obtained by spatial splines, taking into account the station elevation for the monthly averages. The high-resolution EURO4M-APGD Alpine dataset (Isotta et al., 2014) opts for a similar approach with a base field calculated with an adapted PRISM method (Daly et al., 1994; Schwarb et al., 2001) and daily values obtained via a modified version of the SYMAP algorithm, which is a form of inverse distance weighting (Shepard, 1984); this algorithm (adapted by Antolini et al., 2016) is also used to produce the ARCIS dataset (Pavan et al., 2018). KLIMAGRID (Mohr, 2008, 2009) instead chooses an approach based on Delaunay triangulation, in order to minimise smoothing at station points and keep extremes intact. The HYRAS (Rauthe et al., 2013) high-resolution dataset over Germany uses the REGNIE method (Weerts et al., 2008): for each different climatological area, mean fields and climatologies are calculated using least-squares multiple linear regression (against location, slope, height and exposition) and inverse distance weighting. The Austrian dataset SPARTACUS (Hiebl and Frei, 2017) calculates a base field with kriging and topographic predictors, to which SYMAP daily anomalies are applied.

To our knowledge, there is limited literature comparing the performance of these interpolation methods for high-resolution gridded precipitation data. A general validation was carried over by Hofstra et al. (2008), which ultimately resulted in the choice of interpolation technique for the E-OBS dataset mentioned above.

3.3.2 The chosen spatial grid

The choice of grid is dictated by station density and convenience. With an average station spacing of about 10 km, the grid choice fell on the 12 km EURO-CORDEX one used by the Regional Climate Model RegCM. The resulting 95×110 grid (figure 3.9) has a constant grid spacing of 12 km on a Lambert Conformal Conic projection. Unlike more common regular latitude-longitude grids, using a curvilinear grid preserves constant grid cell areas, which simplifies later calculations.

3.3.3 Gridding procedure

In this work, due to technical constraints, a simple interpolation technique (which minimises the smoothing of extreme phenomena) is chosen to regrid the cleansed station data obtained after the manual and automatic filtering steps seen in section 3.2[3]. The method is based on SciPy's (Jones et al., 2007) `interpolate.griddata`, which employs the Qhull library[4] (Barber et al., 1996). Both the linear and the cubic variant were taken into consideration, but since no significant climatological difference was found between the two methods, the linear version was employed. This method

[3] The regridding software was adapted for use on this project from a program provided by Graziano Giuliani from Earth System Physics (ESP) section of the International Centre for Theoretical Physics (ICTP), who also helped at various stages of this project with general software consulting. Graziano's help was irreplaceable and greatly appreciated.

[4] http://www.qhull.org

FIGURE 3.9: Grid of the hourly rain dataset GRIPHO over Italy, projected over Esri© World Imagery tiles in Mercator projection (EPSG code 3857).

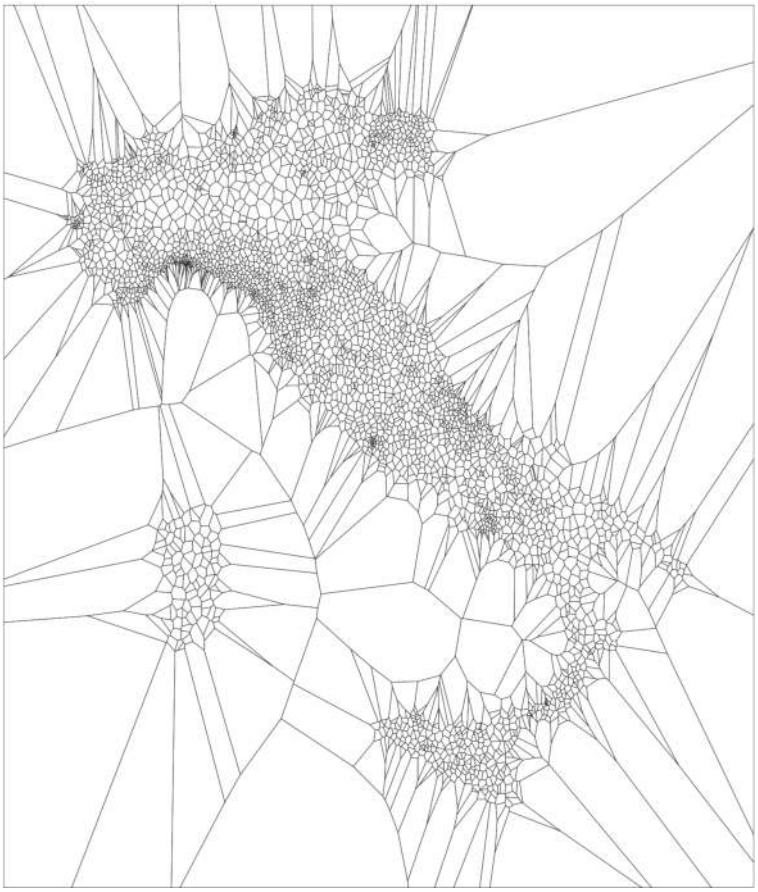

FIGURE 3.10: Voronoi diagram corresponding to the Delaunay triangulation of all stations. Example given for the timestep with the highest number of valid stations for the gridded Italian station-based precipitation dataset GRIPHO.

performs a Delaunay triangulation (Aurenhammer, 1991) on all the available points separately for each timestep, creating a grid of triangular cells whose corner values are linearly interpolated to evaluate the cell values on the underlying rectangular grid. In this sense, this procedure is similar to the works of Mohr (2008) and Velasquez et al. (2011), which also used Delaunay triangles to perform interpolation of sparse rainfall data sources. An example Voronoi diagram associated to the Delaunay triangulation of the timestep containing the highest number of stations is showed in figure 3.10. After the interpolation, values over the sea are forcefully set to missing. The result of the interpolation is, of course, more reliable for periods and regions with high station density; for this reason regions with low station density are also set to missing during the interpolation procedure. This results in a dataset which can have both spatial and temporal empty zones, which is similar to what other station-based datasets have (the E-OBS dataset from Hofstra et al., 2008, for example, also has varying missing values). The interpolation was separately carried out in parallel for each time slice, with no information crossing time boundaries. Figure 3.11 shows the Probability Density Function of GRIPHO in its gridded and non-gridded (raw) form: as expected,

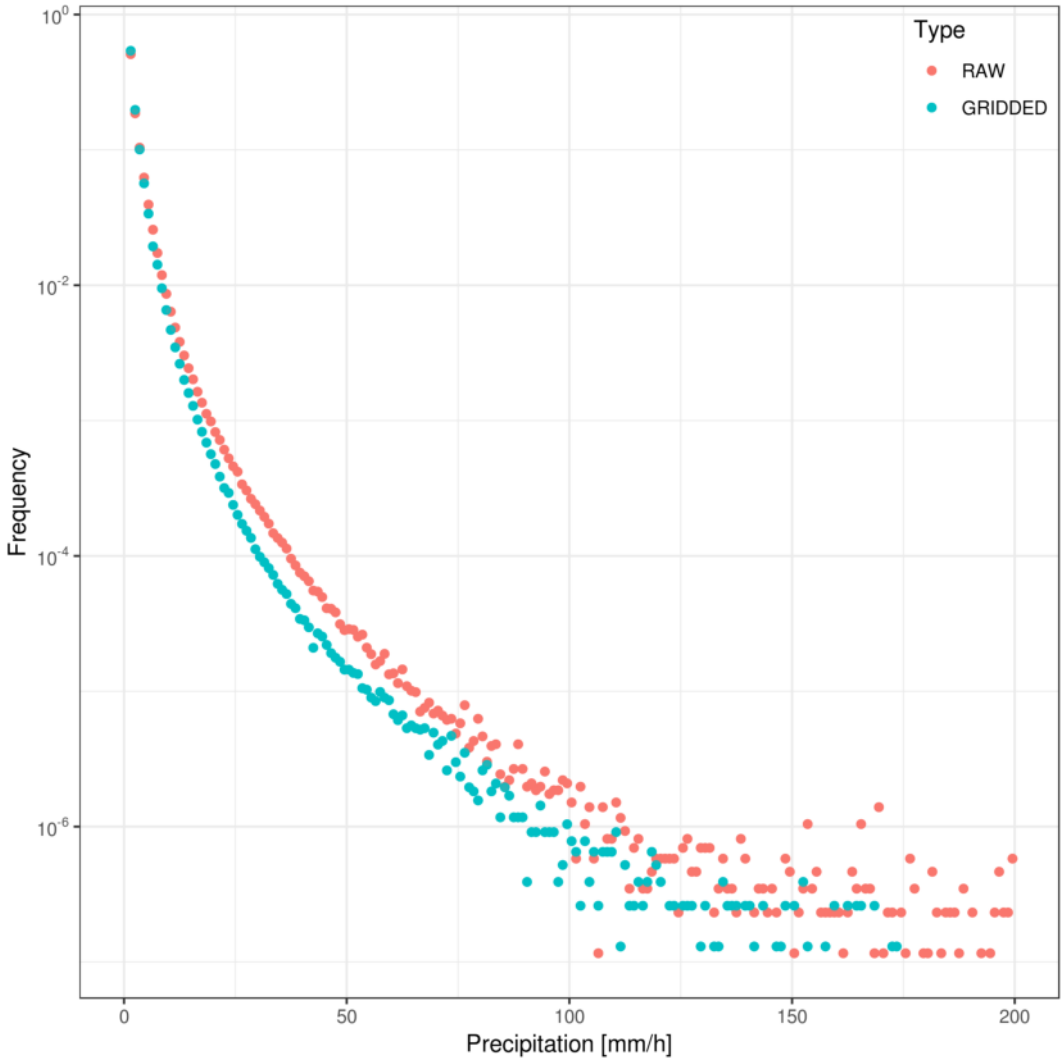

FIGURE 3.11: Comparison of the precipitation distributions from the gridded (teal) and raw (red) hourly precipitation datasets. As is to be expected, gridding introduces a general smoothing of precipitation extremes.

gridding introduces a general smoothing of precipitation extremes. The effect is however quite small, thanks to the choice of interpolation method, and most extreme events are retained. Compared to most of the techniques seen in section 3.3.1, this approach is much faster but also more basic; improving this method will certainly be the goal of future research. Additional information on the interpolation methodology, including tests with different algorithms, are presented in (Fantini et al., 2019, in preparation).

3.3.4 Output format

Once again, the chosen output format is CF-compliant losslessly-compressed netCDF-4. The complete GRIPHO dataset resulted in 192 monthly files, for a total of 561021

quarter-hourly timesteps over the 95×110 grid. The total size of the dataset is 647 MB when adding up the sizes of each separate month, or 507 MB if considering a single aggregated file; the two sizes differ because of the higher compression efficiency resulting from compressing the single, larger file. For the aggregated file, the compression ratio, when compared to an uncompressed dataset, is $44x$.
Due to the aforementioned low amount of sub-hourly values an additional, hourly dataset was created by aggregating sub-hourly data. This version has 140256 timesteps and is 404 MB in size.

For ease of use and download, both these versions were also further compressed by applying a lossy procedure, reducing data precision to 0.1 mm h^{-1}. In these versions, the data is stored as short (16-bit) integers, instead of 32-bit floats; a CF-standard `scale_factor` attribute indicates these are to be rescaled to floats when read. This further reduces the size of the dataset to 248 MB, or 184 MB for the hourly version.

An additional GRIPHO version, containing a variable optimised for reading along the time axis, one timeseries at a time, was also produced. These multiple versions should cover all possible needs and requirements of potential users, and exceed the technical standards usually followed in producing observational datasets for climate.

3.4 Validation against other precipitation datasets

In this section, the new gridded hourly precipitation product presented in this chapter is validated against some of the datasets available over the Italian territory (see section 2.1.3 and table 2.1). Only a basic validation is presented herein, further analysis is described in detail in Fantini et al. (2019, in preparation).

3.4.1 Methodology and metrics

Due to the lack of a suitable reference hourly dataset, the validation is carried out solely on the daily scale; analysis on the hourly scale is planned as a future research path. As reported in section 3.2, the GRIPHO dataset had several optimisations: in the following sections GRIPHO will be analysed both in its final form and in a version obtained after the first, automated cleaning (but without the subsequent manual procedures), in order to evaluate the effectiveness of these procedures. In the figures, this version is referred to as "Station (interp.)"
Four main metrics are presented here: annual cycle, mean seasonal precipitation, extreme seasonal precipitation ($R95_{ptot}$ and $R99_{ptot}$, see section 2.1.4) and precipitation distribution (Probability Density Functions). Similarly to the analysis carried out in section 2.1.4, annual cycles and PDFs are subdivided by region: North, Centre, South and Islands. Other than the product presented here, the datasets taken into consideration are EURO4M-APGD and ARCIS (only available in the North) and E-OBS and the HMR reanalysis (for the whole Italian territory). The nominal resolution of EURO4M-APGD, ARCIS and HMR is superior to that of GRIPHO. The ability to

reproduce fine spatial details is however linked with station density: the EURO4M-APGD dataset, for example, is estimated to have an actual resolution of 15 km or less (Isotta et al., 2014). Similarly to section 2.1.4, an observational period of 2000 to 2016 is considered, limited to 2008, 2013 and 2015 in the case of EURO4M-APGD, HMR and ARCIS respectively due to limited data availability.

3.4.2 Results

The annual cycle of precipitation (figure 3.12) has a similar shape in all six datasets, with differences in precipitation intensity: E-OBS usually results the driest, and GRIPHO the wettest. The filtering procedure of section 3.2 successfully removes a spurious peak in the August in the Islands, but has little to no impact on the average annual cycle of the other regions.
Figure 3.13 shows the spatial distribution of mean seasonal precipitation. The spatial patterns and precipitation amounts in Northern Italy are remarkably similar to those from ARCIS and EURO4M-APGD. In the other regions, GRIPHO results wetter than E-OBS and HMR, while showing similar spatial patterns with the latter. The filtering process successfully removes some suspicious high precipitation values in Veneto (north-east, DJF) and (centre-east, JJA), but does not filter out an excessive high value in the Southern tip of Sicily.

Extreme precipitation metrics (figure 3.14, $R99_{ptot}$ not shown) once again show similar spatial patterns in the North compared with ARCIS and EURO4M-APGD and for the whole Italian region, especially compared with HMR especially. Several extreme precipitation highs, such as the East coast of Sardinia in winter and parts of Calabria in autumn, are reproduced by both GRIPHO and HMR, but not as much by E-OBS. The comparison of the first two rows of each plot shows that the manual filtering managed to significantly reduce what appears to be extreme precipitation excess in several areas, such as Abruzzo, Veneto, Valle d'Aosta, Sicily and Tuscany. However, some extremes, most notably in Sicily and in Abruzzo, seem to have escaped the manual checking. For these, a second manual check will be necessary in a future version of GRIPHO.

The analysis of precipitation PDFs (figures 3.15 and 3.16) shows how GRIPHO contains more extreme events, compared to E-OBS and HMR, in all four regions. In the North, the difference with ARCIS and EURO4M-APGD is less striking, and all the datasets perform similarly, albeit GRIPHO seems to show some slightly more intense events than the ones in the other observational datasets. Considering that none of these datasets include any kind of undercatch correction, this increase in extreme events is hard to evaluate. This metric also shows very well how the filtering procedure significantly reduces the amount of extremely high precipitation events. For the North, Centre and Isles the maximum amounts are decreased in all seasons, while no change is detected for the South of Italy.

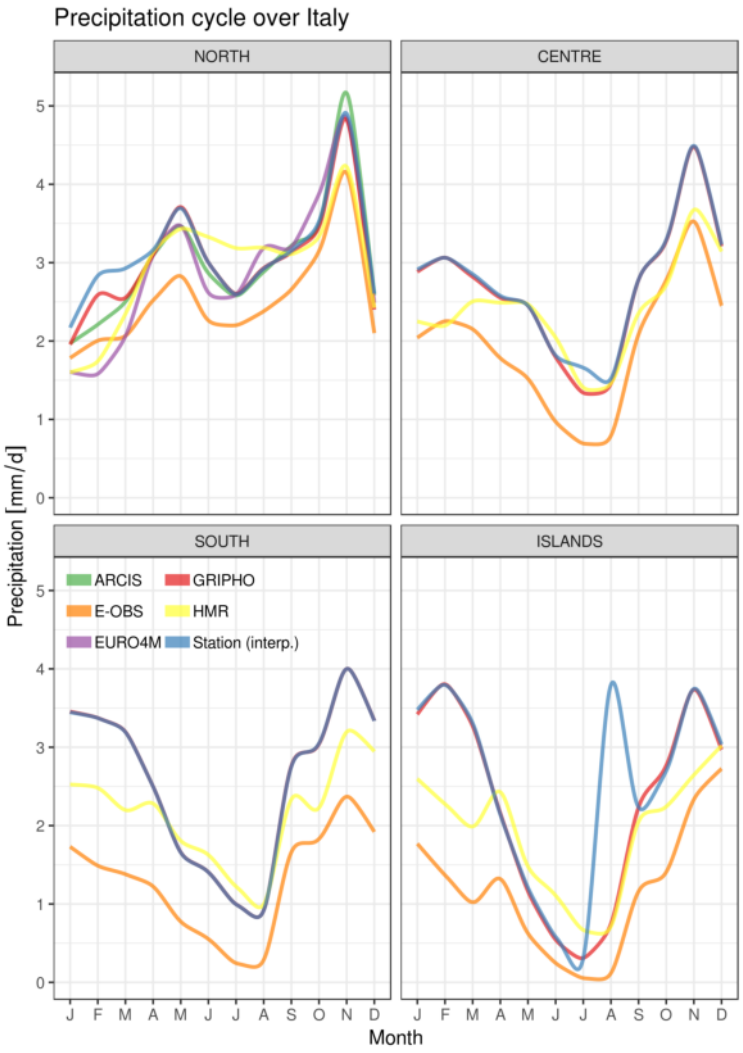

FIGURE 3.12: Average precipitation annual cycle for for the validation of the gridded hourly precipitation dataset. The four summarising regions are highlighted in figures 3.13 and 3.14.

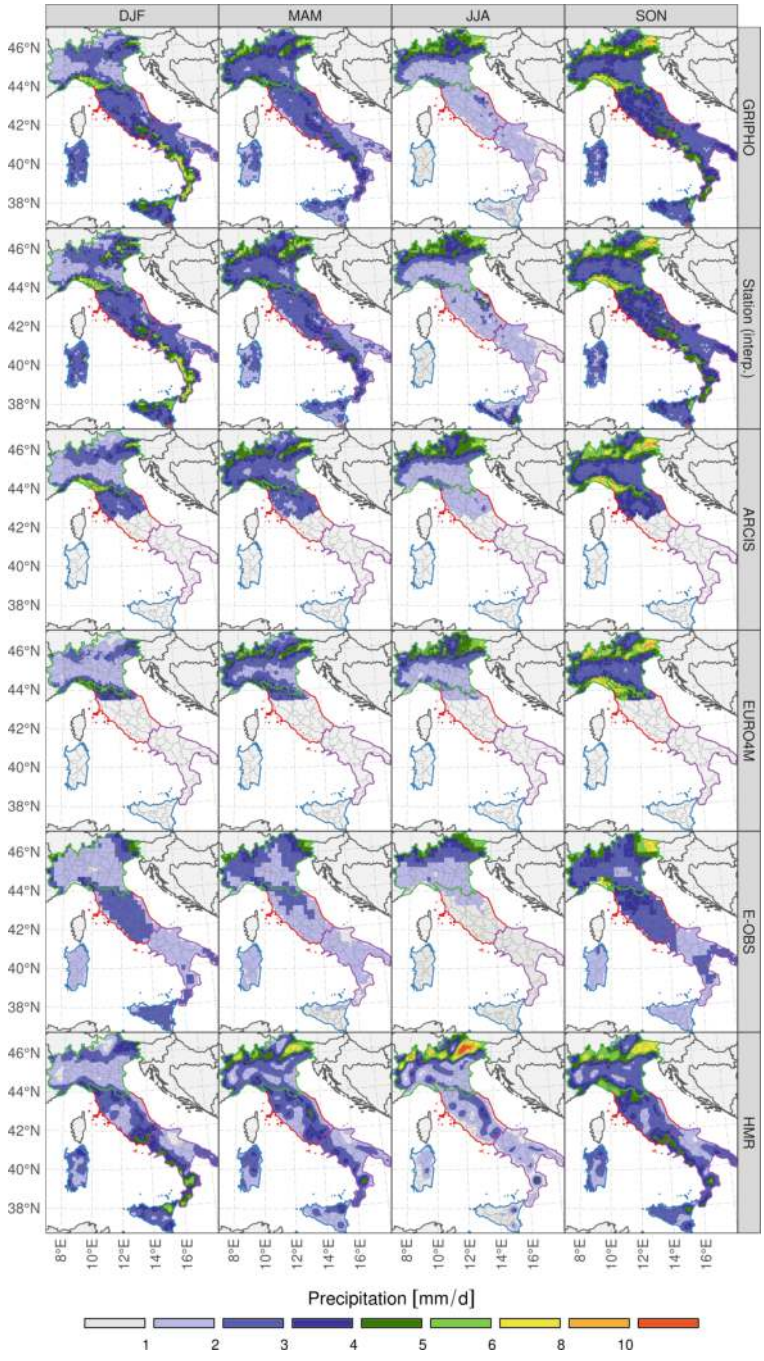

FIGURE 3.13: Average precipitation for the validation of the gridded hourly precipitation dataset. The four summarising regions for the annual cycle (figure 3.12) and the PDFs (figures 3.15 and 3.16) are highlighted in green (North), red (Centre), purple (South) and blue (Islands).

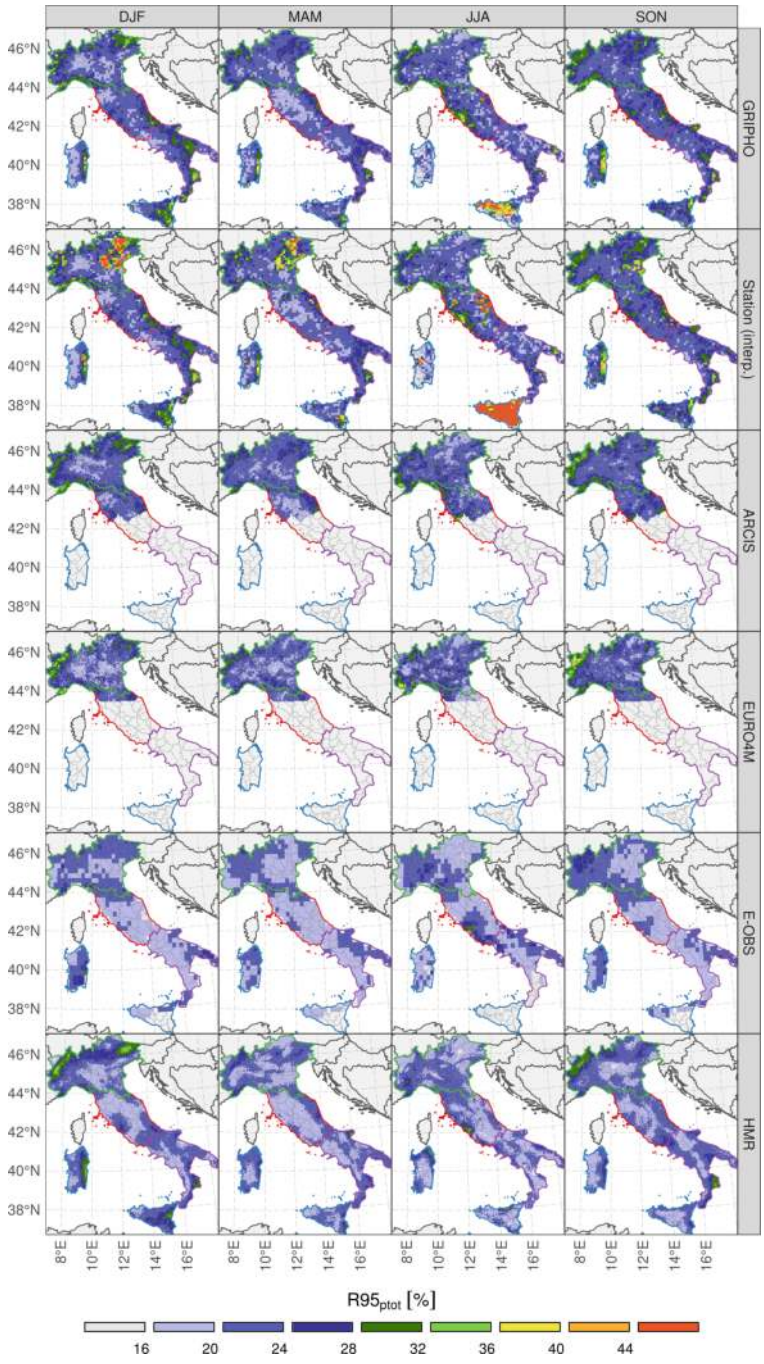

FIGURE 3.14: Extreme R95$_{ptot}$ precipitation for the validation of the gridded hourly precipitation dataset. R95$_{ptot}$ represents the percentage of precipitation due to precipitation events above the 95th percentile.

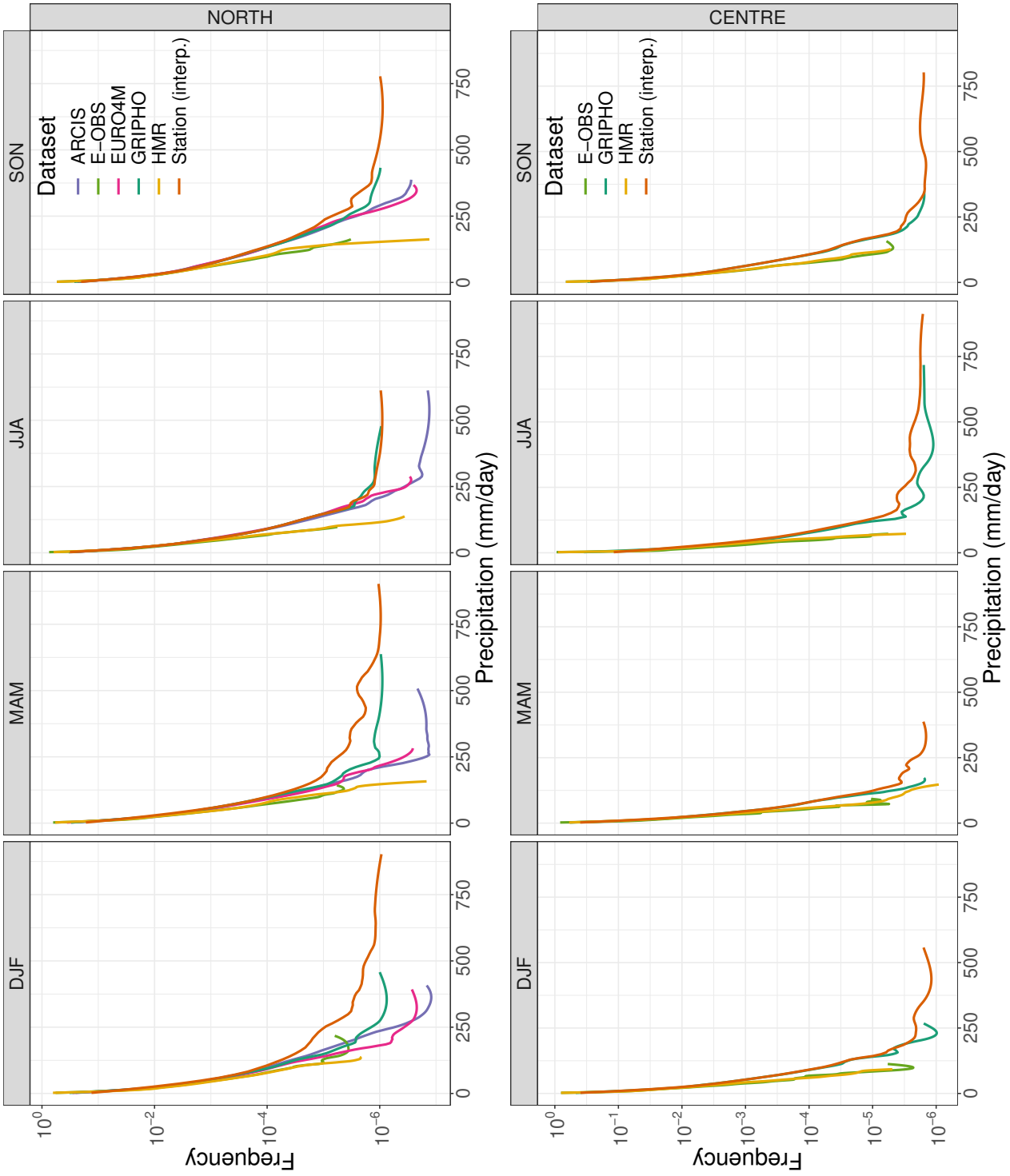

FIGURE 3.15: Daily precipitation Probability Density Functions for the validation of the gridded hourly precipitation dataset for the North and Centre regions. The four summarising regions are highlighted in figures 3.13 and 3.14.

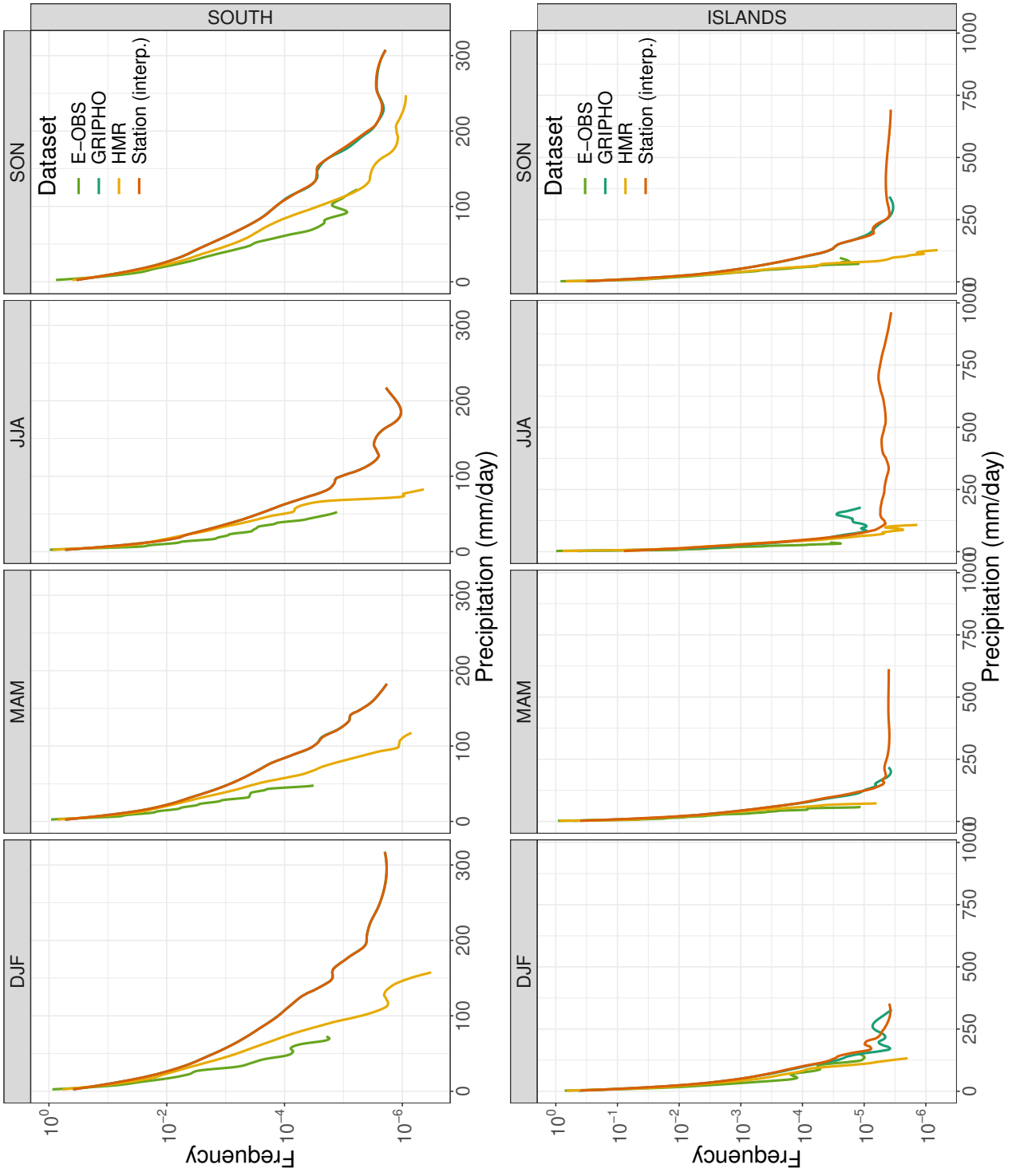

FIGURE 3.16: Daily precipitation Probability Density Functions for the validation of the gridded hourly precipitation dataset for the South and Islands regions. The four summarising regions are highlighted in figures 3.13 and 3.14.

3.5 Summary and outlook

The hourly precipitation dataset GRIPHO represents a first of its kind for the Italian territory. The somewhat limited time availability of the dataset (little more than 15 years) is unfortunate, but no additional data was available for before 2000. The high spatial and temporal resolution are superior to those of E-OBS, which is still the only observation-based dataset available over the whole Italian region. Compared to the ARCIS and EURO4M-APGD datasets, which are only available in Northern Italy, the effective spatial resolution is similar, but the hourly temporal resolution is much finer. Thanks to the high station density, reproduction of extreme events is improved, in particular if compared to E-OBS. The GRIPHO dataset has shown sufficient quality for it to be used to drive the hydrological model CHyM, which is at the core of this thesis work, and to validate the climate simulations performed by RegCM, as detailed in the upcoming chapters.

Availability and additional details on this dataset will be made available in an upcoming paper (Fantini et al., 2019, in preparation), where

- the unexpected behaviour of extreme events in Sicily and Abruzzo will be fixed by applying a further manual conditioning step;
- an analysis of hourly precipitation will be included;
- the choice of interpolation method will be discussed further;
- validation against further datasets available for the area only on a monthly timescale (e.g. the ISAC/CNR dataset) will be included.

Chapter 4

Methods and models

The aim of this project is to evaluate flood hazard in Italy, and to project this evaluation in a possible future scenario. In order to obtain discharge and flood information a hydrological model is used to simulate runoff over the domain. Runoff can then be analysed statistically to provide proxies for floods (such as metrics of extreme discharge) or to drive hydraulic floodplain simulations, capable of spreading the water over the terrain and produce flood extents and water depths.
Figure 4.1 shows flow chart of the thesis work.

The precipitation data that are the main input needed to run hydrological simulations come from two different sources:

High-resolution observations the GRIPHO dataset, described in chapter 3, which provide high-resolution hourly precipitation data.

Regional Climate Model simulations two climate simulations, one run in perfect boundary mode and one with a climate projection.

Section 4.1 will detail the RCM model and simulations, while section 4.2 will describe the hydrological model of choice and its three simulations. Section 4.3 will delineate the statistical procedure used to derive the extreme discharge statistics from the discharge timeseries. Finally, section 4.4 will present the hydraulic model and its simulations.

4.1 The RegCM Regional Climate Model

The ICTP RegCM is a Regional Climate Model developed at the ICTP and maintained primarily by Graziano Giuliani. The project is under very active development and new features, options and schemes are routinely added. RegCM is used by several institutions and research groups worldwide.
The RegCM model was the first limited area model to be developed for long-term climate simulations (Dickinson et al., 1989; Giorgi and Bates, 1989). The model went through the second (Giorgi et al., 1993), third (Pal et al., 2007) and fourth (Giorgi et al., 2012) major revisions and is currently at version 4.7.0.

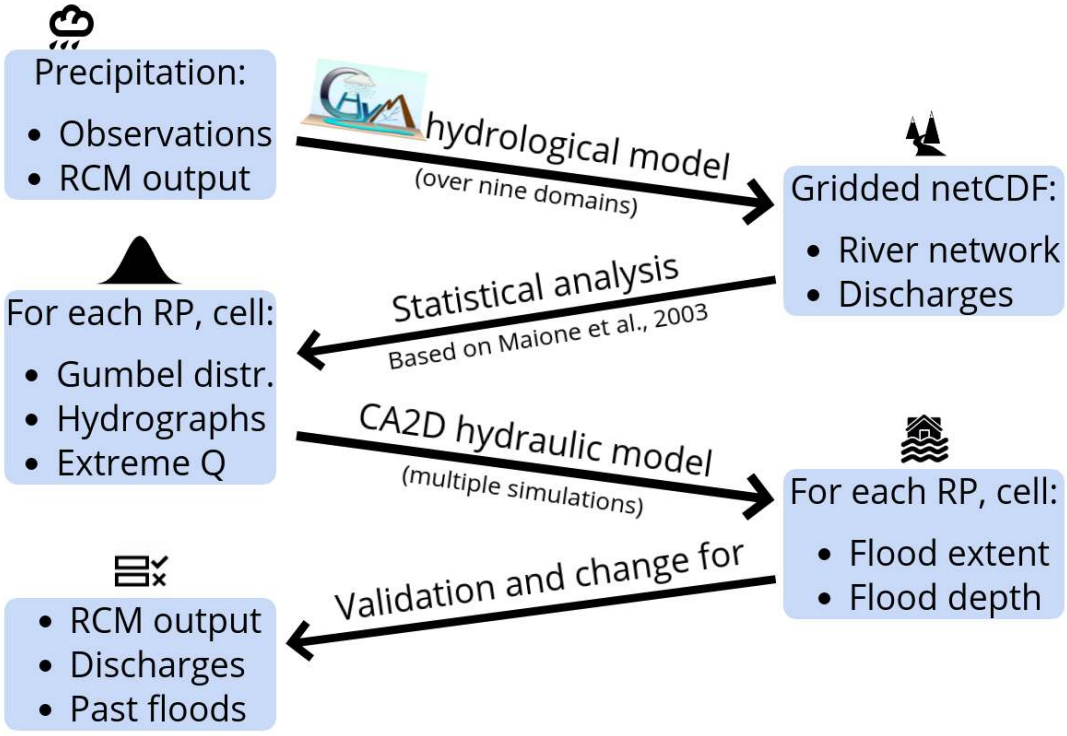

FIGURE 4.1: A schematic description of the methodology employed in this study.

RegCM is a compressible, terrain-following sigma-vertical coordinate model, offering a large selection of physical parameterisations. The dynamics are essentially the same as the NCAR Mesoscale Model 4 or 5, depending on the versions and settings (MM4, MM5, Grell et al., 1994). Recently, the implementation of a non-hydrostatic core from MM5 has allowed to run in convection-permitting mode. RegCM is mainly written in the Fortran programming language and is compliant with the Fortran 2003 ANSI standard; as most other climate models do, RegCM reads and writes files in the netCDF format.

4.1.1 Regional Climate Models: an overview

Regional Climate Models (RCMs) are Limited Area Models (LAMs) usually nested on larger datasets. RCMs are the most common tool used to "zoom in" on a specific area by dynamically *downscaling* lower-resolution climate data. They do this by processing the information provided by the driving dataset at the domain boundaries, adding value thanks to the higher resolution and consequent more accurate representation of physical processes.

The first Regional Climate Models were initially developed in the late ´80s (Dickinson et al., 1989; Giorgi, 1990; Giorgi and Bates, 1989) to perform short, few-days simulations at best. In subsequent years, their use was extended to perform multi-year simulations (Giorgi et al., 1993; Jones et al., 1995). In the last two decades, several

research programs utilising RCMs were put forward to advance the knowledge of climate at small spatial scales: of these, the most recent is the Coordinated Regional Climate Downscaling eXperiment (CORDEX, section 4.1.2).
In the nesting regional climate modelling technique, large scale (atmospheric and oceanic) time-dependent fields drive a higher resolution model over a limited domain. The driving data acts as boundary condition to the driven model and provides the initial conditions. In most cases a one-way nesting scheme is used: the nested model does not influence the boundary driving data, i.e. there is no feedback from the nested model to the coarser model. However, two-way coupled simulations, in which feedback from the driven model is incorporated in the boundary conditions, can be performed with some models (Inatsu and Kimoto, 2009; Lorenz and Jacob, 2005).
By design, RCMs necessitate of external forcings that act as boundary conditions. These are usually of three kinds:

- Model *reanalysis*, such as ERA-Interim (Dee et al., 2011), are weather model simulations of the past which are constrained by a plethora of observed quantities through a complex process of data assimilation. The resulting dataset is uniform in time and space, consistent with observations, physically coherent, and provides all the necessary variables to drive an RCM. Such "perfect boundary condition" simulations are usually performed to validate the ability of an RCM to reproduce a reliable climate.
- Global Climate Models (GCMs) are physical simulations of the general circulation, much like RCMs, however with global extent and, thus, no external forcing other than the initial conditions. GCMs are the most natural choice for long climate projections; they usually have a resolution which, due to computational constraints, is significantly lower than that of RCMs.
- RCMs themselves can be used as driving data for even higher resolution simulations, in what is usually called a multi-nesting simulation. Such simulations are becoming more and more common thanks to the development of convection-permitting models (Clark et al., 2016; Prein et al., 2015), which often have a resolution of 2 km or less and require high-resolution driving data.

Due to the presence of lateral boundary conditions, RCMs necessarily need to take into consideration a so-called *buffer zone*: a number of cells close to the domain edge in which the dynamical equilibrium between the driver and the driven model can be reached and smaller-scale features can develop. The same is true for an initial *spin-up* period, usually of up to one or two years, which is excluded from analysis.

4.1.2 The CORDEX project

In order to properly validate whether climate models perform well, and whether RCMs add value to GCMs and reanalysis, a large number of ensemble simulations,

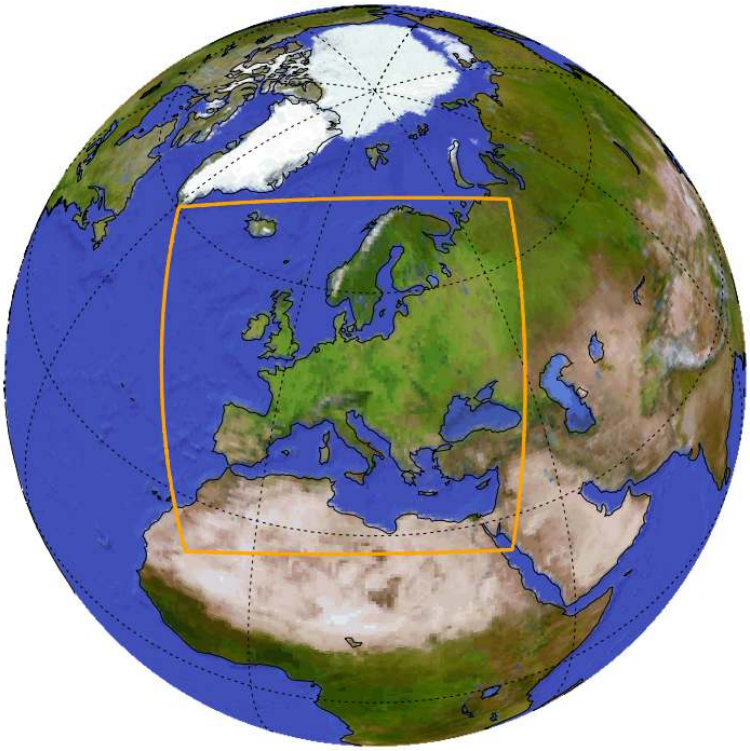

FIGURE 4.2: The approximate EURO–CORDEX domain, from http://www.cordex.org/domains/cordex-region-euro-cordex/

performed on common domains, is advisable. Several international projects have historically provided the basis for this kind of analysis. Some of these are PIRCS, START, CECILIA, CLIM-RUN, MICE, STARDEX, PRUDENCE, SPECS, EUPORIAS, ENSEMBLES, and CORDEX. CORDEX[1] (Giorgi and Gutowski, 2015; Giorgi et al., 2009; Gutowski et al., 2016), a World Climate Research Programme (WCRP) sponsored project, is a framework for downscaling a large number of GCMs using both dynamical and statistical downscaling techniques. 14 common domains are specified (Africa, MENA, North, Central and South America, Antarctica, Arctic, EURO, MED, Australasia, East, Central, South and South-East Asia), mostly covering areas from previous intercomparison projects, with pre-defined resolutions and projections. Two European domains are defined, one covering all of the continent (Jacob et al., 2014, EURO–CORDEX) and one focusing on the Mediterranean (Ruti et al., 2016, Med–CORDEX). Institutions are asked to provide data with a grid resolution of around 12, 25 or 50 km; as will be shown in section 4.1.4, the domain chosen in this work covers the EURO–CORDEX area (figure 4.2) at a resolution of 12 km.

4.1.3 Added value of RCMs

Why use Regional Climate Models, when Global Climate Models are a ever-improving, tried-and-tested approach to simulating climate? The answer is that, even with

[1] CORDEX stands for Coordinated Regional Climate Downscaling eXperiment

today's increasingly powerful computational resources, GCMs are still run at a resolution of several tens of kilometers: for example, the latest Coupled Model Intercomparison Project 6 (CMIP6, Eyring et al., 2016) includes the High Resolution Model Intercomparison Project (HighResMIP, Haarsma et al., 2016), whose simulations are supposed to run with a resolution of "at least 50 km". By contrast, *convection-permitting* RCM simulations with spatial resolutions close to that at which the hydrostatic approximation starts failing (about 10 km Giorgi and Mearns, 1999) are not a rarity anymore (e.g. Clark et al., 2016; Coppola et al., 2018; Prein et al., 2015). Thanks to the increased resolution, the main added value of RCMs is connected with their ability to reproduce otherwise unattainable small scale features (figure 4.3). This is possible because of the better representation of:

Orographic forcing Increased resolution means increased ability to represent slopes, peaks and valleys. Variables that show a pronounced elevation dependency, such as precipitation, temperature and wind speed, greatly benefit from higher ground resolution. This is especially true for complex mountain areas (see e.g. Fischer et al., 2014; Giorgi and Bates, 1989).

Direct representation of processes Some parametrisations can be eliminated altogether at very high resolutions, opting instead for direct representation of the processes. This is the case with the already mentioned convection-permitting models, in which convection is resolved explicitly.

RCMs, thus, usually add information to the global models which they are driven, if there are available observations of sufficient quality and resolution to assess this. This added information, if correct, is referred to as "Added Value". It may seem obvious that increasing the resolution will improve the skill in reproducing climate. However, added value is often hard to predict and identify, as it does not vary linearly with grid size nor is equal on different domains. As the IPCC (IPCC WG1, 2013, section 9.6.3) puts it:

> Although there are indications that model skill increases with higher resolution, it does not do so linearly. Rojas (2006) found more improvement when increasing resolution from 135 km to 45 km than from 45 km to 15 km. Walther et al. (2013) found that the diurnal precipitation cycle and light precipitation improved more when going from 12 km to 6 km resolution than when going from 50 km to 25 km or from 25 km to 12 km. Higher resolution does enable better simulation of extremes (Seneviratne et al., 2012). For example, Pryor et al. (2012) noted that an increase in RCM resolution from 50 km to 6 km increased extreme wind speeds more than the mean wind speed. Kawazoe and Gutowski (2013) compared six RCMs and the two GCMs to high resolution observations, concluding that precipitation extremes were more representative in the RCMs than in the GCMs. Vautard et al. (2013) found that warm extremes in Europe

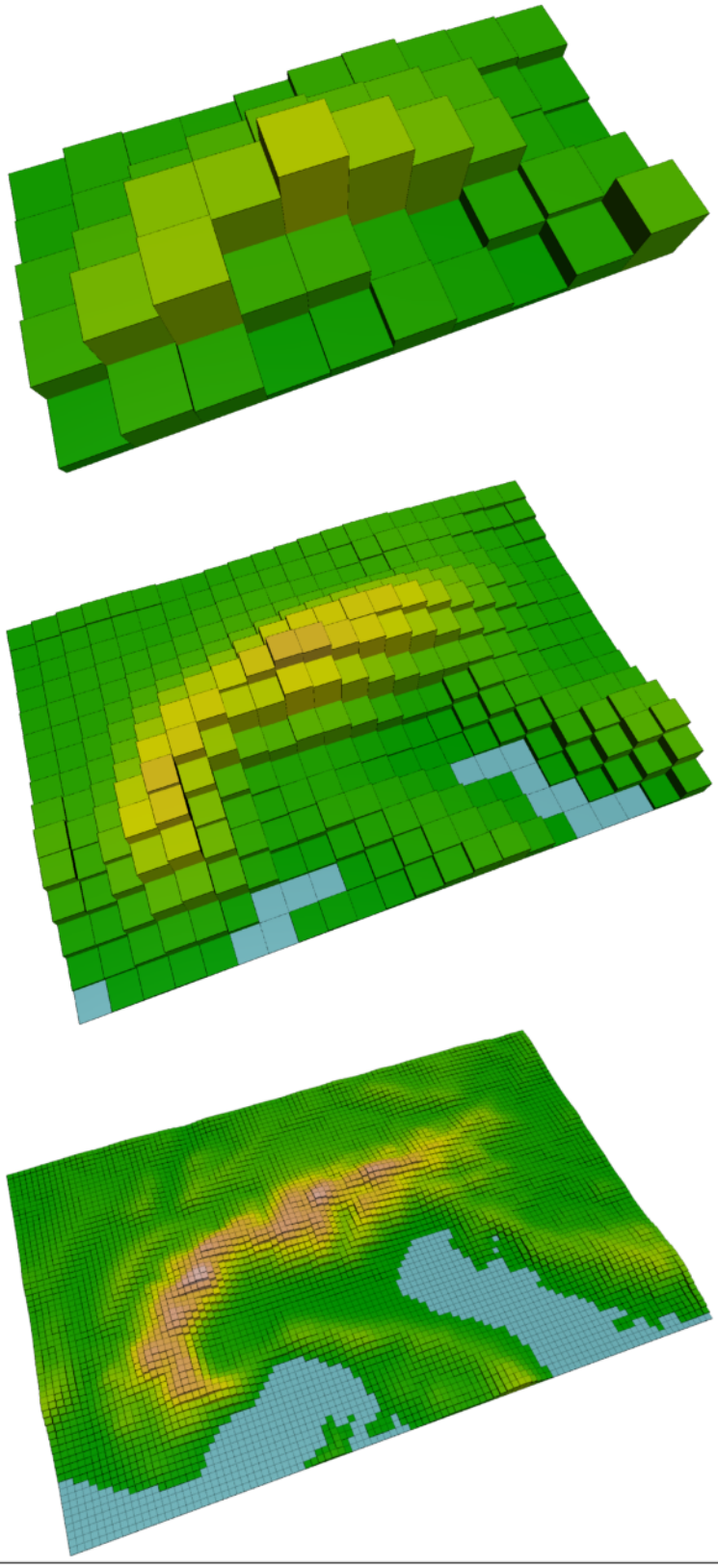

FIGURE 4.3: Representation of topography over the Alps at different resolutions: 1.50°, 0.44° and 0.11°, corresponding to the typical resolutions of GCMs, low-res RCMs and high-res hydrostatic RCMs respectively.

> were generally better simulated in RCMs with 12 km resolution compared to 50 km. Kendon et al. (2012) and Chan et al. (2012) found mixed results in daily precipitation simulated at 12 km and 1.5 km resolution, although the latter had improved sub-daily features, perhaps as convection could be explicitly resolved.

Due to the importance of a reliable representation of extreme precipitation events for flood hazard, the added value that high resolution can provide for this variable deserves greater attention. In a recent study, Fantini et al. (2016) compared 9 EURO– and Med–CORDEX RCMs against high resolution regional observations for several metrics, of which two are extreme precipitation metrics. The performance of the models was assessed at two different resolutions (0.11° and 0.44°). In most regions, the higher resolution RCMs showed better ability to reproduce extreme precipitation compared to the lower resolution ones: in the daily precipitation Probability Density Functions (figure 4.4), for example, the only case in which the performance was clearly degraded (when going from the 0.44° to the 0.11° ensemble) also coincided with the region characterised by the lowest density of stations (the Carpathians); other regions mostly showed better performance on part of the 0.11° ensemble. RCMs performed also significantly better than the driving ERA-Interim (Dee et al., 2011) in all metrics (and in particular in extreme precipitation).
The results of this work are in general agreement, for what concerns extreme precipitation, with other similar works, such as Casanueva et al. (2016), Di Luca et al. (2011), Lucas-Picher et al. (2017), Prein et al. (2016) and Torma et al. (2015), reinforcing the evidence supporting the presence of strong added value for extreme precipitation events in high-resolution RCM simulations. As a result of these considerations, the ICTP RegCM Regional Climate Model was selected to drive the hydrological simulations, both in the present day and in a future scenario. Due to limitations in time and computational resources, no additional model was selected to perform an ensemble simulation in order to reduce uncertainty; this, however, might be an interesting topic for future research.

4.1.4 RegCM experiments

In the framework of this thesis, two regional climate simulations with the ICTP RegCM Regional Climate Model are carried out, both on the complete European continent. One simulation is driven by the European Centre for Medium-range Weather Forecasts (ECMWF) ERA-Interim reanalysis (Dee et al., 2011) and spans 1979–2016, the other is driven by the Met Office Hadley Centre HadGEM2 CMIP5 Global Climate Model (Collins et al., 2011) and covers the period 1971–2099, under the IPCC Representative Concentration Pathway 8.5 (RCP8.5, IPCC, 2008; Riahi et al., 2007). This business-as-usual scenario represents the worst-case future, in which no climate change mitigation measures are taken. This second simulation is part of the

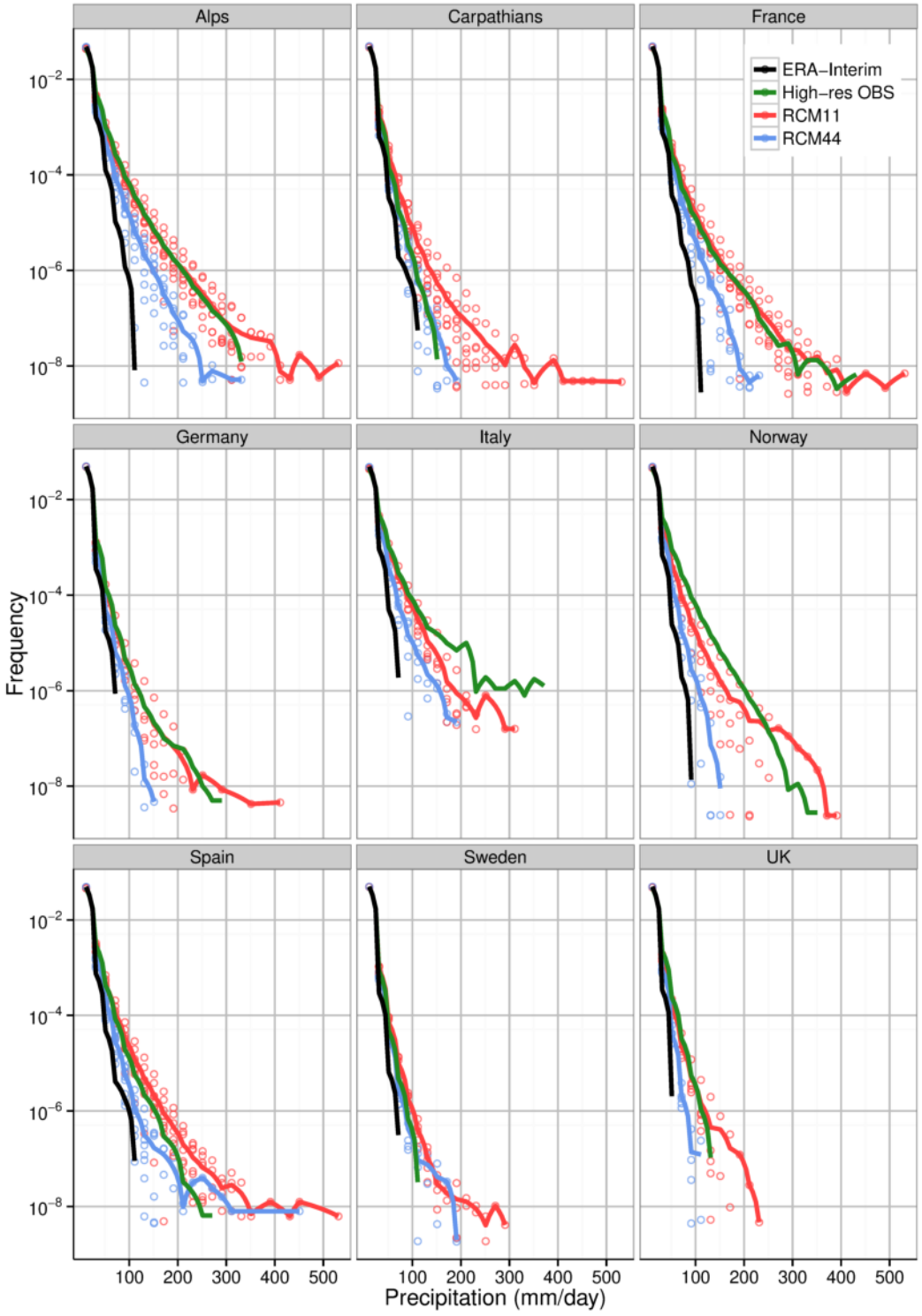

FIGURE 4.4: Probability Density Functions (PDFs) for the ensemble average of the 9 models considered in Fantini et al. (2016) over the 9 regions where high-resolution observations were available. In black, the driving ERA–Interim data; in blue and red, the 0.44° and 0.11° ensembles respectively; in green the regional observations.

PRINCIPLES[2] project.

In order to avoid the several pitfalls in defining a domain and to keep the simulation within the CORDEX project, the EURO-CORDEX domain (figure 4.2) was chosen, with a model resolution of 12 km on a Lambert Conformal Conic projection. RegCM has been run on this domain before, so no adjustment to the domain position, size, and resolution was needed. The initial testing started with the tagged version 4.5.0, but, after subsequent versions were released, the latest (at the time of starting the runs) RegCM 4.6.1 was selected for both simulations.

Model tuning was manually performed by simulating 3-year chunks and comparing them, after removal of a 1-year spinup period, with precipitation and temperature observations from the E-OBS dataset (Haylock et al., 2008). In the case of the simulation driven by the ERA-Interim reanalysis, the first one to be submitted, 92 different tests had to be performed before choosing the final configuration. The simulation driven by HadGEM2, which was started later and whose tuning started off of the first simulation's parameters, required 43 calibration iterations[3].
The first simulation ran on the ICTP ARGO cluster[4] using, on average, 200 processors, for a total actual runtime of about 2500 hours (0.5 million core-hours) for its 38 years of simulation. The second simulation, which extended to 2099 with about 130 years of simulation, was run on the CINECA MARCONI cluster[5] Skylake partition using an average of 816 processors per run, for a total actual runtime of about 3000 hours (2.5 million core-hours) and 90 TB of disk usage before post-processing.
The analysis of the two RegCM simulations will be presented in section 5.1.1.

4.2 The CETEMPS Hydrological Model CHyM

The CETEMPS Hydrological Model (CHyM[6], Coppola et al., 2007; Tomassetti et al., 2005) is a distributed (gridded) hydrological model which simulates surface water runoff, evapotranspiration, percolation, infiltration, melting and return flow. The model uses information from a Digital Elevation Model (section 2.4) to reconstruct a D8 river network employing cellula automata algorithms (Coppola et al., 2006, 2007), and works by assimilating input precipitation from different sources. Routing water through each grid cell is achieved using continuity and momentum equations based on the kinematic shallow water wave approximation of Lighthill and Whitham (1955). The current implementation, provided the necessary input data (at least soil type, elevation, precipitation and temperature), can run on any domain and at any

[2] Producing RegIoNal ClImate Projections Leading to European Services, https://www.gerics.de/science/projects/detail/071974/index.php.en

[3] After the testing phase and the simulation of the historical period, James Ciarlo' from the Earth System Physics (ESP) section of the International Centre for Theoretical Physics (ICTP), took charge of the RegCM simulation driven by HadGEM. Thanks James!

[4] http://argo.ictp.it/

[5] https://www.cineca.it/it/content/marconi

[6] http://cetemps.aquila.infn.it/chym/

resolution.
CHyM was previously used for assessing the hydrological conditions of the Po basin under global warming (Coppola et al., 2014), and is currently used operationally[7] at the CETEMPS Center of Excellence to forecast potential floods using stress indexes (Tomassetti et al., 2005; Verdecchia et al., 2008). The nine Italian domains on which CHyM is operationally run are the same that will be employed in this thesis.

Although part of the model database is stored in Fortran-style binary files, the model was recently updated by Fabio Di Sante and Graziano Giuliani to produce output in the netCDF format, which facilitates postprocessing and analysis. In order to ease the simulation setup, analysis, and monitoring, several tools were put into place to postprocess CHyM output. These include:

- a graphical tool named *chymview* to quickly and effectively visualise simulation outcome;
- automatic tools for the submission of cluster jobs;
- parallel programs for the final postprocessing and rechunking of time-slice netCDF data, for fast reading of discharge timeseries.

4.2.1 Domains and river networks

The first step in simulating the hydrology of the Italian territory is the division in subdomains and the creation of a reliable and plausible river network for each region. As mentioned in the previous section, Italy is already fully covered by nine operational CHyM domains, on which the model has already been run and calibrated over several years of operational work. The domains cover, approximately:

- the Po river basin
- Liguria
- Central Italy
- North-Eastern Italy
- Central-Southern Italy
- Calabria
- Sicily
- Sardinia
- Central-Northern Italy

Figure 4.5 shows the nine domains over the complete Italian territory; some overlap between the domains is necessary in order to include all basins of interest for each

[7] See `http://cetemps.aquila.infn.it/chym/newoper/`, where the current situation is updated daily

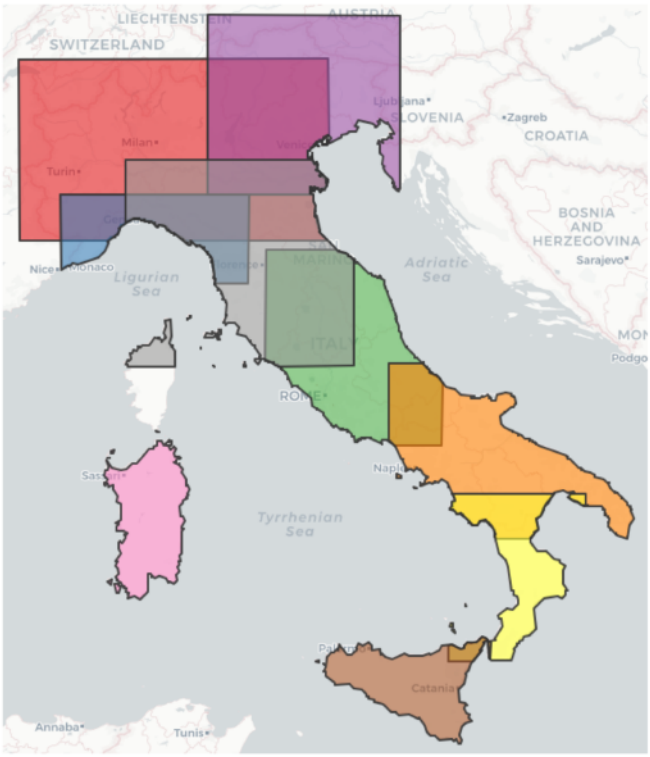

FIGURE 4.5: The nine domains on which the CHyM model is run operationally, which coincide with the domains used in this work.

domain. The setup, resolution and physical configuration for each of the nine domains is different and based on the values suggested by CETEMPS; in particular, resolution ranges from about 300 m (for Liguria, Calabria, Sicily and Sardinia) to about 900 m (for the Po river domain).

Reproducing the river network for all domains represented a challenge. CHyM uses several cellula automata algorithms to smooth the DEM, find no-flow spots, and connect them to the appropriate cells. In this application, a reliable estimation of river network is crucial, in order to be able to assess inundation using the hydraulic model (see section 4.4). Initial tests with the default 300 m Italian DEM shipped with CHyM did not lead to satisfactory results. After further testing and tuning, we resorted to the HydroSHEDS hydrologically-conditioned DEM, which allowed for a more precise representation of river channels, thanks to the built-in river carving. The configuration for the DEM smoothing and connection algorithms was tuned by automatically running several hundred preprocessing cycles with different parameters; the resulting river networks were then manually selected via an interactive web map (see figure 4.6 for an example). Especially in the case of the Po plain, which is extremely flat and is simulated at a coarse resolution, the final reconstructed river network is within the limitations imposed by the resolution of the DEM. Additional tests at an higher model resolution did slightly improve the river representation, but also increased the computational cost significantly.

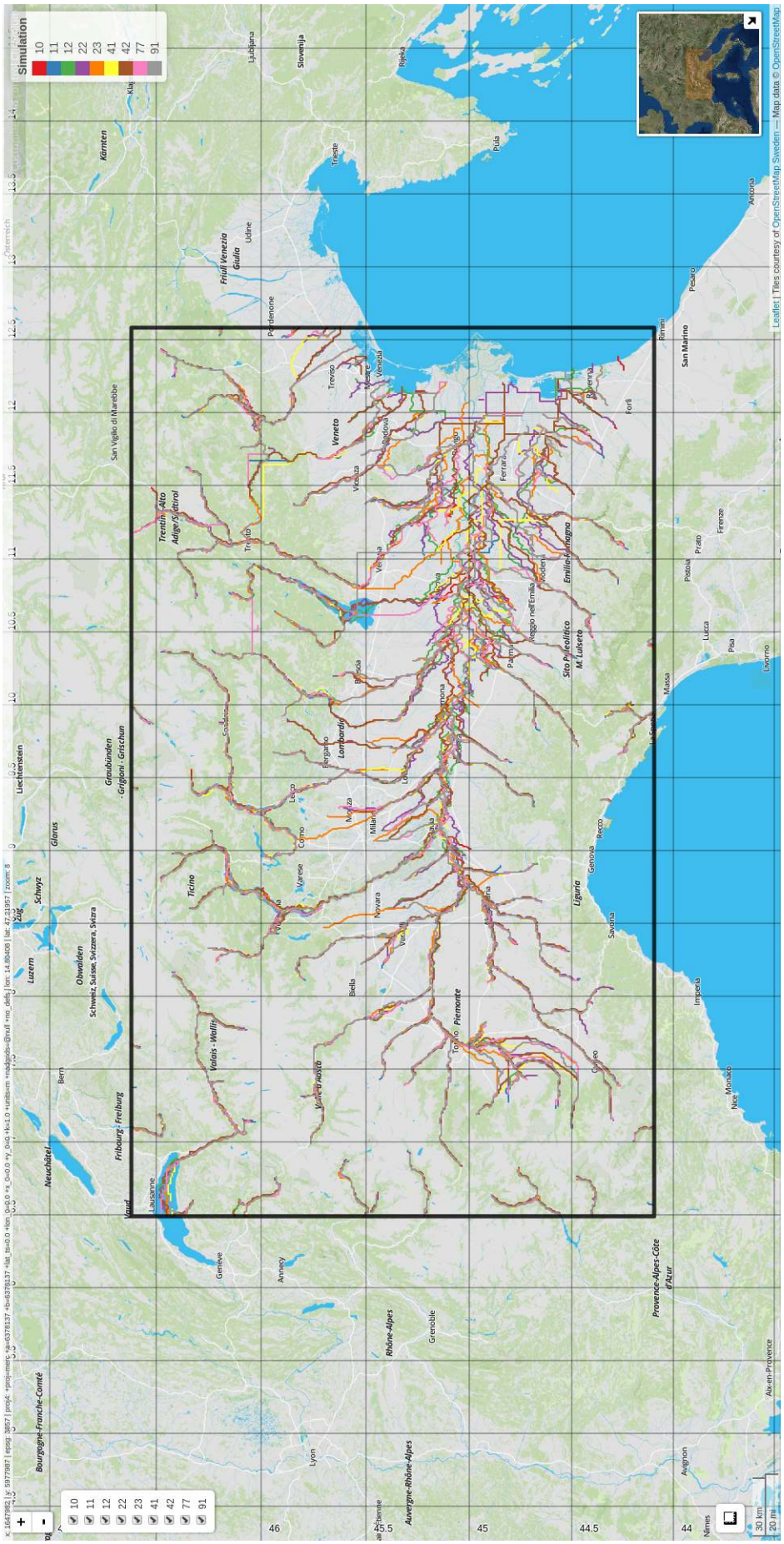

FIGURE 4.6: Example of the river network creation experiments in the Po river basin. In order to obtain the most reliable representation of rivers, the candidate river networks are manually evaluated on top of a real world map.

Driver	Period	Cluster	Disk usage
Observations	2001–2016	ARGO	5.6TB
RegCM (ERA-Interim)	1979–2016	ARGO	7.2TB
RegCM (HadGEM)	1971–2099	MARCONI	21TB

TABLE 4.1: Details on the three CHyM simulations. The disk usage refers to the final usage of the postprocessed output.

Discharge stations (see section 2.2) have been manually repositioned on the simulated river network to insure proper comparison between model and observations.

4.2.2 The three simulations

Three CHyM simulations were run using the same configuration. They differed in the driving component: one was driven by the GRIPHO observational data presented in chapter 3, one by the ERA-Interim-driven RegCM simulation, and one by the HadGEM-driven RegCM simulation (see table 4.1). Each simulation was run on all the nine regions, for a total of 27 simulations. GRIPHO's spatial and temporal coverage of the domains is not complete due to periods where station data is missing: the regions of Sicily and Puglia, in particular, are only covered for around 60% of the timesteps over the 2001–2016 period. For any timesteps and areas with missing data, daily weather forecasts performed with the operational MM5 model (Grell et al., 1994) were used to fill in the gaps. The MM5 model has been in use at CETEMPS for this particular purpose for almost two decades; for what concerns validation on the specific domain of application see, for example, Bianco et al. (2006).

The computational requirements necessary to run CHyM are much lower than those of RegCM, but running on a cluster is still advisable. The HadGEM-based simulation was run, similarly to its RegCM driver (see section 4.1.4), on the CINECA MARCONI cluster, while the other two simulations were run on the local ICTP ARGO cluster. Although the CHyM model is parallel, its scaling is weak: for this reason, it was run limiting to one single compute node in both clusters (20 and 48 cores for ARGO and MARCONI SKL respectively). However, the nine separate domains were run in parallel, effectively greatly reducing simulation time, which amounted in total to approximately 3000 runtime hours (or about 100000 core-hours) and almost 35 TB of postprocessed output data.

4.3 The climatological-hydrological-hydraulic approach

The flood hazard estimation method developed in this project follows the footsteps of similar approaches as illustrated in section 1.2.2: a hydrological model (section 4.2), driven by observations (chapter 3) or by a Regional Climate Model (section 4.1), reproduces discharge data over several different Italian domains and for a period of several years; these discharges are then fitted statistically to an extreme value

distribution which allows to extend the simulation of extreme events to any Return Period, with decreasing accuracy as the rarity of the event increases. The typical discharge for a selected number of Return Periods for each point is then modelled via a hydraulic model ((section 4.4)) to produce flood extent maps. In our case, the statistical procedure, studied and devised by Francesca Raffaele from the ICTP's ESP section, is based on the work of Maione et al. (2003), who present a procedure for the construction of "typical" flood discharge curves (called Synthetic Design Hydrographs) for any point of a river. Maione et al. (2003) derive their methodology by estimating SDHs for gauged sites in the Po river basin, and extending the SDH definition to ungauged sites with a relation depending on the drained area. This allows for a unique, consistent methodology to be applied across the whole catchment for every river cell — in our case, the derivation of the SDHs is performed for selected locations along the river network (see section 4.4), starting from CHyM discharge data (section 4.2). In the following, the technical details and the formulae necessary to perform the calculations which result in the input data for the hydraulic model are described.

Given any river or station point, from model or observed data, the input to the statistical analysis is the complete timeseries of discharge for that specific location. Other than this, the analysis we performed is completely independent of location, albeit a few assumptions had to be made to generalise the process.
The aim is to obtain curves describing, for the given Return Period, the typical discharge timeseries of the event at that river point. These $Q_{RP}(t)$ curves will be called Synthetic Design Hydrographs (SDHs) and give the discharge (Q) of a typical extreme event as a function of the Return Period (RP) and the time (t). SDHs are required by the hydraulic model (see section 4.4) to simulate flood extent.

We start by defining the Flow Duration Frequency reduction curve (FDF) ($Q_D\,(RP)$, which is the discharge averaged over a duration D (usually in hours) around the flood peak with Return Period RP. As a consequence, the instantaneous FDF ($D = 0$) represents the peak flood discharge $Q_0\,(RP)$. The FDF is usually obtained from statistical analysis of historical hydrographs, but its formulation, as we shall see, can be generalised.

Similarly to the work of Maione et al. (2003), we perform with the reasonable assumption that the reduction ratio (ε_D), which is the ratio of the FDF and the peak flood discharge ($Q_0\,(RP)$), is constant for any Return Period RP, so that:

$$\varepsilon_D = \varepsilon_D\,(RP) = \frac{Q_D\,(RP)}{Q_0\,(RP)}\,, \tag{4.1}$$

which means that the reduction ratio only depends on the duration D, as also reported by the Natural Environment Research Council (Great Britain) NERC (1975). As in Maione et al. (2003), when performing the calculation of the FDF around each historical flood peak, the centring of the duration window of width D is chosen as to

maximise the average computed discharge Q_D:

$$\text{FDF} = Q_D = \frac{1}{D} max \int_t^{t+D} Q(\tau)\, d\tau\,, \tag{4.2}$$

where t and τ represent time. Note that the product $Q_D \times D$ represents in fact the volume of water flowed in the duration D. The shape of the final synthetic hydrograph will be determined by the peak-duration ratio r_D: the ratio of the time before the peak and the total duration D of the averaging window. The smaller the r_D, the more skewed the hydrograph will be towards steeper (flatter) rising (falling) limbs of the hydrograph. An example is given in figure 4.7, which shows a possible high discharge event and the graphical representation of the FDF.

Centring on $t = 0$ as the peak flood timing, the two limbs of the hydrograph can be described as:

$$\int_{-r_D D}^{t=0} Q(\tau) = r_D D Q_D(RP) \tag{4.3}$$

and

$$\int_{t=0}^{(1-r_D)D} Q(\tau) = (1-r_D)\, D Q_D(RP)\,, \tag{4.4}$$

where $Q_D(RP)$ is the typical FDF curve for the Return Period RP. The SDH is constructed imposing that the maximum discharges for each duration coincides with the value obtained from FDF curves. Differentiating with respect to D we get, for the falling limb:

$$\text{SDH} = Q_t(RP) = \frac{d/dD\left[(1-r_D)\, D Q_D(RP)\right]|_{D=D(t)}}{d/dD\left[(1-r_D)\, D\right]|_{D=D(t)}}\,, \tag{4.5}$$

where $t = (1-r_D)\, D$. Once the reduction ratio (r_D) and the FDF ($Q_D(RP)$) are known, this formula will allow to calculate the SDH.

In the context of this work, similarly to Alfieri et al. (2014), we chose to assume symmetry of the hydrograph, that is:

$$r_D = \frac{1}{2}\,, \tag{4.6}$$

meaning that the duration windows are always centered on the flood peak and that the peak is in the centre of the hydrograph. Additionally, by definition, this also results in $t = \frac{1}{2}D$.

The maximum flood discharge $Q_0(RP)$ for any given Return Period RP must then be calculated by fitting an appropriate extreme distribution. Following Alfieri et al. (2015a) and Maione et al. (2003), we chose the Gumbel distribution, so that:

$$Q_0(RP) = u - \alpha \ln\left[-\ln\left(1 - \frac{1}{RP}\right)\right]\,, \tag{4.7}$$

where the parameters u and α are estimated from the fit. Given the timeseries of

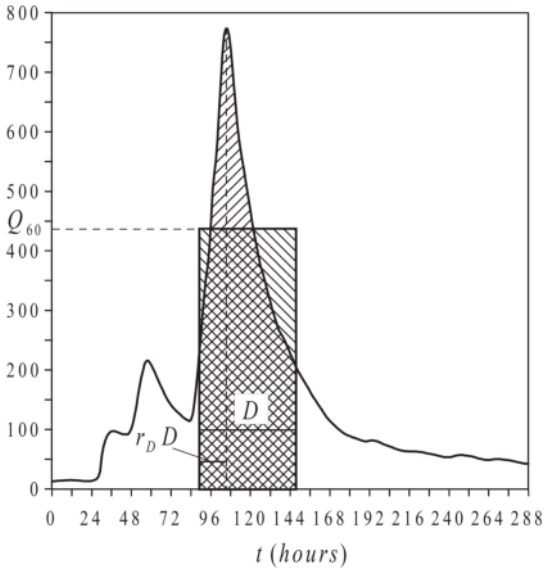

FIGURE 4.7: Example for the calculation of the Flow Duration Frequency curve, from (Maione et al., 2003, figure 1). D is the chosen duration (60 h in this image), r_D the peak-duration ratio, Q_{60} the value which maximises the integral of the discharge (or running average, for discrete data) for the given D.

yearly discharge maxima Q_y, the parameters are estimated by fitting equation (4.7) for the selected Return Period, using the following initial parameters for scale (α) and location (u):

$$\alpha = \frac{\sqrt{6}}{\pi}\sigma\left(Q_y\right) \quad ; \quad u = \mu\left(Q_y\right) - \gamma\alpha\,, \tag{4.8}$$

where γ is the Euler-Mascheroni constant (equal to approximately 0.5772) and μ and σ the mean and standard deviation operators respectively. Different fitting methods did not provide significantly different results in initial testing, so a simple maximum likelyhood method was selected.

We resort to the following approximation for the reduction ratio ε_D :

$$\varepsilon_D \simeq \sqrt{p_2\left[2 + p_1 - \frac{3}{2}p_2\left(1 - p_1\right)\right]}\,, \tag{4.9}$$

where

$$p_1 = e^{-4D/\theta} \quad \text{and} \quad p_2 = \frac{\theta}{2D} \tag{4.10}$$

and θ, the scale of fluctuation, is a parameter which, in our case, is considered to have a linear relationship with the drained area, as in Maione et al. (2003). The approximation in equation (4.9) is suited for large catchments; in this work, however, it is assumed to hold reasonably well for smaller basins. Differentiating equation (4.5),

the falling limb of the SDH can be expressed as:

$$\begin{aligned} \mathrm{SDH} = Q_t\left(RP\right) &= \frac{Q_o\left(RP\right)\left(p_2 - p_1 - p_2 p_1\right)}{\varepsilon_D} \\ &= \frac{\left\{u - \alpha \ln\left[-\ln\left(1 - \frac{1}{RP}\right)\right]\right\}\left(p_2 - p_1 - p_2 p_1\right)}{\sqrt{p_2\left[2 + p_1 - \frac{3}{2} p_2\left(1 - p_1\right)\right]}} \end{aligned} \tag{4.11}$$

This equation allows us to calculate a typical flood event discharge timeseries for any location and Return Period, starting only from the timeseries of yearly maximum discharges Q_y.

Tuning and testing for the method was carried over on the upper Po basin. The region was chosen due to previous experience with the hydrological model on this domain (Coppola et al., 2014), availability of reliable observed discharge data, and lack of large water management structures. Due to the relatively small size of the simulated domains, the calculation was carried over for durations up to 240 h. As highlighted, this approach requires some strong assumptions; the results however are reasonable despite these approximations. Estimating and reducing the uncertainty deriving from the mentioned assumptions would certainly be a possible avenue for future work. An example SDH, obtained from discharge data from the European Water Archive (see section 2.2) for a station on the Tevere river, is shown in figure 4.8; figure 4.9 instead shows the SDHs for the seven discharge stations in the MV1 dataset (which covers the Po river, see figure 2.10). The SDHs are similar to those produced by Maione et al. (2003), indicating that the procedure is correct.

This procedure, as shown in the following chapters, was applied both with observational data and with data coming from a Regional Climate Model. 9 domains covering the complete Italian territory were simulated, but no limitation is in place that would prevent this technique to be applied to any domain worldwide. For each domain, a large number of small flood simulations was performed in order to cover all segments of the river courses.

4.4 The CA2D hydraulic model

Floodplain hydraulic simulations are modelled with a modified version of the CA2D hydraulic model, initially introduced in Dottori and Todini (2010) and described and validated in great detail in Dottori and Todini (2011). CA2D is based on the LISFLOOD-FP model (Bates et al., 2005), a a coupled 1D/2D hydraulic model based on a raster grid which has been extensively used in flood hazard mapping (see e.g. Neal et al., 2011; Skinner et al., 2015; Thomas Steven Savage et al., 2016). Instead of solving the full shallow water equations, CA2D is a reduced complexity model which uses a 2D cellular automata approach. It is significantly faster than LISFLOOD-FP thanks to a number of optimisations and assumptions: in particular, an inertial formulation (Bates et al., 2010) for the computation of discharges and

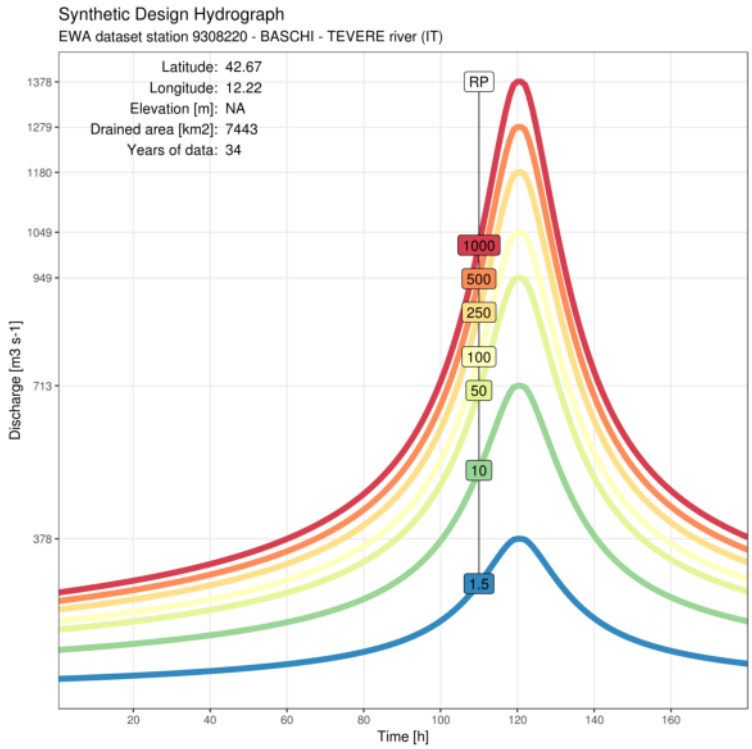

FIGURE 4.8: Example Synthetic Design Hydrograph computed following the procedure described in section 4.3 for a station on the Tevere River, in Central Italy. Seven Return Periods (1.5, 10, 50, 100, 250, 500 and 1000 years) are shown. Discharge data taken from the European Water Archive; see section 2.2 for additional details.

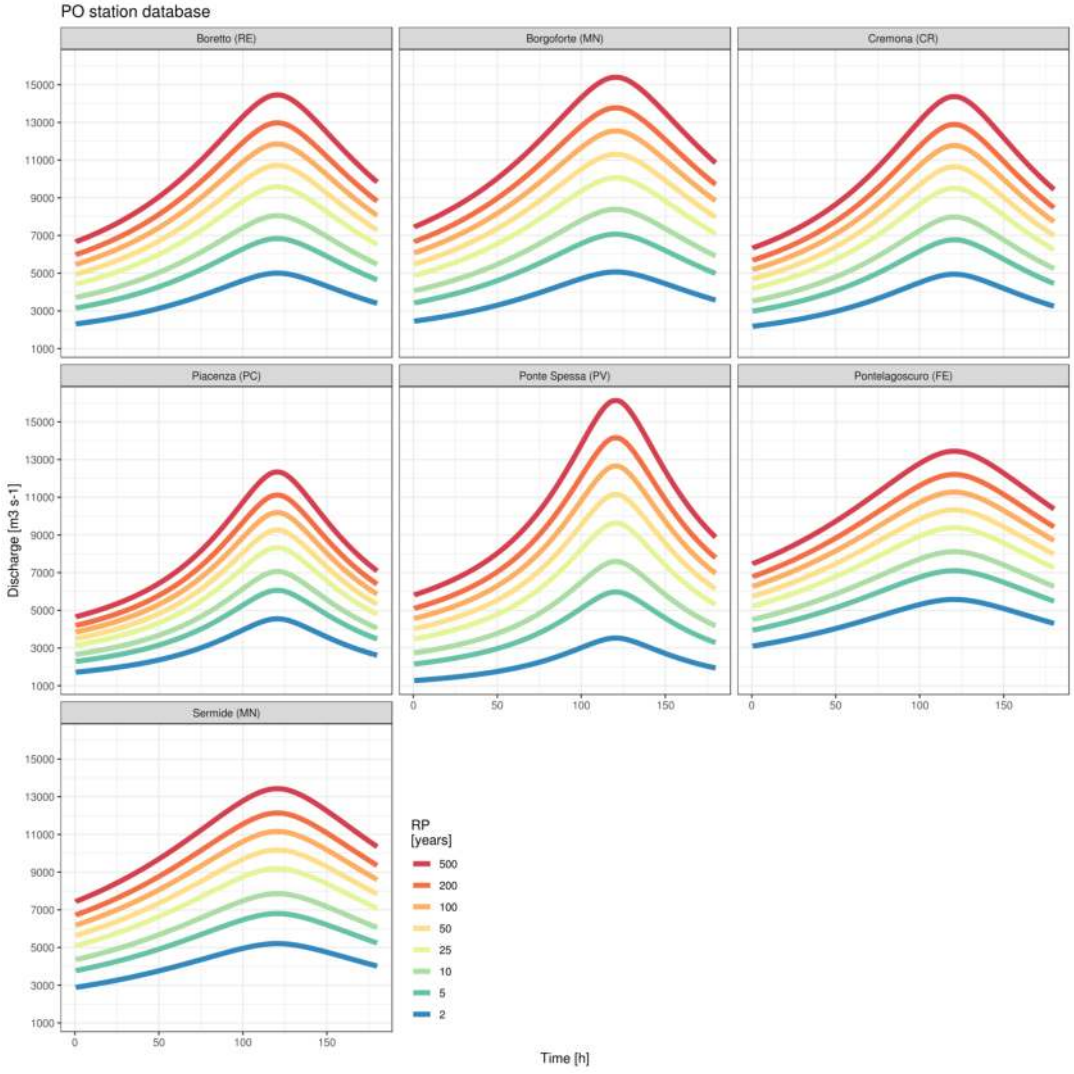

FIGURE 4.9: Synthetic Design Hydrographs for the seven discharge stations in the MV1 dataset (see table 2.3), which covers the Po river; the results are in line with Maione et al. (2003).

the use of a local adaptive timestep (Zhang et al., 1994) enabled a 97 % reduction in computation time compared to LISFLOOD-FP (Dottori and Todini, 2011). This makes high-resolution simulations possible even on a large scale. The model was modified by Rita Nogherotto from the ICTP's ESP section to run in parallel, further speeding up the computation. Rita also took care of running, organising and postprocessing all of the CA2D simulations. The model uses as input the Synthetic Design Hydrographs created starting from CHyM-simulated discharge data using the procedure described in the previous section.

A 90 m resolution, corresponding to the resolution of the underlying HydroSHEDS void-filled DEM (see section 2.4), is selected for all simulations. Due to its high resolution, CA2D cannot be run for the whole domain in a single simulation. To overcome this, a large number of small scale simulations, evenly spaced along the river network, is run in parallel for each of the nine CHyM domains (see section 4.2.1 and figure 4.5). Each of these simulations includes exactly one "virtual station", which represents the water source. Each water source itself corresponds to a specific SDH (figure 4.8) generated from CHyM discharge data for the corresponding river cell. Practical and computational considerations led to the choice of a spacing among stations varying linearly with the drained area of each point and capped between 5 and 10 km. This resulted in a total of 5548 simulations with an extent of $0.2° \times 0.2°$. The connection between CHyM's river network and CA2D's "virtual stations" is performed automatically with a nearest neighbour method, and is manually checked for accuracy. This approach allowed the creation of a ensemble of small, high resolution hydraulic simulation covering the complete river network over each of the nine CHyM domains, while remaining computationally feasible; figures 4.10 and 4.11 show example distributions and density for the "virtual stations".
The outputs of these small-scale simulations, once converted to netCDF, are merged together to create a large scale flood hazard map for each Return Period. This implies an assumption of independence between simulations which, while strong, is necessary to this approach.

Further details regarding the choice of DEM, the conditioning it requires and the spacing of "virtual station" are provided in Nogherotto et al. (2019, in preparation). Currently, only the simulation driven by the CHyM (GRIPHO) has been completed, while other runs driven by RegCM (ERA-Interim and HadGEM) are currently ongoing. All simulations are run on the ICTP ARGO cluster.

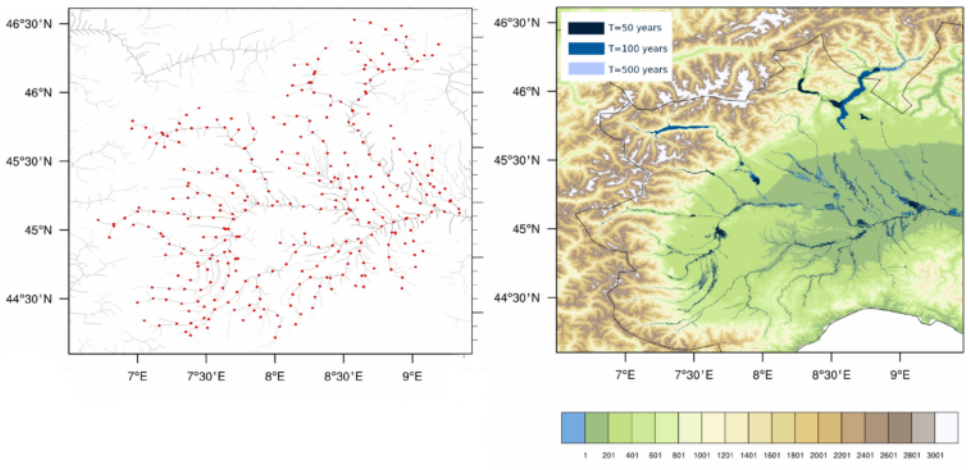

FIGURE 4.10: "Virtual stations" (left) and preliminary flood results (right) of a CA2D test simulation performed over the upper Po basin. From Nogherotto et al. (2019), in preparation.

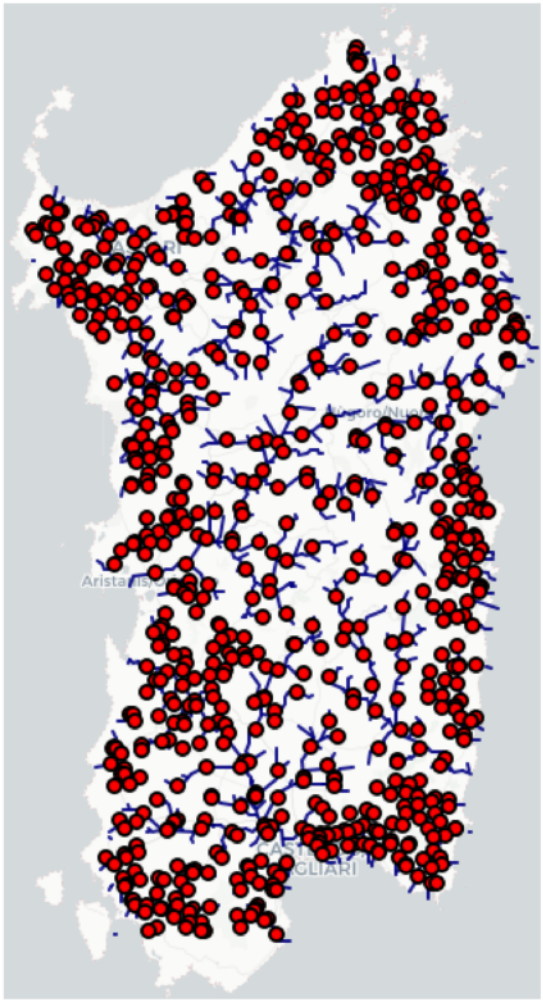

FIGURE 4.11: "Virtual stations" (red dots) over the Sardinia domain, including river network (blue lines) for major rivers.

Chapter 5

Results

This chapter will discuss the results obtained during the development of this PhD project. As described in the previous chapter, a cascade of three modelling tools were employed: a climate model (RegCM, section 4.1), a hydrological model (CHyM, section 4.2) and a hydraulic model (CA2D, section 4.4). The three models were applied in sequence, with the hydrological model utilising rainfall from the RCM, and the hydraulic model taking as input the discharge data processed with the procedure described in section 4.3.

In the following, the RegCM simulations driven by ERA-Interim and HadGEM will be referred to as RegCM-ERA and RegCM-HAD respectively. Similarly, the CHyM simulations driven by RegCM-ERA and RegCM-HAD are called CHyM-ERA and CHyM-HAD, while the simulation driven by GRIPHO is referred to as CHyM-OBS. The four climatological seasons displayed are defined as DJF, MAM, JJA and SON, which refers to the initials of their respective months; in the following, they are referred as winter, spring, summer and autumn. Whenever possible, the analysis was split by four macroregions with different climatic characteristics: North, Centre, South and Islands. These macroregions are identical to those used in the validation of the GRIPHO dataset (section 3.4).

Five different timeslices are used through this analysis:

2001–2016 Validation period for CHyM-OBS.

1980–2016 Validation period for RegCM-ERA and CHyM-ERA.

1976–2005 Validation period for RegCM-HAD and CHyM-HAD. This period is also used as reference period for change assessment against the future scenario and is referred to as *historical* or *reference*.

2020–2049 First time slice for the future scenario simulated by RegCM-GEM and CHyM-HAD. Referred to as *near future*.

2070–2099 Second time slice for the future scenario simulated by RegCM-HAD and CHyM-HAD. Referred to as *far future* or *end of century*.

The chapter is organised as follows. In section 5.1 the validation and future change of mean and extreme precipitation in the RegCM simulations will be presented and discussed. Section 5.2 will describe the results from the hydrological simulations for both the present day and for the future scenario, including several proxies for future changes in flood hazard. Section 5.3 will present the preliminary results obtained in creating flood hazard maps for the entire Italian territory, together with a case study regarding a flooding event in north-western Italy.

5.1 Validation and future changes of precipitation in the RegCM simulations

The two climate simulations described in section 4.1.4 are here analysed with particular attention towards extreme precipitation events. The same precipitation metrics described in section 3.4 are employed. They are: annual cycle, mean seasonal precipitation, extreme seasonal precipitation ($R95_{ptot}$ and $R99_{ptot}$) and daily precipitation distribution (Probability Density Functions). Both a present day evaluation and an assessment of future changes (only for the HadGEM-driven simulation) are carried out. When calculating $R95_{ptot}$ and $R99_{ptot}$ metrics for the future scenario, the 95th and 99th percentile thresholds of the reference period have been used, to provide a uniform reference value.

5.1.1 Validation of present-day model performance

Figure 5.1 shows the annual cycle of precipitation over the four macroregions. the performance of the models in reproducing the precipitation annual cycle and the seasonal precipitation respectively, compared against the best available precipitation datasets (see sections 2.1.4 and 3.4 for a comparison of observations). The annual cycle is approximately correct in the models, with a underestimation (overestimation) of average precipitation occurs in both simulations in the North in autumn (spring). In particular, the RegCM-ERA simulation is capable of reproducing the November precipitation peak in the Centre, South and Islands.

Figure 5.2 Average precipitation peaks over the Alps are correctly reproduced, although the models show a tendency to create isolated precipitation hot-spots. Autumn and winter precipitations over the west coast of Central and Southern Italy (present in GRIPHO, but not in E-OBS) are correctly reproduced, while an underestimation is present in winter over Liguria and the Gulf of Genoa; an underestimation in the Po plain in winter is present, compared to all the observational datasets. Overall, the performance of the two RegCM simulations with mean precipitation metrics is good. The climatologies of the two RegCM simulations are very similar, indicating that a stable equilibrium is reached and that the model is able to create its own climatic features, independently of the driving data. This gives us confidence in using the RegCM model in future climate projections.

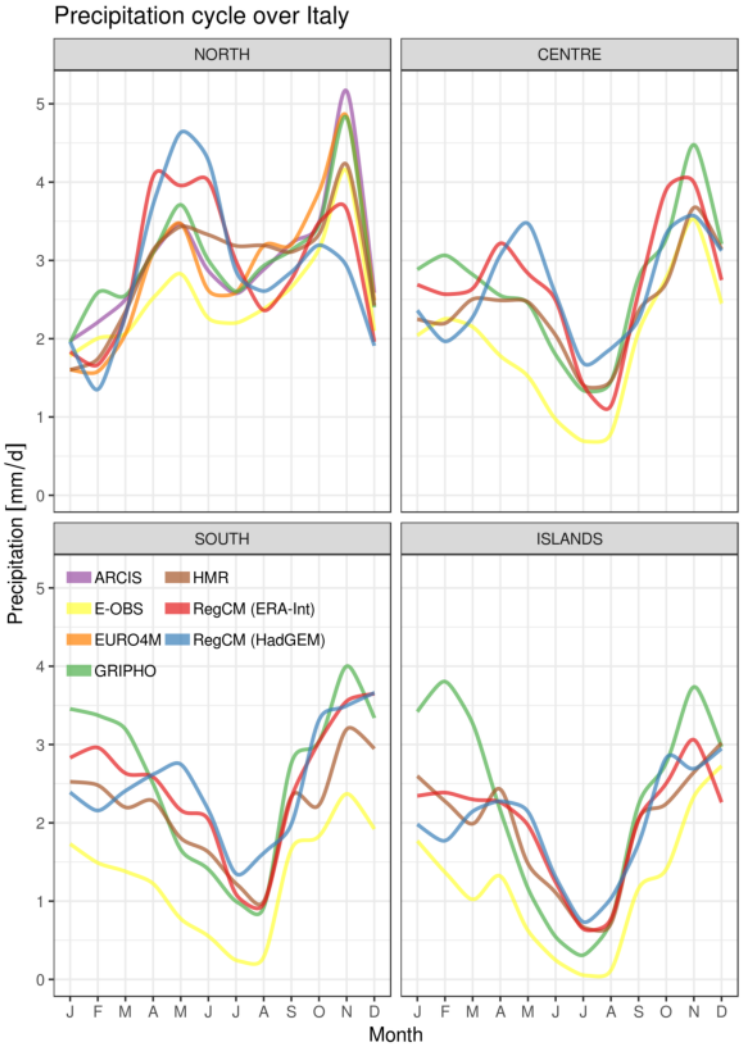

FIGURE 5.1: Annual cycle of precipitation as reproduced by observations (see section 3.4) and models (section 4.1.4). The time period for each dataset varies according to availability. The four macroregions selected are the same as for previous evaluations (sections 2.1.4 and 3.4).

Extreme precipitation is assessed via maps of $R95_{ptot}$ (figure 5.3) and $R99_{ptot}$ (not shown, but similar to $R95_{ptot}$), where the spatial features are well reproduced. The models tend to slightly overestimate extreme precipitation hot-spots especially over the Alps and the prealpine areas of North-Eastern Italy, while slightly underestimating in the South when compared to GRIPHO. Of the two simulations, the ERA-Interim-driven one usually produces more extreme precipitation. PDFs of daily precipitation (figures 5.4 and 5.5) for the four regions and seasons generally show a slight underestimation of extremely strong events compared to the GRIPHO gridded dataset presented in chapter 3, with intermediate values lower than 200 mm d^{-1} slightly more underestimated. In the North, the PDFs of the models resemble more closely the high resolution datasets (GRIPHO, ARCIS, EURO4M) than the lower resolution E-OBS. In

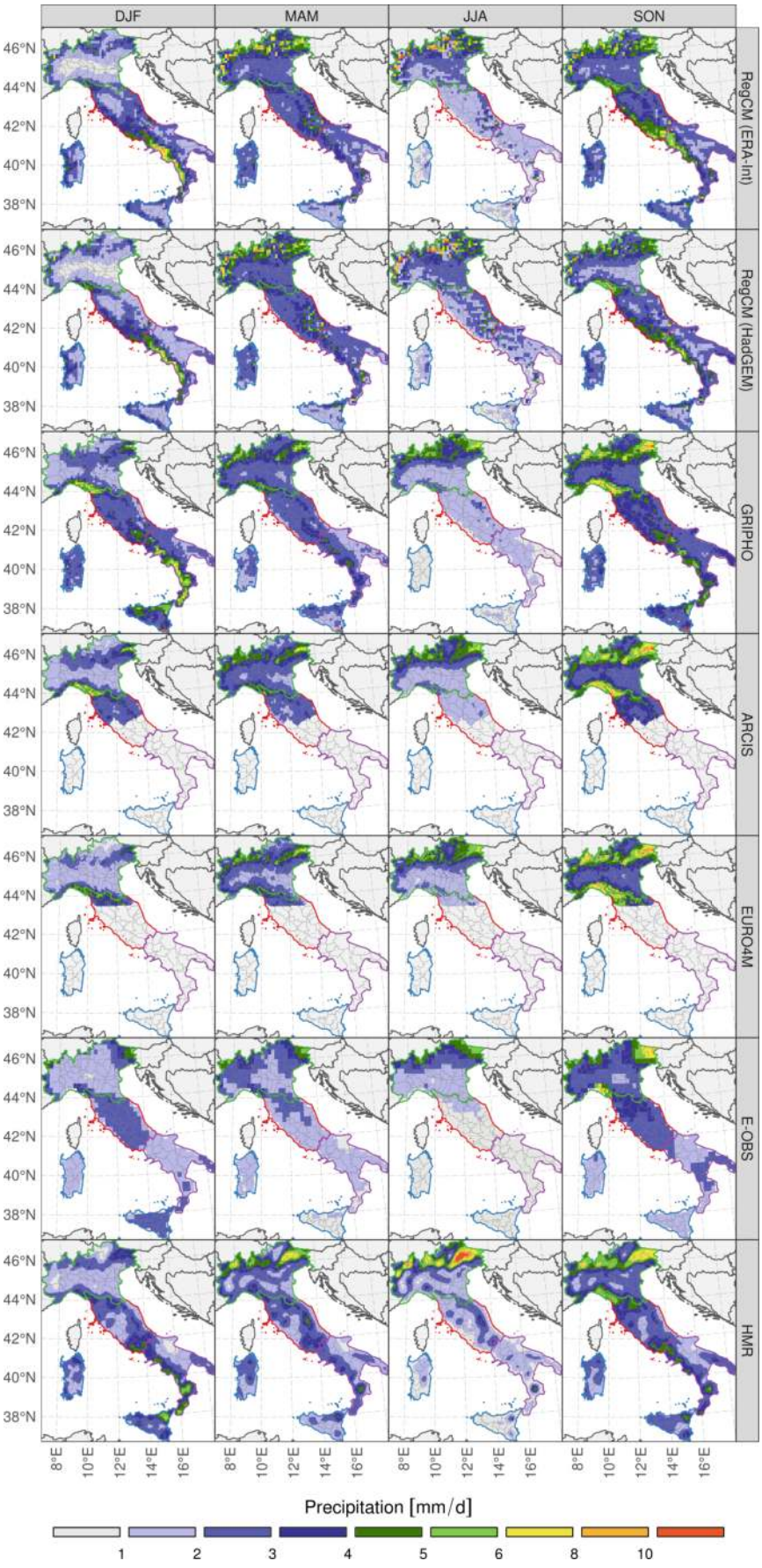

FIGURE 5.2: Average seasonal precipitation for the two climate model simulations (top two rows) and five selected precipitation datasets.

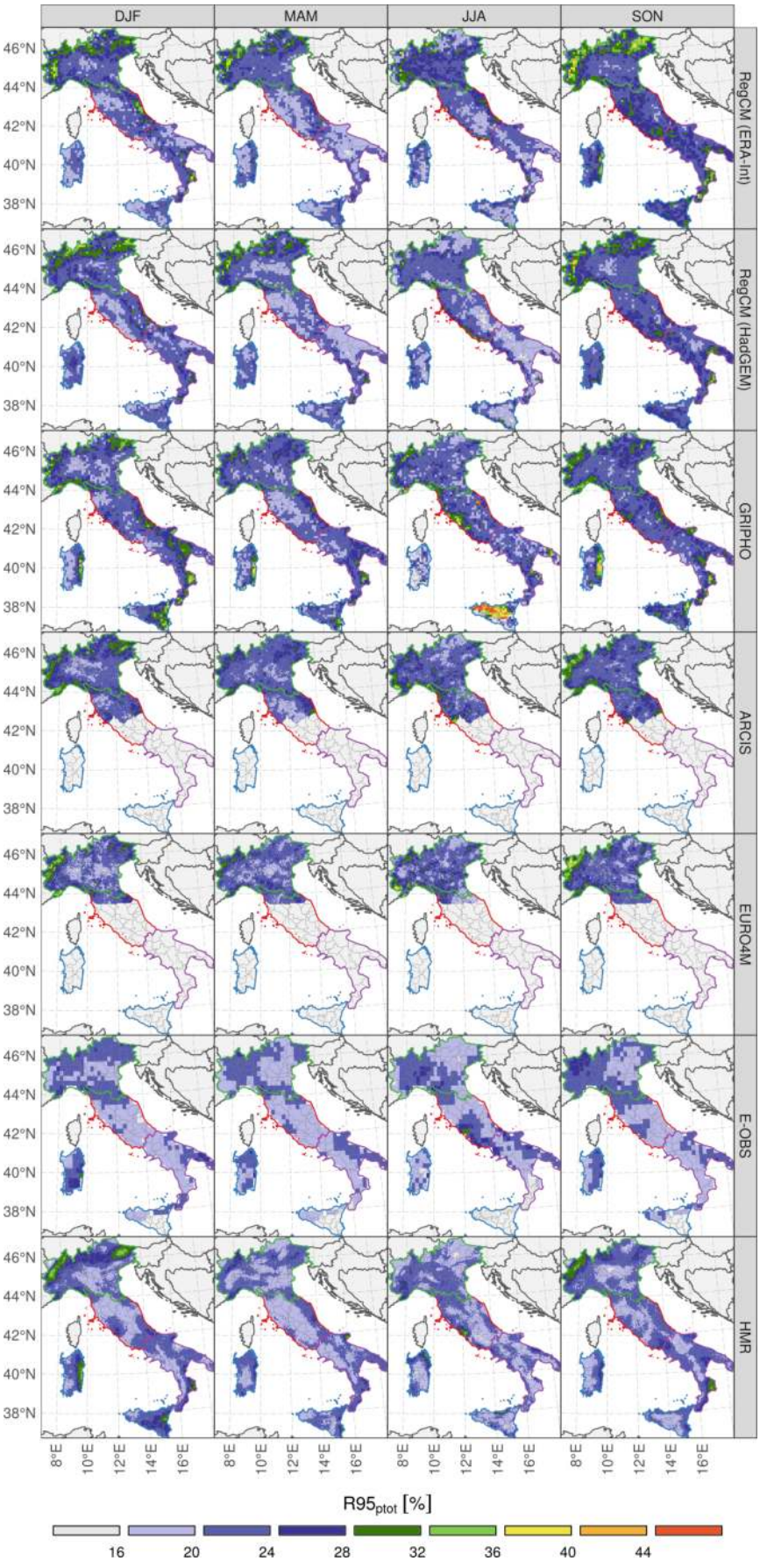

FIGURE 5.3: Seasonal $R95_{ptot}$ maps for the two climate model simulations (top two rows) and five selected precipitation datasets.

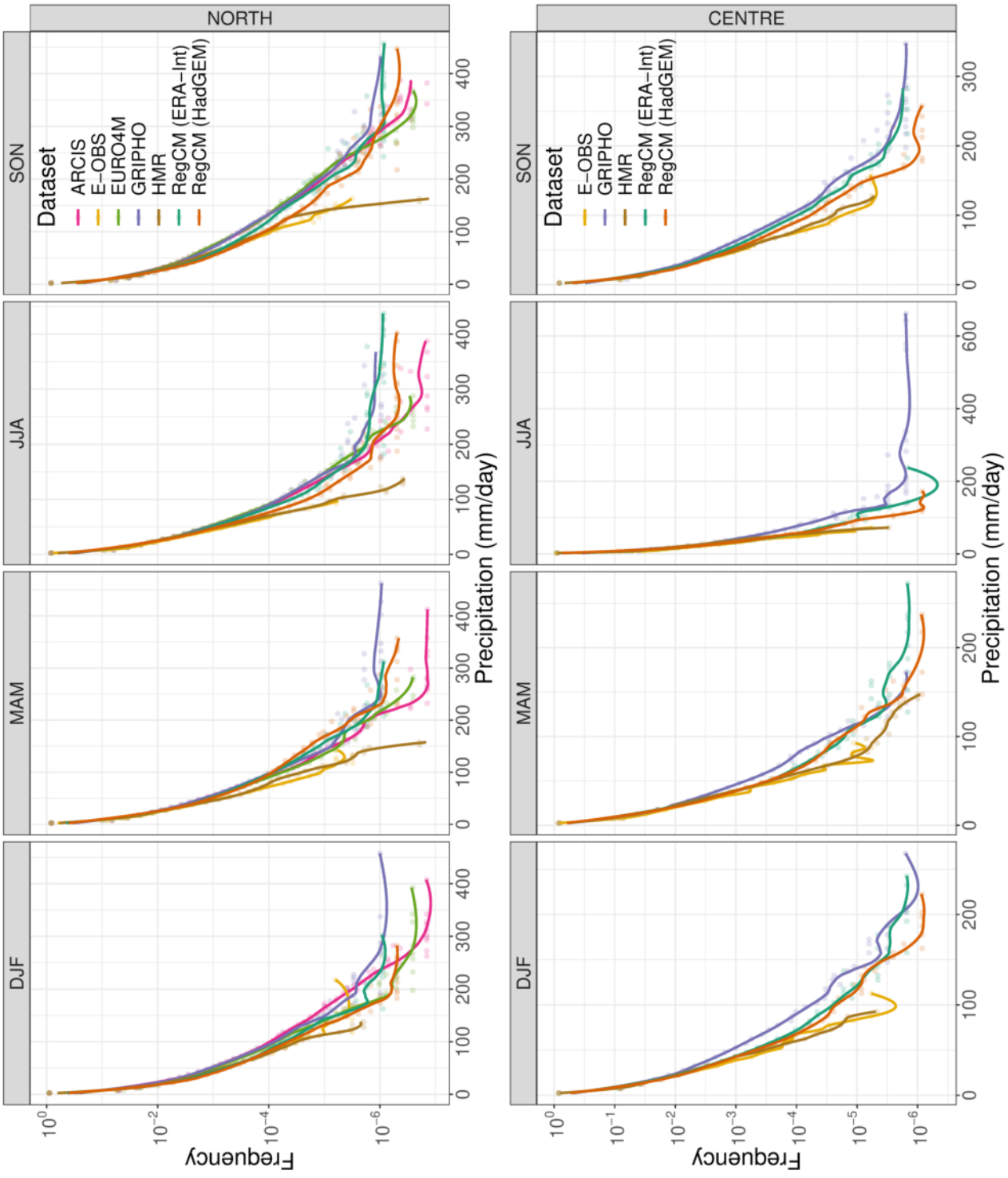

FIGURE 5.4: Daily precipitation Probability Density Functions for the validation of the RegCM simulations for the North and Centre regions. The four summarising regions are highlighted in figures 5.2 and 5.3. The solid lines are smoothed fits.

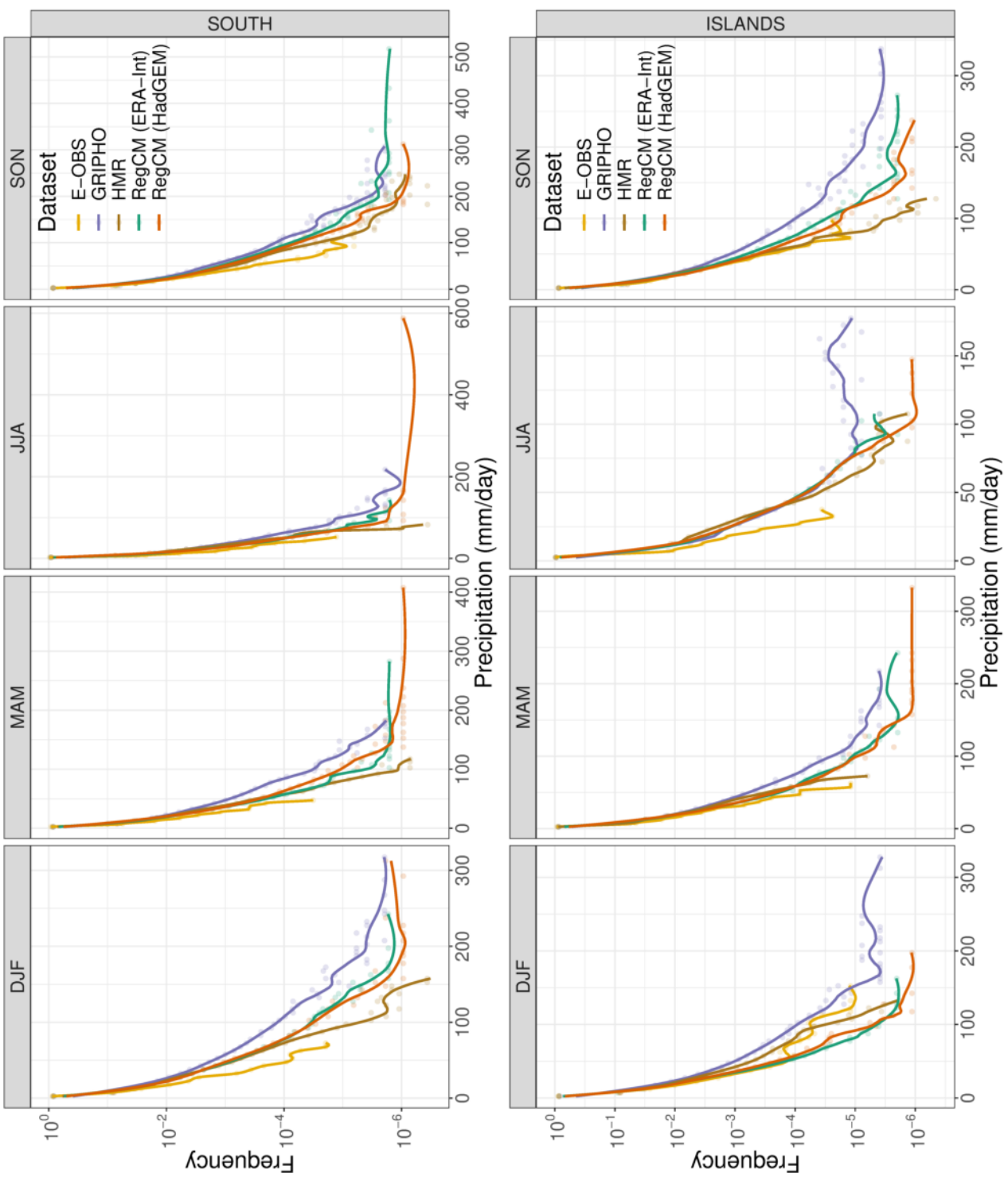

FIGURE 5.5: As figure 5.4, but for the South and Islands regions.

Central Italy in summer RegCM-HAD slightly underestimates extreme precipitations compared to GRIPHO, which however is likely affected by erroneous station data for a few grid points in summer over that region (see section 3.4). Neither model can reproduce the high precipitations found in winter and spring on the east coast of Sardinia, which both GRIPHO and HMR (but not E-OBS) show. The extreme precipitation over Mount Etna in Sicily, reported by HMR, is also underestimated. Comparing RegCM-ERA and RegCM-HAD reveals a difference in the extreme tail of the distribution, where the former generally produces more precipitation extremes (except in summer in the South). Compared to E-OBS and HMR extremes are systematically overestimated, which is likely due to the low station density of these datasets. This underlines the necessity of high-resolution datasets with a large number of stations in order to properly validate extreme precipitations. Similar conclusions were reached before in other studies (Fantini et al., 2016; Prein et al., 2016; Prein and Gobiet, 2017).

Evaluation of simulated temperature, which is not as strongly linked to flood events as precipitation, is presented in appendix A. Both model simulations show good ability to simulate temperature patterns and averages across the complete study domain.

5.1.2 Changes in future climate in the RegCM (HadGEM) simulation

As seen in section 1.3, future precipitation is projected to move towards fewer, more extreme precipitation events. We expect this trend to be also highlighted in RegCM-HAD under the RCP8.5 scenario.
Figure 5.6 shows the annual cycle of mean precipitation across the three timeslices for RegCM-HAD. No strong shift in precipitation seasonality, but rather a general decrease of precipitation all year round, except for winter precipitation in the North, which slightly increases. In the far future, April-May-June precipitation is projected to decrease in all regions but the North An interesting dual mode of precipitation is produced in the far future in the north, where September precipitation is increased and October precipitation decreases. Note that the near future average is very close to the reference (1976–2005), due to the nature of the selected RCP, which substantially increases the greenhouse gases forcing only starting from the second half of the century. Spatial patterns of mean precipitation (figure 5.7) further highlight the increase in average precipitation in the colder months in the North in both time slices ($+18\%$ for 2020–2049, $+13\%$ for 2070–2099). A precipitation decrease is instead present in the Islands in all seasons and especially in spring (-23%) and summer (-31%) by the end of the century. In the other regions, a reduction of summer precipitation can be noted, especially for the far future, with reductions of 14, 13 and 34% for the Centre, South and Islands respectively.

Changes in precipitation extremes are more relevant for this project. Figure 5.8 shows the evolution across the three timeslices of the extreme $R95_{ptot}$ metric, which is

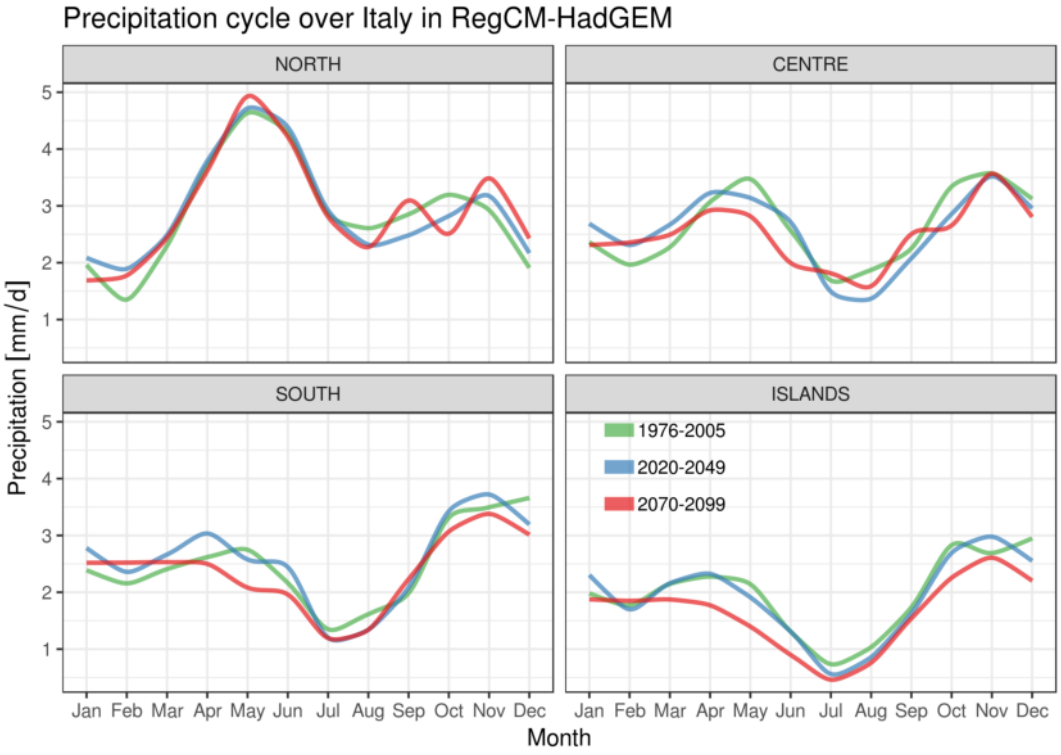

FIGURE 5.6: The precipitation annual cycle for RegCM-HAD in the three timeslices selected, for the four macroregions (see sections 2.1.4 and 3.4).

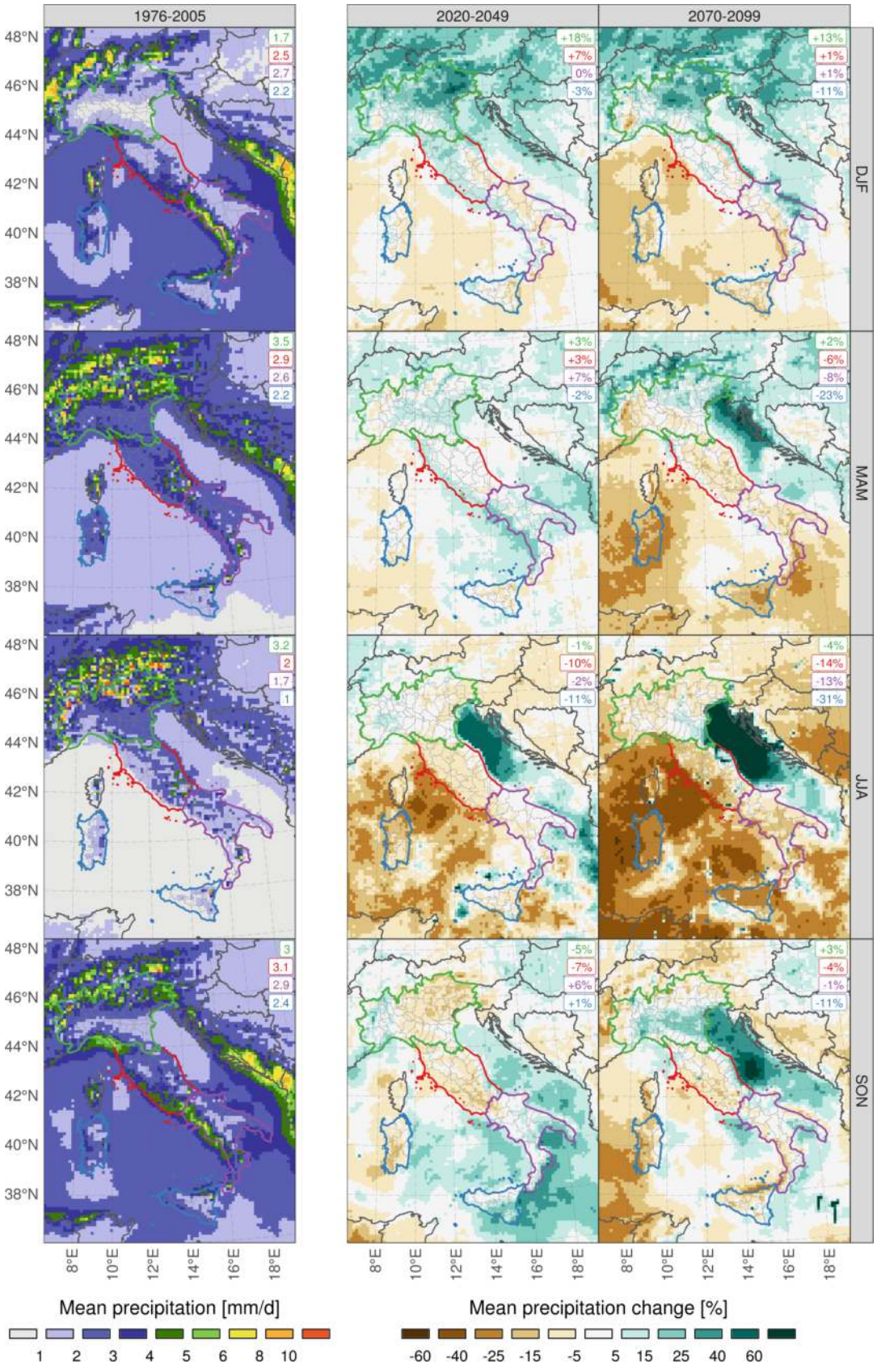

FIGURE 5.7: Average seasonal precipitation for RegCM-HAD for the reference period (left column) and % change w.r.t. it (centre and right column, in percentage). The four rows represent seasons. In the top right corner of each map, the colour-coded average for each of the four macroregions is shown.

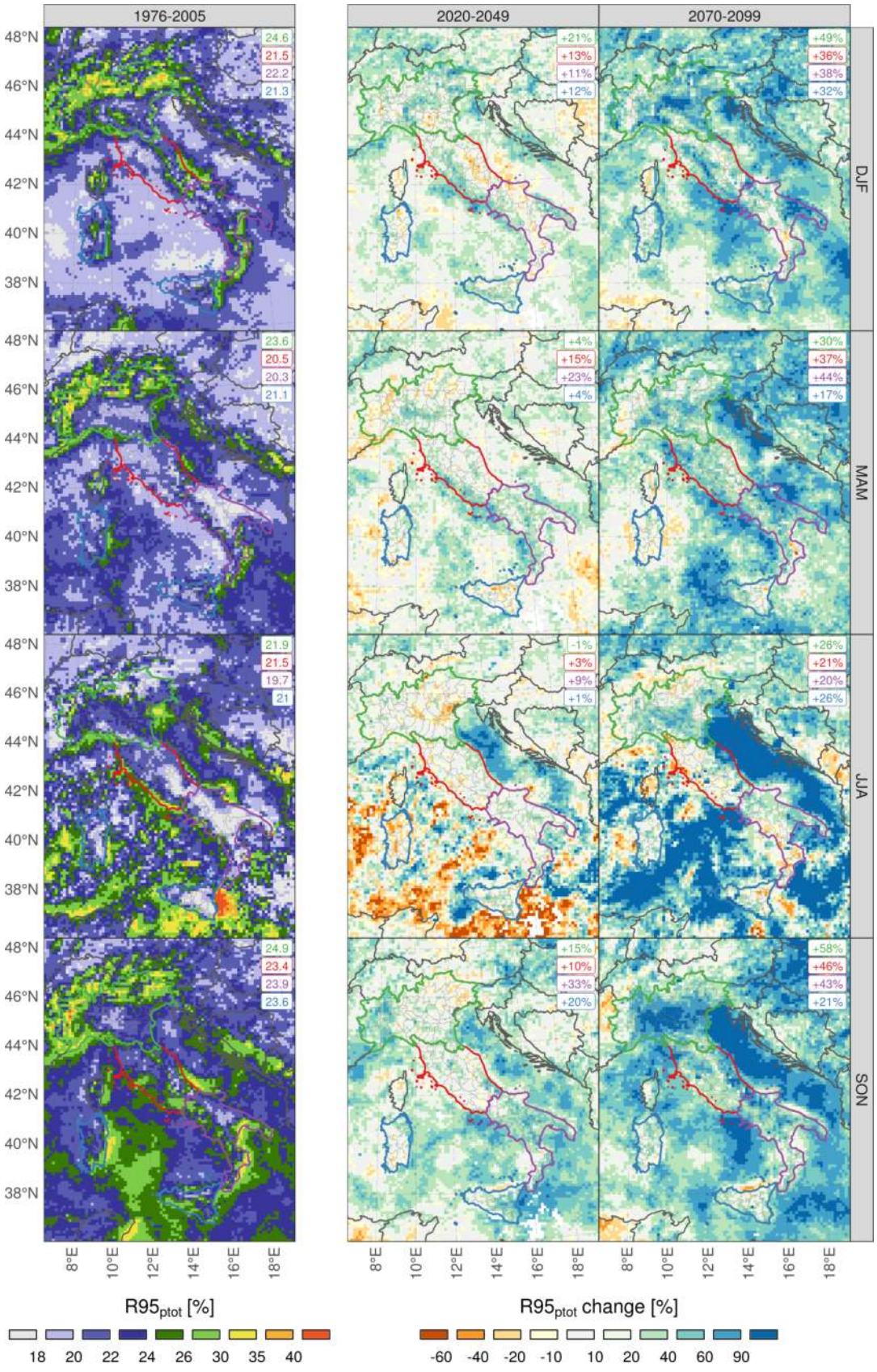

FIGURE 5.8: Seasonal $R95_{ptot}$ for RegCM-HAD for the reference period (left column) and % change w.r.t. it (centre and right column, in percentage). The four rows represent seasons. In the top right corner of each map, the colour-coded average for each of the four macroregions is shown.

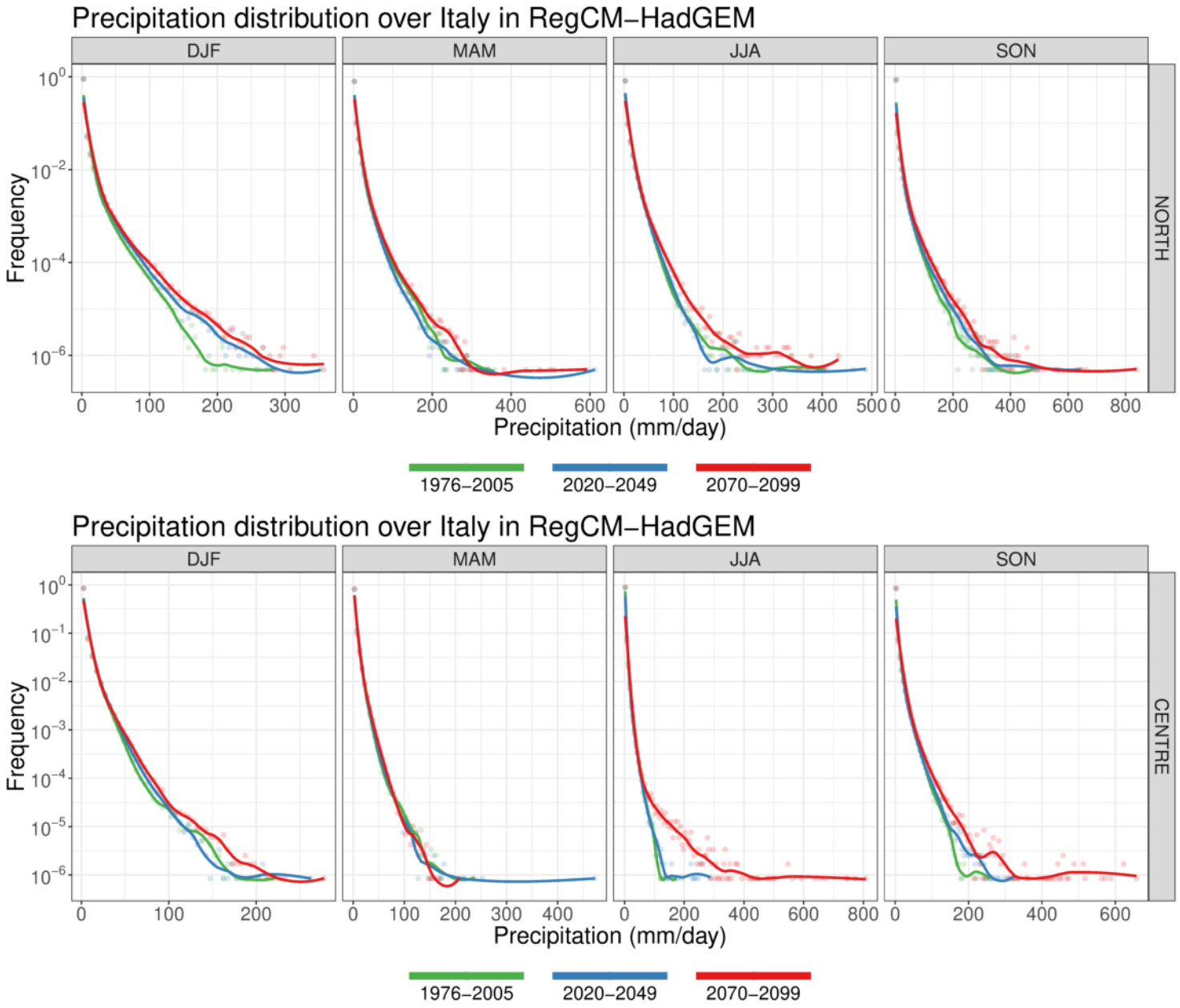

FIGURE 5.9: Daily precipitation Probability Density Functions for the three timeslices of RegCM-HAD for the North and Centre regions. The solid lines are smoothed fits.

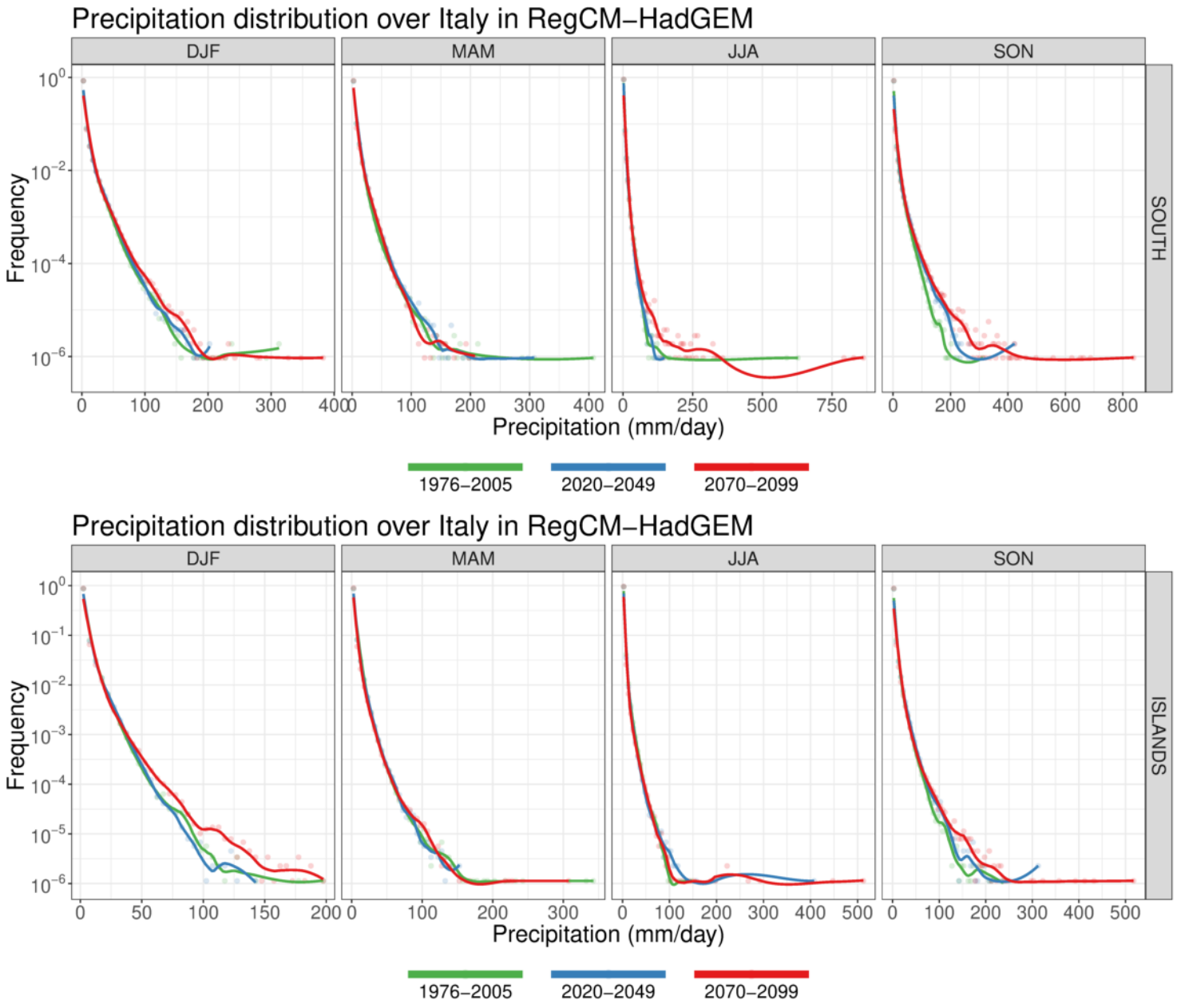

FIGURE 5.10: As figure 5.9, but for the South and Islands regions.

characterised by a general increase in all regions towards the end of the century, with average changes ranging from +17% to +58%. For $R99_{ptot}$ (not shown), the changes are even larger and range from +52% to +155% in the end of the century period. Over land, the area that shows the largest signal is the Po plain, especially in winter and autumn, followed by the south-eastern region. Over high elevations, changes seem to be generally negligible or even slightly negative in all seasons. Spatial trends across the two future timeslices are similar, but there are nonetheless areas (such as Central Italy in autumn) in which the change signal differs between the two timeslices. The daily precipitation PDFs (figures 5.9 and 5.10) also show a similar increase, with stronger extreme events being more pronounced in the far future and, in several cases, with presence of events of a magnitude not recorded in the historical period. The changes greatly depend on the region and the season: Central Italy shows barely any change in winter, but in summer strong events with a magnitude of 100 mm d^{-1} or greater are ten times more frequent in the far future timeslice than in the reference period.
For all regions, autumn shows the largest increase in extreme precipitation, with freater values in Central and Southern Italy Overall, the general tendency of increased extreme precipitation is confirmed, even in regions where average precipitation is projected to decrease.

Results on extreme temperature are deferred to appendix A. The changes are mainly limited to an overall, spatially uniform increase in temperature of about 4 and 6 °C in winter and summer respectively.

5.2 The Italian hydrology in the three CHyM simulations

The findings of section 5.1.2, which indicate a general increase in extreme precipitation over Italy by the end of the century, can be linked to a change in flood hazard over all domains. In the upcoming sections, we'll look at the performance of the CHyM model and discuss how the the projected changes in discharge extremes can be linked to the changes in precipitation. Following the literature (e.g. Alfieri et al., 2015a), this is accomplished through several metrics. For the comparison of CHyM simulation with station data, we used the following metrics:

SDH Synthetic Design Hydrographs, derived from models and observations via the statistical procedure described in section 4.3.

KGE Kling-Gupta efficiency, a metric for analysing model efficiency similar to the Nash-Sutcliffe coefficient, devised by Gupta et al. (2009) and Kling et al. (2012). Varies between $-\inf$ and 1, with values closer to 1 meaning better performance.

d Index of agreement, a standard metric for assessing model performance by Willmott (1984). Varies between 0 and 1, with 0 meaning no agreement and 1 perfect match.

r Pearson correlation coefficient; varies between -1 and 1.

For evaluation of future change in average and extreme discharges, the following four metrics will be used:

$\overline{Q}$ Average discharge.

Q_{ymax} Average maximum discharge calculated over each year in the given record.

Q_{RP} Projected peak discharge for the given Return Period RP, obtained by fitting a Gumbel distribution to the discharge data (see section 4.3).

POT Peak Over Threshold, the number of times (or fraction of timesteps) a discharge climatology surpasses a given threshold, usually given by the Q_{RP} for a given Return Period.

The last three metrics, which represent extreme discharges, are chosen in order to act as proxies for flood events.

5.2.1 Validation of the CHyM simulations

The three CHyM simulations are here validated. The two simulations CHyM-OBS and CHyM-ERA, driven by GRIPHO and RegCM-ERA, can be compared directly to the available discharge data (section 2.2) with standard metrics mentioned in the the beginning of this chapter. Unfortunately, due to the low station availability (both in number of stations and length of the timeseries), most domains contain few or no discharge stations sharing a long enough period with the CHyM simulations. The validation is thus carried out only for the two domains where station availability is more complete (the Po basin and Central Italy). The results are, however, affected by the low quality of the provided observed discharge data, which present several irregularities, inhomogeneities and suspicious values.

For brevity, only a few of the maps are shown here. Figure 5.11 shows the index of agreement and Kling-Gupta efficiency for the GRIPHO-driven simulation over the Po basin, which is the largest basin in Italy. Both metrics show good agreement with observations in most of the domain except the northernmost stations, located in Switzerland. This is also confirmed by the correlation (not shown), which is higher than 0.6 for most stations. Larger basin tend to perform better better in these metrics. Results in Central Italy (see figure 5.12 for the index of agreement and the correlation) show generally acceptable performance for the GRIPHO-driven simulation. Nevertheless, several stations in the eastern part of the domain indicate correlation values smaller than 0.5, suggesting that the model is not performing as good as before in this part of the domain. This is also confirmed by the other metrics. However, the Tevere river basin, which is the main catchment of the region, is showing good results in all metrics.

In regional climate simulations, even if laterally driven by reanalysis, the timing and intensity of heavy precipitation events, which is crucial for a proper representation of discharge, can be quite different from reality. This is reflected by the worsening

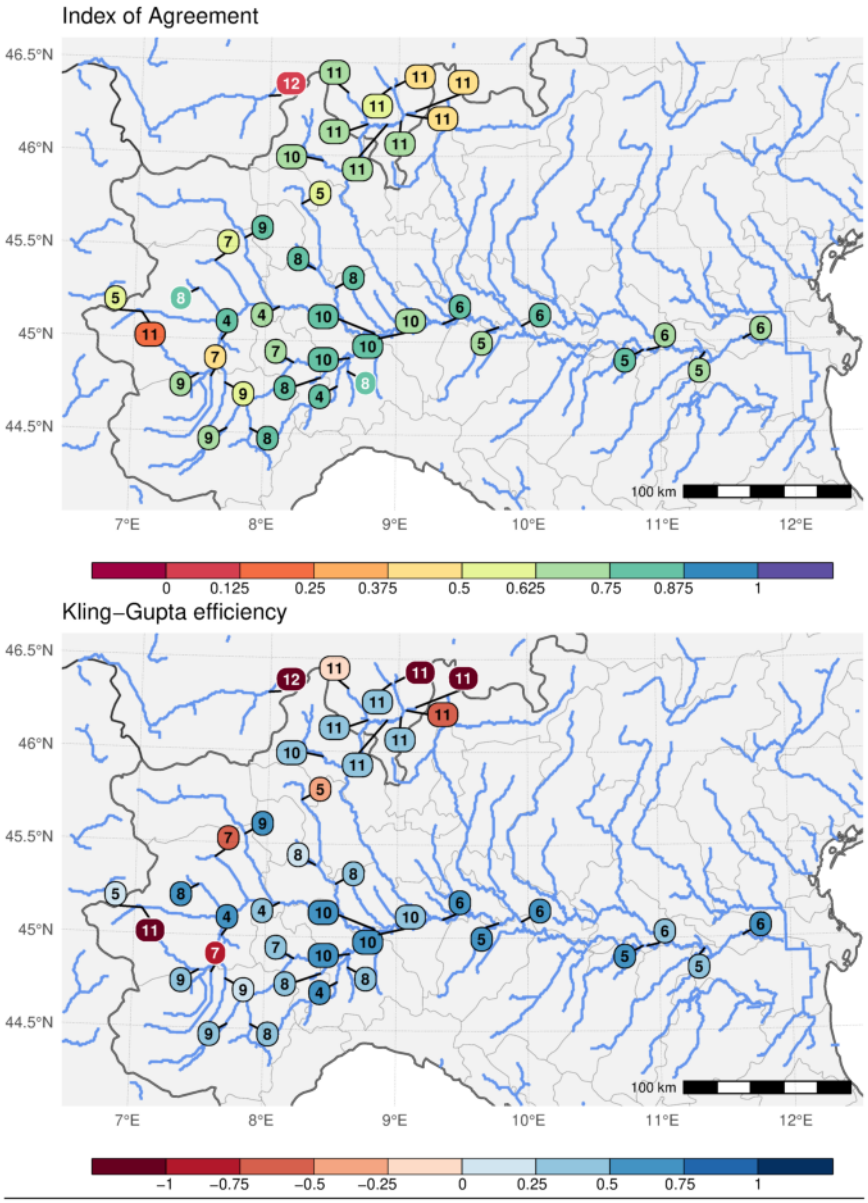

FIGURE 5.11: Index of agreement (top) and Kling-Gupta Efficiency (bottom) for the CHyM simulation driven by GRIPHO over the Po basin, compared with observations. Colours indicate the value of the metric, numbers the total length of the time period in common with observations (in years).

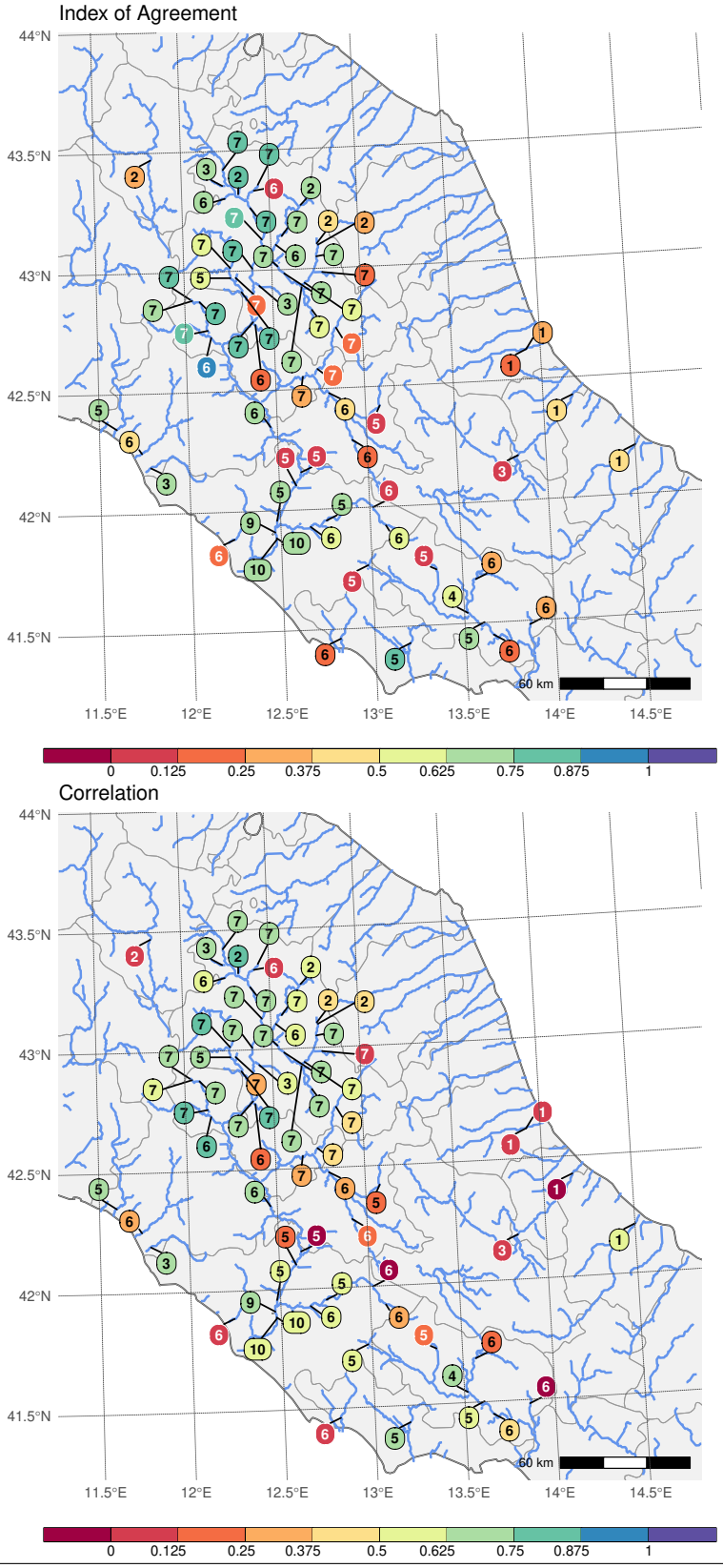

FIGURE 5.12: Index of agreement (top) and correlation (bottom) for the CHyM simulation driven by GRIPHO over Central Italy, compared with observations. Colours indicate the value of the metric, numbers the total length of the time period in common with observations (in years).

of correlation and KGE values in RegCM-ERA (figure 5.13) are still mostly positive, but generally low. The Po river basin, which, due to its large size, is less sensitive to precipitation timing, is the one which is better reproduced.

Validating the performance of CHyM-HAD, the CHyM simulation driven by RegCM-HAD, is more difficult. In this case, since climate simulations do not represent real timing of the events, but rather only a statistical representation of it, no direct comparison with observations can be made. One way to validate the simulations is to use the Synthetic Design Hydrographs that are computed by fitting yearly maxima to an extreme value distribution (see section 4.3 for details). These Hydrographs, which represent the typical discharge timeseries of an extreme event, can be calculated for any river point and can be compared between two points with different time coverage, being them only a statistical representation of the discharge of a given river segment. This approach works best if a long timeseries of discharge data is available. For CHyM model runs driven by RegCM at least 30 years are considered, while the simulation driven by GRIPHO has only 16 years of data. The length of the time period for discharge observations from station data varies by station; only stations with more than 10 years of data are considered here.
Figures 5.14 and 5.15 show Synthetic Design Hydrographs for selected stations, compared with CHyM-OBS, CHyM-ERA and CHyM-HAD. The latter is shown across the three selected timeslices and is generally found to increase discharge by the end of the century; this topic will be more widely discussed in the next section. In particular, figure 5.14 shows SDHs for two selected stations in the Po river basin, which were initially used for testing the methodology. These stations are known to be reliable and relatively unaffected by upstream water management. The three CHyM-OBS, CHyM-ERA and CHyM-HAD simulations show here similar results to the observations for the present day, but an overestimation in the peak discharge at the Isola Sant'Antonio Po station can be found in the CHyM-OBS and CHyM-ERA simulations. Figure 5.15 shows instead example SDHs for two stations in Central Italy, characterised by widely different drained areas (16361 and 53 km^2). In both cases, peak discharges are close to those obtained from observations.
Model performance across different basin sizes is good, albeit, on average across all stations, an overestimation of peak discharges if generally found to be present in all simulations. This might partially be due to the fact that discharge rating curves generally tend to underestimate extreme flows (Di Baldassarre and Montanari, 2009).

5.2.2 Future changes in mean and extreme discharges over Italy

The CHyM-HAD simulation, which covers the period 1975 to 2100, allows us to analyse the possible changes in discharge in a future climate scenario. In figure 5.16, the change in average discharge between the two future timeslices and the reference period is shown for the nine domains used to cover the complete Italian territory.

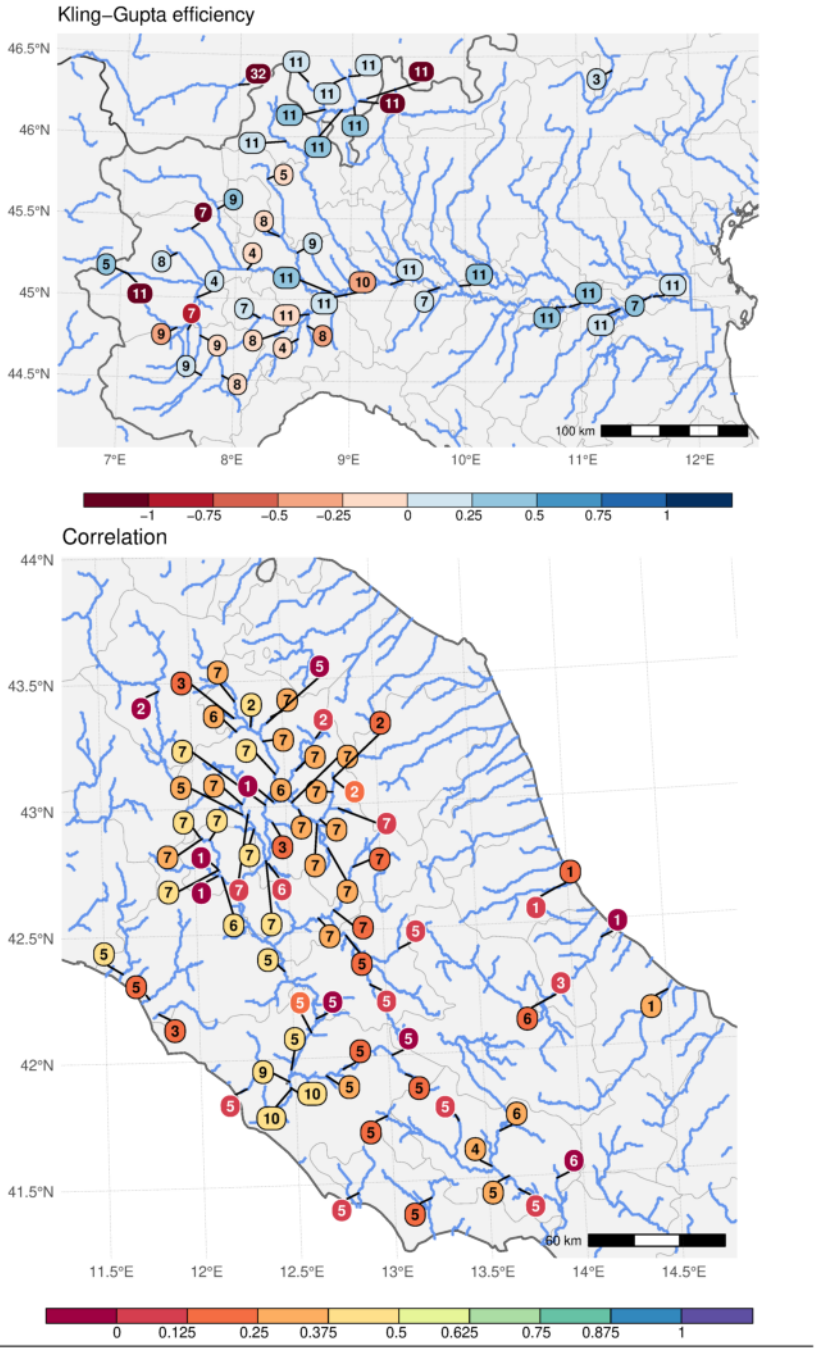

FIGURE 5.13: Kling-Gupta Efficiency (top, over the Po basin) and index of agreement (bottom, over Central Italy) for CHyM-HAD, compared with observations. Colours indicate the value of the metric, numbers the total length of the time period in common with observations (in years).

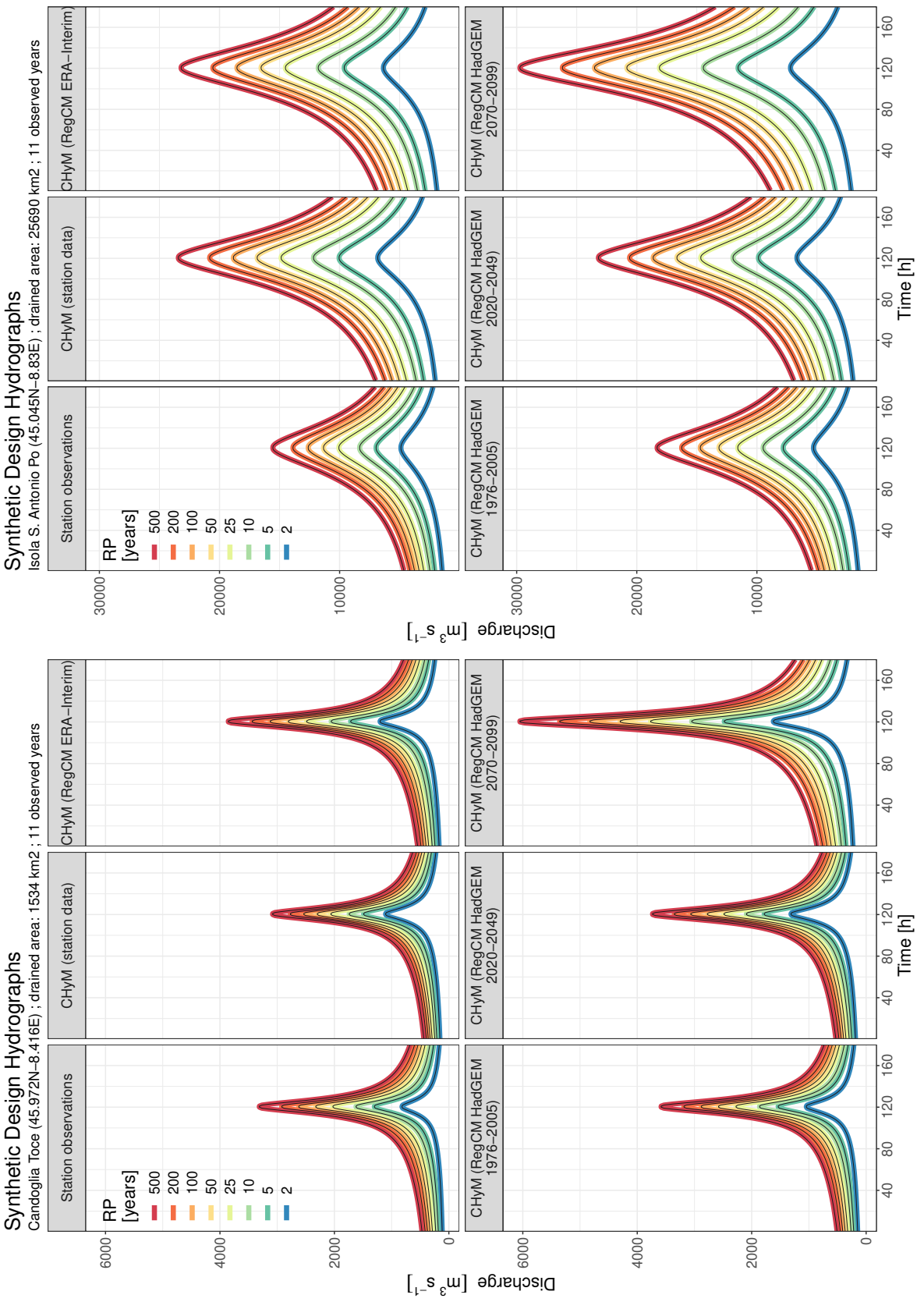

FIGURE 5.14: Example SDHs for two station locations in the Po basin. These stations were among the ones used for the initial definition of the methodology.

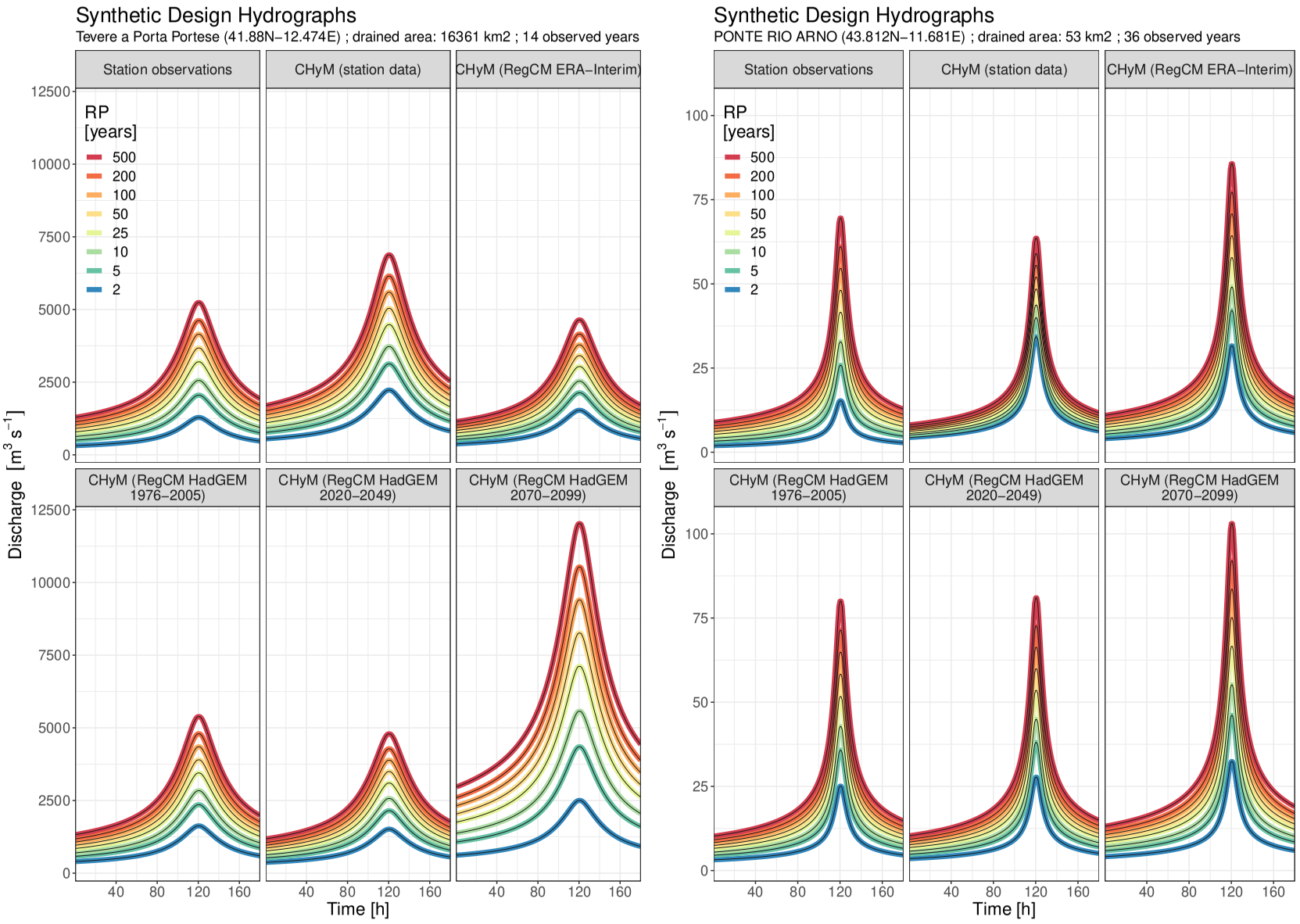

FIGURE 5.15: Example SDHs for two station locations in Central Italy with drastically different basin sizes.

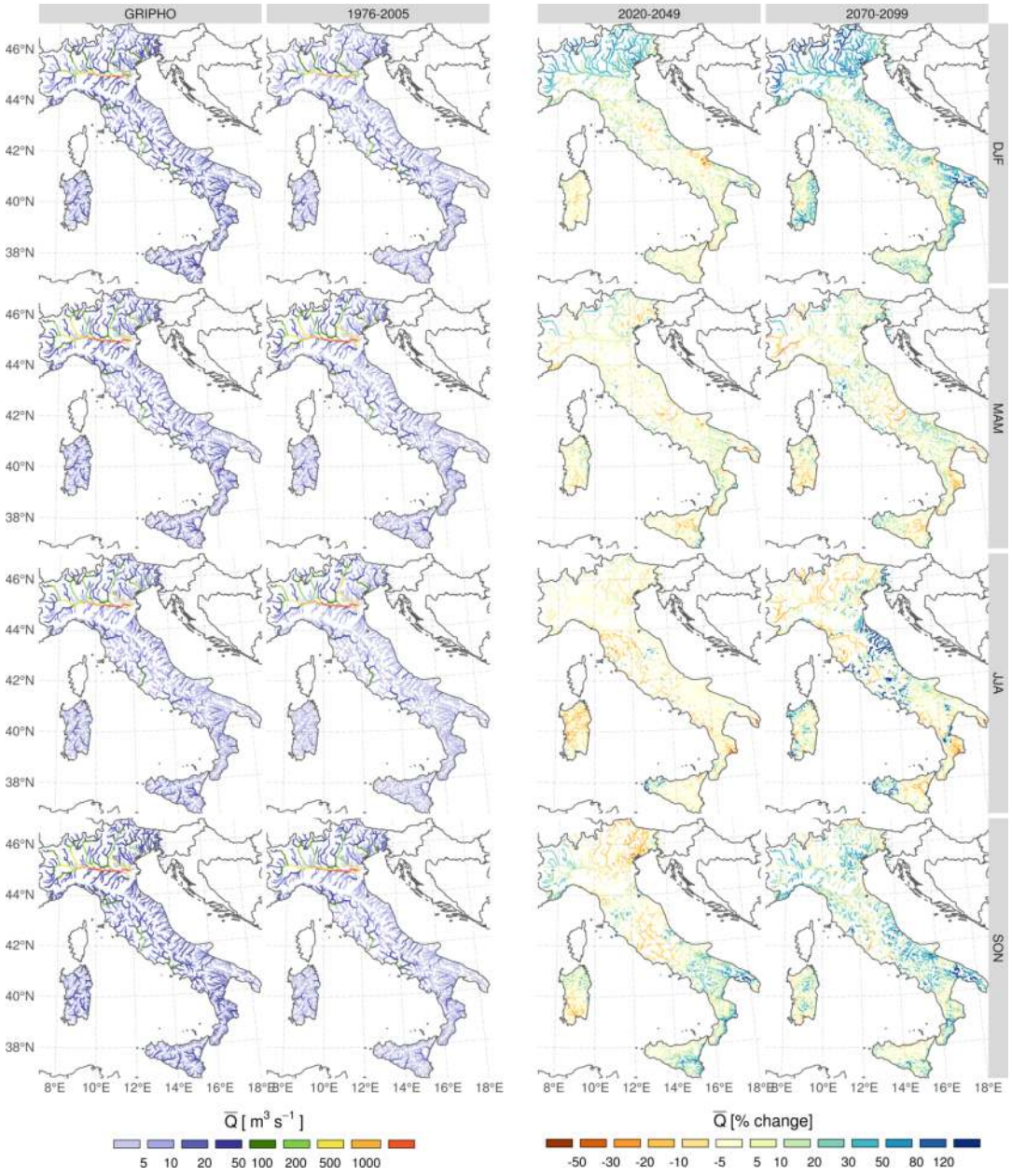

FIGURE 5.16: Average discharge for CHyM-OBS and CHyM-HAD (leftmost two columns) and percentage change for near and far future (leftmost two columns), over the four seasons. To avoid overlaps and overplotting, only the basins completely enclosed in each of the nine simulation domains are plotted and only the major rivers are shown for each basin.

Average discharges obtained from the CHyM-OBS, also plotted as a reference, show good agreement with CHyM-HAD, which covers a similar period of time. Increases (decreases) in mean discharge are larger in the North in winter (summer), which can be directly linked to the changes in mean precipitation (figure 5.7) and snow melt (Coppola et al., 2014). By the end of the century, Central Italy is the only region which shows increased discharges in summer, except for the Tevere river, the main of the region. In autumn in the far future, discharges increase all over Italy, especially for smaller rivers. An exception is the Tevere, the principal river of the second largest Italian basin, which shows a negative change of about 25%. Both increasing and decreasing signals are on average stronger in the far future compared to the near future. The general trends between the two periods are not linear: Sardinia, for example, shows decreased average summer discharges in the near future, but slight increases by the end of the century (despite decreasing precipitation); in autumn, average discharges increase over most of the country, despite little to no change in average precipitation.

As a basic metric for high discharge, the mean annual maximum discharge (Q_{ymax}) over the three selected 30-year periods is displayed in figure 5.17. Compared to CHyM-OBS, in agreement with the RegCM results, CHyM-HAD for the reference period shows generally good performance, despite a slight underestimation for winter in the Po plain. By the end of the century, maximum yearly discharges increase in winter and autumn across most of Italy, with changes often above $+50\%$. In summer and spring, results are more mixed and depend on the region: central Italy shows an increase in summer (including the Tevere river basin, contrarily to mean discharge), while areas such as Sardinia and the Alps show a slight decrease in the same season. Once again changes by the end of the century are higher than in the near future and, in some cases (e.g. Central Italy), of opposite sign. These changes can in general be linked to extreme precipitation changes in the driving model (figure 5.8), which show similar patterns across the domain; there are however some notable differences, such as the marked decrease in 2070-2099 summer Q_{ymax} over Sardinia (not mirrored by $\mathrm{R95}_{ptot}$).

Figure 5.18 shows Q_{RP}: it is the peak projected discharge for the 2, 10, 20, 50 and 100 year Return Periods, calculated using the methodology described in section 4.3. Compared to the mean annual maximum discharge, this metric is more representative of extreme events, but it can only be computed on a yearly basis. These extreme discharges are in line with CHyM-OBS or even somewhat underestimated for some rivers. As for projections, in the near future changes appear to be relatively small and mixed across the domain; for the end of the century, instead, this metric shows a consistent increase in extreme discharges over the whole Italian territory, with only some areas (mainly in the southern region of Calabria) showing a slight decrease. Some large rivers, such as the Po and the Tevere, show more than doubled values of the peak 100-year discharge, compared to 1976–2005. The change results for the five Return Periods are almost identical, which is to be expected given the fact that the

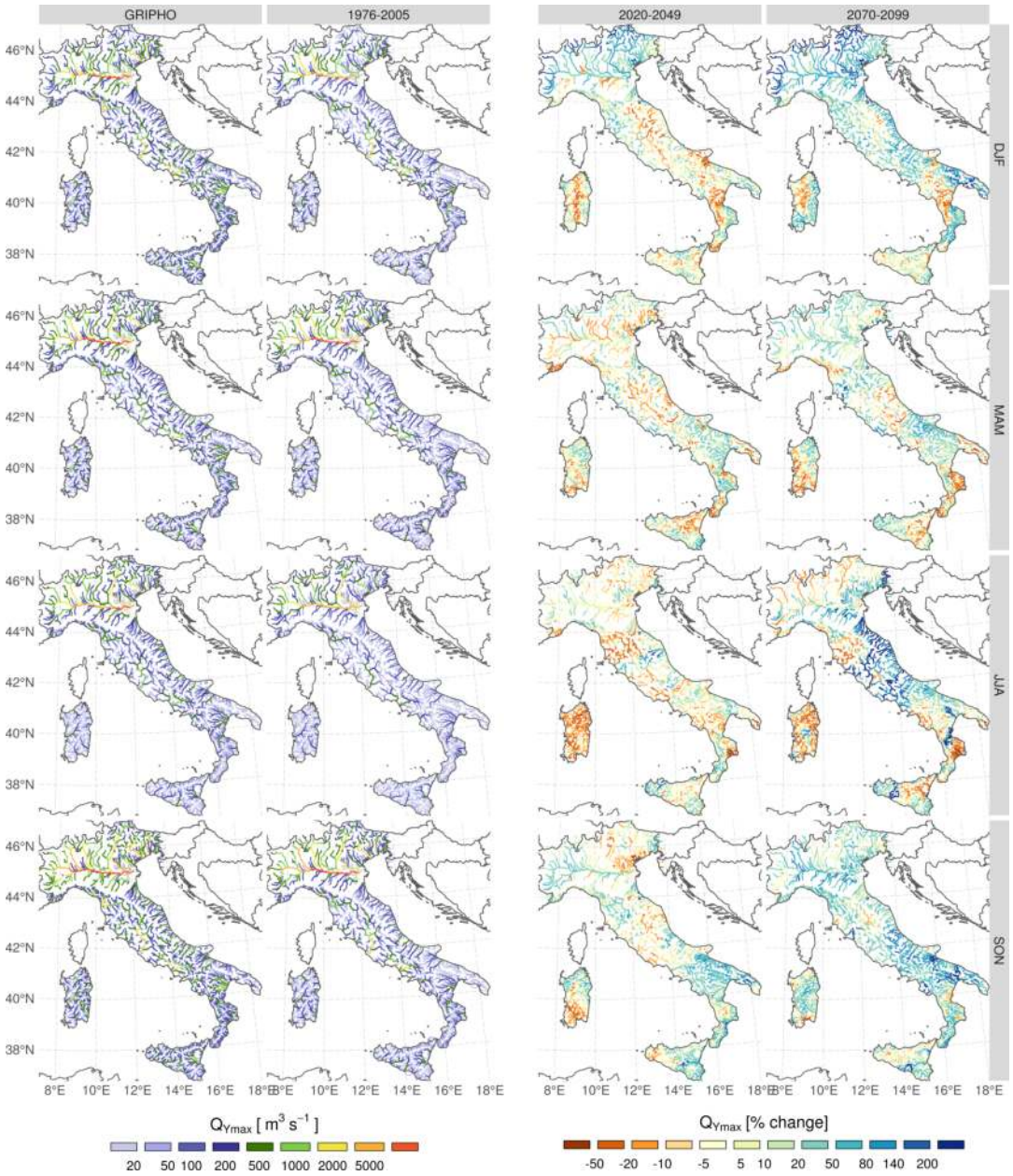

FIGURE 5.17: Like figure 5.16, but for Q_{ymax}, the mean annual maximum discharge.

discharges are calculated using the same constant parameters, only changing the RP. Another standard metric for extreme discharge is the number of times the discharge is higher than a chosen threshold. This Peak Over Threshold (POT) metric is calculated using as reference the peak projected discharge for different Return Periods (the same as in Q_{RP}, figure 5.18). Contrarily to the previous extreme metrics, this metric shows an overestimation on the side of CHyM-HAD compared to CHyM-OBS (figure 5.19), which prompts for caution with drawing conclusions from this data. The maps of POT change clearly show a strong increase in the frequency of future events, for each return period. In particular, for the end of the century, the less frequent the event (more severe floods, higher Return Period), the higher the frequency increase: the frequency of exceedance of 100-year thresholds increases more than 500% and up to tenfold over most of the domain, while the POT of 2-year events increases, on average, by a factor 2 or 3.

Since floods are closely linked with extreme discharges, Q_{ymax}, Q_{RP} and POT can all be considered proxies for flood events. This simulation then unambiguously shows a strong increase in flood hazard towards the end of the century, if the current business-as-usual policy towards climate change is not subject to intervention.

5.3 Flood hazard maps for the Italian territory

The CA2D hydraulic model is able to reproduce flood extent and water depth for the complete Italian domain, as described in section 4.4. Due to the lack of observational data, validation of CA2D against real inundation events is challenging. As an example of validation, a case study was analysed by Rita Nogherotto from the ICTP Earth System Physic group: in November 2016 heavy rainfall over the north-west of Italy, and in particular in the regions of Piemonte and Liguria, led to increase of hydrometric levels over the danger thresholds for several rivers in the Po basin, such as the Bormida and the Tanaro. The event caused vast damages and one casualty[1]. When utilising discharge data from CHyM-OBS, CA2D is able to reproduce with remarkable similarity the flooded extent as reported by COSMO-SkyMed satellite images, in figure 5.20. The actual flooded extents (top panels) are within the boundaries of the 100- and 500-year Return Period extents as simulated with the model (bottom panels) in both the areas considered. This validation, although only partial, suggests the methodology described so far is reasonable.

Figure 5.21 shows preliminary results on flood hazard maps for the complete Italian territory and for four Peturn Periods (50, 100, 250 and 500 years), as reproduced by the CA2D model using discharge data from CHyM-OBS. The results are similar to the official ISPRA flood maps (figure 1.7), even though these maps tend to show a larger flooded extent compared to our product, in compatible Return Periods. However,

[1] For additional information about the event, refer to https://it.wikipedia.org/wiki/Alluvione_del_Piemonte_del_2016 (in Italian)

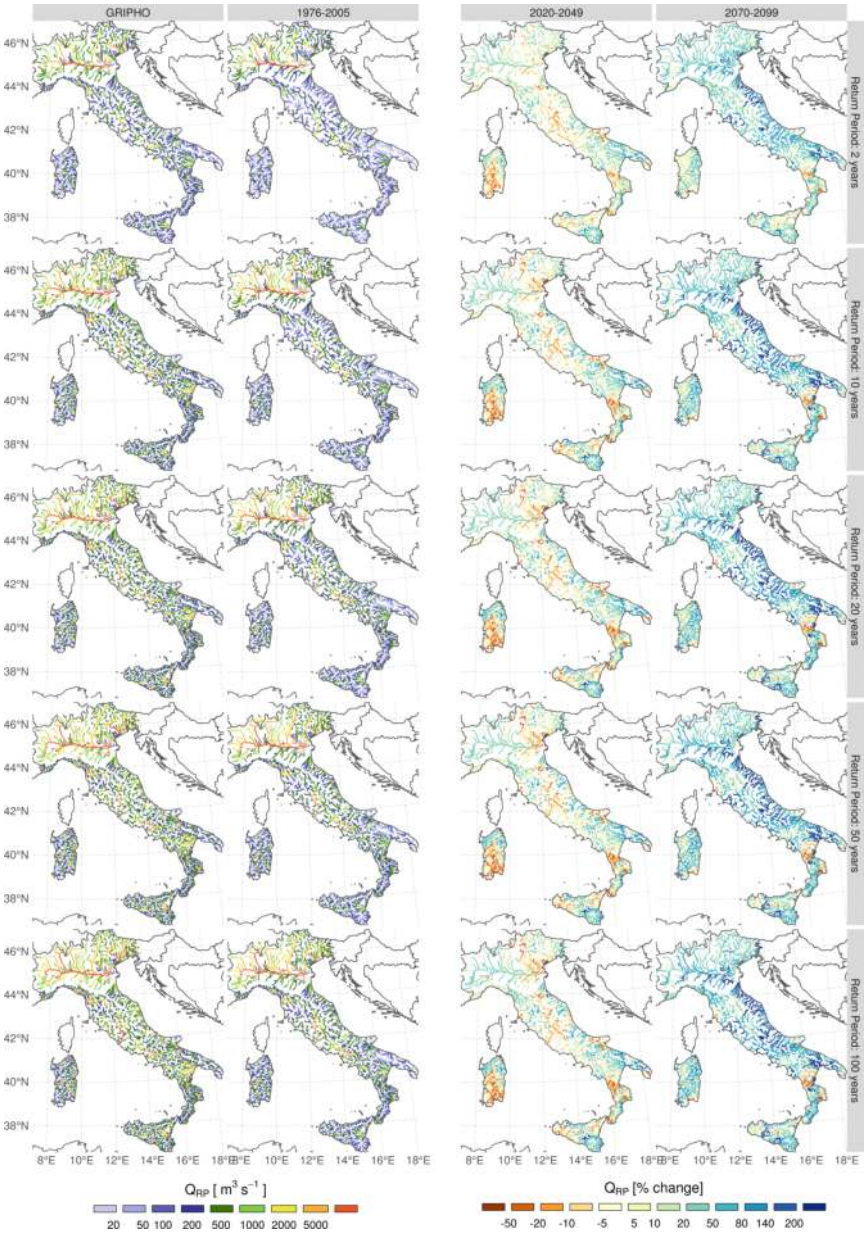

FIGURE 5.18: Like figure 5.16, but for Q_{RP}, the peak projected discharge, calculated for 5 Return Periods: 2, 10, 20, 50 and 100 years.

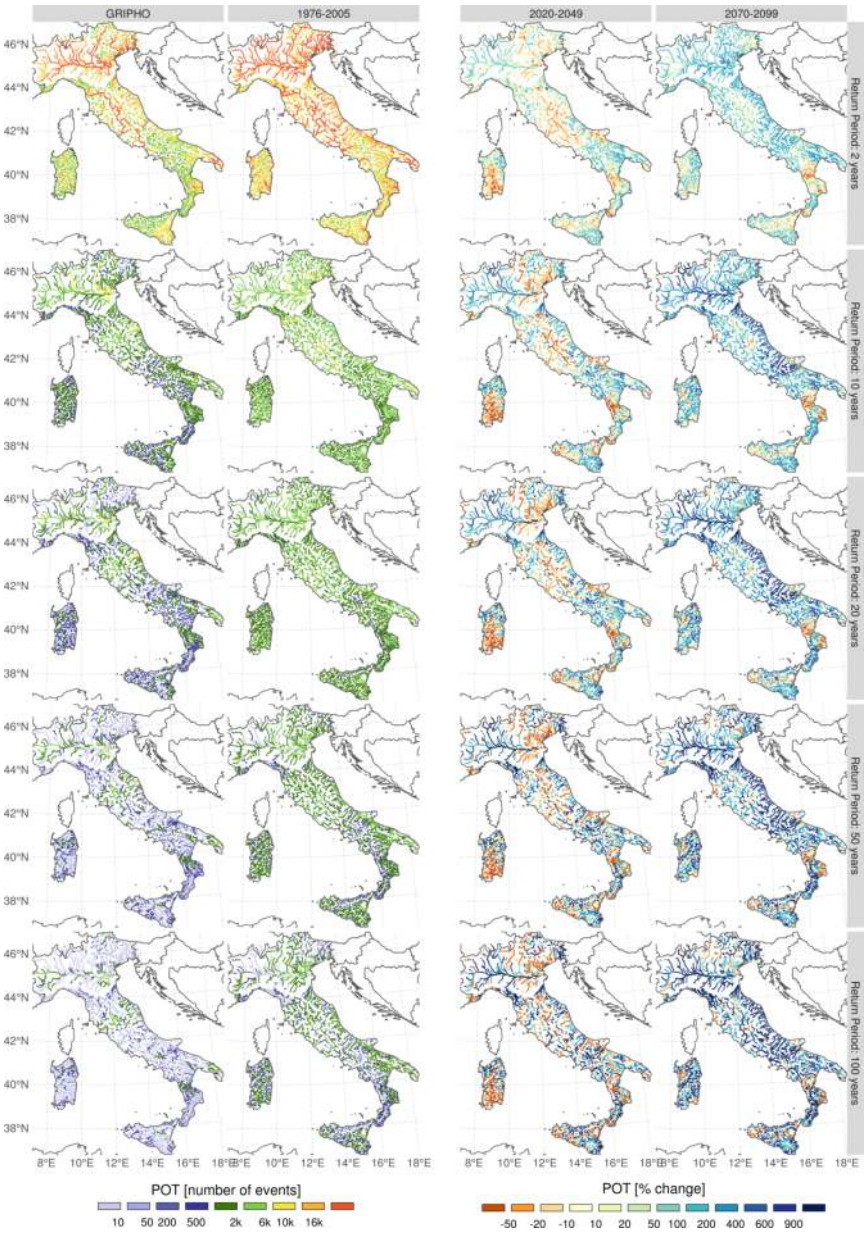

FIGURE 5.19: Like figure 5.16, but for number (and % change) of Peak Over Threshold events above the relative Q_{RP} (see figure 5.18) for 5 Return Periods: 2, 10, 20, 50 and 100 years.

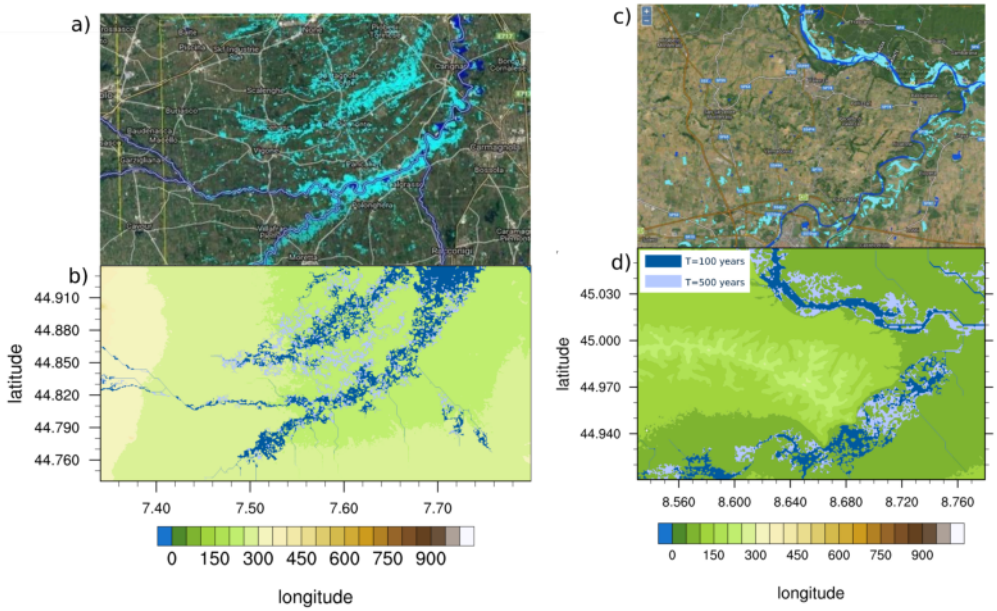

FIGURE 5.20: Case study for the Piemonte 2016 flood, used for the validation of the methodology: left, an area south of Turin; right, close to Alessandria. The panels on top show the floods as acquired by the COSMO-SkyMed satellite constellation, while the lower panels show the flood as modelled by the integrated CHyM-CA2D method for Return Periods of 100 and 500 years. From Nogherotto et al. (2019), in preparation.

the ISPRA maps are an ensemble of estimates obtained from the regional agencies, which might vary in quality and methodology. The maps here produced are instead created via an approach based on a reproducible chain of high-resolution physical models. These preliminary results are encouraging and lay the foundation for the future research avenues discussed in the next chapter.

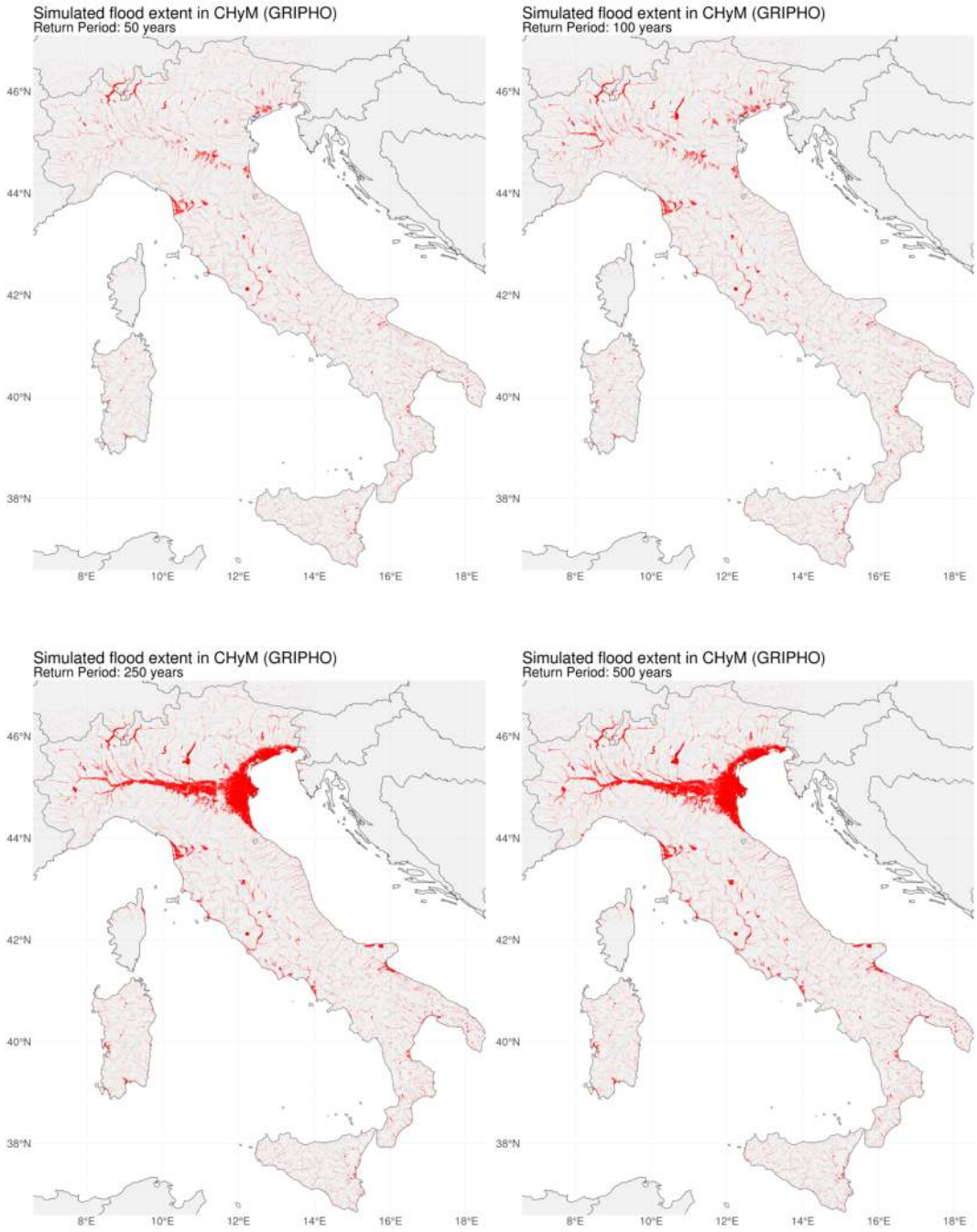

FIGURE 5.21: Preliminary results on the flooded area for four different Return Periods (50, 100, 250 and 500 years), computed by CA2D using data from an observation-driven CHyM simulation.

Chapter 6

Summary and outlook

The primary aim of this PhD project was to evaluate current flood hazard in Italy and to project changes in a future scenario. This was accomplished through a model chain of a climate, a hydrological and a hydraulic model, using an approach similar to that already employed in the literature (see section 1.3, but tailored to be able to work for the the Italian peninsula and the data available over this area. The final aim is to reproduce a much finer spatial details, including as many small catchments as possible over the whole area.

As part of the project, we developed and validated a first version of GRIPHO (GRidded Italian Precipitation Hourly Observations, chapter 3), a new high resolution hourly gridded precipitation database over Italy, for the period 2001 to 2016. To our knowledge, this is the first high resolution station-based precipitation dataset covering the complete Italian territory and having a time frequency greater than daily data. GRIPHO shows good performance in all the tested metrics, which focused on mean and extreme precipitation. In Northern Italy, GRIPHO performs similarly to the existing daily high resolution datasets. In the South, where no such dataset previously existed, GRIPHO shows significantly finer details compared to the state of the art 25 km E-OBS dataset. The creation of GRIPHO required a significant effort for data cleaning and quality control. Some erroneous station values, however, passed through the checking procedures and need to be addressed in a future version. Furthermore, the validation of GRIPHO was not possible on a sub-daily timescale, due to the lack of a suitable hourly comparison dataset, and was limited to a small set of mean and extreme precipitation metrics. We aim to address all of these deficiencies in future works (Fantini et al., 2019, in preparation).
In the context of the development of GRIPHO, we performed (section 2.1.3) an analysis of uncertainty in the available precipitation products over Italy, finding large variations across the different datasets. This analysis confirmed the need, already noted in several works (Fantini et al., 2016; Prein et al., 2016; Prein and Gobiet, 2017), for high resolution, high station density precipitation datasets, especially when considering extreme precipitation metrics. These findings are further discussed in Fantini and Coppola (2019, in preparation).

Two 12 km Regional Climate Model simulations with the ICTP RegCM model were performed on the EURO-CORDEX domain, one as a perfect boundary (ERA-Interim) experiment and one driven by a GCM (HadGEM) under the RCP8.5 scenario. These simulations were validated over the Italian territory in terms of mean and extreme precipitation and temperature, showing good model performance and entitling us to use the model for future projections. In particular, the model is capable of reproducing precipitation extremes when compared with observations. In the scenario simulation, coherently with most literature (see section 1.3), precipitation extremes are projected to strongly increase by the end of the century, even in regions where average precipitation decreases. More intense extreme events, such as those evaluated by the $R99_{ptot}$ metric, are projected to increase more than less intense extremes ($R95_{ptot}$).

Three simulations with the CHyM hydrological model were performed, in which the input precipitation data was provided by GRIPHO, RegCM (ERA-Interim) and RegCM (HadGEM) respectively. Nine separate domains, corresponding to the CHyM operational regions, were chosen and run at a resolution ranging from 300 to 900 m. Validation of the historical simulations (section 5.2), limited to two of the nine domains (the Po basin and Central Italy) due to lack of reliable observational data, showed acceptable performance on part of the model, especially when driven by the GRIPHO observations. We plan to expand this validation by performing additional data cleaning and checks on the discharge datasets considered (section 2.2).
The CHyM scenario simulation driven by RegCM (HadGEM) can be used to assess the impact of climate change on the mean and extreme discharge for the Italian river network. Being this a single scenario simulation, we are well aware of the limitations, for example, on assessing the uncertainty of the projected signal. Therefore, a possible future development would be to repeat the study in an ensemble context. The analysis of this hydrological scenario simulation shows that by comparing the 2070–2099 timeslice with the historical (1976–2005), changes in the mean are rather mixed: discharges generally increase in autumn and winter and decrease in summer, but significant regional differences are present. The Alpine area, which is the water tower for the largest Italian river catchment, the Po basin, which is often flooded, shows significantly increased mean discharges, especially in the colder months.
By the end of the century, the three metrics chosen for extreme discharges all indicate strong increases, in some cases up to tenfold the reference values, for both large and small basins. Since these metrics can be considered proxies for flood hazard, it is likely that floods are also going to increase significantly in this scenario for each of the return period examined in this thesis. These findings are generally in agreement with those found in the literature, however our approach provides a much finer look on smaller basins than previous works, which covered the entire European continent (see e.g. Alfieri et al., 2015a; Alfieri et al., 2015b).

By using the calibrated output of the hydrological model, flood extent maps were

created at a resolution of 90 m using the hydraulic model CA2D (section 5.3) and validated in a case study for the Piemonte 2016 flood. Good agreement between 100- and 500-year Return Period maps and the observed inundation is observed. Larger scale validation is limited by the lack of observations on the flooded extent in real world flood events.
Preliminary flood hazard maps were produced for the present day and compared to the maps assembled by ISPRA starting from flood data from the Italian regional agencies (figure 1.7). Similar features and extents can be found in the two products, despite the differences in the approaches employed in their creation. Compared to the ISPRA maps, our approach has the significant advantage of ensuring that the methodology is coherent across the whole Italian territory and, additionally, it provides a simple route to simulate future hazard. Currently, flood hazard maps under an RCP8.5 scenario (utilising the CHyM output analysed in this thesis) are being computed and will provide a useful tool on top of which future policies can be based.

The work presented in this thesis answers the three main research questions posed in section 1.1.1. Our model chain can reproduce flood hazard over the Italian domain, and first tests suggest good performance both in a case study and in comparison with existing maps. Our simulations project flood hazard proxies to increase in the RCP8.5 business-as-usual scenario for most of the Italian catchments, with changes often exceeding +100% by the end of the century. A good example of this is the increases in mean annual maximum discharge (Q_{Ymax}) in Northern Italy (in winter) and in Central Italy (in summer) by the end of the century.
The near and far future timeslices often show different patterns and change intensities: the peak projected 100-year discharge (Q_{100}), for example, shows only moderate changes in the 2020–2049 timeslice, but very marked increases across most of the country by 2070–2099.
In general, changes can vary from one region to the other, supporting the thesis of the necessity of high resolution studies which are capable of resolving even small river basins. Even at this local scale, changes can be non uniform: in Sardinia, for example, changes in Q_{Ymax} show different sign in different areas, despite their closeness and similar climatic characteristics.
Changes in flood hazard proxies and average discharges usually follow the changes in the respective precipitation metrics, but some exceptions suggest that ground and snow interactions also play an important role in the projections of future hydrology, which cannot only be limited to precipitation analysis. This non linearity can be seen, for example, when comparing average discharge and precipitation over the whole Italy in autumn, or extreme precipitation ($R95_{ptot}$) and discharge (Q_{Ymax}) for Central and Northern Italy in summer in the 2070–2099 timeslice. It is clear that care must be exercised when employing extreme precipitation metrics (such as $R95_{ptot}$) for estimating flood hazard, since other discharge-related proxies can sometimes paint a different picture.

The major limitations of our approach are threefold.
Firstly, the whole procedure completely ignores water management and man-made structures such as dams, dykes and canals. Consequently, it is likely that flood control procedures, such as floodplain reservoirs and river defences, might reduce flood hazard compared to our estimation. To take this factor into account on such a large scale would require significant added complexity and was not planned for this work. Secondly, the procedure described in this thesis is purposefully limited to at most 30-year timeslices: we then describe 100-year floods by extending the available data with an extreme value distribution. The uncertainty associated with this approach should not be easily dismissed, since it can represent a sizeable fraction of the signal. Schulz and Bernhardt (2016), for example, have shown that using 30-year timeslices to estimate 100-year discharges can lead to an error of up to $\pm$30%. The possibility of using the whole 130 years of scenario simulation, however, is ruled out by the need to extrapolate a climate change signal between the far future and the reference period. Thirdly, all of the work carried out in this project is based on a single model chain and a single future scenario (RCP8.5). As highlighted by Dankers and Feyen (2009) and Rojas et al. (2012), who use ensemble approaches, driving different hydrological models with a set of climate models would allow a basic estimation of the uncertainty associated with this method and improve the overall reliability of the projections. As already noted, expanding the current methodology to at least take into account several driving RCMs might be an interesting future research path. Currently, simulations with the climate change mitigation scenario RCP2.6 are planned, to validate the impact of a significantly less extreme degree of climate change which represents the best case scenario of current mitigation policies.

Despite these limitations, we believe that the approach and the tools described in this thesis are useful for evaluating and projecting flood hazard over Italy. Moreover, the methodology we followed is extremely flexible and has the potential for being applied anywhere in the world. In particular, tests on a European-wide 1 km grid have already started, with the intent of extending the evaluation of discharge flood proxies over the whole continent.

In conclusion, we developed, tested and validated a generic methodology for estimation of flood hazard in any domain where terrain and climatic information are available. The results show good agreement with the available observations. The procedure required a large amount of preparation, and in particular the completion of two regional climate simulations for the EURO-CORDEX domain and one scenario hydrological simulation over the entire Italian peninsula, not yet present in the literature. Moreover, the creation and validation of a novel high resolution hourly precipitation dataset named GRIPHO, which currently is the only dataset of this kind available over Italy, has been accomplished.

Appendix A

Temperature validation and change for the RegCM simulations

The two RegCM simulations described in section 4.1.4 are here briefly analysed for what concerns temperature. In the reference period, the comparison is performed against the UDEL(Willmott and Matsuura, 2001), CRU(Harris et al., 2014) and E-OBS (Haylock et al., 2008) datasets. Figure A.1 show the annual cycle of the two simulations, compared with that of observations. In both cases, biases with observations are relatively minor, with the model being slightly too cold in winter in all regions, and slightly too hot (cold) in the North (South) in summer.
A spatial comparison is presented in figure A.2. Average seasonal temperatures are significantly easier for the model to simulate compared to precipitation, and all major features are well reproduced. An overestimation of summer temperatures in the Po plain is found, together with a general underestimation of high elevation temperatures in winter. Uncertainties between observations are also greatly reduced for this variable, with all the three dataset showing similar spatial patterns and values.

For the RegCM (HadGEM) simulation, future changes in temperature can be reduced to a general increase, pretty uniform across all of the domain. Land areas warm up slightly more than water surfaces. The temperature changes range from to 3 to 7 °C, with average changes of 3.7 to 6.2 °C. The increase is stronger in summer and weaker in winter.
Temperature PDFs (not shown) are also mainly characterised by a uniform, constant increase across all the frequencies, seasons and regions. This means that extremely cold days generally disappear in the 2070–2099 timeslice, while high temperature events that can be considered extreme in the reference period become much more common by the end of the century: 30 °C summer days in Sardinia and Sicily, for example, become more than ten times more frequent.

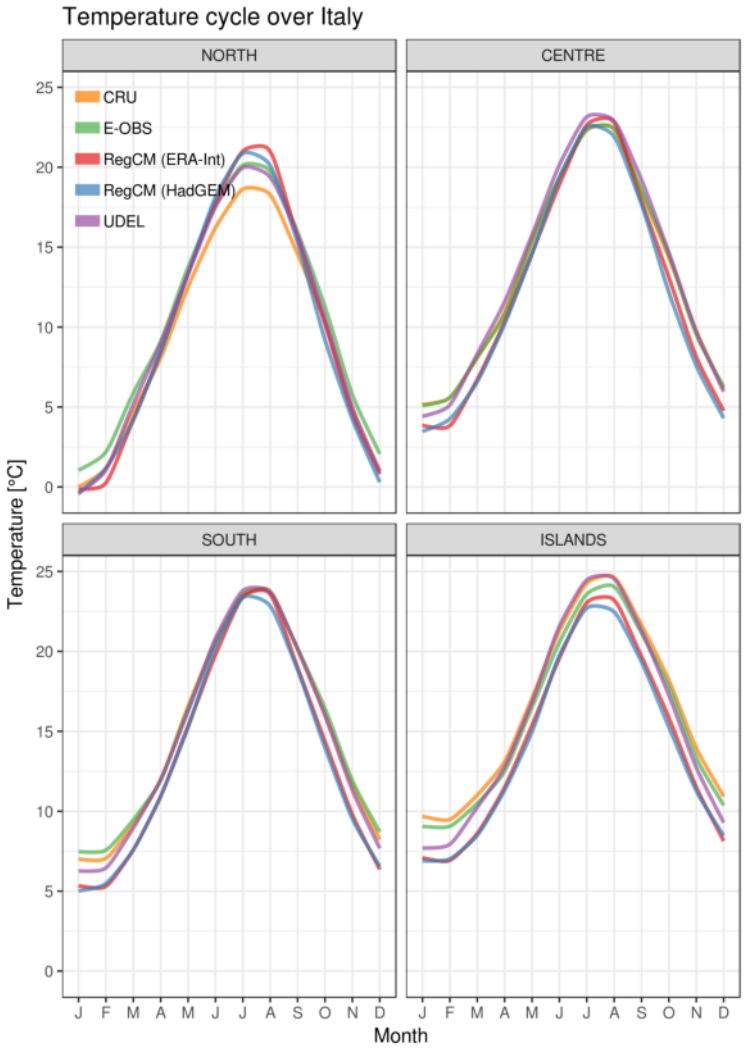

FIGURE A.1: Annual cycle of temperature as reproduced by observations and models (section 4.1.4). The time period for each dataset varies according to availability. The four macroregions selected are the same as in previous evaluations (sections 2.1.4 and 3.4).

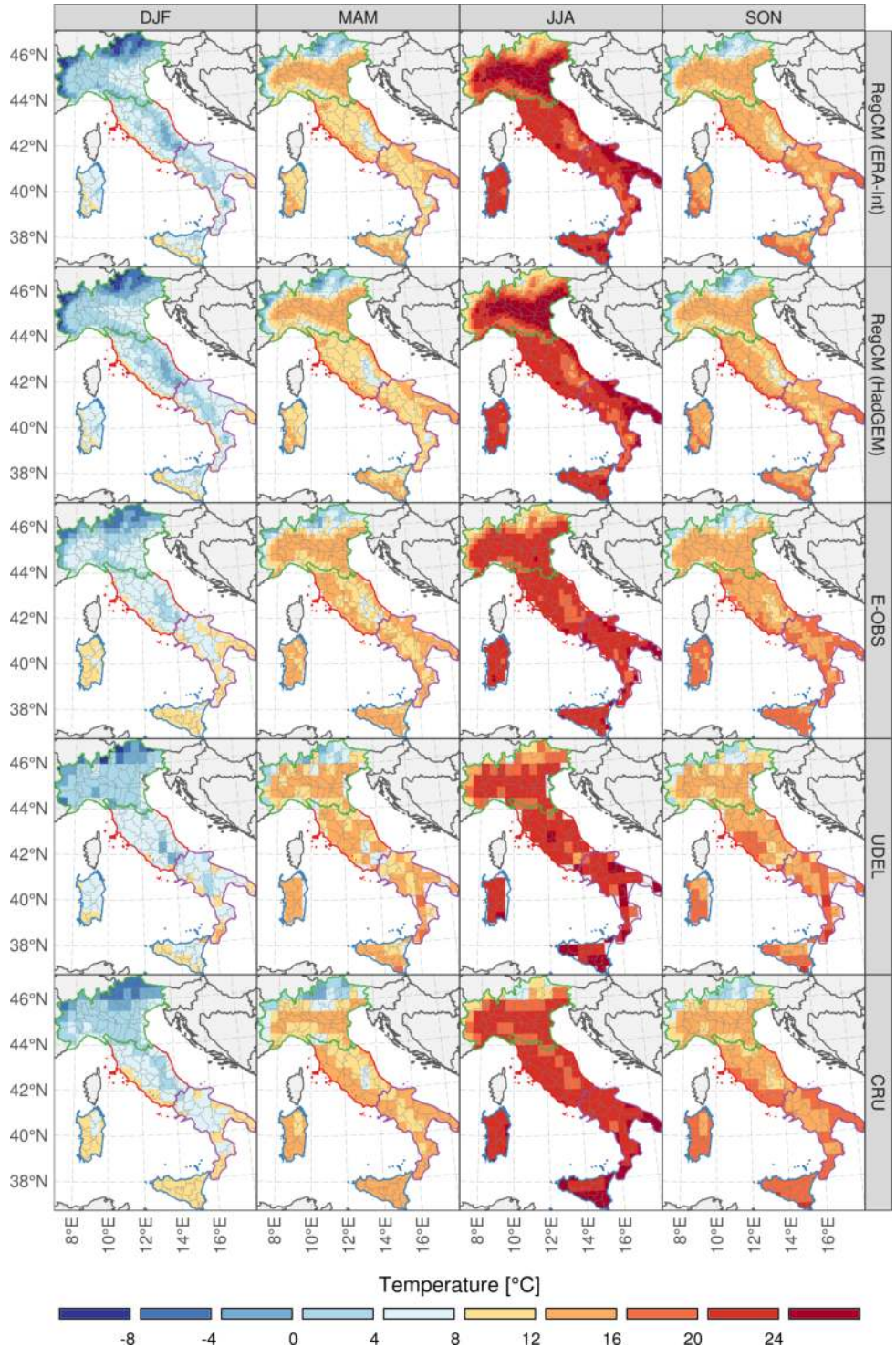

FIGURE A.2: Average seasonal temperature for the two climate model simulations (top two rows) and three selected temperature datasets.

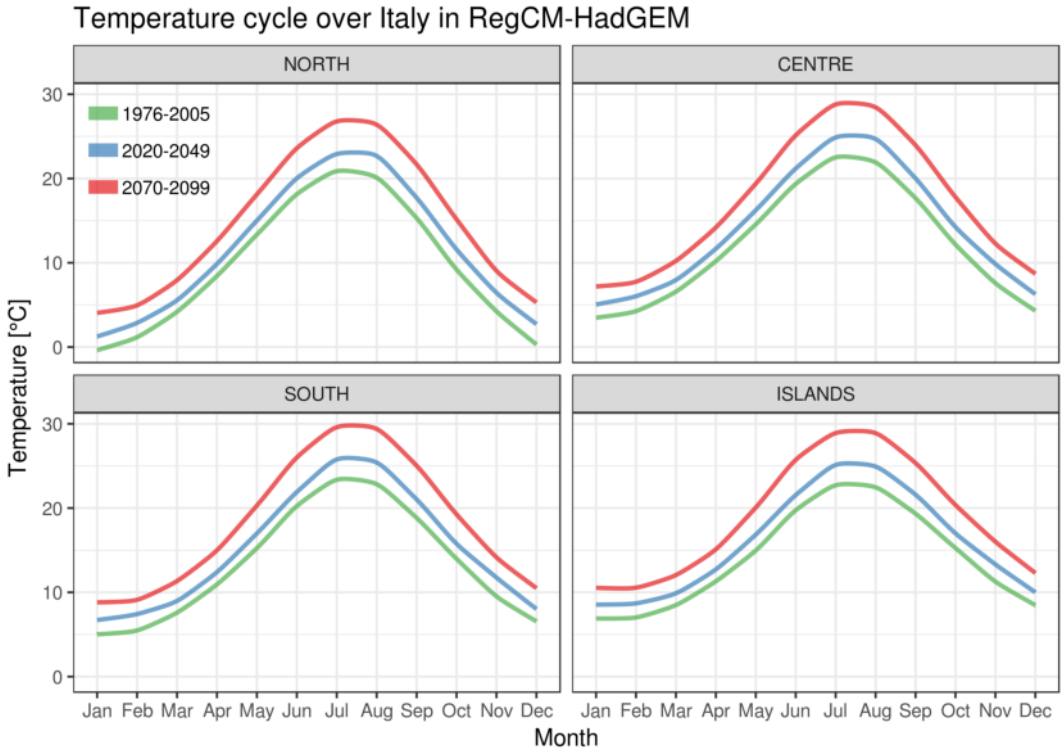

FIGURE A.3: The temperature annual cycle for the RegCM (HadGEM) simulation in the three timeslices selected, for the four macroregions (see sections 2.1.4 and 3.4).

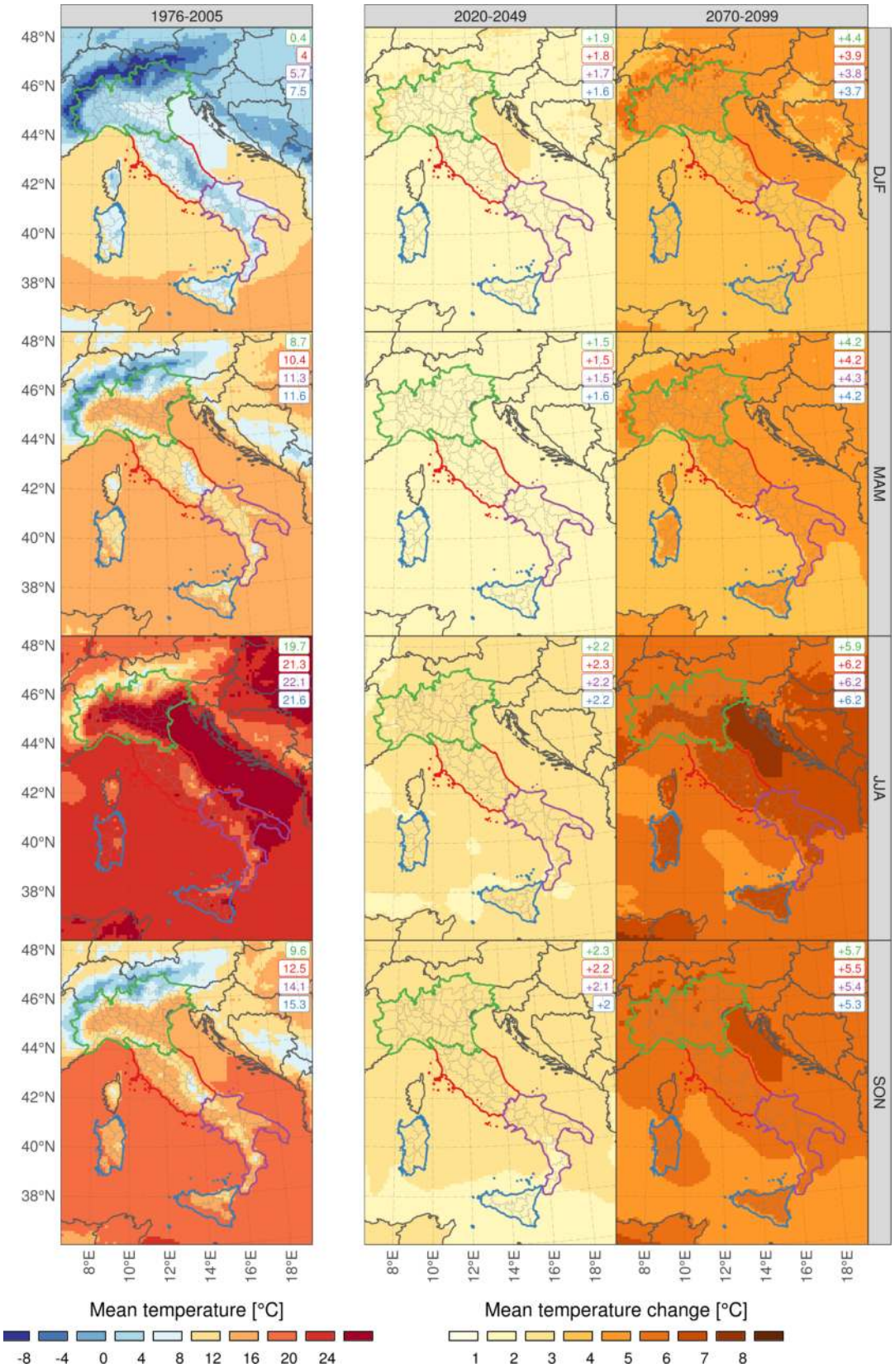

FIGURE A.4: Average seasonal temperature for the RegCM (HadGEM) simulation for the reference period (left column) and change w.r.t. it (centre and right column). The four rows represent seasons. In the top right corner of each map, the colour-coded average for each of the four macroregions is shown.

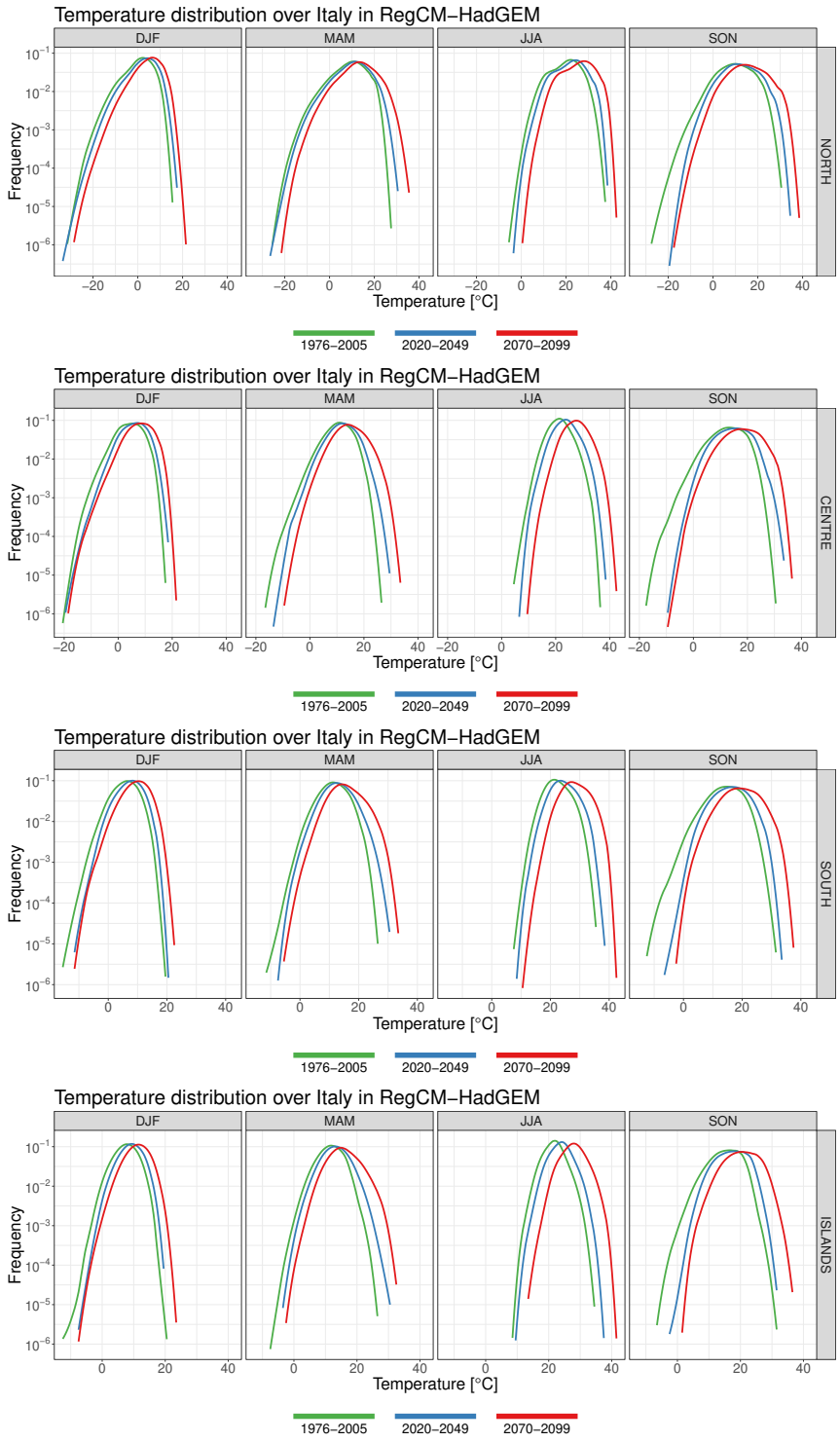

FIGURE A.5: Daily seasonal temperature Probability Density Functions for the RegCM (HadGEM) simulation, across the three timeslices. The four rows represent macroregions, the four columns the seasons.

Appendix B

Software and programs used in this thesis

This PhD project required a vast amount of computing, preprocessing, analysis and plotting. None of this would have been possible without the large number of different software packages used, all of which are free to use, and most of which are open source. The following is a non-comprehensive list of the software used:

R R Core Team (2018)

CDO Schulzweida (2018)

NCO Zender (2008)

Python Python Software Foundation (2018)

netCDF Unidata (2018)

ScyPy Jones et al. (2007)

GDAL GDAL/OGR contributors (2018)

Most of the data analysis and plotting was carried out using R. Several R packages were extremely useful and deserve a special mention:

ncdf4 Pierce (2017)

ggplot2 Wickham (2016)

patchwork Pedersen (2017)

ggspatial Dunnington (2018)

ggrepel Slowikowski (2018)

RColorBrewer Neuwirth (2014)

sf Pebesma (2018a)

stars Pebesma (2018b)

raster Hijmans (2018)

rnaturalearth South (2018)

mapedit Appelhans and Russell (2018)

leaflet Cheng et al. (2018)

shiny Chang et al. (2018)

dplyr Wickham et al. (2018)

tidyr Wickham and Henry (2018)

glue Hester (2018)

readr Wickham et al. (2017)

profvis Chang and Luraschi (2018)

purrr Henry and Wickham (2018)

furrr Vaughan and Dancho (2018)

future Bengtsson (2018)

futile.logger Rowe (2016)

optparse Davis (2018)

lubridate Grolemund and Wickham (2011)

This thesis was typeset in LaTeX.

Bibliography

Adam, Jennifer C and Dennis P Lettenmaier (2003). 'Adjustment of global gridded precipitation for systematic bias'. In: *Journal of Geophysical Research: Atmospheres (1984–2012)* 108.D9. URL: http://onlinelibrary.wiley.com/doi/10.1029/2002JD002499/full.

Adler, Robert F. et al. (2018). 'The Global Precipitation Climatology Project (GPCP) monthly analysis (New Version 2.3) and a review of 2017 global precipitation'. In: *Atmosphere*. ISSN: 20734433. DOI: 10.3390/atmos9040138.

Albano, Raffaele, Leonardo Mancusi and Andrea Abbate (2017). 'Improving flood risk analysis for effectively supporting the implementation of flood risk management plans: The case study of "Serio" Valley'. In: *Environmental Science and Policy*. ISSN: 18736416. DOI: 10.1016/j.envsci.2017.05.017.

Alfieri, L., P. Burek, E. Dutra, B. Krzeminski, D. Muraro, J. Thielen and F. Pappenberger (2013). 'GloFAS-global ensemble streamflow forecasting and flood early warning'. In: *Hydrology and Earth System Sciences*. ISSN: 10275606. DOI: 10.5194/hess-17-1161-2013.

Alfieri, L., P. Burek, L. Feyen and G. Forzieri (2015a). 'Global warming increases the frequency of river floods in Europe'. In: *Hydrology and Earth System Sciences*. ISSN: 16077938. DOI: 10.5194/hess-19-2247-2015.

Alfieri, Lorenzo, Peter Salamon, Alessandra Bianchi, Jeffrey Neal, Paul Bates and Luc Feyen (2014). 'Advances in pan-European flood hazard mapping'. In: *Hydrological Processes*. ISSN: 10991085. DOI: 10.1002/hyp.9947.

Alfieri, Lorenzo, Luc Feyen, Francesco Dottori and Alessandra Bianchi (2015b). 'Ensemble flood risk assessment in Europe under high end climate scenarios'. In: *Global Environmental Change*. ISSN: 09593780. DOI: 10.1016/j.gloenvcha.2015.09.004.

Alfieri, Lorenzo, Luc Feyen and Giuliano Di Baldassarre (2016). 'Increasing flood risk under climate change: a pan-European assessment of the benefits of four adaptation strategies'. In: *Climatic Change*. ISSN: 15731480. DOI: 10.1007/s10584-016-1641-1.

Alfieri, Lorenzo, Berny Bisselink, Francesco Dottori, Gustavo Naumann, Ad de Roo, Peter Salamon, Klaus Wyser and Luc Feyen (2017). 'Global projections of river flood risk in a warmer world'. In: *Earth's Future*. ISSN: 23284277. DOI: 10.1002/2016EF000485.

Alfieri, Lorenzo, Francesco Dottori, Richard Betts, Peter Salamon and Luc Feyen (2018). 'Multi-Model Projections of River Flood Risk in Europe under Global Warming'. In: *Climate*. ISSN: 2225-1154. DOI: 10.3390/cli6010006.

Allen, Myles R. and William J. Ingram (2002). *Constraints on future changes in climate and the hydrologic cycle*. DOI: 10.1038/nature01092.

Amadio, Mattia, Jaroslav Mysiak, Silvano Pecora and Alberto Agnetti (2013). 'Looking Forward from the Past: Assessing the Potential Flood Hazard and Damage in Polesine Region by Revisiting the 1950 Flood Event'.

Anderegg, William R L, James W Prall, Jacob Harold and Stephen H Schneider (July 2010). 'Expert credibility in climate change.' In: *Proceedings of the National Academy of Sciences of the United States of America* 107.27, pp. 12107–9. ISSN: 1091-6490. DOI: 10.1073/pnas.1003187107. URL: http://www.pubmedcentral.nih.gov/articlerender.fcgi?artid=2901439&tool=pmcentrez&rendertype=abstract.

Antolini, G., L. Auteri, V. Pavan, F. Tomei, R. Tomozeiu and V. Marletto (2016). 'A daily high-resolution gridded climatic data set for Emilia-Romagna, Italy, during 1961-2010'. In: *International Journal of Climatology*. ISSN: 10970088. DOI: 10.1002/joc.4473.

Appelhans, Tim and Kenton Russell (2018). *mapedit: Interactive Editing of Spatial Data in R*. URL: https://cran.r-project.org/package=mapedit.

Arheimer, B. and G. Lindström (2015). 'Climate impact on floods: Changes in high flows in Sweden in the past and the future (1911-2100)'. In: *Hydrology and Earth System Sciences*. ISSN: 16077938. DOI: 10.5194/hess-19-771-2015.

Arnell, Nigel W. and Simon N. Gosling (2016). 'The impacts of climate change on river flood risk at the global scale'. In: *Climatic Change*. ISSN: 15731480. DOI: 10.1007/s10584-014-1084-5.

Ashouri, Hamed, Kuo Lin Hsu, Soroosh Sorooshian, Dan K. Braithwaite, Kenneth R. Knapp, L. Dewayne Cecil, Brian R. Nelson and Olivier P. Prat (2015). 'PERSIANN-CDR: Daily precipitation climate data record from multisatellite observations for hydrological and climate studies'. In: *Bulletin of the American Meteorological Society*. ISSN: 00030007. DOI: 10.1175/BAMS-D-13-00068.1.

Auer, Ingeborg et al. (2007). 'HISTALP - Historical instrumental climatological surface time series of the Greater Alpine Region'. In: *International Journal of Climatology*. ISSN: 08998418. DOI: 10.1002/joc.1377.

Aurenhammer, Franz (1991). 'Voronoi diagrams—a survey of a fundamental geometric data structure'. In: *ACM Computing Surveys*. ISSN: 03600300. DOI: 10.1145/116873.116880.

Barber, C. Bradford, David P. Dobkin and Hannu Huhdanpaa (1996). 'The quickhull algorithm for convex hulls'. In: *ACM Transactions on Mathematical Software*. ISSN: 00983500. DOI: 10.1145/235815.235821.

Barredo, J. I. (2009). 'Normalised flood losses in Europe: 1970-2006'. In: *Natural Hazards and Earth System Science*. ISSN: 16849981. DOI: 10.5194/nhess-9-97-2009.

Barredo, Jose I., A. de Roo and C. Lavalle (2007). 'Flood risk mapping at European scale'. In: *Water Science and Technology*. ISBN: 1843395991. DOI: 10.2166/wst.2007.531.

Bartsotas, N. S., E. N. Anagnostou, E. I. Nikolopoulos and G. Kallos (2018). 'Investigating Satellite Precipitation Uncertainty Over Complex Terrain'. In: *Journal of Geophysical Research: Atmospheres*. ISSN: 21698996. DOI: 10.1029/2017JD027559.

Bashfield, a., a. Keim, A. Bashfielda and A. Keimb (2011). 'Continent-wide DEM Creation for the European Union'. In: *34th International Symposium on Remote Sensing of Environment - The GEOSS Era: Towards Operational Environmental Monitoring*.

Bates, Paul, Matt Horritt, Matt Wilson and Neil Hunter (2005). 'LISFLOOD-FP User manual and technical note'. In: *Geographical*. ISSN: 0304419X. DOI: 10.1016/S0304-419X(99)00021-9.

Bates, Paul D., Matthew S. Horritt and Timothy J. Fewtrell (2010). 'A simple inertial formulation of the shallow water equations for efficient two-dimensional flood inundation modelling'. In: *Journal of Hydrology*. ISSN: 00221694. DOI: 10.1016/j.jhydrol.2010.03.027.

Bell, V. A., A. L. Kay, R. G. Jones and R. J. Moore (2007). 'Use of a grid-based hydrological model and regional climate model outputs to assess changing flood risk'. In: *International Journal of Climatology*. ISSN: 08998418. DOI: 10.1002/joc.1539.

Bengtsson, Henrik (2018). *future: Unified Parallel and Distributed Processing in R for Everyone*. URL: https://cran.r-project.org/package=future.

Bertato, Mirko, Dario B. Giaiotti, Agostino Manzato and Fulvio Stel (2003). 'An interesting case of tornado in Friuli-Northeastern Italy'. In: *Atmospheric Research*. ISSN: 01698095. DOI: 10.1016/S0169-8095(03)00043-7.

Bianco, L., B. Tomassetti, E. Coppola, A. Fracassi, M. Verdecchia and G. Visconti (2006). 'Thermally driven circulation in a region of complex topography: Comparison of wind-profiling radar measurements and MM5 numerical predictions'. In: *Annales Geophysicae*. ISSN: 14320576. DOI: 10.5194/angeo-24-1537-2006.

Blöschl, Günter et al. (2017). 'Changing climate shifts timing of European floods'. In: *Science*. ISSN: 10959203. DOI: 10.1126/science.aan2506.

Bowman, Kenneth P. (2005). 'Four years of precipitation retrievals from the Tropical Rainfall Measuring Mission (TRMM) satellite are compared with data from 25 surface rain gauges on the National Oceanic and Atmospheric Administration/Pacific Marine Environment Laboratory (NOAA/PMEL'. In: *Journal of Climate*. ISSN: 08948755. DOI: 10.1175/JCLI3259.1.

Braca, Giovanni (2008). *STAGE – DISCHARGE RELATIONSHIPS IN OPEN CHANNELS : PRACTICES AND PROBLEMS*. Tech. rep. DOI: 10.1002/art.37735. URL: http://www.ing.unitn.it/dica/tools/download/Quaderni/Foralps_TR_11.pdf.

Brakenridge, G R, E Andersona, S V Nghiemb, S Caquard and T B Shabaneh (2003). 'Flood Warnings , Flood Disaster Assessments , and Flood Hazard Reduction : The Roles of Orbital Remote Sensing'. In: *30th International Symposium on Remote Sensing of Environment*.

Brunetti, Michele (2004). 'Changes in daily precipitation frequency and distribution in Italy over the last 120 years'. In: *Journal of Geophysical Research*. ISSN: 0148-0227. DOI: 10.1029/2003JD004296.

Brunetti, Michele, Maurizio Maugeri and Teresa Nanni (2001). 'Changes in total precipitation, rainy days and extreme events in Northeastern Italy'. In: *International Journal of Climatology*. ISSN: 08998418. DOI: 10.1002/joc.660.

Brunetti, Michele, Letizia Buffoni, Franca Mangianti, Maurizio Maugeri and Teresa Nanni (2004). 'Temperature, precipitation and extreme events during the last century in Italy'. In: *Global and Planetary Change*. ISBN: 0921-8181. DOI: 10.1016/S0921-8181(03)00104-8.

Brunetti, Michele, Maurizio Maugeri, Fabio Monti and Teresa Nanni (2006). 'Temperature and precipitation variability in Italy in the last two centuries from homogenised instrumental time series'. In: *International Journal of Climatology*. ISSN: 08998418. DOI: 10.1002/joc.1251.

Bytheway, Janice L. and Christian D. Kummerow (2013). 'Inferring the uncertainty of satellite precipitation estimates in data-sparse regions over land'. In: *Journal of Geophysical Research Atmospheres*. ISSN: 21698996. DOI: 10.1002/jgrd.50607.

Casanueva, A. et al. (2016). 'Daily precipitation statistics in a EURO-CORDEX RCM ensemble: added value of raw and bias-corrected high-resolution simulations'. In: *Climate Dynamics*. ISSN: 14320894. DOI: 10.1007/s00382-015-2865-x.

CEA (2007). 'Reducing the Social and Economic Impact of Climate Change and Natural Catastrophes Insurance Solutions and Public-Private Partnerships'. In: July, p. 40. URL: http://www.eaee.gr/cms/sites/default/files/cea_report_on_climate_change_and_natural_catastrophes.pdf.

Chan, S. C., E. J. Kendon, H. J. Fowler, S. Blenkinsop, C. A. T. Ferro and D. B. Stephenson (2012). 'Does increasing resolution improve the simulation of United Kingdom daily precipitation in a regional climate model?' In: *Climate Dynamics*. DOI: 10.1007/s00382-012-1568-9.

Chang, Winston and Javier Luraschi (2018). *profvis: Interactive Visualizations for Profiling R Code*. URL: https://cran.r-project.org/package=profvis.

Chang, Winston, Joe Cheng, J J Allaire, Yihui Xie and Jonathan McPherson (2018). *shiny: Web Application Framework for R*. URL: https://cran.r-project.org/package=shiny.

Chen, Mingyue and Pingping Xie (2008). 'CPC Unified Gauge-based Analysis of Global Daily Precipitation'. In: *2008 Western Pacific Geophysics Meeting*. ISBN: 0026-0576. DOI: http://dx.doi.org/10.1016/S0026-0576(07)80022-5.

Cheng, Joe, Bhaskar Karambelkar and Yihui Xie (2018). *leaflet: Create Interactive Web Maps with the JavaScript 'Leaflet' Library*. URL: https://cran.r-project.org/package=leaflet.

Christensen, O. B. and J. H. Christensen (2004). 'Intensification of extreme European summer precipitation in a warmer climate'. In: *Global and Planetary Change*. ISSN: 09218181. DOI: 10.1016/j.gloplacha.2004.06.013.

Clark, Peter, Nigel Roberts, Humphrey Lean, Susan P. Ballard and Cristina Charlton-Perez (2016). *Convection-permitting models: A step-change in rainfall forecasting*. DOI: 10.1002/met.1538.

Clement, M. A., C. G. Kilsby and P. Moore (2017). 'Multi-temporal synthetic aperture radar flood mapping using change detection'. In: *Journal of Flood Risk Management*. ISSN: 1753318X. DOI: 10.1111/jfr3.12303.

Collins, W. J. et al. (2011). *Development and evaluation of an Earth-system model – HadGEM2*. DOI: 10.5194/gmdd-4-997-2011.

Coppola, E., B. Tomassetti, M. Verdecchia, F.S. Marzano and G. Visconti (2006). 'Small-catchment flood forecasting and drainage network extraction using computational intelligence'. In: *The 2006 IEEE International Joint Conference on Neural Network Proceedings*. DOI: 10.1109/IJCNN.2006.246773.

Coppola, E., B. Tomassetti, L. Mariotti, M. Verdecchia and G. Visconti (2007). 'Cellular automata algorithms for drainage network extraction and rainfall data assimilation'. In: *Hydrological Sciences Journal*. ISSN: 02626667. DOI: 10.1623/hysj.52.3.579.

Coppola, Erika, Marco Verdecchia, Filippo Giorgi, Valentina Colaiuda, Barbara Tomassetti and Annalina Lombardi (Sept. 2014). 'Changing hydrological conditions in the Po basin under global warming'. In: *Science of the Total Environment* 493, pp. 1183–96. ISSN: 1879-1026. DOI: 10.1016/j.scitotenv.2014.03.003. URL: http://www.sciencedirect.com/science/article/pii/S0048969714003271http://www.ncbi.nlm.nih.gov/pubmed/24656403.

Coppola, Erika et al. (2018). *A first-of-its-kind multi-model convection permitting ensemble for investigating convective phenomena over Europe and the Mediterranean*. Springer Berlin Heidelberg. ISBN: 0123456789. DOI: 10.1007/s00382-018-4521-8. URL: http://dx.doi.org/10.1007/s00382-018-4521-8.

Covello, F., F. Battazza, A. Coletta, E. Lopinto, C. Fiorentino, L. Pietranera, G. Valentini and S. Zoffoli (2010). 'COSMO-SkyMed an existing opportunity for observing the Earth'. In: *Journal of Geodynamics*. ISSN: 02643707. DOI: 10.1016/j.jog.2010.01.001.

Crespi, A., M. Brunetti, G. Lentini and M. Maugeri (2017). '1961–1990 high-resolution monthly precipitation climatologies for Italy'. In: *International Journal of Climatology*. ISSN: 10970088. DOI: 10.1002/joc.5217.

Dai, Aiguo (2016). 'Historical and Future Changes in Streamflow and Continental Runoff: A Review'. In: *Terrestrial Water Cycle and Climate Change: Natural and Human-Induced Impacts*. ISBN: 9781118971772. DOI: 10.1002/9781118971772.ch2.

Dai, Aiguo, Taotao Qian, Kevin E. Trenberth and John D. Milliman (2009). 'Changes in continental freshwater discharge from 1948 to 2004'. In: *Journal of Climate*. ISSN: 08948755. DOI: 10.1175/2008JCLI2592.1.

Daly, Christopher, Ronald P. Neilson and Donald L. Phillips (1994). 'A Statistical-Topographic Model for Mapping Climatological Precipitation over Mountainous Terrain'. In: *Journal of Applied Meteorology*. ISSN: 0894-8763. DOI: 10.1175/1520-0450(1994)033<0140:ASTMFM>2.0.CO;2.

Dankers, Rutger and Luc Feyen (2009). 'Flood hazard in Europe in an ensemble of regional climate scenarios'. In: *Journal of Geophysical Research Atmospheres*. ISSN: 01480227. DOI: 10.1029/2008JD011523.

Dankers, Rutger et al. (2014). 'First look at changes in flood hazard in the Inter-Sectoral Impact Model Intercomparison Project ensemble'. In: *Proceedings of the National Academy of Sciences*. ISSN: 0027-8424. DOI: 10.1073/pnas.1302078110.

Davis, Trevor L (2018). *optparse: Command Line Option Parser*. URL: https://cran.r-project.org/package=optparse.

De Moel, H., J. Van Alphen and J. C.J.H. Aerts (2009). 'Flood maps in Europe - Methods, availability and use'. In: *Natural Hazards and Earth System Science*. ISSN: 16849981. DOI: 10.5194/nhess-9-289-2009.

Dee, D. P. et al. (Apr. 2011). 'The ERA-Interim reanalysis: configuration and performance of the data assimilation system'. In: *Quarterly Journal of the Royal Meteorological Society* 137.656, pp. 553–597. ISSN: 00359009. DOI: 10.1002/qj.828. URL: http://doi.wiley.com/10.1002/qj.828.

Demir, Vahdettin and Ozgur Kisi (2016). 'Flood Hazard Mapping by Using Geographic Information System and Hydraulic Model: Mert River, Samsun, Turkey'. In: *Advances in Meteorology*. ISSN: 16879317. DOI: 10.1155/2016/4891015.

Di Baldassarre, G. and A. Montanari (2009). 'Uncertainty in river discharge observations: A quantitative analysis'. In: *Hydrology and Earth System Sciences*. ISSN: 16077938. DOI: 10.5194/hess-13-913-2009.

Di Luca, Alejandro, Ramón de Elía and René Laprise (Apr. 2011). 'Potential for added value in precipitation simulated by high-resolution nested Regional Climate Models and observations'. In: *Climate Dynamics* 38.5-6, pp. 1229–1247. ISSN: 0930-7575. DOI: 10.1007/s00382-011-1068-3. URL: http://link.springer.com/article/10.1007/s00382-011-1068-3http://link.springer.com/10.1007/s00382-011-1068-3.

Di Salvo, Cristina, Giancarlo Ciotoli, Francesco Pennica and Gian Paolo Cavinato (2017). 'Pluvial flood hazard in the city of Rome (Italy)'. In: *Journal of Maps*. ISSN: 17445647. DOI: 10.1080/17445647.2017.1333968.

Diaconescu, Emilia Paula, Philippe Gachon and René Laprise (2015). 'On the Remapping Procedure of Daily Precipitation Statistics and Indices Used in Regional Climate Model Evaluation'. In: *Journal of Hydrometeorology*. ISSN: 1525-755X. DOI: 10.1175/JHM-D-15-0025.1. URL: https://journals.ametsoc.org/doi/full/10.1175/JHM-D-15-0025.1.

Dickinson, Robert E, Ronald M Errico, Filippo Giorgi and Gary T Bates (1989). 'A regional climate model for the western United States'. In: *Climatic Change* 15.3, pp. 383–422.

Do, Hong X., Seth Westra and Michael Leonard (2017). 'A global-scale investigation of trends in annual maximum streamflow'. In: *Journal of Hydrology*. ISSN: 00221694. DOI: 10.1016/j.jhydrol.2017.06.015.

Donnelly, Chantal, Wouter Greuell, Jafet Andersson, Dieter Gerten, Giovanna Pisacane, Philippe Roudier and Fulco Ludwig (2017). 'Impacts of climate change on European hydrology at 1.5, 2 and 3 degrees mean global warming above preindustrial level'. In: *Climatic Change*. ISSN: 15731480. DOI: 10.1007/s10584-017-1971-7.

Dottori, F. and E. Todini (2010). 'A 2D Flood Inundation Model Based on Cellular Automata Approach'. In: *XVIII International Conference on Water Resources*.

– (2011). 'Developments of a flood inundation model based on the cellular automata approach: Testing different methods to improve model performance'. In: *Physics and Chemistry of the Earth*. ISSN: 14747065. DOI: 10.1016/j.pce.2011.02.004.

Dottori, Francesco, Rui Figueiredo, Mario L.V. Martina, Daniela Molinari and Anna Rita Scorzini (2016). 'INSYDE: A synthetic, probabilistic flood damage model based on explicit cost analysis'. In: *Natural Hazards and Earth System Sciences*. ISSN: 16849981. DOI: 10.5194/nhess-16-2577-2016.

Duchon, Claude E. and Gavin R. Essenberg (2001). 'Comparative rainfall observations from pit and aboveground rain gauges with and without wind shields'. In: *Water Resources Research*. ISSN: 00431397. DOI: 10.1029/2001WR000541.

Dunnington, Dewey (2018). *ggspatial: Spatial Data Framework for ggplot2*. URL: https://cran.r-project.org/package=ggspatial.

Durman, C. F., J. M. Gregory, D. C. Hassell, R. G. Jones and J. M. Murphy (2001). 'A comparison of extreme European daily precipitation simulated by a global and a regional model for present and future climates'. In: *Quarterly Journal of the Royal Meteorological Society*. ISSN: 00359009. DOI: 10.1256/smsqj.57315.

Eaton, Brian et al. (2009). *NetCDF Climate and Forecast (CF) Metadata Conventions*. Tech. rep.

European Union Floods Directive (2007). *DIRECTIVE 2007/60/EC OF THE EUROPEAN PARLIAMENT AND OF THE COUNCIL: on the assessment and management of flood risks*.

EWA (2014). *European Water Archive (EWA) of EURO-FRIEND-Water*. URL: https://www.bafg.de/GRDC/EN/04_spcldtbss/42_EWA/ewa_node.html.

Eyring, Veronika, Sandrine Bony, Gerald A. Meehl, Catherine A. Senior, Bjorn Stevens, Ronald J. Stouffer and Karl E. Taylor (2016). 'Overview of the Coupled Model Intercomparison Project Phase 6 (CMIP6) experimental design and organization'. In: *Geoscientific Model Development*. ISSN: 19919603. DOI: 10.5194/gmd-9-1937-2016.

Fantini, Adriano and Erika Coppola (2019). 'Uncertainty in gridded precipitation datasets over Europe'. In: *in preparation*.

Fantini, Adriano et al. (2016). 'Assessment of multiple daily precipitation statistics in ERA-Interim driven Med-CORDEX and EURO-CORDEX experiments against high resolution observations'. In: *Climate Dynamics* 51.2, pp. 877–900. ISSN: 14320894. DOI: 10.1007/s00382-016-3453-4. URL: https://link.springer.com/article/10.1007/s00382-016-3453-4.

Fantini, Adriano, Erika Coppola, Marco Verdecchia and Graziano Giuliani (2019). 'GRIPHO : a gridded high-resolution hourly precipitation dataset over Italy'. In: *in preparation*.

Feyen, Luc, Rutger Dankers, Katalin Bódis, Peter Salamon and José I. Barredo (2011). 'Fluvial flood risk in Europe in present and future climates'. In: *Climatic Change*. ISSN: 01650009. DOI: 10.1007/s10584-011-0339-7.

Fischer, Andreas, Denise Keller, Mark Liniger, Jan Rajczak and Christoph Schär (2014). 'Projected changes in precipitation intensity and frequency over complex topography : a multi-model perspective'. In: 16, p. 9916. ISSN: 08998418. DOI: 10.1002/joc.4162.

Førland, E.J. et al. (1996). *Manual for Operational Correction of Nordic Precipitation Data*. Tech. rep. Norwegian Meteorological Institute. URL: https://www.met.no/publikasjoner/met-report/met-report-1996/_/attachment/download/ea2cb006-688a-408f-a60c-9f6306843cc0:e16a138129a1d1896cff764ab3eb2cc42aefb160/MET-report-24-1996.pdf.

Forzieri, Giovanni, Alessandro Cescatti, Filipe Batista e Silva and Luc Feyen (2017). 'Increasing risk over time of weather-related hazards to the European population: a data-driven prognostic study'. In: *The Lancet Planetary Health*. ISSN: 25425196. DOI: 10.1016/S2542-5196(17)30082-7.

Forzieri, Giovanni, Alessandra Bianchi, Filipe Batista e. Silva, Mario A. Marin Herrera, Antoine Leblois, Carlo Lavalle, Jeroen C.J.H. Aerts and Luc Feyen (2018). 'Escalating impacts of climate extremes on critical infrastructures in Europe'. In: *Global Environmental Change*. ISSN: 09593780. DOI: 10.1016/j.gloenvcha.2017.11.007.

Fowler, H. J. and C. G. Kilsby (2003). 'Implications of changes in seasonal and annual extreme rainfall'. In: *Geophysical Research Letters*. ISSN: 00948276. DOI: 10.1029/2003GL017327.

Frei, Christoph, Regina Schöll, Sophie Fukutome, Jürg Schmidli and Pier Luigi Vidale (2006). 'Future change of precipitation extremes in Europe: Intercomparison of scenarios from regional climate models'. In: *Journal of Geophysical Research Atmospheres* 111. ISSN: 01480227. DOI: 10.1029/2005JD005965.

Funk, Chris et al. (2015). 'The climate hazards infrared precipitation with stations - A new environmental record for monitoring extremes'. In: *Scientific Data*. ISSN: 20524463. DOI: 10.1038/sdata.2015.66.

Gao, Y. C. and M. F. Liu (2013). 'Evaluation of high-resolution satellite precipitation products using rain gauge observations over the Tibetan Plateau'. In: *Hydrology and Earth System Sciences*. ISSN: 10275606. DOI: 10.5194/hess-17-837-2013.

GDAL/OGR contributors (2018). *{GDAL/OGR} Geospatial Data Abstraction software Library*. URL: http://gdal.org.

Germann, Urs, Gianmario Galli, Marco Boscacci and Martin Bolliger (2006). 'Radar precipitation measurement in a mountainous region'. In: *Quarterly Journal of the Royal Meteorological Society*. ISSN: 00359009. DOI: 10.1256/qj.05.190.

Giorgi, Filippo (Sept. 1990). 'Simulation of Regional Climate Using a Limited Area Model Nested in a General Circulation Model'. In: *Journal of Climate* 3.9, pp. 941–963. ISSN: 0894-8755. DOI: 10.1175/1520-0442(1990)003<0941:SORCUA>2.0.CO;2. URL: http://journals.ametsoc.org/doi/abs/10.1175/1520-0442%281990%29003%3C0941%3ASORCUA%3E2.0.CO%3B2.

Giorgi, Filippo and Gary T. Bates (1989). 'The Climatological Skill of a Regional Model over Complex Terrain'. In: *Monthly Weather Review*. ISSN: 0027-0644. DOI: 10.1175/1520-0493(1989)117<2325:TCSOAR>2.0.CO;2.

Giorgi, Filippo and William J. Gutowski (2015). 'Regional Dynamical Downscaling and the Cordex Initiative'.

Giorgi, Filippo and Linda O Mearns (1999). 'Introduction to special section- Regional climate modeling revisited'. In: *Journal of Geophysical Research: Atmospheres (1984–2012)* 104.D6, pp. 6335–6352. URL: http://onlinelibrary.wiley.com/doi/10.1029/98JD02072/full;http://onlinelibrary.wiley.com/doi/10.1029/98JD02072/pdf.

Giorgi, Filippo, Maria Rosaria Marinucci and Gary T. Bates (Oct. 1993). 'Development of a Second-Generation Regional Climate Model (RegCM2). Part I: Boundary-Layer and Radiative Transfer Processes'. In: *Monthly Weather Review* 121.10, pp. 2794–2813. ISSN: 0027-0644. DOI: 10.1175/1520-0493(1993)121<2794:DOASGR>2.0.CO;2. URL: http://journals.ametsoc.org/doi/abs/10.1175/1520-0493%281993%29121%3C2794%3ADOASGR%3E2.0.CO%3B2.

Giorgi, Filippo, Colin Jones and GR Asrar (2009). 'Addressing climate information needs at the regional level: the CORDEX framework'. In: *... Organization (WMO) Bulletin* 58.July, pp. 175–183. URL: http://wcrp.ipsl.jussieu.fr/cordex/documents/CORDEX_giorgi_WMO.pdf.

Giorgi, Filippo et al. (Mar. 2012). 'RegCM4: model description and preliminary tests over multiple CORDEX domains'. In: *Climate Research* 52, pp. 7–29. ISSN: 0936-577X. DOI: 10.3354/cr01018. URL: http://www.int-res.com/abstracts/cr/v52/p7-29/.

Gobiet, Andreas, Sven Kotlarski, Martin Beniston, Georg Heinrich, Jan Rajczak and Markus Stoffel (2014). '21st century climate change in the European Alps-A review'. In: *Science of the Total Environment*. ISSN: 18791026. DOI: 10.1016/j.scitotenv.2013.07.050.

Gosling, S. N., R. G. Taylor, N. W. Arnell and M. C. Todd (2011). 'A comparative analysis of projected impacts of climate change on river runoff from global and catchment-scale hydrological models'. In: *Hydrology and Earth System Sciences*. ISSN: 10275606. DOI: 10.5194/hess-15-279-2011.

Gosling, Simon N. et al. (2017). 'A comparison of changes in river runoff from multiple global and catchment-scale hydrological models under global warming scenarios of 1 °C, 2 °C and 3 °C'. In: *Climatic Change*. ISSN: 15731480. DOI: 10.1007/s10584-016-1773-3.

Goubanova, K. and L. Li (2007). 'Extremes in temperature and precipitation around the Mediterranean basin in an ensemble of future climate scenario simulations'. In: *Global and Planetary Change*. ISSN: 09218181. DOI: 10.1016/j.gloplacha.2006.11.012.

G.R.Brakenridge (2015). *Global Active Archive of Large Flood Events*. URL: http://floodobservatory.colorado.edu/Archives/index.html.

Grell, Georg a, J. Dudhia and D. Stauffer (1994). *A description of the fifth-generation Penn State/NCAR Mesoscale Model (MM5)*. Tech. rep. December, p. 121. DOI: 10.5065/D60Z716B.

Grolemund, Garrett and Hadley Wickham (2011). 'Dates and Times Made Easy with {lubridate}'. In: *Journal of Statistical Software* 40.3, pp. 1–25. URL: http://www.jstatsoft.org/v40/i03/.

Guha-sapir, Debarati, Philippe Hoyois and Regina Below (2011). *Annual Disaster Statistical Review 2010: The numbers and trends*. Tech. rep. DOI: 10.1093/rof/rfs003.

Gupta, Hoshin V., Harald Kling, Koray K. Yilmaz and Guillermo F. Martinez (2009). 'Decomposition of the mean squared error and NSE performance criteria: Implications for improving hydrological modelling'. In: *Journal of Hydrology*. ISSN: 00221694. DOI: 10.1016/j.jhydrol.2009.08.003.

Gutowski, J. William et al. (2016). 'WCRP COordinated Regional Downscaling EXperiment (CORDEX): A diagnostic MIP for CMIP6'. In: *Geoscientific Model Development*. ISSN: 19919603. DOI: 10.5194/gmd-9-4087-2016.

Haarsma, Reindert J. et al. (2016). 'High Resolution Model Intercomparison Project (HighResMIP v1.0) for CMIP6'. In: *Geoscientific Model Development*. ISSN: 19919603. DOI: 10.5194/gmd-9-4185-2016.

Hall, J. et al. (2014). 'Understanding flood regime changes in Europe: A state-of-the-art assessment'. In: *Hydrology and Earth System Sciences*. ISSN: 16077938. DOI: 10.5194/hess-18-2735-2014.

Harris, I., P. D. Jones, T. J. Osborn and D. H. Lister (2014). 'Updated high-resolution grids of monthly climatic observations - the CRU TS3.10 Dataset'. In: *International Journal of Climatology*. ISSN: 08998418. DOI: 10.1002/joc.3711.

Haylock, M R, N. Hofstra, A.M.G. Klein Tank, E.J. Klok, P.D. Jones and M New. (2008). 'A European daily high-resolution gridded dataset of surface temperature and precipitation'. In: *Journal of Geophysical Research-Atmospheres*. ISSN: 0148-0227. DOI: 10.1029/2008JD010201.

Henry, Lionel and Hadley Wickham (2018). *purrr: Functional Programming Tools*. URL: https://cran.r-project.org/package=purrr.

Hester, Jim (2018). *glue: Interpreted String Literals*. URL: https://cran.r-project.org/package=glue.

Hiebl, Johann and Christoph Frei (2017). 'Daily precipitation grids for Austria since 1961—development and evaluation of a spatial dataset for hydroclimatic monitoring and modelling'. In: *Theoretical and Applied Climatology*. ISSN: 14344483. DOI: 10.1007/s00704-017-2093-x.

Hijmans, Robert J (2018). *raster: Geographic Data Analysis and Modeling*. URL: https://cran.r-project.org/package=raster.

Hirabayashi, Yukiko and Shinjiro Kanae (2009). 'First estimate of the future global population at risk of flooding'. In: *Hydrological Research Letters*. ISSN: 1882-3416. DOI: 10.3178/hrl.3.6.

Hirabayashi, Yukiko, Shinjiro Kanae, Seita Emori, Taikan Oki and Masahide Kimoto (2008). 'Global projections of changing risks of floods and droughts in a changing climate'. In: *Hydrological Sciences Journal*. ISSN: 02626667. DOI: 10.1623/hysj.53.4.754.

Hirabayashi, Yukiko, Roobavannan Mahendran, Sujan Koirala, Lisako Konoshima, Dai Yamazaki, Satoshi Watanabe, Hyungjun Kim and Shinjiro Kanae (2013). 'Global flood risk under climate change'. In: *Nature Climate Change*. ISSN: 1758678X. DOI: 10.1038/nclimate1911.

Hofstra, Nynke, Malcolm Haylock, Mark New, Phil Jones and Christoph Frei (2008). 'Comparison of six methods for the interpolation of daily, European climate data'. In: *Journal of Geophysical Research Atmospheres*. ISSN: 01480227. DOI: 10.1029/2008JD010100.

Hou, Arthur Y., Ramesh K. Kakar, Steven Neeck, Ardeshir A. Azarbarzin, Christian D. Kummerow, Masahiro Kojima, Riko Oki, Kenji Nakamura and Toshio Iguchi (2014). 'The global precipitation measurement mission'. In: *Bulletin of the American Meteorological Society*. ISSN: 00030007. DOI: 10.1175/BAMS-D-13-00164.1.

Huffman, George J., David T. Bolvin, Eric J. Nelkin, David B. Wolff, Robert F. Adler, Guojun Gu, Yang Hong, Kenneth P. Bowman and Erich F. Stocker (2007). *The TRMM Multisatellite Precipitation Analysis (TMPA): Quasi-Global, Multiyear, Combined-Sensor Precipitation Estimates at Fine Scales*. DOI: 10.1175/JHM560.1.

Hughes, D. A. (2006). 'Comparison of satellite rainfall data with observations from gauging station networks'. In: *Journal of Hydrology*. ISSN: 00221694. DOI: 10.1016/j.jhydrol.2005.11.041.

Huntjens, Patrick, Claudia Pahl-Wostl and John Grin (2010). 'Climate change adaptation in European river basins'. In: *Regional Environmental Change*. ISSN: 14363798. DOI: 10.1007/s10113-009-0108-6.

Inatsu, Masaru and Masahide Kimoto (2009). *A Scale Interaction Study on East Asian Cyclogenesis Using a General Circulation Model Coupled with an Interactively Nested Regional Model*. DOI: 10.1175/2009MWR2825.1.

IPCC (2000). *Special Report Emissions Scenarios*. Tech. rep. DOI: http://dx.doi.org/10.1111/sode.12035.

– (2008). *Towards New Scenarios for Analysis of Emissions, Climate Change, Impacts and Response Strategies*. Ed. by Richard H Moss, p. 132. ISBN: 9789291691241. URL: http://www.osti.gov/energycitations/product.biblio.jsp?osti_id=940991.

– (2012). 'Determinants of risk: Exposure and vulnerability'. In: *Managing the Risks of Extreme Events and Disasters to Advance Climate Change Adaptation: Special Report of*

the Intergovernmental Panel on Climate Change. ISBN: 9781139177245. DOI: 10.1017/CBO9781139177245.005.

IPCC (2014). 'Climate Change 2014: Impacts, Adaptation, and Vulnerability'. In: *Assessment Report 5*. DOI: 10.1017/CBO9781107415379.

– (2018). *Global Warming of 1.5 °C*. Tech. rep. IPCC. URL: https://www.ipcc.ch/report/sr15/.

IPCC WG1 (2013). *Climate Change 2013: The Physical Science Basis. Contribution of Working Group I to the Fifth Assessment Report of the Intergovernmental Panel on Climate Change*. Tech. rep. Cambridge University Press, Cambridge, United Kingdom and New York, NY, USA, p. 1535. URL: http://inis.iaea.org/search/search.aspx?orig_q=RN:45042273.

Isotta, Francesco a. et al. (Apr. 2014). 'The climate of daily precipitation in the Alps: development and analysis of a high-resolution grid dataset from pan-Alpine rain-gauge data'. In: *International Journal of Climatology* 34.5, pp. 1657–1675. ISSN: 08998418. DOI: 10.1002/joc.3794. URL: http://doi.wiley.com/10.1002/joc.3794.

Istituto di Ricerca per la Protezione Idrologica and Consiglio Nazionale delle Ricerche (2018). *Polaris - Rapporto Periodico 2017 sul Rischio posto alla Popolazione italiana da Frane e Inondazioni*. Tech. rep. IRPI/CNR. URL: http://polaris.irpi.cnr.it/wp-content/uploads/report-2017.pdf.

Jacob, Daniela et al. (2014). 'EURO-CORDEX: New high-resolution climate change projections for European impact research'. In: *Regional Environmental Change* 14, pp. 563–578. ISSN: 1436378X. DOI: 10.1007/s10113-013-0499-2.

Jiménez Cisneros, B.E., T. Oki, N.W. Arnell, G. Benito, J.G. Cogley, P. Döll, T. Jiang and S.S. Mwakalila (2014). *Freshwater resources. In: Climate Change 2014: Impacts,Adaptation, and Vulnerability. Part A: Global and Sectoral Aspects. Contribution of Working Group II to the Fifth Assessment Report of the Intergovernmental Panel on Climate Change*. Tech. rep., pp. 229–269. DOI: 10.2134/jeq2008.0015br. URL: http://www.ncbi.nlm.nih.gov/entrez/query.fcgi?cmd=Retrieve&db=PubMed&dopt=Citation&list_uids=15236969.

Johansson, B. (2002). 'Estimation of areal precipitation for hydrological modelling'. PhD thesis. Earth Sciences Centre, Göteborg University.

Jones, Eric, Travis Oliphant, Pearu Peterson and Others (2007). *SciPy: Open source scientific tools for Python*. DOI: 10.1109/MCSE.2007.58. URL: https://www.scipy.org/.

Jones, R. G., J. M. Murphy and M. Noguer (July 1995). 'Simulation of climate change over europe using a nested regional-climate model. I: Assessment of control climate, including sensitivity to location of lateral boundaries'. In: *Quarterly Journal of the Royal Meteorological Society* 121.526, pp. 1413–1449. ISSN: 00359009. DOI: 10.1002/qj.49712152610. URL: http://doi.wiley.com/10.1002/qj.49712152610.

Jongman, Brenden, Philip J. Ward and Jeroen C.J.H. Aerts (2012). 'Global exposure to river and coastal flooding: Long term trends and changes'. In: *Global Environmental Change*. ISSN: 09593780. DOI: 10.1016/j.gloenvcha.2012.07.004.

Joyce, Robert J., John E. Janowiak, Phillip A. Arkin and Pingping Xie (2004). 'CMORPH: A Method that Produces Global Precipitation Estimates from Passive Microwave and Infrared Data at High Spatial and Temporal Resolution'. In: *Journal of Hydrometeorology*. ISSN: 1525-755X. DOI: 10.1175/1525-7541(2004)005<0487:CAMTPG>2.0.CO;2.

Józsa, Edina, Szabolcs Ákos Fábián and Mónika Kovács (2014). 'An evaluation of EU-DEM in comparison with ASTER GDEM, SRTM and contour-based DEMs over the Eastern Mecsek Mountains'. In: *Hungarian Geographical Bulletin*. ISSN: 20645031. DOI: 10.15201/hungeobull.63.4.3.

Kawazoe, Sho and William J. Gutowski (Aug. 2013). 'Regional, Very Heavy Daily Precipitation in NARCCAP Simulations'. In: *Journal of Hydrometeorology* 14.4, pp. 1212–1227. ISSN: 1525-755X. DOI: 10.1175/JHM-D-12-068.1. URL: http://journals.ametsoc.org/doi/abs/10.1175/JHM-D-12-068.1.

Kendon, Elizabeth J., Nigel M. Roberts, Catherine A. Senior and Malcolm J. Roberts (Sept. 2012). 'Realism of Rainfall in a Very High-Resolution Regional Climate Model'. In: *Journal of Climate* 25.17, pp. 5791–5806. ISSN: 0894-8755. DOI: 10.1175/JCLI-D-11-00562.1. URL: http://journals.ametsoc.org/doi/abs/10.1175/JCLI-D-11-00562.1.

Kharin, V. V., F. W. Zwiers, X. Zhang and M. Wehner (2013). 'Changes in temperature and precipitation extremes in the CMIP5 ensemble'. In: *Climatic Change* 119, pp. 345–357. ISSN: 01650009. DOI: 10.1007/s10584-013-0705-8.

Kidd, C. and V. Levizzani (2011). 'Status of satellite precipitation retrievals'. In: *Hydrology and Earth System Sciences*. ISSN: 10275606. DOI: 10.5194/hess-15-1109-2011.

Kjeldsen, T. R. et al. (2014). *Documentary evidence of past floods in Europe and their utility in flood frequency estimation*. DOI: 10.1016/j.jhydrol.2014.06.038.

Klein Tank, A. M G and G. P. Können (2003). 'Trends in Indices of daily temperature and precipitation extremes in Europe, 1946-99'. In: *Journal of Climate*. ISSN: 08948755. DOI: 10.1175/1520-0442(2003)016<3665:TIIODT>2.0.CO;2.

Kling, Harald, Martin Fuchs and Maria Paulin (2012). 'Runoff conditions in the upper Danube basin under an ensemble of climate change scenarios'. In: *Journal of Hydrology*. ISSN: 00221694. DOI: 10.1016/j.jhydrol.2012.01.011.

Kochendorfer, John et al. (2017a). 'Analysis of single-Alter-shielded and unshielded measurements of mixed and solid precipitation from WMO-SPICE'. In: *Hydrology and Earth System Sciences*. ISSN: 16077938. DOI: 10.5194/hess-21-3525-2017.

Kochendorfer, John et al. (2017b). 'The quantification and correction of wind-induced precipitation measurement errors'. In: *Hydrology and Earth System Sciences*. ISSN: 16077938. DOI: 10.5194/hess-21-1973-2017.

Kochendorfer, John et al. (2018). 'Testing and development of transfer functions for weighing precipitation gauges in WMO-SPICE'. In: *Hydrology and Earth System Sciences*. ISSN: 16077938. DOI: 10.5194/hess-22-1437-2018.

Kron, Wolfgang (2002). 'Keynote lecture: Flood risk= hazard× exposure× vulnerability'. In: *Proceedings of the Flood Defence*.

– (2005). 'Flood risk = hazard • values • vulnerability'. In: *Water International*. ISSN: 02508060. DOI: 10.1080/02508060508691837.

Kundzewicz, Zbigniew (2012). *Changes in Flood Risk in Europe*. ISBN: 978-1-907161-28-5. DOI: 10.1201/b12348.

Kundzewicz, Zbigniew W., Yukiko Hirabayashi and Shinjiro Kanae (2010). 'River Floods in the Changing Climate-Observations and Projections'. In: *Water Resources Management*. ISSN: 09204741. DOI: 10.1007/s11269-009-9571-6.

Kundzewicz, Zbigniew W. et al. (2013). 'Flood risk and climate change: global and regional perspectives'. In: *Hydrological Sciences Journal*. ISSN: 0262-6667. DOI: 10.1080/02626667.2013.857411.

Landelius, T., P. Dahlgren, S. Gollvik, A. Jansson and E. Olsson (2016). 'A high-resolution regional reanalysis for Europe. Part 2: 2D analysis of surface temperature, precipitation and wind'. In: *Quarterly Journal of the Royal Meteorological Society*. ISSN: 1477870X. DOI: 10.1002/qj.2813.

Lehner, B, K Verdin and A Jarvis (2013). 'HydroSHEDS Technical Documentation Version 1.2'. In: *EOS Transactions*. DOI: WorldWildlifeFundUS,Washington,DC.Availablefrom:<http://hydrosheds.cr.usgs.gov>..

Lehner, Bernhard, Petra Döll, Joseph Alcamo, Thomas Henrichs and Frank Kaspar (2006). 'Estimating the impact of global change on flood and drought risks in Europe: A continental, integrated analysis'. In: *Climatic Change*. ISSN: 01650009. DOI: 10.1007/s10584-006-6338-4.

Lehner, Bernhard, Kristine Verdin and Andy Jarvis (2008). 'New global hydrography derived from spaceborne elevation data'. In: *Eos*. ISSN: 00963941. DOI: 10.1029/2008EO100001.

Lighthill, M. J. and G. B. Whitham (1955). 'On Kinematic Waves. I. Flood Movement in Long Rivers'. In: *Proceedings of the Royal Society A: Mathematical, Physical and Engineering Sciences*. ISSN: 1364-5021. DOI: 10.1098/rspa.1955.0088.

Lorenz, Philip and Daniela Jacob (2005). 'Influence of regional scale information on the global circulation: A two-way nesting climate simulation'. In: *Geophysical Research Letters* 32, pp. 1–4. ISSN: 00948276. DOI: 10.1029/2005GL023351.

Lucas-Picher, Philippe, René Laprise and Katja Winger (2017). 'Evidence of added value in North American regional climate model hindcast simulations using ever-increasing horizontal resolutions'. In: *Climate Dynamics*. ISSN: 14320894. DOI: 10.1007/s00382-016-3227-z.

Luo, Tianyi (2015). *Aqueduct Global Flood Analyzer*. URL: https://www.wri.org/resources/maps/aqueduct-global-flood-analyzer.

Maggioni, Viviana, Mathew R. P. Sapiano and Robert F. Adler (2016). 'Estimating Uncertainties in High-Resolution Satellite Precipitation Products: Systematic or Random Error?' In: *Journal of Hydrometeorology*. ISSN: 1525-755X. DOI: 10.1175/JHM-D-15-0094.1.

Maione, Ugo, Paolo Mignosa and Massimo Tomirotti (2003). 'Regional estimation of synthetic design hydrographs'. In: *International Journal of River Basin Management*. ISSN: 18142060. DOI: 10.1080/15715124.2003.9635202.

Mallakpour, Iman and Gabriele Villarini (2015). 'The changing nature of flooding across the central United States'. In: *Nature Climate Change*. ISSN: 17586798. DOI: 10.1038/nclimate2516.

Marchesini, I, M Rossi, P Salvati, M Donnini, S Sterlacchini and F Guzzetti (2016). 'Delineating flood prone areas using a statistical approach'. In: *PeerJ preprints*. ISSN: 2167-9843. DOI: 10.7287/peerj.preprints.1937v2.

Marchi, L., M. Borga, E. Preciso and E. Gaume (2010). 'Characterisation of selected extreme flash floods in Europe and implications for flood risk management'. In: *Journal of Hydrology*. ISSN: 00221694. DOI: 10.1016/j.jhydrol.2010.07.017.

Martinis, Sandro and Christoph Rieke (2015). 'Backscatter analysis using multi-temporal and multi-frequency SAR data in the context of flood mapping at River Saale, Germany'. In: *Remote Sensing*. ISSN: 20724292. DOI: 10.3390/rs70607732.

Martinis, Sandro, André Twele, Christian Strobl, Jens Kersten and Enrico Stein (2013). 'A multi-scale flood monitoring system based on fully automatic MODIS and terraSAR-X processing chains'. In: *Remote Sensing*. ISSN: 20724292. DOI: 10.3390/rs5115598.

Masoero, Alessandro, Pierluigi Claps, Nathalie E.M. Asselman, Erik Mosselman and Giuliano Di Baldassarre (2013). 'Reconstruction and analysis of the Po River inundation of 1951'. In: *Hydrological Processes*. ISSN: 08856087. DOI: 10.1002/hyp.9558.

Merz, B., A. H. Thieken and M. Gocht (2007). 'Flood risk mapping at the local scale: Concepts and challenges'. In: *Advances in Natural and Technological Hazards Research*. ISBN: 978-1-4020-4200-3. DOI: 10.1007/978-1-4020-4200-3{_}13.

Merz, B. et al. (2014). 'Floods and climate: Emerging perspectives for flood risk assessment and management'. In: *Natural Hazards and Earth System Sciences*. ISSN: 16849981. DOI: 10.5194/nhess-14-1921-2014.

Middelkoop, H. et al. (2001). 'Impact of climate change on hydrological regimes and water resources management in the Rhine basin'. In: *Climatic Change*. ISSN: 01650009. DOI: 10.1023/A:1010784727448.

Milly, P. C.D., R. T. Wetherald, K. A. Dunne and T. L. Delworth (2002). 'Increasing risk of great floods in a changing climate'. In: *Nature*. ISSN: 00280836. DOI: 10.1038/415514a.

Mitchell, James K. (2003). *European river floods in a changing world*. DOI: 10.1111/1539-6924.00337.

Mohr, Matthias (2008). 'New Routines for Gridding of Temperature and Precipitation Observations for "seNorge. no"'. In: *Met. no Report*. ISSN: 0027-8424. DOI: 10.1073/pnas.93.13.6830.

– (2009). 'Comparison of versions 1.1 and 1.0 of gridded tem- perature and precipitation data for Norway'. In: Met.no not.19.

Morelli, Stefano, Alessandro Battistini and Filippo Catani (2014). 'Rapid assessment of flood susceptibility in urbanized rivers using digital terrain data: Application to the arno river case study (Firenze, northern Italy)'. In: *Applied Geography*. ISSN: 01436228. DOI: 10.1016/j.apgeog.2014.06.032.

Munich RE (2000). *Topics 2000: Natural catastrophes – the current position*. Tech. rep.

– (2015). 'Weather catastrophes and climate change'. In: *Münchener Rückversicherungs-Gesellschaft*.

Natural Environment Research Council (Great Britain) NERC (1975). *Flood Studies Report in Five Volumes*. Tech. rep. Natural Environment Research Council (Great Britain).

Neal, J., G. Schumann, T. Fewtrell, M. Budimir, P. Bates and D. Mason (2011). 'Evaluating a new LISFLOOD-FP formulation with data from the summer 2007 floods in Tewkesbury, UK'. In: *Journal of Flood Risk Management*. ISSN: 1753318X. DOI: 10.1111/j.1753-318X.2011.01093.x.

Nešpor, Vladislav and Boris Sevruk (1999). 'Estimation of wind-induced error of rainfall gauge measurements using a numerical simulation'. In: *Journal of Atmospheric and Oceanic Technology*. ISSN: 07390572. DOI: 10.1175/1520-0426(1999)016<0450:EOWIEO>2.0.CO;2.

Neuwirth, Erich (2014). *RColorBrewer: ColorBrewer Palettes*. URL: https://cran.r-project.org/package=RColorBrewer.

Nigro, Joseph, Daniel Slayback, Frederick Policelli and G Robert Brakenridge (2014). 'NASA/DFO MODIS Near Real-Time (NRT) Global Flood Mapping Product Evaluation of Flood and Permanent Water Detection'. In: *Evaluation, Greenbelt, MD*.

Nogherotto, Rita, Adriano Fantini, Francesca Raffaele, Erika Coppola and Filippo Giorgi (2019). 'An integrated hydrological and hydraulic modelling approach for the flood risk assessment over Po river basin: a case study for the ALLIANZ Insurance Company'. In: *in preparation*.

Norbiato, Daniele, Marco Borga, Marco Sangati and Francesco Zanon (2007). 'Regional frequency analysis of extreme precipitation in the eastern Italian Alps and the August 29, 2003 flash flood'. In: *Journal of Hydrology*. ISSN: 00221694. DOI: 10.1016/j.jhydrol.2007.07.009.

Pal, Jeremy S., Filippo Giorgi and Xunqiang Bi (2004). 'Consistency of recent European summer precipitation trends and extremes with future regional climate projections'. In: *Geophysical Research Letters*. ISSN: 00948276. DOI: 10.1029/2004GL019836.

Pal, Jeremy S. et al. (2007). 'Regional climate modeling for the developing world: The ICTP RegCM3 and RegCNET'. In: *Bulletin of the American Meteorological Society* 88, pp. 1395–1409. ISSN: 00030007. DOI: 10.1175/BAMS-88-9-1395.

Paprotny, Dominik, Oswaldo Morales-Nápoles and Sebastiaan N. Jonkman (2017). 'Efficient pan-European river flood hazard modelling through a combination of statistical and physical models'. In: *Natural Hazards and Earth System Sciences*. ISSN: 16849981. DOI: 10.5194/nhess-17-1267-2017.

Pavan, Valentina et al. (2018). 'High resolution climate precipitation analysis for north-central Italy, 1961–2015'. In: *Climate Dynamics* 0.0, pp. 1–19. ISSN: 14320894. DOI: 10.1007/s00382-018-4337-6. URL: http://dx.doi.org/10.1007/s00382-018-4337-6.

Pebesma, Edzer (2018a). 'Simple Features for R: Standardized Support for Spatial Vector Data'. In: *The R Journal*. URL: https://journal.r-project.org/archive/2018/RJ-2018-009/index.html.

– (2018b). *stars: Scalable, Spatiotemporal Tidy Arrays*. URL: https://github.com/r-spatial/stars/.

Pedersen, Thomas Lin (2017). *patchwork: The Composer of ggplots*. URL: https://github.com/thomasp85/patchwork.

Pekel, Jean François, Andrew Cottam, Noel Gorelick and Alan S. Belward (2016). 'High-resolution mapping of global surface water and its long-term changes'. In: *Nature*. ISSN: 14764687. DOI: 10.1038/nature20584.

Pierce, David (2017). *ncdf4: Interface to Unidata netCDF (Version 4 or Earlier) Format Data Files*. URL: https://cran.r-project.org/package=ncdf4.

Pierdicca, N., L. Pulvirenti, M. Chini, L. Guerriero and L. Candela (2013). 'Observing floods from space: Experience gained from COSMO-SkyMed observations'. In: *Acta Astronautica*. ISSN: 00945765. DOI: 10.1016/j.actaastro.2012.10.034.

Prein, A. F. et al. (2016). 'Precipitation in the EURO-CORDEX 0.11 and 0.44 simulations: high resolution, high benefits?' In: *Climate Dynamics*. ISSN: 14320894. DOI: 10.1007/s00382-015-2589-y.

Prein, Andreas F. and Andreas Gobiet (2017). 'Impacts of uncertainties in European gridded precipitation observations on regional climate analysis'. In: *International Journal of Climatology*. ISSN: 10970088. DOI: 10.1002/joc.4706.

Prein, Andreas F. et al. (2015). *A review on regional convection-permitting climate modeling: Demonstrations, prospects, and challenges*. DOI: 10.1002/2014RG000475.

Prudhomme, Christel, Dörte Jakob and Cecilia Svensson (2003). *Uncertainty and climate change impact on the flood regime of small UK catchments*. DOI: 10.1016/S0022-1694(03)00065-9.

Pryor, S. C., G. Nikulin and C. Jones (Feb. 2012). 'Influence of spatial resolution on regional climate model derived wind climates'. In: *Journal of Geophysical Research* 117.D3, p. D03117. ISSN: 0148-0227. DOI: 10.1029/2011JD016822. URL: http://doi.wiley.com/10.1029/2011JD016822.

Púčik, Tomáš et al. (2017). 'Future changes in European severe convection environments in a regional climate model ensemble'. In: *Journal of Climate*. ISSN: 08948755. DOI: 10.1175/JCLI-D-16-0777.1. URL: https://journals.ametsoc.org/doi/pdf/10.1175/JCLI-D-16-0777.1.

Pulvirenti, L., M. Chini, N. Pierdicca, L. Guerriero and P. Ferrazzoli (2011). 'Flood monitoring using multi-temporal COSMO-skymed data: Image segmentation and signature interpretation'. In: *Remote Sensing of Environment*. ISSN: 00344257. DOI: 10.1016/j.rse.2010.12.002.

Python Software Foundation (2018). *Python Language Reference*. URL: http://www.python.org.

R Core Team (2018). *R: A Language and Environment for Statistical Computing*. DOI: 10.1007/978-3-540-74686-7. URL: https://www.r-project.org/.

Rajczak, J., P. Pall and C. Schär (May 2013). 'Projections of extreme precipitation events in regional climate simulations for Europe and the Alpine Region'. In: *Journal of Geophysical Research Atmospheres* 118.9, pp. 3610–3626. ISSN: 21698996. DOI: 10.1002/jgrd.502972013. URL: http://doi.wiley.com/10.1002/jgrd.50297.

Rauthe, Monika, Heiko Steiner, Ulf Riediger, Alex Mazurkiewicz and Annegret Gratzki (2013). 'A Central European precipitation climatology - Part I: Generation and validation of a high-resolution gridded daily data set (HYRAS)'. In: *Meteorologische Zeitschrift* 22, pp. 235–256. ISSN: 09412948. DOI: 10.1127/0941-2948/2013/0436.

Reed, Duncan W. (2002). 'Reinforcing flood-risk estimation'. In: *Philosophical Transactions of the Royal Society A: Mathematical, Physical and Engineering Sciences*. DOI: 10.1098/rsta.2002.1005.

Refice, Alberto, Domenico Capolongo, Guido Pasquariello, Annarita Daaddabbo, Fabio Bovenga, Raffaele Nutricato, Francesco P. Lovergine and Luca Pietranera (2014). 'SAR and InSAR for flood monitoring: Examples with COSMO-SkyMed data'. In: *IEEE Journal of Selected Topics in Applied Earth Observations and Remote Sensing*. ISSN: 21511535. DOI: 10.1109/JSTARS.2014.2305165.

Riahi, Keywan, Arnulf Grübler and Nebojsa Nakicenovic (2007). 'Scenarios of long-term socio-economic and environmental development under climate stabilization'. In: *Technological Forecasting and Social Change* 74, pp. 887–935. ISSN: 00401625. DOI: 10.1016/j.techfore.2006.05.026.

Ridal, Martin, Esbjörn Olsson, Per Unden, Klaus Zimmermann and Alexandra Ohlsson (2017). *HARMONIE reanalysis report of results and dataset*. Tech. rep. SMHI.

Rizzoli, Paola et al. (2017). 'Generation and performance assessment of the global TanDEM-X digital elevation model'. In: *ISPRS Journal of Photogrammetry and Remote Sensing*. ISSN: 09242716. DOI: 10.1016/j.isprsjprs.2017.08.008.

Robson, Alice J. (2002). 'Evidence for trends in UK flooding'. In: *Philosophical Transactions of the Royal Society A: Mathematical, Physical and Engineering Sciences*. ISBN: 1364-503X. DOI: 10.1098/rsta.2002.1003.

Rojas, Maisa (Aug. 2006). 'Multiply Nested Regional Climate Simulation for Southern South America: Sensitivity to Model Resolution'. In: *Monthly Weather Review* 134.8, pp. 2208–2223. ISSN: 0027-0644. DOI: 10.1175/MWR3167.1. URL: http://journals.ametsoc.org/doi/abs/10.1175/MWR3167.1.

Rojas, R., L. Feyen, A. Bianchi and A. Dosio (2012). 'Assessment of future flood hazard in Europe using a large ensemble of bias-corrected regional climate simulations'. In: *Journal of Geophysical Research Atmospheres*. ISSN: 01480227. DOI: 10.1029/2012JD017461.

Rojas, Rodrigo, Luc Feyen and Paul Watkiss (2013). 'Climate change and river floods in the European Union: Socio-economic consequences and the costs and benefits of adaptation'. In: *Global Environmental Change*. ISSN: 09593780. DOI: 10.1016/j.gloenvcha.2013.08.006.

Rossi, Mauro, Dalia Kirschbaum, Daniela Valigi, Alessandro Mondini and Fausto Guzzetti (2017). 'Comparison of Satellite Rainfall Estimates and Rain Gauge Measurements in Italy, and Impact on Landslide Modeling'. In: *Climate*. ISSN: 2225-1154. DOI: 10.3390/cli5040090.

Roudier, Philippe, Jafet C.M. Andersson, Chantal Donnelly, Luc Feyen, Wouter Greuell and Fulco Ludwig (2016). 'Projections of future floods and hydrological droughts in Europe under a +2°C global warming'. In: *Climatic Change*, pp. 341–355. ISSN: 15731480. DOI: 10.1007/s10584-015-1570-4.

Rowe, Brian Lee Yung (2016). *futile.logger: A Logging Utility for R*. URL: https://cran.r-project.org/package=futile.logger.

Ruti, Paolo M. et al. (2016). 'Med-CORDEX initiative for Mediterranean climate studies'. In: *Bulletin of the American Meteorological Society*. ISSN: 00030007. DOI: 10.1175/BAMS-D-14-00176.1.

Salvati, P., C. Bianchi, M. Rossi and F. Guzzetti (2010). 'Societal landslide and flood risk in Italy'. In: *Natural Hazards and Earth System Science*. ISSN: 16849981. DOI: 10.5194/nhess-10-465-2010.

Santo, A., G. Di Crescenzo, S. Del Prete and L. Di Iorio (2012). 'The Ischia island flash flood of November 2009 (Italy): Phenomenon analysis and flood hazard'. In: *Physics and Chemistry of the Earth*. ISSN: 14747065. DOI: 10.1016/j.pce.2011.12.004.

Sarachi, Sepideh, Kuo-lin Hsu and Soroosh Sorooshian (2015). 'A Statistical Model for the Uncertainty Analysis of Satellite Precipitation Products'. In: *Journal of Hydrometeorology*. ISSN: 1525-755X. DOI: 10.1175/JHM-D-15-0028.1.

Schlaffer, Stefan, Patrick Matgen, Markus Hollaus and Wolfgang Wagner (2015). 'Flood detection from multi-temporal SAR data using harmonic analysis and change detection'. In: *International Journal of Applied Earth Observation and Geoinformation*. ISSN: 03032434. DOI: 10.1016/j.jag.2014.12.001.

Schneider, Udo, Andreas Becker, Peter Finger, Anja Meyer-Christoffer, Markus Ziese and Bruno Rudolf (2014). 'GPCC's new land surface precipitation climatology based on quality-controlled in situ data and its role in quantifying the global water cycle'. In: *Theoretical and Applied Climatology*. ISSN: 14344483. DOI: 10.1007/s00704-013-0860-x.

Schulz, Karsten and Matthias Bernhardt (2016). 'The end of trend-estimation for extreme floods under climate change?' In: *Hydrological Processes*. ISSN: 10991085. DOI: 10.1002/hyp.10816.

Schulzweida, Uwe (2018). *CDO User's Guide*. DOI: 10.1111/j.1600-0447.2011.01711.x. URL: https://code.mpimet.mpg.de/projects/cdo/.

Schwarb, M, C Daly, C Frei and C Schär (2001). 'Mean annual precipitation throughout the European Alps, 1971–1990'. In: *Hydrologic atlas of Switzerland (Plate 2.6)*.

Seneviratne, Sonia I et al. (2012). *IPCC special report on Managing the Risks of Extreme Events and Disasters to Advance Climate Change Adaptation (SREX)*. Ed. by Christopher B. Field, Vicente Barros, Thomas F. Stocker and Qin Dahe. Cambridge: Cambridge University Press. ISBN: 9781139177245. DOI: 10.1017/CBO9781139177245. URL: http://dx.doi.org/10.1017/CBO9781139177245.006http://ebooks.cambridge.org/ref/id/CBO9781139177245.

Serinaldi, Francesco and Chris G. Kilsby (2017). 'A Blueprint for Full Collective Flood Risk Estimation: Demonstration for European River Flooding'. In: *Risk Analysis*. ISSN: 15396924. DOI: 10.1111/risa.12747.

Shepard, D S (1984). 'Computer mapping: The SYMAP interpolation algorithm'. In: *Spatial Statistics and Models*. ISBN: 978-90-481-8385-2. DOI: 10.1007/978-94-017-3048-8{_}7.

Skinner, Christopher J., Thomas J. Coulthard, Daniel R. Parsons, Jorge A. Ramirez, Liam Mullen and Susan Manson (2015). 'Simulating tidal and storm surge hydraulics with a simple 2D inertia based model, in the Humber Estuary, U.K'. In: *Estuarine, Coastal and Shelf Science*. ISSN: 02727714. DOI: 10.1016/j.ecss.2015.01.019.

Slowikowski, Kamil (2018). *ggrepel: Automatically Position Non-Overlapping Text Labels with 'ggplot2'*. URL: https://cran.r-project.org/package=ggrepel.

Smith, Laurence C. (1997). 'Satellite remote sensing of river inundation area, stage, and discharge: a review'. In: *Hydrological Processes*. ISSN: 08856087. DOI: 10.1002/(SICI)1099-1085(199708)11:10<1427::AID-HYP473>3.3.CO;2-J.

Sole, A., L. Giosa, L. Nolè, V. Medina and A. Bateman (2008). 'Flood risk modelling with LiDAR technology'. In: *WIT Transactions on Ecology and the Environment*. ISSN: 17433541. DOI: 10.2495/FRIAR080031.

South, Andy (2018). *rnaturalearth: World Map Data from Natural Earth*. URL: https://github.com/ropensci/rnaturalearth.

Stephens, E. M., P. D. Bates, J. E. Freer and D. C. Mason (2012). 'The impact of uncertainty in satellite data on the assessment of flood inundation models'. In: *Journal of Hydrology*. ISSN: 00221694. DOI: 10.1016/j.jhydrol.2011.10.040.

Stevens, Andrew J., Derek Clarke and Robert J. Nicholls (2016). 'Trends in reported flooding in the UK: 1884–2013'. In: *Hydrological Sciences Journal*. ISSN: 21503435. DOI: 10.1080/02626667.2014.950581.

Tadono, T., H. Nagai, H. Ishida, F. Oda, S. Naito, K. Minakawa and H. Iwamoto (2016). 'Generation of the 30 M-MESH global digital surface model by alos prism'. In: *International Archives of the Photogrammetry, Remote Sensing and Spatial Information Sciences - ISPRS Archives*. DOI: 10.5194/isprsarchives-XLI-B4-157-2016.

Tadono, Takeo, Junichi Takaku, Fumi Ohgushi, Masanori Doutsu and Ken Ichiro Kobayashi (2017). 'Updates of 'AW3D30' 30 M-MESH global digital surface model

dataset'. In: *International Geoscience and Remote Sensing Symposium (IGARSS)*. ISBN: 9781509049516. DOI: 10.1109/IGARSS.2017.8128290.

Tarquini, Simone, Ilaria Isola, Massimiliano Favalli, Francesco Mazzarini, Marina Bisson, Maria Teresa Pareschi and Enzo Boschi (2007). 'TINITALY/01: A new Triangular Irregular Network of Italy'. In: *Annals of Geophysics*. ISSN: 15935213. DOI: 10.4401/ag-4424. URL: http://tinitaly.pi.ingv.it/.

Tarquini, Simone, Stefano Vinci, Massimiliano Favalli, Fawzi Doumaz, Alessandro Fornaciai and Luca Nannipieri (2012). 'Release of a 10-m-resolution DEM for the Italian territory: Comparison with global-coverage DEMs and anaglyph-mode exploration via the web'. In: *Computers and Geosciences*. ISSN: 00983004. DOI: 10.1016/j.cageo.2011.04.018. URL: http://tinitaly.pi.ingv.it/.

Thober, Stephan et al. (2018). 'Multi-model ensemble projections of European river floods and high flows at 1.5, 2, and 3 degrees global warming'. In: *Environmental Research Letters*. ISSN: 17489326. DOI: 10.1088/1748-9326/aa9e35.

Thomas Steven Savage, James, Francesca Pianosi, Paul Bates, Jim Freer and Thorsten Wagener (2016). 'Quantifying the importance of spatial resolution and other factors through global sensitivity analysis of a flood inundation model'. In: *Water Resources Research*. ISSN: 19447973. DOI: 10.1002/2015WR018198.

Tian, Yudong and Christa D. Peters-Lidard (2010). 'A global map of uncertainties in satellite-based precipitation measurements'. In: *Geophysical Research Letters*. ISSN: 00948276. DOI: 10.1029/2010GL046008.

Tomassetti, B., E. Coppola, M. Verdecchia and G. Visconti (2005). 'Coupling a distributed grid based hydrological model and MM5 meteorological model for flooding alert mapping'. In: *Advances in Geosciences*. ISSN: 16807359. DOI: 10.5194/adgeo-2-59-2005.

Torma, Csaba, Filippo Giorgi and Erika Coppola (2015). 'Added value of regional climate modeling over areas characterized by complex terrain-precipitation over the Alps'. In: *Journal of Geophysical Research*. ISSN: 21562202. DOI: 10.1002/2014JD022781.

Tramblay, Yves and Samuel Somot (2018). 'Future evolution of extreme precipitation in the Mediterranean'. In: *Climatic Change*, pp. 1–14. ISSN: 0165-0009. DOI: 10.1007/s10584-018-2300-5. URL: https://link.springer.com/article/10.1007/s10584-018-2300-5.

Trigila, Alessandro, Carla Iadanza, Martina Bussettini and Barbara Lastoria (2018). *Dissesto idrogeologico in Italia: pericolosità e indicatori di rischio*. Tech. rep. ISPRA, Rapporti 287/2018. URL: http://www.isprambiente.gov.it/files2018/pubblicazioni/rapporti/rapporto-dissesto-idrogeologico/Rapporto_Dissesto_Idrogeologico_ISPRA_287_2018_Web.pdf.

Unidata (2018). *Network Common Data Form (netCDF)*. DOI: http://doi.org/10.5065/D6H70CW6. URL: https://www.unidata.ucar.edu/software/netcdf/.

USGS (1996). *Global 30 Arc-Second Elevation (GTOPO30)*. DOI: https://lta.cr.usgs.gov/GTOPO30.

Valentini, R., L.M. Bouwer, E. Georgopoulou, D. Jacob, E. Martin, M. Rounsevell and J.-F. Soussana (2014). *Europe. In: Climate Change 2014: Impacts, Adaptation, and Vulnerability. Part B: Regional Aspects. Contribution of Working Group II to the Fifth Assessment Report of the Intergovernmental Panel on Climate Change*. Tech. rep., pp. 1267–1326. URL: https://www.ipcc.ch/report/ar5/wg2/.

Van Alphen, J., F. Martini, R. Loat, R. Slomp and R. Passchier (2009). 'Flood risk mapping in Europe, experiences and best practices'. In: *Journal of Flood Risk Management*. ISSN: 1753318X. DOI: 10.1111/j.1753-318X.2009.01045.x.

Vaughan, Davis and Matt Dancho (2018). *furrr: Apply Mapping Functions in Parallel using Futures*. URL: https://cran.r-project.org/package=furrr.

Vautard, Robert et al. (Apr. 2013). 'The simulation of European heat waves from an ensemble of regional climate models within the EURO-CORDEX project'. In: *Climate Dynamics* 41.9-10, pp. 2555–2575. ISSN: 0930-7575. DOI: 10.1007/s00382-013-1714-z. URL: http://link.springer.com/10.1007/s00382-013-1714-z.

Veijalainen, Noora, Eliisa Lotsari, Petteri Alho, Bertel Vehviläinen and Jukka Käyhkö (2010). 'National scale assessment of climate change impacts on flooding in Finland'. In: *Journal of Hydrology*. ISSN: 00221694. DOI: 10.1016/j.jhydrol.2010.07.035.

Velasquez, Nicolas, Veronica Botero and Jaime Ignacio Velez (2011). 'Rainfall distribution based on a Delaunay triangulation method'. In: *Lecture Notes in Computer Science (including subseries Lecture Notes in Artificial Intelligence and Lecture Notes in Bioinformatics)*. ISBN: 9783642252488. DOI: 10.1007/978-3-642-25249-5{_}7.

Verdecchia, M. et al. (2008). 'Flood forecast in complex orography coupling distributed hydro-meteorological models and in-situ and remote sensing data'. In: *Meteorology and Atmospheric Physics*. ISSN: 01777971. DOI: 10.1007/s00703-007-0278-z.

Vidal, Jean Philippe, Eric Martin, Laurent Franchistéguy, Martine Baillon and Jean Michel Soubeyroux (2010). 'A 50-year high-resolution atmospheric reanalysis over France with the Safran system'. In: *International Journal of Climatology*. ISSN: 08998418. DOI: 10.1002/joc.2003.

Walther, Alexander, Jee-Hoon Jeong, Grigory Nikulin, Colin Jones and Deliang Chen (Jan. 2013). 'Evaluation of the warm season diurnal cycle of precipitation over Sweden simulated by the Rossby Centre regional climate model RCA3'. In: *Atmospheric Research* 119, pp. 131–139. ISSN: 01698095. DOI: 10.1016/j.atmosres.2011.10.012. URL: http://linkinghub.elsevier.com/retrieve/pii/S0169809511003395.

Weerts, A. H., D. Meißner and S. Rademacher (2008). *input data Rainfall-Runoff Model Operational Systems FEWS-NL and FEWS-DE*. Tech. rep. Deltares.

Westerhoff, R. S., M. P.H. Kleuskens, H. C. Winsemius, H. J. Huizinga, G. R. Brakenridge and C. Bishop (2013). 'Automated global water mapping based on wide-swath orbital synthetic-aperture radar'. In: *Hydrology and Earth System Sciences*. ISSN: 10275606. DOI: 10.5194/hess-17-651-2013.

Whitfield, P. H. (2012). *Floods in future climates: A review*. DOI: 10.1111/j.1753-318X.2012.01150.x.

Wickham, Hadley (2016). *ggplot2: Elegant Graphics for Data Analysis*. Springer-Verlag New York. ISBN: 978-3-319-24277-4. URL: http://ggplot2.org.

Wickham, Hadley and Lionel Henry (2018). *tidyr: Easily Tidy Data with 'spread()' and 'gather()' Functions*. URL: https://cran.r-project.org/package=tidyr.

Wickham, Hadley, Jim Hester and Romain Francois (2017). *readr: Read Rectangular Text Data*. URL: https://cran.r-project.org/package=readr.

Wickham, Hadley, Romain François, Lionel Henry and Kirill Müller (2018). *dplyr: A Grammar of Data Manipulation*. URL: https://cran.r-project.org/package=dplyr.

Willmott, C. J. and K. Matsuura (2001). *Terrestrial Air Temperature and Precipitation: Monthly and Annual Time Series (1950 - 1999)*. URL: http://climate.geog.udel.edu/~climate/html_pages/README.ghcn_ts2.html.

Willmott, Cort J. (1984). 'On the Evaluation of Model Performance in Physical Geography'. In: *Spatial Statistics and Models*. ISBN: 9048183855. DOI: 10.1007/978-94-017-3048-8{_}23.

Wolff, M. A., K. Isaksen, A. Petersen-ØVerleir, K. Ødemark, T. Reitan and R. Brækkan (2015). 'Derivation of a new continuous adjustment function for correcting wind-induced loss of solid precipitation: Results of a Norwegian field study'. In: *Hydrology and Earth System Sciences*. ISSN: 16077938. DOI: 10.5194/hess-19-951-2015.

World Meteorological Organization (2008). *Guide to Meteorological Instruments and Methods of Observation*. ISBN: 978-92-63-10008-5. DOI: Guidetometeorologicalinstrumentandobservingpr

Wüest, Marc, Christoph Frei, Adrian Altenhoff, Martin Hagen, Michael Litschi and Christoph Schär (2010). 'A gridded hourly precipitation dataset for Switzerland using rain-gauge analysis and radar-based disaggregation'. In: *International Journal of Climatology*. ISSN: 08998418. DOI: 10.1002/joc.2025.

Zender, Charles S. (2008). 'Analysis of self-describing gridded geoscience data with netCDF Operators (NCO)'. In: *Environmental Modelling and Software*. ISSN: 13648152. DOI: 10.1016/j.envsoft.2008.03.004.

Zhang, X. D., J. Y. Trepanier, M. Reggio and R. Camarero (1994). 'Time-accurate local time stepping method based on flux updating'. In: *The American Institute of Aeronautics and Astronautics Journal* 32.9, pp. 1926–1929. ISSN: 0001-1452. DOI: 10.2514/3.12195.